Insulin signalling in endothelial cells

Philippeos, Christina

Awarding institution:
King's College London

Insulin signalling in endothelial cells

By

Christina Philippeos

thesis submitted to King's College London

for the degree of Doctor of Philosophy, April 2014

Randall Division of Cell and Molecular Biophysics

King's College London

2nd floor New Hunt's House

London SE1 1UL

Abstract

Insulin is known to act as an anti-inflammatory agent and protect vascular endothelial cells during ischaemic damage *in vivo*. Although it is known that insulin signals in part through phosphatidylinositol 3-kinases (PI3Ks) and Akt, its effects on endothelial junctions and actin cytoskeleton are unknown. This study aimed to characterise endothelial responses to insulin, identify endothelial insulin-induced changes in protein phosphorylation and determine the roles of these changes in regulating endothelial functions.

Insulin stimulation induced dose-dependent Akt activation in both primary human umbilical vein endothelial cells (HUVECs) and an endothelial cell line, human bone-marrow endothelial cells (HBMECs). Insulin decreased basal HUVEC permeability, increased angiogenic loop formation *in vitro* and increased cell migration in a wound-healing model, compared to untreated cells.

Insulin-stimulated changes in protein phosphorylation were identified using a 14-3-3 affinity purification proteomic screen, as 14-3-3 proteins interact specifically with phosphorylated Ser/Thr residues within 14-3-3-binding motifs. A total of 390 14-3-3-binding proteins were identified from insulin-stimulated HBMECs, from which 12 proteins were selected based on predicted roles in endothelial cytoskeleton regulation. Validation of these hits, performed by Far-Western overlay analysis, identified 4 IGF-I-regulated 14-3-3-binding proteins: Parg1 (ARHGAP29), RICH-1 (ARHGAP17), LMO7 and Epsin2.

Parg1 depletion in HUVECs induced stress fibre formation, increased endothelial permeability, severely decreased angiogenic loop formation and decreased cell migration, compared to siRNA control-treated cells. This suggests that Parg1 regulates contractility and hence could affect endothelial cell-cell junctional stability. Depletion of RICH-1 and LMO7 in HUVECs resulted in mislocalisation of the tight junction protein ZO-1. However, this did not affect endothelial permeability, suggesting that these proteins are important for maintaining tight junction integrity. LMO7 and Epsin2 depletion each resulted in an increase in angiogenic loop formation, but did not detectably affect cell migration. Insulin stimulation of Epsin2 might increase lamellipodium formation, although further studies are required to establish the mechanisms involved.

In conclusion, this thesis describes a 14-3-3-based proteomic screen that identified novel regulators of endothelial function. These proteins could contribute to the anti-inflammatory roles of insulin.

Acknowledgements

"If I have seen further, it is by standing on the shoulders of giants."

<div align="right">Isaac Newton</div>

A major research project like this is never the work of anyone alone. First and foremost, I would like to express my deepest gratitude to my two supervisors, Professor Anne Ridley and Professor Carol MacKintosh. Anne, thank you for your constant guidance, encouragement and infinite patience during my PhD. It has been an honour to work under your leadership and gain insight into the perplexing field of cell signalling and migration. I was fortunate to have had the opportunity to spend three months in the MacKintosh laboratory in Dundee. The skills and experiences I gained during this time were invaluable. Carol, I am deeply grateful for your continual support and advice throughout this project. I would also like to express my gratitude to The British Heart Foundation for their financial support.

To all the past and present members of the Ridley laboratory, it has been a privilege to go on this journey with you. This PhD has been an extremely challenging experience, however I am doing the best happy dance of my life right now! I hope the legacy of the happy dance lives on throughout your many future successes and discoveries. A very special thank you goes to Silvia Mele, my partner in crime. I could not have gone through this experience without you. I will miss our lengthy scientific discussions about weird and wonderful results, scrutinizing the English language and, of course, your singing at the lab bench. Elvira Infante and Barbara Borda d'Água, I am truly grateful to both of you for taking me under your wing when I first joined the lab, and for teaching me all the little tricks of the trade. To my dearest Ritu Garg, thank you for always being a constant source of reassurance, positivity and support in the laboratory to another butterfly. Special thanks also goes to my rock-star post docs, Nicolas Reymond, Audrey Colomba, Virginia Tajadura-Ortega and Silvia Giampieri, for all the scientific discussions and jokes along the way. Many thanks to Richard Foxon for being so resourceful.

Thank you to everyone who welcomed me into the MacKintosh laboratory. I am particularly grateful for the technical assistance and support given by Kumara Dissanayake, Catherine Johnson and Gerta Hoxhaj. A big thank you goes to Michele Tinti for being my bioinfomatics knight, and for always being a Skype message away in times of need. Many thanks to all the support staff in the MRC Protein Phosphorylation unit and DSTT at the University of Dundee. In particular, Rachel Toth for her amazing cloning work and David Campbell and the mass spectrometry team.

I have to thank all my friends around the world for your endless support. I would love to name you all individually, but I have a word limit ☺ Thank you for being the amazing people you are. I am truly blessed.

Finally and above all, my deepest wholehearted gratitude goes to my family. Mom, Annie, Maria, Demetri and little Ariana, thank you for your boundless love and encouragement.

I would like to dedicate this work in memory of my Father, who taught me that anything is possible through hard work and determination.

Table of Contents

List of Figures

List of Tables

Supplementary movies

Abbreviations

ADF	actin-dissociating protein
AJs	adherens junctions
AmBic	ammonium bicarbonate
Amot	angiomotin
AMPK	AMP-activated protein kinase
aPKC	atypical protein kinase C
APS	adaptor protein with a PH and SH2 domain
Arp2/3	actin-related protein 2/3
ATP	Adenosine triphosphate
BAR	Bin/amphiphysin/Rvs
BCA	bicinchoninic acid
BMH	brain neuromodulin homologue
BSA	bovine serum albumin
CAMs	cell adhesion molecules
CH	Calponin Homology
CHO	Chinese hamster ovary
CIP4	Cdc42-interacting protein 4
CVD	Cardiovascular disease
DAPI	4',6-diamidino-2-phenylindole
DEPC	diethyl pyrocarbonate
DH	Dbl homology
DIG	digoxygenin
DMEM	Dulbecco's modified eagle medium
DMSO	dimethyl sulphoxide
DNA	deoxyribonucleic acid
DNA-PK	DNA-dependent protein kinase
DRF1	diaphanous-related formin 1
DTT	dithiothreitol
EBM	endothelial basal medium
EC	enzyme commission
ECL	enhanced chemiluminescence
ECM	extracellular matrix
ECs	endothelial cells
EDTA	ethylene-diamine-tetra-acetic acid
EGF	epidermal growth factor
EGFP	enhanced green fluorescence protein
EGM	endothelial growth medium
EMED	Emery-Dreifuss muscular dystrophy
eNOS	endothelial nitric oxide synthase
ENTH	epsin N-terminal homology
Epsin	Eps15-interacting protein
ER	endoplasmic reticulum
ERM	ezrin/radixin/moesin
ESAM	endothelial cell selective adhesion molecule

ET-1	endothelin-1
F-actin	filamentous actin
FBS	foetal bovine serum
FITC	fluorescein isothiocyanate
FN	fibronectin
G-actin	globular actin
Gab-1	GRB2-associated-binding protein 1
GAP	GTPase-activating protein
GAPDH	glyceraldehyde 3-phosphate dehydrogenase
GDI	guanine nucleotide dissociation inhibitor
GDP	guanosine diphosphate
GEF	guanine nucleotide exchange factor
GFP	green fluorescent protein
GIK	glucose, insulin and potassium
GMIP	GEM-interacting protein
GST	glutathione S-transferase
GTP	guanosine triphosphate
HBMEC	human bone marrow endothelial cell
HDL	high-density lipoprotein
HEK293	human embryonic kidney 293
HEPES	4-(2-hydroxyethyl)-1-piperazine-ethanesulphonic acid
HGF	hepatocyte growth factor
HMHA1	Minor histocompatibility protein HA-1
HRP	horseradish peroxidase
HUVECs	human umbilical vein endothelial cells
ICAM	intercellular adhesion molecule
IF	immunofluorescence
IGF-I	Insulin-like growth factor I
IGF-IR	insulin-like growth factor I receptor
IL-1	interleukin-1
IP	immunoprecipitation
IPTG	isopropyl β-D-1-thiogalactopyranoside
IR	insulin receptor
IRS	insulin receptor substrate
IRSp53	insulin-receptor substrate p53
JAM	junction adhesion molecule
LB	luria broth
LDL	low-density lipoprotein cholesterol
LIMK	LIM kinase
LMO7	LIM domain only 7
MAPK	Ras-mitogen-activated protein kinase
mDia1	mammalian diaphanous 1
MEK	MAPK and ERK kinase
MI	myocardial infarction
MLC	myosin regulatory light chain
MLCK	myosin regulatory light chain kinase

MLCP	myosin light chain phosphatase
MMP	matrix metalloproteinase
MRTFs	myocardin-related transcription factors
MS	mass spectrometry
mTOR	mammalian target of rapamycin
MYPT1	Myosin phosphatase-targeting subunit 1
NES	nuclear export sequence
NLS	nuclear localisation sequence
NO	nitric oxide
NPF	nucleation promoting factor
p90RSK	protein kinase p90 ribosomal S6 kinase
PAK	p21 activated kinase
PANK2	Pantothenate kinase 2
PAR	partitioning-defective
Parg1	PTPL1-associated RhoGAP 1
PBS	phosphate buffered saline
PCR	polymerase chain reaction
PDGF	platelet-derived growth factor
PDK1	3-phosphoinositide-dependent protein kinase 1
PECAM-1	platelet endothelial adhesion molecule-1
PEI	polyethylenimine
PFA	paraformaldehyde
PH	pleckstrin-homology
PI3K	phosphatidylinositol 3-kinase
PIP$_2$	phosphatidylinositol 4,5-diphosphate
PIP$_3$	phosphatidylinositol 3,4,5-trisphosphate
PKA	cAMP-dependent protein kinase
PKB	protein kinase B
PKC	Protein kinase C
PKG	cGMP-dependent protein kinase
PSGL1	P-selectin glycoprotein ligand1
PSSM	position-specific scoring matrix
PTB	phosphotyrosine-binding
PTPs	protein tyrosine phosphatases
Rho	Ras homologous
RICH-1	RhoGAP interacting with CIP4 homologues
RNAi	RNA interference
ROCK	Rho-associated kinase
ROS	reactive oxygen species
RPMI	Roswell park memorial institute
SDS-PAGE	sodium dodecyl sulphate-polyacrylamide gel electrophoresis
SGK	serum and glucocorticoid-regulated kinase
SH2	src homology-2
siRNA	small interfering RNA
SIRP	signal-regulatory protein
SOS	Son-of-sevenless

SRF	serum response factor
TBS	tris buffered saline
TCFs	ternary complex factors
TE	Tris-EDTA
TEAB	triethylammonium bicarbonate
TEM	transendothelial migration
TJs	tight junctions
TNF-α	tissue necrosis factor α
UIM	ubiquitin-interacting motifs
VASP	vasodilator-stimulated phosphoprotein
VCAM1	vascular cell-adhesion molecule 1
VE-cadherin	vascular endothelial cadherin
VE-PTP	vascular endothelial protein tyrosine phosphatase
VEGF	vascular endothelial growth factor
VEGFR-2	VEGF receptor 2
WASP	Wiskott Aldrich syndrome protein
WAVE	WASP-family verprolin homology protein
WB	Western blot
ZO	zonula occludens

1   Introduction

1.1   Cardiovascular disease

Cardiovascular disease (CVD) is the number one cause of death globally (Alwan, 2011; Murray et al., 2012). A better understanding of the disease has led to improved prevention and therapy resulting in the decline of CVD. However, an estimated 17.3 million people still die from CVD every year, which is equivalent to approximately 30% of all deaths worldwide. Although many diseases affect the cardiovascular system, the greatest numbers of deaths are due to myocardial infarction (MI) and ischaemic stroke caused by atherosclerosis (Libby et al., 2013). Hypertension, high levels of low-density lipoprotein cholesterol (LDL), and low levels of high-density lipoprotein (HDL) have all been identified as risk factors associated with an increased incidence of cardiovascular disease (Ferri, 2013).

Atherosclerosis is a progressive disease characterised by the accumulation of lipids and fibrous elements in the large and medium-sized arteries resulting in blot clots (thrombosis) or severe narrowing of the vessels (stenosis) (Libby, 2012). Accelerated atherosclerosis is observed in diabetics, resulting in CVD developing on average 15 years earlier (Booth et al., 2006) and having more than a two-fold increase in the risk of dying from CVD than non-diabetics (Seshasai et al., 2011). Previously, it was believed that atherosclerosis resulted from a passive build up of cholesterol in the artery wall. However, new evidence implicates inflammation and immune effector mechanisms in the pathogenesis of this disease (reviewed in (Libby, 2012). Atherogenesis develops when oxidative, haemodynamic, and/or biochemical stimuli and inflammatory factors change the permeability of the endothelium (see section 1.2) and promote the entry and retention of monocytes and cholesterol-containing LDL particles from the blood. This triggers a cascade of inflammatory and biochemical modifications that results in endothelial and smooth-muscle cell proliferation, producing extracellular matrix molecules. A fibrous cap is formed over the developing atheromatous plaque and this leads to clinical symptoms by producing flow-limiting stenosis (causing stable angina), or the

formation of thrombi that interrupt blood flow resulting in myocardial ischaemia on either a temporary basis (causing unstable angina) or a permanent one (causing myocardial infarction or stroke). If the plaque ruptures, it exposes procoagulant material within the core of the plaque to coagulation proteins and platelets in the blood, which triggers thrombosis (Nabel and Braunwald, 2012). Identifying the key events that trigger inflammation and understanding the regulation of these signalling pathways could provide potential new preventative and treatment strategies, specifically targeting CVD. The mechanisms involved in inflammation will be discussed in section 1.2.5.

1.2   The vascular endothelium

The endothelium is a single layer of endothelial cells (ECs) that form the inner cellular lining of the entire vascular system. Blood vessels (arteries, veins and capillaries) and lymphatic vessels are lined by ECs, however for the purpose of this thesis, focus will be placed on vascular ECs. This monolayer is in direct contact with the blood and acts as a physical barrier separating blood and circulating cells from the surrounding tissue. The ECs attach to a basal lamina that provides the scaffold of all blood vessels, with the ECs lining the inside of scaffold and the outer layer covered with smooth muscle cells or pericytes, depending on the site in the vasculature. ECs can produce almost all the proteins comprising the basal lamina and enzymes involved in its remodelling (Félétou, 2011). Endothelial shape varies across the vasculature, but these cells are generally approximately 50–70 μm long, 10–30 μm wide and 0.1–10 μm thick, and slightly elongated in the direction of blood flow, due to the shear stress forces exerted by the flowing blood. ECs are highly sensitive to their surroundings, as they need to be able to respond to and resist haemodynamic forces. Perturbations of endothelial structure and function are usually early key events in developing atherosclerosis (Endemann and Schiffrin, 2004).

1.2.1 Endothelial cell function

EC structure and functional integrity are necessary to maintain the vessel wall and provide a semi-selective permeable barrier between the blood and the tissues. This versatile and multifunctional monolayer not only controls oxygen and nutrient exchange but also has many other physiological roles. ECs control blood fluidity, platelet aggregation and vascular tone, as well as regulate immune and inflammatory responses and angiogenesis (Sumpio et al., 2002). When the endothelium is at rest, under normal unstimulated conditions, blood flow is laminar and platelets and leucocytes do not adhere to ECs due to the anticoagulant and non-thrombogenic properties of the luminal surface of quiescent ECs (reviewed in (Pober and Sessa, 2007). ECs sense mechanical stimuli, such as pressure and shear stress, hormonal and chemical stimuli, such as thrombin, histamine and tissue necrosis factor α (TNF-α) (Ehringer et al., 1996; Endemann and Schiffrin, 2004; McKenzie and Ridley, 2007). These stimuli alter EC adhesion molecules, cell-cell junctions and the cytoskeleton, as well as influence the smooth muscle cells of the vessels resulting in the EC regulation of vasomotor function, inflammatory processes, and controlling haemostasis (Endemann and Schiffrin, 2004). Failure of ECs to adequately perform any of these physiological functions constitutes 'endothelial cell dysfunction'.

1.2.2 Cell-cell junctions

ECs tightly regulate the infiltration of solutes, plasma proteins and circulating cells from the blood into the vessel wall and underlying tissue (Wojciak-Stothard and Ridley, 2002). This vascular permeability is achieved by specialised transcellular systems of transport vesicles and by the regulated opening and closing of cell-cell junctions (Dejana, 2004). ECs are in constant, dynamic interaction with their neighbouring cells and are attached via transmembrane homophilic adhesion proteins localised at cell-cell junctions (Bazzoni and Dejana, 2004). The cell-cell junctions are stabilised by specific intracellular partners that anchor the transmembrane adhesion proteins to the actin cytoskeleton. These complex structures serve many purposes, and are not just necessary to maintain adhesion

between cells. Cell-cell junctions mediate intracellular signals that communicate cell position, and contact-dependent inhibition of growth, maintain cell shape and establish cell polarity. Furthermore, junction signalling is implicated in angiogenesis, shear stress responses and leucocyte extravasation and infiltration into inflamed areas (Bazzoni and Dejana, 2004). Junctional signalling can either occur directly by engaging signalling proteins or growth-factor receptors, or indirectly by binding transcription factors at the cell membrane, preventing them from translocating to the nucleus (Dejana, 2004). An example of indirect intracellular signalling regulation is the junctional protein β-catenin, which can translocate to the nucleus and act as a transcription factor. Furthermore, binding of β-catenin to the cell-cell junctions prevents it from being degraded (Sadot et al., 1998). Adhesion proteins are always in a dynamic equilibrium, even after contacts have been stably formed, and recycle continuously between plasma membrane and intracellular compartments (Bazzoni and Dejana, 2004). Usually, changes in endothelial permeability are reversible and the gaps close quite rapidly, unless episodes of chronic inflammation occur (Dejana and Orsenigo, 2013).

The endothelial adhesive complexes comprise three types of junctions: the tight junctions (TJs), adherens junctions (AJs) and gap junctions (Bazzoni and Dejana, 2004) (Figure 1.1). Moreover, adjacent quiescent ECs may overlap resulting in the formation of contact regions where AJ components arrange in a reticular distribution and are termed reticular AJs (Fernandez-Martin et al., 2012). In addition to the defined junctional complexes, other adhesion proteins contribute to cell-cell adhesion, such as platelet endothelial adhesion molecule-1 (PECAM-1), and intercellular adhesion molecule 2 (ICAM-2) (Dejana and Giampietro, 2012; Dejana et al., 2008) (Figure 1.1).
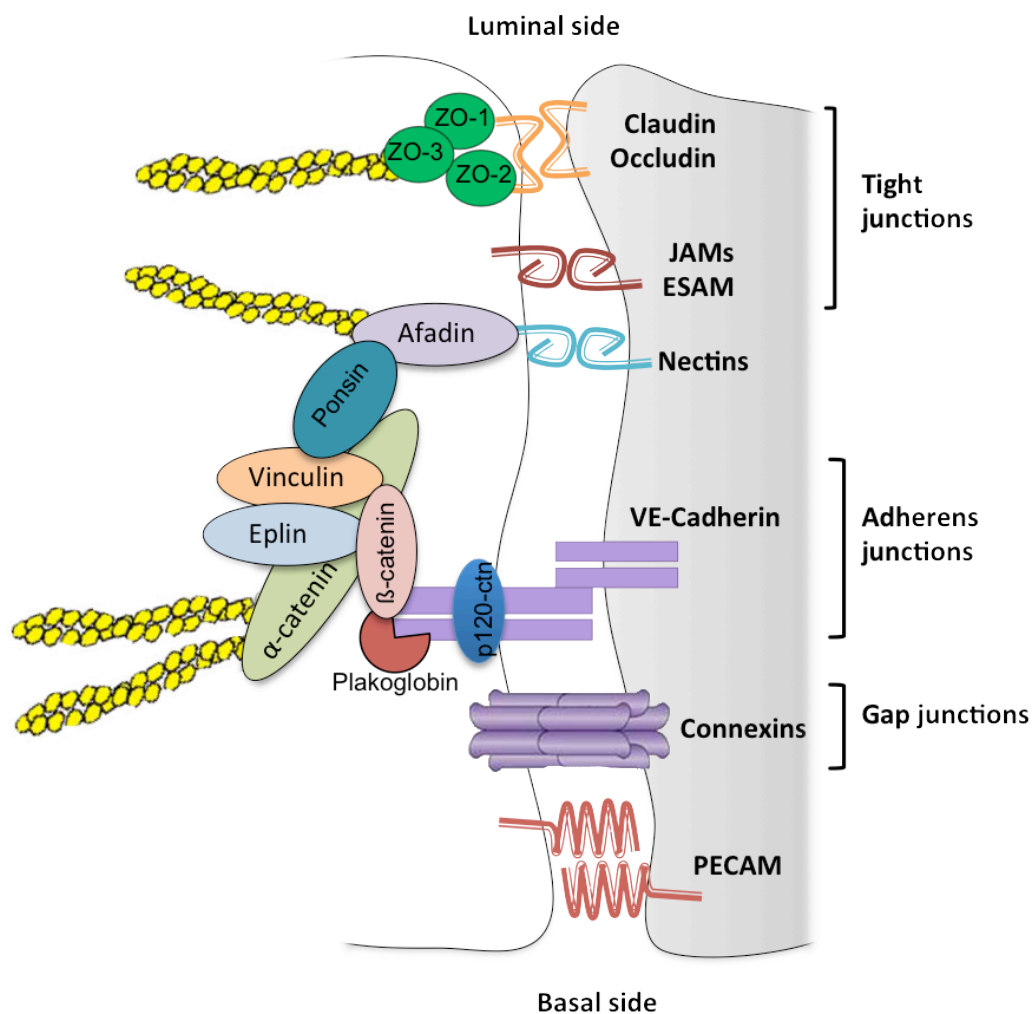
Figure 1.1 Schematic representation of junctions between endothelial cells

Junctions in endothelial cells include tight junctions, adherens junctions, gap junctions and PECAM-1 and the nectin-afadin system. TJs are comprised of claudins and occludin, as well as members of the JAM family and ESAM. The ZO family of proteins are cytoplasmic components of the TJs. The AJs consist of a transmembrane VE-cadherin that binds to p120-catenin, β-catenin and plakogloblin. The adherens junctions are connected to the actin cytoskeleton via actin-binding proteins including α-catenin, vinculin and α-actinin, among others.

AJs are formed at early stages of intercellular contact and are followed by TJ organization (Dejana et al., 2009). TJs act as a primary barrier to the diffusion of solutes through the intercellular space, they create a boundary between the apical and the basolateral plasma membrane domains, and they maintain cell polarity by recruiting various cytoskeletal as well as signalling molecules at their cytoplasmic surface (Tsukita et al., 2001). In epithelia, TJs occupy the most apical position between the neighbouring cells, sealing the cleft edges towards the luminal surface and limiting the free movement of lipids and proteins between the apical and the basolateral cell surfaces (Dejana et al., 2009; Lampugnani, 2012). However, in the endothelium, TJs are frequently intermingled with AJs throughout the cell-cell boundaries (Dejana, 2004). AJs promote TJ maturation and maintenance. In addition to controlling cell permeability, AJs are required for the correct organisation of new vessels in angiogenesis (Bazzoni and Dejana, 2004). Gap junctions serve as communication structures between adjacent cells allowing the passage of small molecular weight solutes, however they are not involved in the control of endothelial barrier function (Dejana et al., 2009).

Junctions between ECs have a variable organisation throughout the vascular tree, depending on the organ-specific requirements (Simionescu, 2000). For example, the endothelium in the brain is rich in TJs, as strict control of permeability is required for the blood-brain barrier; whereas areas that have dynamic trafficking of circulating cells and plasma proteins, such as postcapillary venules, display fewer TJ (Engelhardt, 2003; Wolburg and Lippoldt, 2002). Although endothelial junctions share several morphological and molecular similarities with junctions of other cell types, they also have important cell-specific features (Dejana and Orsenigo, 2013).

1.2.2.1   Molecular organisation of adherens junctions

Transmembrane adhesion proteins of the cadherin family form adherens junctions. Cadherins are Ca^{2+}-dependent cell adhesion molecules (CAMs) mediating homophilic adhesion and are organized in multimeric complexes at the cell borders (reviewed in (Bazzoni and Dejana, 2004). In ECs, a specific cadherin called vascular endothelial cadherin (VE-cadherin) is the key component of endothelial AJs (Dejana

et al., 1999). VE-cadherin is present in all ECs, in all types of vessels, and forms a zipper-like structure along cell-cell borders by dimerising laterally in *cis* with *trans* VE-cadherin on the adjacent cell (Bazzoni and Dejana, 2004; Dejana and Giampietro, 2012). VE-cadherin is anchored to the actin cytoskeleton by linking to a large number of intracellular proteins through its cytoplasmic tail. This interaction is vital for junctional stability and also for the dynamic opening and closing of junctions (see section 1.2.3). The carboxy-terminal region of VE-cadherin directly binds to β-catenin, plakoglobin (also known as γ-catenin) and p120-catenin (Dejana and Giampietro, 2012) (Figure 1.1).

Both β-catenin and plakoglobin bind to the actin binding protein α–catenin. The cadherin–catenin complex interacts with the actomyosin cytoskeleton, which is vital for cell adhesion stability (Pokutta and Weis, 2007; Vestweber, 2008). However, the role of α-catenin in AJs has not been fully elucidated. Although it might serve as a linker that directly connects the cadherin–β-catenin complex to filamentous actin (F-actin), the binding of α-catenin to β-catenin or F-actin is believed to be mutually exclusive (Yamada et al., 2005). Several other actin binding proteins that are located at AJs have been shown to bind to α-catenin and to localize to cell–cell contacts including: afadin (Pokutta et al., 2002), zonula occludens protein 1 (ZO-1) (Itoh et al., 1997), eplin (Abe and Takeichi, 2008), α-actinin (Nieset et al., 1997) and vinculin (Huveneers et al., 2012; Weiss et al., 1998). The roles of these proteins and the exact molecular organisation in cell–cell junctions are partially defined, but they may provide additional linkages to F-actin. Interestingly, ZO-1 is commonly considered a cytoplasmic component of TJs (see section 1.2.2.2), but is found in AJs at early stages of their organisation and only localises in TJs once when junctions are stabilized (Dejana, 2004; Itoh et al., 1997).

ECs express other cadherins such as neural (N) -cadherin, T-cadherin and P-cadherin (Dejana et al., 2008). T-cadherin and P-cadherin are non-cell type specific cadherins and are variably expressed in different types of ECs (Ivanov et al., 2001). While abundant in the endothelium, N-cadherin does not localise at the cell-cell junctions and it has been suggested that N-cadherin may be responsible for the anchorage of

the endothelium to the surrounding mesenchymal cells, such as vascular smooth muscle cells or pericytes (mesenchymal cells that associate with the walls of small blood vessels) (Navarro et al., 1998).

Recent findings have elucidated the establishment of AJs in ECs (Hoelzle and Svitkina, 2012). Migrating human umbilical vein endothelial cells (HUVECs) initiate interaction with each other by protruding lamellipodia (thin sheet-like protrusions that are filled with a branched network of F-actin with barbed ends facing the leading edge (Mattila and Lappalainen, 2008)). The subsequent retraction of the lamellipodia results in the formation of filopodium-like bridges (finger-like structures that are filled with tight parallel bundles of F-actin). These bridges are bundled by fascin, VE-cadherin accumulates at points of contact, and the recruitment of non-muscle myosin II matures these bridges into stress-fibre like structures. These bridges link adjacent cells that lead to subsequent junction expansion (Hoelzle and Svitkina, 2012). Discontinuous AJs in ECs have a similar structure where adjacent cells are linked by stress-fibres and VE-cadherin is localised in short linear structures that are orthogonal to cell-cell borders (Millan et al., 2010). In contrast, continuous AJs have a linear morphology along cell boundaries. The regulation of vascular permeability and the switch from continuous to discontinuous AJs will be discussed in section 1.2.3.

1.2.2.2   Molecular organisation of tight junctions

Tight junctions comprise three distinct types of integral membrane proteins, claudin, occludin, and an additional, structurally different protein, junction adhesion molecule (JAM) (Figure 1.1). TJs have been extensively studied in epithelial cells, however relatively little is known about cell-specific characteristics of TJs in ECs. There are over 20 members in the claudin family, however only a few are expressed in the endothelium with claudin5 expressed primarily in ECs of blood vessels (Dejana et al., 2009). Another transmembrane component of TJs is occludin. Although not necessary for TJ formation, it contributes to TJ stabilization and optimal barrier function (reviewed in (Cummins, 2012)). Claudins and occludin are

linked to a variety of intracellular signalling and structural mediators. These include actin binding ZO proteins (ZO-1, -2 and -3) and AF-6/afadin, which link TJs to the actin cytoskeleton; as well as PAR-3, cingulin and 7H6 antigen, also present in epithelial TJs (Bazzoni and Dejana, 2004) (Figure 1.1).

JAMs are localized at intercellular contacts and participate in the assembly and maintenance of junctions, signalling to cytoskeleton-associated proteins and recruiting cell-polarity proteins to the junctions via their PDZ-domain-binding motif (Weber et al., 2007). ECs express JAM-A, JAM-B and JAM-C. JAM-A co-localises with occludin, claudins, ZOs and cingulin at the level of TJs, and JAM-B and JAM-C are specifically enriched in certain vessels, such as high endothelial venules (Weber et al., 2007). The intracellular proteins of all the endothelial junctions are able to interact with each other. ZO-1 can bind to JAMs, the AJ protein α-catenin, as well as the gap junction connexion-43 (Harhaj and Antonetti, 2004). Interestingly, occludin also interacts with a gap junction protein, connexin-32, co-localizing at TJs (Kojima et al., 1999). ESAM (endothelial cell selective adhesion molecule) is an endothelial-specific transmembrane Ig protein related to JAMs that mediates homophilic binding, and its only known cytoplasmic binding partner is MAGI-I (Wallez and Huber, 2008). It is probable that the different junction systems interact and cooperate with each other to regulate barrier integrity.

1.2.2.3   **Other adhesive complexes**

In addition to AJs and TJs, ECs express other adhesive proteins that are concentrated at the intercellular cleft but are not specifically confined to AJs or TJs. Nectins participate in the initial step of junction formation and play a fundamental role in the establishment of polarity (Takai et al., 2003). They are Ca^{2+}-independent immunoglobulin-like CAMs and the nectin family comprises four members, nectin-1, nectin-2, nectin-3 and nectin-4 (reviewed in (Rikitake et al., 2012). Nectins are connected to the actin cytoskeleton through the binding of their cytoplasmic tails to the PDZ-containing protein afadin, which also binds to ponsin (Reymond et al., 2000; Takahashi et al., 1999). Ponsin binds afadin, vinculin, and α-catenin (Bazzoni

and Dejana, 2004) (Figure 1.1). Both vinculin and α-catenin are part of the AJs, and therefore provide the link between the cadherin and nectin systems (Wallez and Huber, 2008). Nectins can also interact with TJs through ZO-1, and through the interaction of afadin and JAM-A (Ebnet et al., 2000). These interactions may depend on the specific localization of these proteins and the on the cell type in relation to the junctional complex arrangement.

PECAM-1/CD31 is another endothelial adhesive protein that does not co-localise with AJs or TJs. It is a transmembrane immunoglobulin-like CAM concentrated at intercellular contacts in the endothelium (Bazzoni and Dejana, 2004). PECAM-1 is also expressed by leucocytes and platelets and is required for leucocyte transendothelial migration (TEM) (Mamdouh et al., 2003). A recent study showed that PECAM-1 coordinates with AJs to maintain endothelial barrier function (Fernandez-Martin et al., 2012).

1.2.3   Mechanisms regulating endothelial permeability

There are two main types of endothelial permeability: i) basal permeability, which occurs at the level of capillaries, the major site of exchange in the vascular bed, and ii) induced permeability that is associated with inflammation, predominantly involving post-capillary venules (Félétou, 2011). In a state of acute or chronic inflammation, ischaemia–reperfusion and atherosclerosis, mediators (such as histamine and thrombin), cytokines, growth factors (such as vascular endothelial growth factor (VEGF)) and reactive oxygen species induce EC retraction, which increases the intercellular space and subsequently the permeability to solutes and plasma proteins (Félétou, 2011). In normal conditions, endothelial cells control the passage of plasma proteins and circulating cells from blood to tissues by two different routes: the transcellular or paracellular pathways (reviewed in (Komarova and Malik, 2010)). The transcellular pathway involves the passage of plasma components through the endothelial cytoplasm by the action of vesicular transport systems, specialized pore-like structures called fenestrae, and biochemical transporters. Molecules are transported inside the vesicles either in solid phase (i.e.

bound to membrane receptors) or in fluid phase (i.e. diluted in the vesicular content) (Bazzoni and Dejana, 2001). Leucocytes can transmigrate through the endothelial barrier via both the transcellular and paracellular routes. With the assistance of intracellular vesicular structures, indentation of the apical plasma membrane of an endothelial cell would lead to fusion with the basal plasma membrane that could serve to bridge the gap between the two sides, providing a channel that allows a leucocyte to traverse through the thin cell body (Feng et al., 2002). It was observed that 7 to 11% of neutrophils, monocytes, or lymphocytes migrate via a transcellular route through the monolayer of HUVECs (Vestweber, 2012b).

The paracellular route of endothelial permeability regulation is mediated by the rearrangement of endothelial cell-cell junction complexes (Bazzoni and Dejana, 2004). Endothelial cell contacts need to be opened to allow leucocytes to pass through the junctions of the endothelial barrier (Vestweber, 2008) and ECs dynamically regulate this paracellular permeability in response to diverse stimuli, such as histamine, thrombin or VEGF (Bogatcheva and Verin, 2008).

1.2.3.1   Adherens junctions and regulation of vascular permeability

VE-cadherin plays a central role in regulating endothelial permeability. There are four interconnected biochemical routes whereby permeability-increasing agents or inflammatory stimuli lead to the loss of VE-cadherin function, and ultimately an increase of vascular permeability: (1) phosphorylation-driven VE-cadherin/catenin complex destabilization, (2) reduction of VE-cadherin cell surface levels, (3) crosstalk with tight junctions, and (4) tension and mechanical forces (Gavard, 2009). For example, VEGF induces VE-cadherin tyrosine phosphorylation and disrupts VE-cadherin/catenin binding (Esser et al., 1998). Tyrosine phosphorylation of VE-Cadherin causes subtle changes in the organisation of AJs and is associated with destabilizing junctions and impaired barrier control. Interestingly, it has recently been shown that hemodynamic forces can also result in tyrosine phosphorylation of VE-cadherin *in vivo* via Src kinase in veins, but not in arteries (Orsenigo et al., 2012).

Phosphorylation of VE-cadherin by the non-receptor tyrosine kinase Src is not sufficient to decrease endothelial barrier function (Adam et al., 2010), but it is thought to serve as a priming mechanism to sensitise veins to other permeability inducing agents such as inflammatory cytokines (Orsenigo et al., 2012). Full understanding of the direct and indirect interactions of VE-cadherin that regulate paracellular permeability are still unknown. However, it has been suggested that VE-cadherin forms different complexes in response to different needs of the vasculature, such as low or tight control of permeability, growing or resting of vessels, and in response to inflammation (Dejana and Giampietro, 2012).

The VE-cadherin–catenin complex is a central target for the opening of endothelial junctions during leucocyte extravasation. This complex is focally lost at endothelial contacts where monocytes transmigrate under flow conditions (Allport et al., 2000) and mice with strongly stabilised endothelial junctions (modified with a VE-cadherin-α-catenin fusion protein) exhibited impaired leucocyte extravasation *in vivo* under various inflammatory situations (Schulte et al., 2011).

AJs are also destabilized by the internalization of VE-cadherin. Tyrosine phosphorylation of VE-cadherin by permeability-increasing agents or inflammatory stimuli promotes the internalization of VE-cadherin through clathrin-coated vesicles (Dejana and Orsenigo, 2013; Gavard and Gutkind, 2006). However, the binding of p120-catenin to VE-cadherin maintains VE-cadherin localization at the membrane and p120-catenin selectively prevents the clathrin-dependent endocytic machinery from targeting VE-cadherin for endocytosis (Xiao et al., 2005). Internalization of VE-cadherin requires p120-catenin dissociation.

Several protein tyrosine phosphatases (PTPs) associate with and dephosphorylate VE-cadherin. Vascular endothelial protein tyrosine phosphatase (VE-PTP) is the only known endothelial specific receptor-type tyrosine phosphatase and its activity enhances VE-cadherin mediated cell–cell adhesion, decreasing endothelial barrier permeability (Nawroth et al., 2002). VEGF is able to dissociate VE-PTP from VE-cadherin, resulting in AJ destabilisation (Vestweber, 2012b). Interestingly, VE-PTP is

thought to participate in leucocyte transmigration as leucocytes also trigger the dissociation of VE-PTP from VE-cadherin (Nottebaum et al., 2008), supporting the idea that leucocytes induce changes in the phosphorylation state of VE-cadherin to enhance their transmigration (Harris and Nelson, 2010).

Not only is VE-cadherin relocated and phosphorylated upon stimulation by diverse permeability inducing agents, but it has also been shown to influence tight junctional assembly. VE-cadherin can directly enhance the expression level of claudin-5 by tethering repressive transcription factors away from the nucleus and claudin-5 promoter (Taddei et al., 2008).

The shape of the endothelial cell also determines the integrity of the endothelial barrier. The tension exerted by actomyosin contraction can disrupt AJs. This will be discussed further in section 1.4.4, when the regulators of actomyosin contractility are described.

1.2.3.2   Tight junctions and the regulation of vascular permeability

In comparison to AJs, the regulation of TJs in the endothelial barrier is not as well understood. Expression levels of occludin and its localization at TJs in the endothelium correlate with the permeability of different segments in the vascular tree. Occludin is expressed at high levels in brain endothelial cells with a continuous distribution, and at much lower levels in ECs of non-neural tissues, exhibiting a discontinuous distribution (Harhaj et al., 2006). Like VE-cadherin, endothelial specific Claudin 5 levels and cellular localization are regulated by phosphorylation (reviewed in (Gonzalez-Mariscal et al., 2008)). Protein kinase C (PKC) is an important TJ mediator. PKC activation supports assembly of growing TJs, but impairs the integrity of established TJs (Bazzoni, 2006). This suggests that phosphorylation of TJ proteins has a different effect on the endothelium depending on whether the TJ are in an assembled or disassembled state. VEGF activates PKC in primary retinal ECs, stimulating the phosphorylation of occludin resulting in an increase in endothelial permeability (Harhaj et al., 2006). It is unclear whether

occludin is a direct target of PKC activity, or if VEGF induces a cascade of occludin phosphorylation that requires more than PKC activation alone.

JAM expression is upregulated in response to inflammation and ischaemia (Weber et al., 2007). Although the role of JAMs in the mechanism of increased permeability is not yet determined, JAM-A responds to permeability-increasing cytokines by dissociating from the actin cytoskeleton and destabilising TJs (Vandenbroucke et al., 2008). Long-term stimulation of ECs with TNF-α leads to reduced localisation of occludin and JAM-A at TJs (McKenzie and Ridley, 2007). JAM-B is unregulated in chronic inflammation (Aurrand-Lions et al., 2001) and both JAM-A and JAM-C are upregulated in ECs obtained from atherosclerotic vessels (Keiper et al., 2005; Ostermann et al., 2005).

In summary, the loss of function and/or mislocalisation of most of the key components of TJs result in increased paracellular permeability.

1.2.4   **The actin cytoskeleton**

ECs require a strong and dynamic structure that is able to maintain cell-cell and cell-matrix tethering, as well as provide mechanical support to facilitate cell migration. The cytoskeleton provides these essential functions by forming an intracellular scaffold that links integral membrane proteins to the interior of the cell, and responds to environmental signals by coordinating changes in cell shape required for cell motility and membrane protrusion. The cytoskeleton is made up of three types of polymers: actin filaments, microtubules and intermediate filaments. Each component has a specific role to play in the cell; actin filaments provide mechanical structure and motility, microtubules are responsible for separating chromosomes and transport of large particles, and intermediate filaments function as intracellular ligaments and tendons to resist mechanical forces (Pollard and Cooper, 2009). Reinforcement of the cytoskeleton occurs through the interaction of these three components.

Soluble globular monomers of actin (G-actin) assemble into insoluble filamentous polymers (F-actin), depending on cellular demand. In general the amount of G-actin and F-actin is always in equilibrium in the cell (Stossel et al., 1985). The polymerisation process begins slowly, as small oligomers of actin are very unstable, but once filaments have been created, actin polymerizes rapidly (Pollard and Cooper, 2009). Actin filaments are polarised, they possess a 'fast growing' barbed end and a slow growing pointed end with all the subunits in the filament oriented in the same direction (reviewed in (Pollard and Borisy, 2003)). Adenosine triphosphate (ATP) is bound to magnesium ions in a deep cleft in actin that stabilises the molecule but is not required for polymerisation (Asakura, 1961). Once incorporated at the barbed end, ATP-actin hydrolyses its bound ATP. The ADP-actin molecules are left on the filament and eventually dissociate at the pointed end. ADP-actin monomers are subsequently reloaded with ATP and shuttle back to the barbed ends for a new round of polymerisation (Lambrechts et al., 2004). This simple steady state polymerization/depolymerisation mechanism is known as actin filament treadmilling (Dominguez, 2009). However, this simple mechanism cannot account for the vast variety of actin-dependent processes and actin networks observed in cells. Actin polymerisation in eukaryotic cells is a dynamic process that depends on interactions of actin monomers and filaments with numerous other proteins to initiate polymerization, restrict the length of actin filaments, regulate the assembly and turnover of actin filaments, and cross-link filaments into networks or bundles (Pollard and Cooper, 2009). New actin filaments are formed in three ways: i) by growing a branch on the side of an existing filament, ii) severing a filament to create two new ends, or iii) starting up a filament from monomers. Several actin-binding proteins have been identified that are responsible for modulating the organisation and function of the actin cytoskeleton (Pollard and Borisy, 2003). For example, capping proteins, like Gelsolin or Eps8, terminate active polymerisation by capping barbed ends of the actin filament. The regulation of cytoskeleton dynamics will be discussed in more detail in section 1.4.2.

Similar to the endothelial cell-cell junctions (see section 1.2.2), the organisation of actin and the signal transduction events that control it vary across the vascular tree

and contribute greatly to differences in barrier function. The actin cytoskeleton is organized principally into 3 distinct structures in ECs: i) the membrane skeleton, ii) the actin cortex and iii) actomyosin-based stress fibres (Prasain and Stevens, 2009).

1.2.4.1   The membrane skeleton

The membrane skeleton (also known as the cortical web or spectrin-based membrane skeleton) is immediately adjacent to the plasma membrane and plays an important role in determining the organisation, stability and shape of the membrane (De Matteis and Morrow, 2000). It is composed of an evolutionarily conserved rod-shaped protein called spectrin, originally identified in erythrocytes, which associates with actin filaments to form a 2D meshwork at the cytoplasmic border of the plasma membrane (Heltianu et al., 1986). Spectrins bind transmembrane adhesion proteins within the plasma membrane either directly, or through adapter proteins such as ankyrin and protein 4.1 (Pradhan et al., 2001). α-catenin tethers the membrane skeleton to the plasma membrane through AJs (see section 1.2.2.1).

1.2.4.2   The actin cortex

A dense ring of actin fibres is organised and stabilised just beneath the spectrin-based membrane skeleton and serves to support the cell periphery (Bogatcheva and Verin, 2008). The attachment of the actin cortex to the membrane and its dynamic rearrangement is modulated by the array of actin and/or membrane-binding proteins. These include endothelial junction proteins such as ZO-1 (Itoh et al., 1997), α-catenin (Muller et al., 2005) connexin-43 (Toyofuku et al., 1998) and members of the Enabled/vasodilator-stimulated phosphoprotein (Ena/VASP) protein family (Benz et al., 2008; Comerford et al., 2002). The ezrin/radixin/moesin (ERM) family are also actin-binding proteins that integrate cell surface receptors and proteins with the actin cortex (Ivetic and Ridley, 2004).

Stabilisation of the actin cortex is regulated via phosphorylation of actin-binding proteins such as filamin. Constitutively phosphorylated filamin cross-links F-actin to membrane glycoproteins, stabilising the actin cortex at the membrane (Stossel et al., 2001).

1.2.4.3   Structure and function of stress fibres

The actin cytoskeleton responds dynamically to changes in the environment. Quiescent ECs are characterised by a thick actin cortex and the absence of stress fibres, however when the cells are activated by stimuli such as thrombin, a rapid reorganization of actin structures results in a reduction of cortical actin and an increase in stress fibres (Bogatcheva and Verin, 2008). Stress fibres are thick contractile bundles of actin and myosin II filaments with alternating polarity in non-muscle cells (reviewed in (Naumanen et al., 2008; Pellegrin and Mellor, 2007; Tojkander et al., 2012). These bundles are cross-linked by α-actinin with the double-headed myosin II motor protein between consecutive α-actinin-foci, forming bipolar filaments (Langanger et al., 1986). Interestingly, stress fibres do not contract uniformly along their lengths due to the widths of myosin–α-actinin bands varying in different regions (Peterson et al., 2004). While the membrane skeleton and actin cortex are situated close to the cell membrane, stress fibres extend throughout the cell cytoplasm generating a centripetal (inward) tension that counteracts the centrifugal (outward) tension established by the cortical actin (Prasain and Stevens, 2009). This maintains straight non-adherent cell borders (Thery et al., 2006).

At least three different categories of stress fibres are present in cultured mammalian cells *in vitro*, based on their sub-cellular localization and interactions with integrin-rich focal adhesions (molecular complexes that connect the actin cytoskeleton with the extracellular matrix). These include: ventral stress fibres, dorsal stress fibres and transverse arcs (Small et al., 1998) (Figure 1.2). Stress fibre bundles on the ventral cell surface lie along the base of the cell and are typically associated with focal adhesions at both ends. Ventral stress fibres are responsible for the tail retraction by occasional contraction cycles that facilitate cell movement

(Chen, 1981), and also work against membrane tension at cell borders (Thery et al., 2006). Dorsal stress fibres are attached to a focal adhesion at their distal ends, tethering them to the base of the cell, with their other end rising towards the dorsal surface and terminating in a loose matrix of actin filaments. Dorsal stress fibres cannot contract, as they do not typically contain myosin II (Tojkander et al., 2011), and thus are not true stress fibres by definition. However they do provide a scaffold for the assembly of other types of stress fibres that tether them to focal adhesions (Hotulainen and Lappalainen, 2006). Transverse arcs are bundles of F-actin that form beneath the dorsal surface of migrating cells, just behind the protrusive lamella. These structures are typically not directly attached to focal adhesions, but they are connected to the substrate via dorsal stress fibres. In migrating cells, they sweep backwards from the leading edge towards the nucleus, where they disassemble (Heath, 1983). This process, known as retrograde flow, is driven by the continuous contraction of transverse arcs (Zhang et al., 2003).
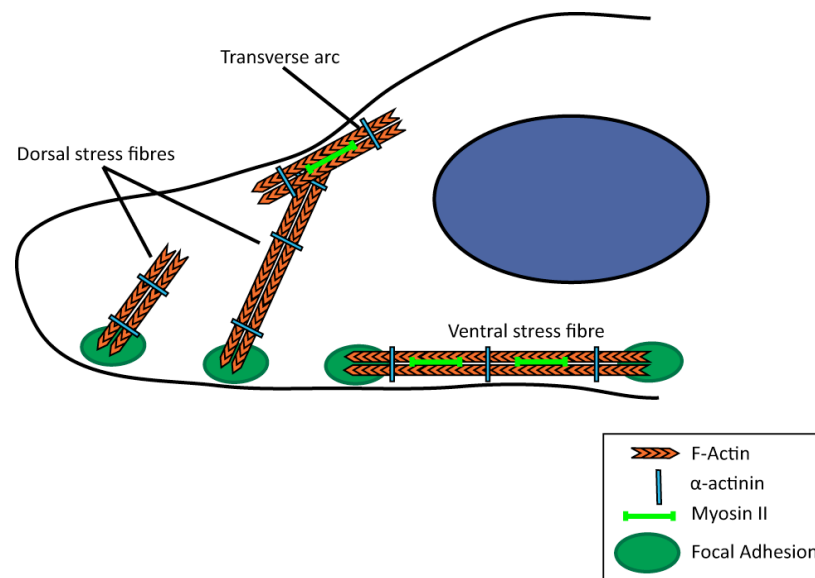
Figure 1.2 Actin stress fibres

Schematic illustration of the different stress fibre networks in migrating mammalian cells. Dorsal stress fibres arise from focal adhesions at the cell periphery and elongate up through the cell to join transverse arcs at the cell surface. Ventral stress fibres attach to focal adhesions at both ends along the base of the cell.

The activity of myosin and its interaction with actin filaments in non-muscle cells is regulated by phosphorylation of the myosin regulatory light chain (MLC). MLC-phosphorylation-mediated contractility of stress fibres is controlled by at least two distinct pathways: i) MLC kinase (MLCK) in a Ca^{2+}/calmodulin-dependent pathway, and ii) Rho kinase/ROCK in a Rho-dependent pathway (Katoh et al., 2001). This will be discussed in section 1.4.2 Rho GTPases as regulators of cytoskeleton dynamics in endothelial cells.

The function of stress fibres that is particularly relevant to this thesis is their role in the vasculature. Stress fibres are found in both motile and non-motile ECs. In non-motile cells such as confluent vascular ECs, stress fibres elongate both over and under the nucleus and orient in a specific direction in response to fluid shear stress (Wojciak-Stothard and Ridley, 2003). They are thought to be required for endothelial cells to remain flat under flow conditions, reducing shear stress and providing rigidity to the cell to resist these forces (Pellegrin and Mellor, 2007). Interestingly, there are few focal adhesions in confluent endothelial monolayers, however adherens junctional complexes can act as substitutes to anchor these cells (Millan et al., 2010).

1.2.5   Inflammation and the endothelium

Acute inflammation occurs in the endothelium in response to infectious microbes or injured tissue. The innate immune response recruits and activates neutrophils locally to eliminate the stimulus by killing microbes or removing cellular debris, and if this fails the inflammatory process will persist and evolve (Pober and Sessa, 2007). However, while serving their protective role, inflammatory responses could contribute to tissue damage. Many diseases are caused by dysregulated inflammatory responses that are initiated in the absence of a stimulus or persist even after resolution of the inciting infection or injury (Taqueti et al., 2006). During tissue damage, such as ischaemia, proinflammatory cytokines are released that lead to the induction of endothelial adhesion molecules and the presentation of chemokines and other chemotactic factors on the luminal endothelial surface

(Vestweber, 2012a). This initiates the inflammatory process by activating the leucocyte adhesion cascade, which involves rolling of the leucocyte, followed by adhesion strengthening and arrest, intraluminal crawling, paracellular and/or transcellular migration and finally results in TEM (also known as diapedesis) (reviewed in (Muller, 2011)).

The capture and rolling of leucocytes are mediated by transmembrane glycoproteins known as selectins. L-selectins are expressed on leucocytes, and E- and P-selectins are expressed on endothelial cells that interact with P-selectin glycoprotein ligand1 (PSGL1) and other glycosylated ligands. Leucocytes adhere to inflamed endothelium under conditions of blood flow because L-selectin and P-selectin actually require shear stress to strengthen the bonds and support adhesion (Ley et al., 2007). Resting ECs do not interact with leucocytes as basal production of nitric oxide (NO) sequesters E- and P-selectin, as well as other adhesion molecules such as vascular cell-adhesion molecule 1 (VCAM1) and intracellular adhesion molecule I (ICAM-1) (De Caterina et al., 1995). The expression of endothelial adhesion molecules P-selectin, E-selectin and VCAM-1 has also been implicated in atherosclerosis (Dong and Wagner, 1998). These are induced by multiple factors including oxidized LDL, inflammatory cytokines such as interleukin-1 (IL-1) or TNF-α, as well as biomechanical forces such as shear stress (reviewed in (Libby, 2012)). The rolling of leucocytes on the blood wall allows the cells to slow down and to detect chemokines on the endothelium surface. Chemokines activate leucocyte integrin receptors promoting adhesion to ICAM-1 (Yang et al., 2005) and VCAM-1, stabilising leucocyte adhesion and migration on the activated endothelial cell surface (Ley et al., 2007). As the leucocyte crawls to the EC border, ICAM-1 and VCAM-1 cluster underneath it and transmit a number of signals into the EC. These signals stimulate an increase of cytosolic free Ca^{2+} (Huang et al., 1993) which activates MLCK (Hixenbaugh et al., 1997), and results in stress fibre contraction that induces junctional disruption (see sections 1.2.4.3 and 1.4.2). Inflamed ECs can redistribute junctional molecules that favour TEM. Stimulation of ICAM-1 also leads to the phosphorylation of VE-cadherin by the kinases Src and Pyk2 (Turowski et al., 2008). Phosphorylation of VE-cadherin on the p120- and β-catenin-binding sites inhibits

their binding and destabilises the AJs (Allingham et al., 2007) (see section 1.2.3.1).

The cross-linking of VCAM-1 also leads to AJ disassembly by the activation of Rac1

(see section 1.4) as a result of an increase in reactive oxygen species in ECs (Cook-

Mills et al., 2004; van Wetering et al., 2002). PECAM-1 is an interesting cell

adhesion and signalling molecule in terms of TEM, as it is concentrated at the

borders of endothelial cells and expressed diffusely on platelets and leucocytes

(Muller, 2011). Homophilic interaction between the PECAM molecules of both cells

is required for TEM (Mamdouh et al., 2003; Muller et al., 1993). It is vital to the

regulation of inflammatory responses, and interestingly it has been shown to serve

a variety of both pro-inflammatory and anti-inflammatory functions (reviewed in

(Privratsky et al., 2010)).

1.3   Insulin

The discovery of insulin in 1921 by Frederick Banting, Charles Best, James Bertram

Collip and John James Rickard Macleod (Banting et al., 1922), is considered one of

the great biological and medical advances of the twentieth century (Cohen, 2006).

Insulin was the first protein to have its amino acid sequence determined (Sanger

and Tuppy, 1951), the first protein to be synthesized chemically (Du et al., 1961;

Katsoyannis, 1967), first to be measured by radioimmunoassay (Yalow and Berson,

1961) and first to have its three-dimensional structure solved (Blundell et al., 1971).

Insulin is a peptide hormone produced from pro-insulin in the β-cells of the

pancreas in response to high blood glucose after a meal (Steiner and Oyer, 1967).

Insulin is the primary hormone involved in controlling blood glucose levels in

humans and most vertebrates. As well as maintaining glucose homeostasis, insulin

is also responsible for promoting a number of other cellular events including

regulation of ion and amino acid transport, lipid metabolism, glycogen synthesis,

gene transcription and mRNA turnover, protein synthesis and degradation, and

DNA synthesis (Kahn and White, 1988). It regulates glucose uptake,

gluconeogenesis and glycogenesis in skeletal muscle, adipocytes, and liver by

modifying the activity of a variety of enzymes and transport processes (Chaudhuri

et al., 2012). However, as molecular pathways of insulin signalling are being elucidated, more evidence is developing on many non-metabolic actions of insulin.

1.3.1   Insulin and insulin-like growth factor-1 (IGF-I) receptors

Insulin mediates its actions at the cellular level by binding to a plasma membrane receptor. The insulin receptor (IR) and the insulin-like growth factor I receptor (IGF-IR) are homologues, sharing >50% of their amino acid sequence (Ullrich et al., 1986). Insulin-like growth factor I (IGF-I) is a member of the insulin superfamily of polypeptide hormones that all share the distinctive insulin structural motif (Shabanpoor et al., 2009). The major source of IGF-I is the liver, but synthesis has been shown to take place in numerous tissues and it is an important mediator of cell and tissue growth and differentiation, in response to pituitary growth hormone (GH), which in turn regulates the production and release of IGF-I (Daughaday and Rotwein, 1989). IR and IGF-IR are cell-surface glycoproteins, belonging to the tyrosine kinase family. They consist of an extracellular α-subunit and a transmembrane β-subunit linked by disulphide bonds to form an $\alpha_2\beta_2$-heterotetramer (Cheatham and Kahn, 1995; Kasuga et al., 1982a). The α-subunit contains the ligand-binding site and the β-subunit has the ligand-sensitive tyrosine kinase site that undergoes a conformational change leading to ATP binding and autophosphorylation upon ligand binding (Frattali et al., 1992). IR and IGF-IR have 84% homology in the β-subunit tyrosine kinase domains (Ullrich et al., 1986). Both insulin and IGF-I bind to either receptor at high concentrations but have a 100 to 1000 times higher affinity for their respective receptor (Werner et al., 2008). Hybrid insulin/IGF-I receptors have been found in tissues that co-express both receptors and are composed of half an αβ IR disulphide-linked to an αβ half of the IGF-IR (Moxham et al., 1989). Endothelial cells express insulin and IGF-I receptors as well as hybrid receptors, with HUVECs expressing more IGF-IR than IR. Low concentrations of IGF-I can activate IR and the insulin/IGF-I hybrid receptors; however insulin cannot activate IGF-IR or the hybrid receptors at normal plasma insulin levels (10^{-9} to 10^{-8} M) (Nitert et al., 2005).

1.3.2   Insulin signalling pathways in endothelial cells

The insulin receptor serves two purposes: i) to recognise insulin among all other circulating molecules in the blood by binding it with a high degree of specificity and affinity, and ii) to induce a transmembrane signal that mediates the intracellular action of insulin (Kahn and White, 1988). When insulin binds to the α-subunit of its cognate receptor, a rapid conformational change in the β-subunit results in dimerization and activation of the tyrosine kinase domain (Lee et al., 1997). This in turn, enhances the kinase activity of the receptor enabling it to phosphorylate a series of cytoplasmic substrates (Kasuga et al., 1982b). In addition to tyrosine autophosphorylation, the insulin receptor is also subject to β-subunit serine/threonine phosphorylation (Pessin and Saltiel, 2000). The three-dimensional structure of the insulin–IR complex, demonstrating how insulin engages the IR, has only recently been elucidated (Menting et al., 2013), and this interaction initiates the activation of many signal transduction networks that regulate diverse cellular functions (Nystrom and Quon, 1999). Two major pathways are known to be activated by insulin in endothelial cells: the phosphatidylinositol 3-kinase (PI3K)-Akt/protein kinase B (PKB) pathway and the Ras-mitogen-activated protein kinase (MAPK) pathway (Taniguchi et al., 2006) (Figure 1.3). The IR engages directly with intracellular signalling molecules via interactions between phosphotyrosine motifs in the receptor and downstream molecules containing src homology-2 (SH2) and phosphotyrosine-binding (PTB) domains. At least 11 intracellular substrates of the IR kinase have been identified including 6 members of the insulin receptor substrate (IRS) family (IRS-1, 2, 3, 4, 5, and 6), the Shc adaptor protein isoforms, SIRP (signal-regulatory protein) family members, Gab-1 (GRB2-associated-binding protein 1), Cbl, and APS (adaptor protein with a PH and SH2 domain) (Pessin and Saltiel, 2000).
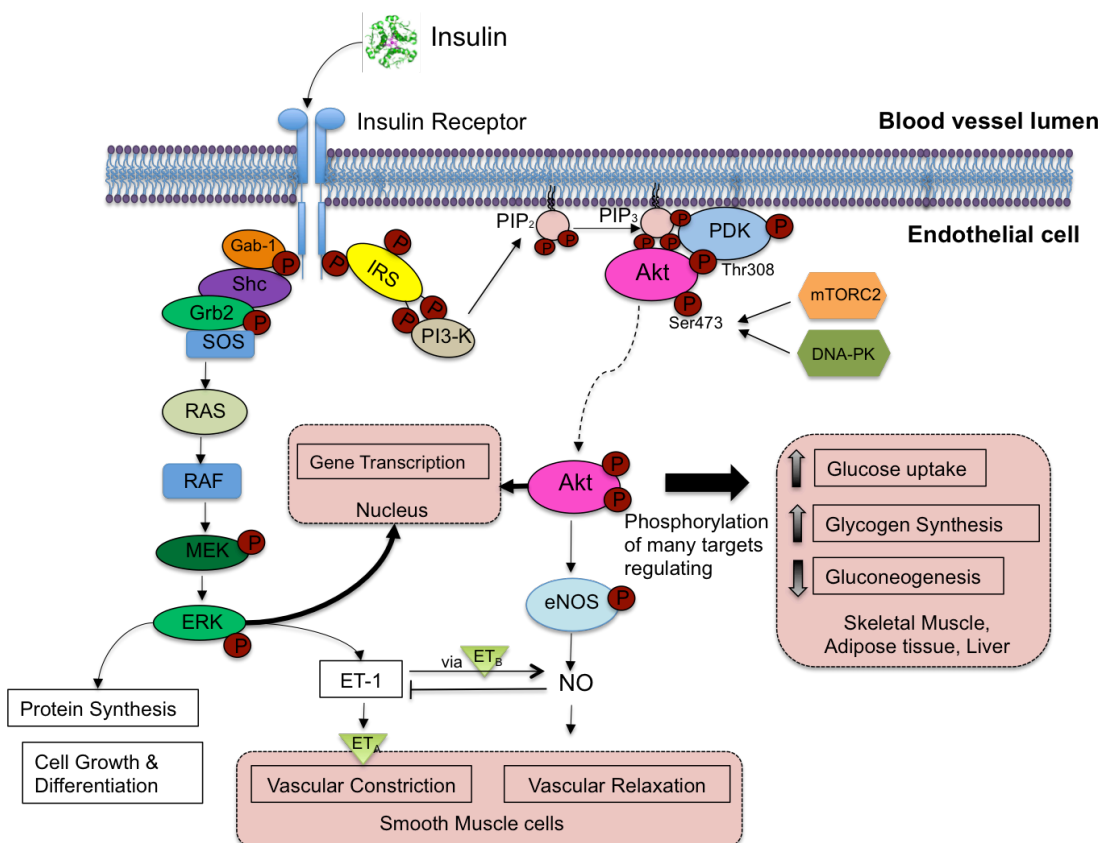
Figure 1.3 Major signalling pathways activated by insulin

Insulin binds to the insulin receptor (IR) inducing tyrosine autophosphorylation and activating two signalling pathways: Ras-mitogen activated protein kinase (MAPK), which results in cell proliferation and differentiation and vasoconstriction by endothelin-1 (ET-1) via ET_A receptors on smooth muscle cells; and phosphatidylinositol 3-kinase (PI3K)-Akt, which mediates the metabolic actions of insulin and vasodilation via nitric oxide (NO). Insulin receptor substrate (IRS) is phosphorylated by the IR, creating Src homology 2 (SH2)-domain binding motifs for the SH2 domain of the regulatory p85 subunit of PI3K. This interaction allosterically activates the PI3K p110 catalytic subunit to convert phosphatidylinositol 4,5-diphosphate (PIP_2) to phosphatidylinositol 3,4,5-trisphosphate (PIP_3). PIP_3 binds Akt and induces a conformational change that promotes Akt-Thr308 phosphorylation by constitutively active 3-phosphoinositide-dependent protein kinase 1 (PDK1). This enables Mammalian target of rapamycin complex 2 (mTORC2) or DNA-dependent protein kinase (DNA-PK) to phosphorylate Akt Ser473 and fully activate it resulting in a cascade of phosphorylation to its many substrates. Darker arrows indicate phosphorylation and regulation of target proteins. In the endothelium, Akt phosphorylates and activates endothelial nitric oxide synthase (eNOS) to produce more NO resulting in vasodilation. Shc and Grb2-associated-binding protein 1 (Gab-1) bind to the IR and recruit Son-of-sevenless (SOS) that activates Ras resulting in a serine kinase cascade activating Raf, MEK (MAPK and ERK kinase) and MAPK (also known as ERK).

**1.3.2.1 The phosphatidylinositol 3-kinase (PI3K) – Akt / protein kinase B (PKB)
         pathway**

The PI3K-Akt pathway is a highly conserved, tightly regulated multistep process (Hemmings and Restuccia, 2012). Although IR phosphorylates many proteins (Schmelzle et al., 2006), IRS-1 and IRS-2 are particularly important players in insulin signalling in endothelial cells (Hanke and Mann, 2009). The IRS proteins contain a pleckstrin-homology (PH) domain, required to anchor IRS proteins to the plasma membrane and a PTB domain, able to bind IR and IGF-IR. The C-terminal region contains more than twenty potential sites for phosphorylation by the IR. Class 1A PI3Ks are one of the best-characterised downstream effectors of IRS proteins, and are responsible for regulating growth and metabolism (Cantley, 2002). PI3Ks are heterodimers consisting of a p85 regulatory subunit and a p110 catalytic subunit, and several isoforms of each subunit exist in mammals (Engelman et al., 2006). The interaction of the SH2 domain of the p85 subunit allosterically activates the pre-associated p110 catalytic subunit to generate the lipid product phosphatidylinositol 3,4,5-trisphosphate [PI(3,4,5)P3 or PIP$_3$] from the substrate phosphatidylinositol 4,5-bisphosphate [PI(4,5)P2 or PIP$_2$] (Hemmings and Restuccia, 2012) (Figure 1.3). PIP$_3$ transmits multiple signals by binding to proteins with PIP$_3$-binding PH domains, localizing them to the same region of the plasma membrane. Several members of the AGC superfamily of serine/threonine protein kinases, guanine-nucleotide exchange proteins of the Rho family and the TEC family of tyrosine kinases are among these proteins (Saltiel and Kahn, 2001).

Akt/PKB binds to PIP$_3$ at the plasma membrane via its PH domain, which induces a conformational change in Akt, enabling co-recruited 3-phosphoinositide-dependent protein kinase 1 (PDK1) to access the activation loop and phosphorylate Akt-Thr308 (Alessi et al., 1997). Phosphorylation of Thr308 increases Akt activity by approximately 100-fold, however maximal Akt activity also requires phosphorylation of Ser473 in the hydrophobic motif (Alessi et al., 1996a). The kinase responsible for Ser473 phosphorylation has been elusive and was provisionally called PDK2. Current evidence suggests that different kinases phosphorylate Ser473 depending on the cellular conditions and could be cell

type/tissue-specific and stimulus-specific Akt. Two potential candidates for PDK2 have been reported: mammalian target of rapamycin complex 2 (mTORC2) phosphorylates Ser473 under conditions of growth and mitogen stimulation (Sarbassov et al., 2005), and DNA-dependent protein kinase (DNA-PK) is the kinase activated in stress situations, such as after DNA damage (Feng et al., 2004) (Figure 1.3). Akt is a serine/threonine kinase belonging to the AGC protein kinase family. It facilitates most of the PI3K-mediated metabolic actions of insulin as well as regulates many cellular processes including proliferation, cell survival, growth and angiogenesis. These processes are mediated through serine and/or threonine phosphorylation of a wide range of downstream substrates including other kinases, signalling proteins and transcription factors (Taniguchi et al., 2006). The Akt family has three closely related mammalian isoforms PKB-α, PKB-β and PKB-γ (referred to as Akt1, Akt2 and Akt3 respectively), which are encoded by distinct genes, and have diverse functions (Hanada et al., 2004). The activation of Akt leads to the phosphorylation of a number of targets that contain sequences with a specific recognition motif of Akt, defined as RxRxx(S/T)B (Alessi et al., 1996b), where x represents any amino acid, B represents bulky hydrophobic residues and S/T the phosphorylation site. The critical requirement for R residues at both the −5 and −3 positions on substrates efficiently phosphorylated by Akt, distinguishes the substrate specificity of Akt from that of other mitogen-stimulated AGC kinases (Manning and Cantley, 2007). Over 100 non-redundant Akt substrates have been reported (Manning and Cantley, 2007). In the endothelium, Akt directly phosphorylates and activates endothelial nitric oxide synthase (eNOS) at Ser1179, leading to an increased production of nitric oxide (NO) and subsequent vasodilation (Dimmeler et al., 1999; Zeng and Quon, 1996) (Figure 1.3). The Akt phosphorylation site on eNOS is essential for its activation, as cells expressing a mutant eNOS S1179A did not produce detectable NO in response to insulin (Montagnani et al., 2001). The consequences of insulin regulation of eNOS on cardiovascular disease are discussed in section 1.3.3.

1.3.2.2   The Ras-mitogen activated kinase (MAPK) pathway

In addition to PI3K-Akt signalling, insulin also stimulates the MAPK/ERK pathway. This pathway does not mediate the metabolic actions of insulin, but is responsible for mitogenic effects leading to differentiation and proliferation, as well as exerting feedback regulatory functions by modulating the secretion of the vasoconstrictor endothelin-1 from the endothelium (Muniyappa et al., 2007). The MAPK/ERK pathway is activated by the binding of Shc and Gab1 to the activated IR, which once phosphorylated binds the adaptor protein growth factor receptor-bound protein 2 (Grb2) (Figure 1.3). Grb2 constitutively associates with the guanyl nucleotide exchange factor Son-of-sevenless (SOS) that mediates the activation of Ras at the membrane (Skolnik et al., 1993). Ras is activated by the exchange of GDP to GTP, and subsequently operates as a molecular switch. GTP-bound active Ras initiates a kinase cascade, involving sequential activation of Raf, MEK (MAPK and ERK kinase) and ERK (extracellular signal-regulated kinase) (Taniguchi et al., 2006) (Figure 1.3).

Activated ERKs phosphorylate and regulate the activity of a number of substrates such as protein kinase p90 ribosomal S6 kinase (p90RSK), and can also translocate into the nucleus and phosphorylate transcription factors such as ternary complex factors (TCFs) and others (Pouyssegur and Lenormand, 2003). Activated ERK also induces the secretion of endothelin-1 (ET-1). ET-1 is a vasoconstrictor secreted by endothelial cells that activates PKC in vascular smooth muscle cells (Marasciulo et al., 2006).

A critical balance between the endothelium-derived relaxing and constricting factors maintains vascular homeostasis.

1.3.3   Insulin and cardiovascular disease

In addition to its metabolic actions, insulin elicits metabolism-independent, anti-inflammatory protection against atherosclerosis and injury caused by myocardial ischaemia (Yu et al., 2011). It is well recognised that diabetic patients have an increased risk of cardiovascular disease (Seshasai et al., 2011). Insulin is fundamental for normal cardiovascular function, as a loss of insulin signalling in the endothelium, as well as endothelium specific insulin resistance, leads to accelerated atherosclerosis (Gage et al., 2013; Rask-Madsen et al., 2010) and endothelial dysfunction (Muniyappa and Sowers, 2013). Insulin also inhibits the development of atherosclerosis in apolipoprotein E–knockout mice, which develop atherosclerosis spontaneously (Shamir et al., 2003). Intensive insulin therapy in critically ill patients protected the endothelium by lowering levels of ICAM-1 and E-selectin, thus reducing the activation of the endothelium, which contributed to the prevention of organ failure and death (Langouche et al., 2005). Insulin exerts significant cardiovascular protection from ischaemia and reperfusion injury. A "metabolic cocktail" comprising glucose, insulin and potassium (GIK) has been shown to reduce mortality in patients with acute myocardial infarction undergoing reperfusion (Diaz et al., 1998). Moreover, the early administration of GIK at the onset of reperfusion significantly reduced infarct size and insulin-mediated cardioprotection was shown to be independent of the presence of glucose (Jonassen et al., 2001). Several mechanisms have been proposed to explain how GIK may be cardioprotective. Insulin induces anti-inflammatory (Li et al., 2009), anti-apoptotic (Gao et al., 2002), and antioxidant effects (Suranadi et al., 2012), as well as a vasodilatory effect through the increased expression of endothelial nitric oxide synthase and subsequent release of NO (Zeng and Quon, 1996). Insulin also appears to inhibit leucocyte-endothelium adherence. GIK administration in a rabbit myocardial ischaemia-reperfusion model significantly decreased coronary endothelial expression of P-selectin and ICAM-1 via Akt-NO signalling, inhibiting polymorphonuclear leucocyte adherence to the endothelium (Li et al., 2009). Insulin-NO signalling and its importance in cardioprotection are reviewed in (Yu et al., 2011).

1.4   Rho GTPases

The Ras homologous (Rho) family guanosine triphosphate (GTP) binding proteins (Rho GTPases) are small molecular switches that regulate many signal transduction pathways in eukaryotic cells (Hall, 2012). They are principally known for their essential role in regulating actin cytoskeletal dynamics, but are also key regulators of adhesion organisation, cell polarity, cell migration, cell division and vesicle trafficking (Heasman and Ridley, 2008). These proteins are highly conserved in evolution and are present in all eukaryotic genomes sequenced thus far including animals, plants and yeast (Boureux et al., 2007). The Rho GTPases belong to the Ras GTPase superfamily and comprise 20 family members organised into 8 subfamilies: i) the RhoA, B and C subfamily, ii) the RhoD and RhoF subfamily, iii) the Rac1, 2, 3 and RhoG subfamily, iv) the Cdc42, RhoJ and RhoQ subfamily, v) the RhoV and RhoU subfamily, vi) the RhoH subfamily, vii) the RhoBTB 1 and 2 subfamily, and viii) the Rnd1, 2 and 3 subfamily (Figure 1.4). The best-characterized members of the family are RhoA, Rac and Cdc42 (reviewed in (Heasman and Ridley, 2008)).
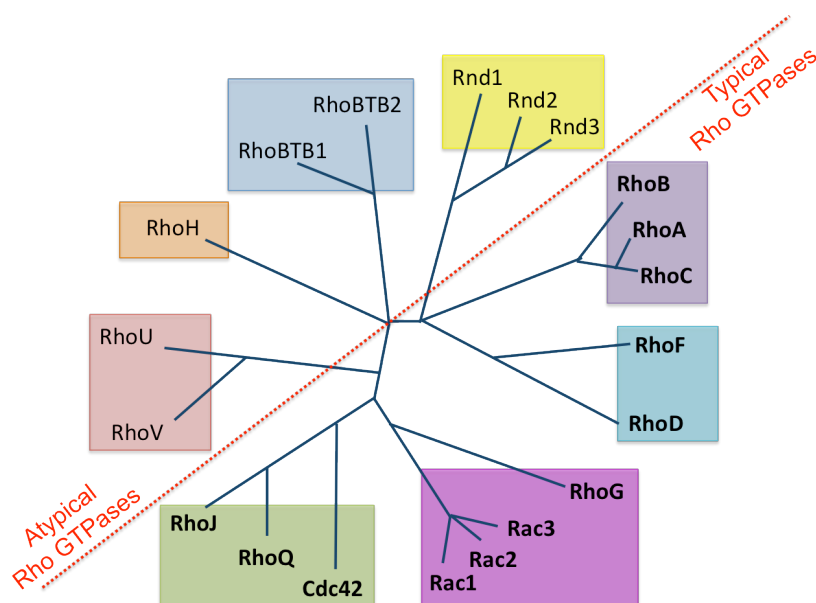
Figure 1.4 The Rho GTPase family tree
The 20 members of the Rho GTPase family are divided into 8 subfamilies, designated by the different coloured boxes. These families can be classified as typical (in bold) or atypical, depending on their type of regulation.

1.4.1   Regulation of Rho GTPase activity

For the Rho GTPases to act as molecular switches they cycle between an active GTP-bound and an inactive GDP-bound state. These transitions are tightly regulated by 3 sets of proteins: i) guanine nucleotide exchange factors (GEFs), ii) GTPase-activating proteins (GAPs), and iii) guanine nucleotide dissociation inhibitors (GDIs). The GTP-bound form activates downstream pathways by binding to effectors (Figure 1.5).

GDP is tightly bound to typical Rho GTPases and therefore require GEFs to facilitate the release of the GDP molecule. This causes the formation of an unstable nucleotide-free intermediate that is then loaded with GTP due to the higher cytosolic GTP levels present in the cell (reviewed in (Cook et al., 2013) and (Rossman et al., 2005)). The RhoGEFs are divided into two major classes. The Dbl family GEFs contain a Dbl homology (DH)–pleckstrin homology (PH; DH-PH) tandem domain and mediates the GDP–GTP exchange through the DH domain. The second class of GEFs for Rho GTPases is the DOCK family GEFs that have no DH-PH tandem domain, but contain a conserved DHR2 domain that directly interacts with Rho GTPases and mediates GDP–GTP exchange (Bos et al., 2007; Rossman et al., 2005).

Rho GTPases have low intrinsic GTPase activity, which is usually slower than the cellular functions they are required to regulate. In order to terminate the signal generated by activated Rho GTPases, GAPs are required to stimulate the intrinsic enzymatic activity leading to hydrolysis of the GTP and consequently to their functional inactivation (Tcherkezian and Lamarche-Vane, 2007). Most Rho GAPs are therefore negative modulators of Rho GTPase function.

Many Rho GTPases exert their functions at the plasma membrane. To ensure they are properly localised in the cell they are post-translationally modified at the C-terminus by the addition of a lipid group, which increases the protein hydrophobicity and facilitates membrane association. The majority of Rho GTPases have a C*AAX* tetrapeptide motif (where C represents cysteine, A is an aliphatic amino acid, and *X* is any amino acid, which determines the type of isoprenyl group)

at the C-terminus that is required for prenylation (Roberts et al., 2008). The lipid can either be a geranylgeranyl or farnesyl group. A lack of prenylation causes mislocalisation of the Rho GTPase to the cytoplasm, resulting in them being functionally inactive. GDIs sequester some GTPases in the cytosol by masking the prenyl lipid groups, preventing the association of Rho GTPases with the membranes and blocking the dissociation of GDP, thus inhibiting their interaction with downstream effectors (reviewed in (Garcia-Mata et al., 2011). Despite the wide diversity in the Rho GTPase family, only three genes encode GDIs in mammals: GDI-1 or −α, GDI-2 or β and GDI-3 or −γ. GDIs ensure a stable soluble pool of inactive Rho GTPases is available in the cytosol, acting as a reservoir that can be rapidly translocated to any membrane in the cell in response to specific signals.

In addition to prenylation, Rho proteins can be regulated by other post-translational modifications. Rho GTPases can be regulated through direct phosphorylation (Lang et al., 1996; Riento et al., 2005b) ubiquitylation (Wei et al., 2013) and palmitoylation (Navarro-Lerida et al., 2012). RhoA was the first Rho protein shown to be subject to phosphorylation. cAMP-dependent protein kinase (PKA) and cGMP-dependent protein kinase (PKG) phosphorylate RhoA at Ser188 (Lang et al., 1996; Sauzeau et al., 2000). However, this phosphorylation does not modify its GTPase activity or its interaction with GEFs and GAPs, but significantly increases its interaction with GDI independently of the nucleotide (GDP or GTP) loaded on the protein, and enhances the ability of GDI to extract RhoA from membranes (Ellerbroek et al., 2003; Forget et al., 2002). Subsequently, other members of the Rho family have been shown to be regulated by serine or tyrosine phosphorylation. Cdc42 is phosphorylated at Tyr64 by Src also resulting in its increased interaction with GDI (Tu et al., 2003). Rnd3 is phosphorylated on multiple sites by Rho-associated kinase 1 (ROCK1) (Riento et al., 2005a) and protein kinase C (PKC)α (Madigan et al., 2009), which causes the cytosolic relocation and increased stability of Rnd3. Rac1 is reported to be phosphorylated at Ser71 by Akt, which inhibits its GTP binding activity without any significant change in GTPase activity. A mutant Rac1 S71A inhibited GTP-binding and GTPase activity (Kwon et al., 2000).

GEFs, GAPs and GDIs therefore play crucial roles in regulating typical Rho GTPases. The typical members include the Rho, Rac, Cdc42, RhoF and RhoD subfamilies. However, the atypical members of the GTPase family, which include the Rnd subfamily members, RhoBTBs and RhoH, do not act as molecular switches and do not cycle between an active/inactive bound form. Instead they stay constitutively bound to GTP as a result of amino acid substitutions in key residues involved in GTP hydrolysis, and have a very low affinity for GDP (Chardin, 2003). The atypical Rho GTPases RhoU and RhoV have a high intrinsic GDP/GTP exchange rate and are therefore mainly in an active form (Shutes et al., 2004). Thus, atypical GTPases have to be regulated by alternative methods and are often positively regulated at the level of expression and negatively regulated by targeted destruction, for example by proteasomal degradation (Aspenstrom et al., 2007). Their function can also be regulated by protein-protein interactions induced by phosphorylation, such as 14-3-3 proteins (see section 1.6). For example, Rnd3 is inactivated by protein phosphorylation and 14-3-3 binding (Riou et al., 2013).
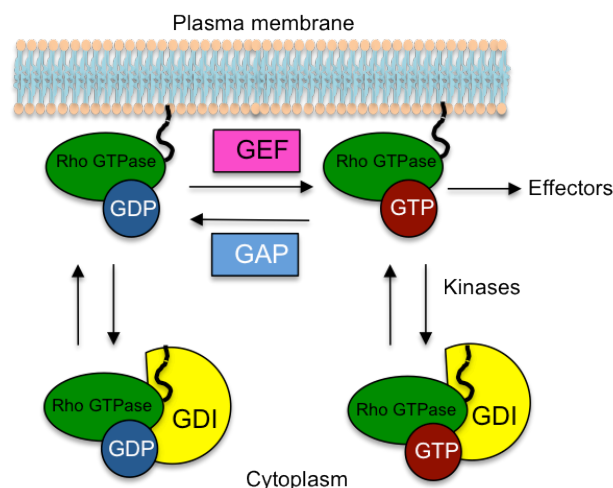
Figure 1.5 Regulation of Rho GTPase activity

Typical members of the Rho GTPase family cycle between an inactive GDP-bound form and an active GTP-bound form. GEFs facilitate the exchange of GDP for GTP promoting the active state, whereas GAPs stimulate the hydrolysis of GTP to GDP and down-regulate the Rho GTPase activity. GDIs sequester several Rho proteins in the cytoplasm, preventing their association with membranes where they mediate their actions. Protein phosphorylation by various kinases, such as the AGC kinases and ROCK1, can also regulate Rho GTPase activity.

1.4.2   Rho GTPases as regulators of cytoskeleton dynamics in endothelial cells

Cells remodel their cytoskeletons by responding to diverse stimuli from the external environment. As key regulators of cytoskeletal dynamics the GTP-bound active Rho GTPases perform their regulatory function by integrating information from a broad spectrum of upstream signals, such as growth factors, chemokines and cell adhesion receptors and interacting with an array of down-stream target (effector) proteins. These effector proteins include serine/threonine kinases, tyrosine kinases, lipid kinases, lipases, oxidases and scaffold proteins (Jaffe and Hall, 2005).

As discussed in section 1.2.4.3, stress fibre contractility is regulated by phosphorylation of the regulatory subunit of the myosin II, MLC. Reversible phosphorylation of MLC stimulates the ATPase activity of myosin II resulting in the assembly of actomyosin filaments (Vicente-Manzanares et al., 2009). The activation of Rho proteins contribute to the formation of contractile actomyosin filaments (see section 1.2.4), and RhoA in particular induces stress-fibre and focal adhesion formation (Ridley and Hall, 1992). RhoA is able to phosphorylate MLC through its downstream effectors ROCK1 and ROCK2 (Naumanen et al., 2008). ROCKs phosphorylate MLC (Amano et al., 1996) and also indirectly increase the pool of phosphorylated MLC (p-MLC) by inactivating the enzyme that dephosphorylates MLC, myosin light chain phosphatase (MLCP) (Kimura et al., 1996). ROCKs play an important role in stress fibre turnover, as they activate the LIM kinase pathway. LIM kinase (LIMK) regulates actin dynamics and increases the stability of stress fibres by inactivating actin-dissociating protein (ADF)/cofilin (Ohashi et al., 2000). Cofilins catalyse depolymerisation of actin filaments by promoting actin monomer dissociation from the pointed end, increasing the rate of actin turnover by providing new actin monomers for polymerization (Carlier et al., 1997). Cofilin can also sever actin filaments, increasing the number of uncapped barbed ends that serve as sites for actin polymerization and filament elongation (Ghosh et al., 2004) (see section 1.2.4).

RhoA can also stimulate actin polymerization in mammalian cells through its effector the diaphanous-related formin 1(DRF1)/ mammalian diaphanous 1 (mDia1) (Watanabe et al., 1997). mDia1 facilitates the polymerization of long parallel actin filaments and is important for the formation of dorsal stress fibres (Hotulainen and Lappalainen, 2006). Furthermore, RhoA can control the composition of the actin cytoskeleton by regulating the transcription of several genes that encode cytoskeletal proteins, through the myocardin-related transcription factor MAL (also known as MRTF-A) and serum response factor (SRF) pathway (Hill et al., 1995; Miralles et al., 2003). Rho activation induces a reduction in cytoplasmic G-actin triggering the dissociation of G-actin from MAL, resulting in the translocation of MAL into the nucleus where it acts as a co-activator of SRF (Miralles et al., 2003).

Rac and Cdc42 are primarily known for their essential roles in cell migration as they regulate actin-rich protrusive lamellipodia and filopodia, respectively (Nobes and Hall, 1995; Ridley et al., 1992). This is described in section 1.4.3. They stimulate actin polymerisation via the actin-related protein 2/3 (Arp2/3) complex. The heptameric Arp2/3 complex nucleates new actin filaments by branching off pre-existing filaments, when activated by nucleation promoting factors (NPFs) (reviewed in (Rotty et al., 2013)). Cdc42 directly binds and activates the NPFs Wiskott–Aldrich syndrome protein (WASP) and neuronal WASP (N-WASP). Rac activates the Arp2/3 complex via WASP family verprolin-homologous protein (WAVE, also known as SCAR). Cdc42 and Rac are also involved in stabilizing actin filaments as they can also activate LIMK via the p21 activated kinase (PAK) family, which phosphorylates and inhibits cofilin (Jaffe and Hall, 2005).

1.4.3   **Rho GTPases as regulators of cell migration in endothelial cells**

An important feature of many cells is their ability to migrate in response to particular chemical or mechanical stimuli. Many physiological processes require cells to be motile, including angiogenesis, tissue repair and immune surveillance, however cell migration also contributes to pathological conditions such as cancer metastasis, chronic inflammation and vascular disease (Ridley et al., 2003). Cell

migration involves many coordinated signalling events that regulate changes to the cytoskeleton and cell adhesion. It requires the cell to polarise in response to extracellular stimuli, extend lamellipodia or blebs at the leading edge, followed by the formation and turnover of new cell-substrate adhesions, and finally contraction of the cell body and tail detachment (reviewed in (Ridley, 2011)). Endothelial cells can directionally migrate toward a gradient of soluble chemoattractants (chemotaxis), immobilized ligands (haptotaxis), or by mechanical forces (mechanotaxis) (Lamalice et al., 2007). The specific mechanisms involved in endothelial cell migration will be discussed in the context of angiogenesis in section 1.5.

The presence of Rho GTPases and their effector proteins at specific loci on the membrane dictates the directionality of cell migration. The major driving force for migration to occur requires actin polymerisation and filament elongation at the front, and actomyosin contraction at the back. The establishment of this cell polarity is tightly regulated, mediated by several positive feedback loops involving Rho GTPases, PI3Ks, integrins, microtubules, and vesicular transport (Ridley et al., 2003). Cdc42 is active at the front of migrating cells and is a key regulator of directional sensing and migration. Cdc42 induces filopodia by activating actin polymerization via three of its targets: i) WASP/N-WASP, which activates the Arp2/3 complex previously discussed; ii) formins, such as mDia2 (Firat-Karalar and Welch, 2011) and iii) insulin-receptor substrate p53 (IRSp53), a membrane deforming and curvature sensing protein (Ridley, 2011). Filopodia act as sensors that navigate cell migration, however the exact molecular mechanisms, by which filopodia are initiated and spatially restricted to specific sites on the plasma membrane, are still unknown (Disanza et al., 2013). Cdc42 is also able to control cell directionality by restricting where lamellipodia form through regulating spatial Rac activation and consequently actin polymerization (Cau and Hall, 2005).

Polarity proteins react to extrinsic or intrinsic polarity cues such as extracellular matrix ligands, growth factor or chemoattractant gradients and assemble into multiprotein complexes, inducing downstream signalling that triggers the

establishment of cellular asymmetry. Cdc42 acts through a polarity protein, partitioning-defective-6 (PAR6), and forms a polarity complex with PAR3 and atypical protein kinase C (aPKC) (Joberty et al., 2000; Lin et al., 2000). For example, active Cdc42 at the leading edge binds PAR6, which stimulates PAR3 in the complex to bind Tiam1, a GEF for Rac, resulting in Rac activation (Nishimura et al., 2005). In endothelial cells, Rho, Rac, and Cdc42 differentially facilitate cell migration depending on the stimulus. ECs polarise in response to shear stress whereby RhoA is initially activated, inducing stress-fibres that cause cell contraction, followed by Rac1 and Cdc42 activation resulting in cells respreading and elongation in the direction of flow. Interestingly, unlike other cell types, endothelial cells do not require Cdc42 to polarise, as Rho and Rac maintain polarized migration in the direction of shear stress (Wojciak-Stothard and Ridley, 2003).

Polarised migrating cells have a stable fan-shaped front called the lamella, from which the highly dynamic lamellipodia protrude, composed of orthogonal arrays of actin filaments with branched actin filaments near the leading edge plasma membrane (Suraneni et al., 2012). The primary mediator of actin polymerization in lamellipodia is Rac activation of the Arp2/3 complex via the WAVE complex, as previously discussed. Other potential actin filament nucleators have also been shown to contribute to lamellipodium extension, such as the members of the formin (Firat-Karalar and Welch, 2011) and Spire families (Ito et al., 2011). The exact molecular mechanisms are still not fully understood, however evidence suggests that the Arp2/3 complex and/or Spires initiate nucleation in lamellipodia, whereas formins promote elongation (Ridley, 2011).

1.4.4   **Rho GTPases as regulators of endothelial cell-cell junctions**

Direct association of the actin cytoskeleton with cell adhesion proteins is essential for barrier function. The molecular mechanisms involved are not fully understood, as the endothelial barrier is rapidly regulated *in vivo*. Thus, *in vitro* models are required to elucidate these dynamic changes. Pro-inflammatory stimuli, such as TNF-α, induce changes in cell-cell junctions, actin stress fibre organisation and an

increase in permeability *in vitro* (McKenzie and Ridley, 2007). As key regulators of the actin cytoskeleton, small Rho GTPases regulate the stability of endothelial intercellular junctions (reviewed in (Wojciak-Stothard and Ridley, 2002)). In addition to the mechanisms that regulate endothelial barrier function discussed in section 1.2.3, increased centripetal tension as a result of actomyosin-induced contractility can open intercellular gaps (Dejana and Orsenigo, 2013). Rho-induced phosphorylation of MLC via ROCK results in the formation of stress fibres (see section 1.2.4.3) that have been shown to be associated with AJs (Millan et al., 2010). Depending on the strength of cell-cell junctions, this actomyosin contractility results in reduced endothelial barrier function. ROCK also phosphorylates occludin, which promotes the disassembly of TJs (Hirase et al., 2001). Therefore, Rho plays a dual role in regulating endothelial permeability through stress fibre formation and destabilizing intercellular junctions (Beckers et al., 2010). However, RhoA is not just responsible for junctional destabilisation as a certain amount of contraction is necessary for tension and remodelling of circumferential actin filaments (Gomez et al., 2011), thus a very fine balance of RhoA is required.

Rac1 and Cdc42 are only activated after RhoA activity subsides (Wildenberg et al., 2006), and function to re-establish cell-cell contact by inducing lamellipodia or filopodia. Rac is activated in response to cadherin contact assembly (Kovacs et al., 2002), whereas Rho is inhibited through a process that involves p190RhoGAP (Noren et al., 2003). Interestingly, Rac1 appears to have a dual role on endothelial intercellular junction maintenance and stabilization, depending on signalling conditions. Rac activity is associated with endothelial junction strengthening, as dominant negative Rac (Wojciak-Stothard et al., 2001) and Rac inhibition (Waschke et al., 2004) increased endothelial permeability, in the absence of vasoactive stimuli. Rac1 and Cdc42 are able to stabilise endothelial cell-cell junctions by regulating the interactions between α-catenin and cadherins, by two different mechanisms. Rac1 and Cdc42 bind to and negatively regulate IQGAP1, which directly interacts with β-catenin and dissociates α-catenin from the cadherin-catenin complex resulting in junctional destabilization (Fukata et al., 1999). They have also been reported to inhibit cadherin endocytosis through the interaction

with IQGAP and actin cytoskeleton reorganization (Izumi et al., 2004). Conversely, Rac1 can weaken junctions by inducing VE-cadherin internalisation after VEGF stimulation, via phosphorylation by the Rac1 downstream target PAK (Gavard and Gutkind, 2006). PAK has also been shown to enhance MLC phosphorylation and increase actomyosin contractility (Stockton et al., 2004). Rac1 activation could possibly destabilise barrier function through the generation of reaction oxygen species (ROS) (van Wetering et al., 2002). Although the same GTPase can participate in junction assembly and destabilisation, the regulators, effectors and cellular processes involved might differ in each case.

1.4.5   Rho GTPases in cardiovascular disease

Statins (3-hydroxy-3-methylglutaryl-coenzyme A reductase inhibitors) are one of the most widely used therapies to prevent and regulate the risk factors of cardiovascular disease (Taylor et al., 2013). However, their anti-atherosclerotic effects may not only be as a result of their lipid-lowering properties, but possibly through other pleiotropic consequences mediated by the inhibition of Rho GTPases (Tanaka et al., 2013). Statins block the synthesis of important isoprenoid intermediates in the cholesterol biosynthetic pathway, required for the post-translational lipid modification of Rho GTPases (see section 1.4.1) (Takemoto and Liao, 2001). Consequently, statins inhibit Ras and Rho isoprenylation, leading to the accumulation of Ras and Rho in the cytoplasm and preventing their signalling. RhoA is particularly important in the pathophysiology of cardiovascular disease, as it has been shown to negatively regulate eNOS expression, a hallmark of endothelial dysfunction (Laufs and Liao, 1998). Moreover, the *RhoA* gene was implicated in contributing to the variation observed in LDL-cholesterol response to statins (Medina et al., 2012). These findings have initiated a new era of drug development, using selective small GTPase inhibitors as potential anti-atherosclerotic and cardioprotective therapies. One of the most extensively studied therapeutic targets in cardiovascular disease is ROCK, the major downstream effector of RhoA (reviewed in (Shi and Wei, 2013; Surma et al., 2011). ROCK inhibitors have been

shown to reduce endothelial dysfunction, inflammatory cell recruitment, hypercontraction of vascular smooth muscle cells, as well as vascular and cardiac remodelling, however the mechanisms involved are yet to be fully elucidated (Noma et al., 2012).

1.5 Angiogenesis

Angiogenesis is the development of new blood vessels from pre-existing structures and is essential in physiological and pathological conditions, including embryonic development, wound healing, tissue regeneration and tumour growth (Lamalice et al., 2007). Angiogenesis involves endothelial cell activation, degradation of the basement membrane, invasion, proliferation, lumen formation and stabilization and is regulated by a balance of pro- and anti-angiogenic molecules (Bayless and Johnson, 2011). The various steps of angiogenesis are coordinated by several key factors, such as growth factors, bioactive lipids, integrins, junctional proteins and transmembrane proteinases to ultimately transduce intracellular signals to the cytoskeleton (Bayless and Johnson, 2011). The scientific literature on angiogenesis is vast, and therefore this section will focus on the links between angiogenesis, endothelial cell-cell junctions and the cytoskeleton, relevant for this thesis.

When the usually quiescent endothelium receives an angiogenic stimulus, such as VEGF induced by wounding and ischaemia, the vascular basement membrane is degraded by matrix metalloproteinases (MMPs) (Carmeliet and Jain, 2011). This relieves pericyte-endothelial contacts and releases extracellular matrix (ECM)-sequestered growth factors (Senger and Davis, 2011). In addition, VEGF destabilises junctions by promoting VE-cadherin internalisation (Gavard and Gutkind, 2006) (as described above in section 1.4.4). Integrin signals, as well as chemoattractants, initiate the next stage of angiogenesis, which is known as sprouting. One endothelial cell, known as the tip cell, becomes selected to lead and guide the emerging vessel sprout towards the angiogenic signal, whilst the neighbouring cells, called stalk cells, proliferate and elongate to form the lumen of the new vessel. This differentiation is determined by the Notch signalling pathway, a key regulator of

cell fate, differentiation and patterning processes in a large variety of tissues and organisms (reviewed in (Thomas et al., 2013).

VEGF exerts its effects by binding to its tyrosine kinase receptors, and VEGF regulated endothelial migration mainly occurs through signalling induced by VEGF receptor 2 (VEGFR-2) (Lamalice et al., 2007). VEGF activates N-WASP, promoting actin nucleation, and also leads to the rapid phosphorylation and inactivation of the actin depolymerisation factor cofilin, via its upstream regulator LIM-kinase (Gong et al., 2004). Therefore, VEGF stimulates the formation of filopodia and lamellipodia via Cdc42 and Rac1 at the leading edge of the tip cell, which then migrates by the general mechanisms described in section 1.4.3. Interestingly, endothelial cells migrate in a coordinated group where the polarized rear of the migrating tip cell is associated with an endothelial stalk cell via VE-cadherin adhesion, causing a 'stretch' response that induces proliferation via Rac1 activation (Liu et al., 2007).

After the initial sprouting phase, endothelial cells undergo complex morphogenesis to assemble as coalesced lumen-bearing cords with a branching structure (reviewed in (Iruela-Arispe and Davis, 2009)). The leading tip cells do not form lumens, however the trailing stalk cells rapidly lumenize by two possible mechanisms. Cord hollowing forms a lumen by altering cell shape and cell-cell junctions of endothelial trunk cells, flattening along the wall of matrix space created by the leading cell. The second method, known as cell hollowing or intracellular vacuolation, forms endothelial luminal structures by coalescing and fusing individual vacuoles with those in neighbouring cells (Davis et al., 2000). Tip cells eventually anastomose with other tip cells from neighbouring sprouts to build new blood vessel circuits. In addition to their roles in sprouting, Rac1 and Cdc42 are essential for regulating these morphological changes, mediated by their various downstream effectors, including Pak2, Pak4, Par3 and Par6. *In vitro* depletion of Rac1 and Cdc42, or their effectors, impairs endothelial cell tube and lumen formation (Bayless and Davis, 2002; Koh et al., 2008).

VE-cadherin is not only fundamental for maintaining quiescent endothelium barrier integrity, but also plays an important role in angiogenesis signalling. Although a loss of VE-cadherin does not prevent vessel development, defects in vascular remodelling and integrity are observed. VE-cadherin is reduced between cells during sprouting by endocytosis as a result of VEGF stimulation, allowing the cells to move more freely (Carmeliet and Jain, 2011). However, VE-cadherin is required for the cessation of sprouting. Localisation of VE-cadherin at the tip cell filopodium allows for the establishment of new contacts with other tip cells and this engagement of junctions leads to increased actomyosin contractility via ROCK, antagonizing VEGF signalling and terminating sprouting (Abraham et al., 2009). The establishment of a functional vasculature then occurs by subsequent pruning and remodelling of the branches, while the endothelial cells become quiescent and cell-cell junctions strengthen, reducing VEGF signalling.

1.6   14-3-3 Proteins

The 14-3-3 protein family are a group of highly conserved 28-33 kDa acidic proteins found in all eukaryotes from fungi to animals and plants. Their unique name was derived from their initial discovery, when they were eluted in the fourteenth DEAE-cellulose chromatography fraction and migrated as spot cluster 3.3 by two-dimensional starch gel electrophoresis during fractionation of extracts of bovine brain (Moore and Perez, 1967). There are seven 14-3-3 isoforms found in mammals (14-3-3 β, ε, η, γ, τ, ζ and σ) that are expressed from different genes, and vary in expression between cell types and tissues (Kleppe et al., 2011). However, the functional distinctions among isoforms is not fully understood. In *Arabidopsis*, 15 isoforms have been identified, whereas only two 14-3-3 proteins are found in the yeast *Saccharomyces cerevisiae*, named BMH1 (brain neuromodulin homologue 1) and BMH2. 14-3-3 proteins exhibit a remarkable degree of amino acid sequence conservation both within and across species (Wang and Shakes, 1996). This high degree of conservation and ubiquity reflects their fundamental importance in many biological processes.

1.6.1   **Structure of 14-3-3 dimers**

Crystal structural studies show that 14-3-3 proteins are highly helical proteins that are able to self assemble into homo- and hetero-dimers (Aitken, 2006). Each L-shaped monomer consists of a bundle of nine antiparallel α-helices (H1-H9) that interact at the N-termini, forming a cup-shape with a central groove approximately 35 Å broad, 35 Å wide and 20 Å deep (Obsil and Obsilova, 2011) (Figure 1.6). Certain family members prefer to homodimerise, such as γ and σ, whereas other members such as ε have a higher affinity for subunits other than itself and hence preferentially heterodimerise (Morrison, 2009). Homodimers have one salt bridge at the interface, while heterodimers are stabilized by up to three (Yang et al., 2006).

The conserved sequences between the different isoforms of the 14-3-3 family are mainly found in the concave surface that contains an amphipathic ligand-binding groove, while variable residues are more likely to be found at the outer convex surface, particularly in the N- and C-termini. The ligand-binding groove is formed by α-helices H3, H5, H7 and H9 and each subunit of the dimer is able to bind one discrete phosphoserine or phosphothreonine containing ligand independently at a distance of 34 Å between (Figure 1.6). These binding sites are either in the same protein or in two independent proteins that are linked by their interaction with 14-3-3 (Xiao et al., 1995). The structure of the 14-3-3 dimer is relatively rigid and little structural change is observed upon binding to its ligands. This rigidity facilitates one of the roles of 14-3-3 proteins to induce conformational changes to their bound target proteins (Obsil and Obsilova, 2011) (see section 1.6.3).
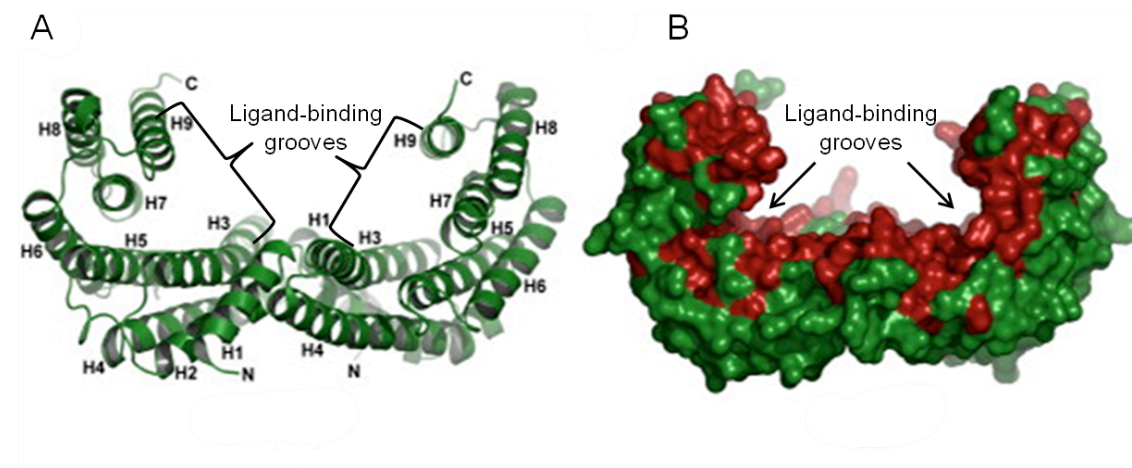
Figure 1.6 The crystal structure of dimeric 14-3-3 proteins
The ribbon representation (A) and the surface representation (B) of human 14-3-3ζ. Dimers are formed by 9 helices (H1-H9) and each L-shaped monomer contains a conserved ligand-binding groove formed by α-helices H3, H5, H7 and H9. Residues depicted in red are conserved among all seven human isoforms. Image adapted from (Obsil and Obsilova, 2011).

1.6.2   14-3-3 interactions with phosphopeptides

14-3-3 dimers interact with a diverse array of cellular proteins, including transcription factors, biosynthetic enzymes, cytoskeletal proteins, signalling molecules, apoptosis factors, tumour suppressors and small GTPases (Morrison, 2009). These interactions are primarily regulated by phosphorylation of the target proteins (Muslin et al., 1996). Oriented peptide library screening identified two canonical motifs found to bind optimally to 14-3-3s, namely RSX(pS/T)XP (mode I) and RXXX(pS/T)XP (mode II) where pS/T represents the phosphoserine or phosphothreonine, and X can be any amino acid (Yaffe et al., 1997). Further analysis of over 200 phosphorylated 14-3-3-binding sites in the literature identified that the proline (P) located at position +2 of the phosphorylation site only occurs in approximately 50% of 14-3-3 binding motifs (Johnson et al., 2010). Interestingly, many target proteins do not contain sequences that conform precisely to these motifs. Binding partners that contain more than one 14-3-3 binding site have a 30-fold higher affinity for the 14-3-3 dimer than a peptide containing a single phosphorylated motif (Yaffe et al., 1997). This means that two imperfect sites could

be sufficient to allow 14-3-3-binding, if they are in antiparallel orientation and able to achieve the correct spacing (Bridges and Moorhead, 2005). In addition to the two canonical binding motifs, 14-3-3 proteins can bind to the C-terminus of several proteins, and the motif R-X-X-pS/pT-X-COOH has been defined as a mode III binding site (Coblitz et al., 2005). The importance of 14-3-3 binding to the C-terminus was recently demonstrated in the Rnd family of Rho GTPases. 14-3-3 simultaneously engages the C-terminal farnesyl group and the adjacent phosphorylated serine residues of Rnd3, inhibiting its translocation from the plasma membrane to the cytosol, which provides a novel mechanism of regulation for this atypical Rho GTPase (Riou et al., 2013).

1.6.3   Functional effects of 14-3-3 binding to target proteins

14-3-3 proteins have no intrinsic enzymatic activity of their own, however they are involved in many cellular processes through their interaction with their many binding proteins. There are three proposed mechanisms to describe how 14-3-3 proteins modify the properties and function of their binding partners. These modes of action are: (i) direct conformational changes of the target protein, (ii) physical occlusion of sequence-specific or structural features, and (iii) scaffolding (Bridges and Moorhead, 2005; Mackintosh, 2004).

Due to their rigid α-helical structure, 14-3-3 proteins can act as a stable support on which target proteins can be reshaped. Many 14-3-3 ligands have two or more 14-3-3-binding motifs that simultaneously engage both subunits in the 14-3-3 dimer. It has been proposed that one site on the target protein acts as a dominant site and once phosphorylated and binding to one monomer occurs, subsequent binding of a weaker secondary site in the ligand protein to the other 14-3-3 monomer follows due to its proximity and conformational changes (Yaffe, 2002). The ability of 14-3-3 proteins to act as conformational clamps can also result in substantial rearrangement of an active site in target enzymes. In addition to inducing these conformational changes, 14-3-3s provide the structural support needed to stabilise

enzyme targets in a specific conformation, thus directly increasing or decreasing their catalytic activity (Mackintosh, 2004).

Binding to 14-3-3 proteins can change the subcellular localisation of a protein, but does not target proteins to one specific location. The effect of 14-3-3 binding on the subcellular localisation of a partner protein depends solely on information encoded within the partner protein and the proximity of that information to a 14-3-3 binding motif. In several cases, if a binding partner contains a nuclear localisation sequence (NLS) or a nuclear export sequence (NES) within close proximity of a 14-3-3–binding site, then the 14-3-3 dimer can interfere with their function by masking or obscuring these sites. This could alter the kinetics of nuclear-cytoplasmic shuttling, and result in a change or protein localisation (Muslin and Xing, 2000). For example, the junctional protein and transcription factor β-catenin is exported out of the nucleus upon binding to 14-3-3 with its antagonist Chibby, thereby suppressing β-catenin signalling activity (Takemaru et al., 2009). Cytoplasmic-endoplasmic reticulum (ER) localisation can also be regulated by 14-3-3 binding. Proteins synthesized in the ER are retained there by a dibasic ER retention motif that could be obscured upon 14-3-3 binding (Bridges and Moorhead, 2005). Binding to 14-3-3 dimers can mask protein-protein sites, protein-DNA sites as well as protect target proteins against dephosphorylation and proteolytic degradation (Obsil and Obsilova, 2011).

The dimeric nature of 14-3-3 proteins with two adjacent phospho-peptide binding sites provides a phosphorylation-dependent scaffold to anchor proteins within close proximity of one another and function as an adaptor (Obsil and Obsilova, 2011). This allows for two phosphorylated residues to dock into the dimer, which may be phosphorylated by different kinases. The 14-3-3 dimer can therefore act as a logic gate that integrates two inputs to generate an action (Johnson et al., 2010).

1.7   Aims of the study

The aim of this research was to identify protein phosphorylation changes in response to insulin treatment of endothelial cells and determine the roles of these changes in regulating endothelial functions. The hypothesis of the study is that insulin protects endothelial cells from damage by phosphorylating proteins that may be involved in stabilising endothelial cell-cell junctions.

The study was divided into three main objectives:

1. The first aim was to establish the cellular model for the study by investigating the effects of insulin on human umbilical vein endothelial cell (HUVEC) barrier function, endothelial migration and angiogenesis.

2. The second objective of the project was to identify new targets, whose phosphorylation and binding to 14-3-3 proteins is stimulated by insulin in endothelial cells. Proteins of interest were validated and selected based on predicted roles in endothelial function specifically in Rho GTPase and PI3K signalling pathways.

3. The third aim of the study was to investigate how these proteins contribute to endothelial functions. The objective was approached by over-expression and protein silencing analysis to identify their roles in ECs.

2   Materials and Methods

Chemicals and salts for solutions were purchased from Sigma-Aldrich, unless otherwise stated.

2.1   Materials

2.1.1   Reagents and Kits

Table 2.1 Reagents and Kits

Reagents/Kits	Source
Amaxa^{TM} HUVEC Nucleofector^{TM} Kit	Lonza
Cell Tracker ^{TM} Orange, CMRA	Invitrogen
Complete, mini EDTA-free protease inhibitor cocktail	Roche Applied Science
Colloidal Coomassie Brilliant Blue-G	Sigma-Aldrich
Coverslips (13 mm)	VWR
Dulbecco's modified eagle medium (DMEM)(+ 4500 mg/L glucose, + L-Glutamine, + 25 mM HEPES, + 110 mg/L sodium pyruvate)	Gibco®, Life Technologies
Dried, skimmed milk	Marvel
Endothelial cell basal medium-2 (EBM-2), supplemented with ascorbic acid, R3-IGF-1, heparin, rhFGF-B, hydrocortisone, GA-1000, rhEGF, VEGF, 2% foetal bovine serum. Supplements provided as part of a bullet kit, SingleQuots®, purchased with the basal medium.	Clonetics®, Lonza
Enhanced chemiluminescence (ECL) reagent	GE Healthcare
Foetal calf serum	Invitrogen
Fibronectin	Calbiochem
FITC-dextran (molecular weight 42,000)	Sigma-Aldrich
Fluorescent mounting medium	DAKO
Gelatin	Sigma-Aldrich
Glutathione sepharose beads	GE Healthcare
Insulin from bovine pancreas	Sigma-Aldrich (cat. no. I1882)
Recombinant human insulin like growth factor-1	Millipore
L-broth	Sigma-Aldrich
BDMatrigel ^{TM} basement membrane matrix	BD Biosciences
Nitrocellulose membranes	Millipore
Nu PAGE® 4-12 % Bis-Tris Gels	Invitrogen
Nu PAGE® MES Running buffer	Invitrogen
Nu PAGE® LDS Sample buffer (4x)	Invitrogen

Novex® Colloidal Coomassie Blue Staining Kit	Invitrogen
Oligofectamine ™	Invitrogen
Opti-MEM + GlutaMax ™	Gibco®, Life Technologies
ORIS™ assay stoppers	Platypus Technologies
HiSpeed Maxiprep kit	Qiagen
Penicillin / Streptomycin (10,000 U/ml/10,000 mg/l)	Gibco®, Life Technologies
Phosphate buffered saline (PBS) (-) CaCl$_2$ / MgCl$_2$ or (+) 100 mg/L CaCl$_2$ / MgCl$_2$	Gibco®, Life Technologies
Pierce® BCA Protein Assay Kit	Thermo Scientific
PI-103	Millipore
Polyethylenimine (PEI), linear, MW ~ 25,000	Polysciences, Inc (cat. no. 23966)
Precision PlusProtein ™ standards	Bio-Rad
Transwell Permeable Supports, 0.4 µm pore size, 12 mm	Costar
Trypsin / EDTA 0.05%	Gibco®, Life Technologies
Vivaspin concentrators (5 000 and 10 000 MWCO)	Vivascience
Whatman 3MM chromatography paper	Whatman
X-ray film	Fujifilm

2.1.2   Buffers and solutions

Table 2.2 Buffers and solutions

Buffer	Composition
Lysis buffer	50 mM Tris-HCl pH 7.5 150 mM NaCl 1 mM EDTA 1 mM EGTA 270 mM Sucrose 1 mM Benzamidine 0.1% β-mercaptoethanol 1% Triton X-100 50 mM NaF 1 mM Na$_3$VO$_4$ 1 mM PMSF 20 nM Calyculin A Complete mini EDTA-free protease inhibitor
NuPAGE® MES SDS running buffer	50 mM MES 50 mM Tris base 0.1% SDS 1 mM EDTA pH 7.3

NuPAGE® MOPS SDS running buffer	50 mM MOPS 50 mM Tris base 0.1% SDS 1 mM EDTA pH 7.7
Transfer buffer	25 mM Tris 192 mM Glycine 20% Methanol pH 8.3
Tris-buffered saline with Tween (TBST)	20 mM Tris-HCl pH 7.6 140 mM NaCl 0.1% Tween-20
Stripping buffer	70 mM Tris 20 mM NaCl pH 2.3
14-3-3 Affinity Purification	
Peptide coupling buffer	0.1 M $NaHCO_3$ pH 8.0 0.5 M NaCl
Blocking buffer	0.1 M Tris-HCl pH 8.0
High pH Buffer	50 mM Tris-HCl pH 8.0 0.5 M NaCl
Low pH Buffer	50 mM NaAcetate pH 4.0 0.5 M NaCl
Buffer A	25 mM Tris-HCl pH 7.5 (4°C) 100 mM NaCl 25 mM NaF
Buffer B	25 mM Tris-HCl pH 7.5 (4°C) 500 mM NaCl 25 mM NaF
Cell lysis buffer	50 mM Tris-HCl pH 7.5 120 mM NaCl 1 mM EDTA 1 mM EGTA 270 mM Sucrose 1 mM Benzamidine 0.1% β-mercaptoethanol 1% Triton X-100 5 mM sodium pyrophosphate 10 mM Na- β-Glycerolphosphate 1 μM microcystin-LR 1 mM Na_3VO_4 50 mM NaF 1 mM PMSF Complete mini EDTA-free protease inhibitor

GFP-Trap pull down	
High salt buffer	50 mM Tris-HCl pH 7.5
	250 mM NaCl

2.1.3 Antibodies

Table 2.3 Primary Antibodies

Western Blot (WB); Immunofluorescence (IF)

Antibody (clone)	Species	Dilution	Supplier and Catalogue number
Akt	Rabbit	WB 1/1000	Sigma-Aldrich #HPA019657
Phospho-Akt (Ser473)	Rabbit	WB 1/1000	Cell Signaling #4060
ARHGAP17	Rabbit	WB 1/500	Abcam #74454
β-Catenin	Rabbit	IF 1/100	Sigma-Aldrich #C2206
Epsin2	Rabbit	WB 1/500	Abcam #ab74942
GAPDH	Mouse	WB 1/5000	Millipore #MAB374
GFP	Rabbit	WB 1/1000	Santa Cruz Biotechnology
LMO (C-5)	Mouse	WB 1/200	Santa Cruz Biotechnology #sc-365515
PARG1 (ARHGAP29)	Mouse	WB 1/2000	Bethyl Laboratories #A301-924A
pan 14-3-3 (K-19)	Rabbit	WB 1/1000	Santa Cruz Biotechnology #sc-629
PECAM1/CD31 (cloneJC70A)	Mouse	IF 1/200	Dako Cytomation
VE-cadherin	Mouse	IF 1/100	BD Biosciences #555289
ZO-1	Rabbit	IF 1/100	Invitrogen #61-7300

Table 2.4 Secondary Antibodies and reagents

Antigen	Species	Conjugate	Dilution	Supplier
Anti-Digoxigenin (Fab fragments)	Sheep	HRP	1/5000	Roche Diagnostics #11 207 733 910
Mouse IgG	Sheep	HRP	1/5000	GE Healthcare #NA931V
Rabbit IgG	Donkey	HRP	1/5000	GE Healthcare #NA934V
Mouse IgG (H+L)	Goat	AlexaFluor® 488	1/300	Molecular Probes #A11001
Mouse IgG (H+L)	Goat	AlexaFluor® 647	1/300	Molecular Probes #A21235
Rabbit IgG (H+L)	Goat	AlexaFluor® 488	1/300	Molecular Probes #A11008
Rabbit IgG (H+L)	Goat	AlexaFluor® 647	1/300	Molecular Probes #A21245
Phalloidin		AlexaFluor® 546	1/400	Molecular Probes #A22283
DAPI		DAPI	1/10000	Molecular Probes # D3571

2.1.4 siRNA oligonucleotides

Table 2.5 siRNA oligonucleotides

All siRNAs were purchased from Dharmacon. Oligo numbers assigned by Dharmacon.

Gene name	Oligo number	Sequence
ARHGAP17	#1	GCAGACAUGUACAACUUUA
	#2	AAACAGAAGUCCUUAGUGA
	#4	CUGAAGAGGUGGAAUUUAA
	#17	GUAAGAAGCAGUGCGUUAA
ARHGAP29	#1	GCAAAGACCUUCUAAGACA
	#2	GAAGUUCUCCCACAUGUUA
	#3	GGAAUGCACUUGGUAGAUA
	#4	GAACUAACAUUGGAAUUCA
EPN2	#1	AGACUACGCUGUUGGAUUU
	#3	CCACUGGGCCCUGCAAUGA
	#4	CCACCAAGCCCGUGUCUGU
	#17	AUUAAAAUCCACUAGAGCGA
LMO7	#1	CUACUGAACUGGAUGAUUA
	#2	GAAGUAUAAUGGAGAUGUU
	#3	UAGCAGGAUUGGAUAAUAU
	#4	GGACUAUUCUCAUUAAGGC

2.1.5 Software

Table 2.6 Software

Software	Supplier
Illustrator CS4	Adobe
Photoshop CS4	Adobe
Metamorph	Molecular Devices
Volocity	Volocity Perkin Elmer, Improvision
LSM + ZEN	Zeiss
ImageJ	National Institutes of Health
VisANT	National Institutes of Health
Jalview	University of Dundee
SigmaPlot Version 12.5	Systat Software, San Jose, CA

2.2   Methods: General molecular biology

2.2.1   Plasmid transformation of *Escherichia coli* (*E. coli*)

Plasmid DNA (100 ng) was added to 100 µl of competent DH5α cells (Invitrogen) and incubated on ice for 15 min. The suspension was heat-shocked at 42°C for 45 sec and then placed on ice for 5 min. After addition of 500 µl of antibiotic-free LB (Luria broth) the cells were allowed to grow at 37°C for 1 h. Transformed plasmid DNA suspensions (100 µl) were streaked onto LB agar plates containing the appropriate antibiotic for selection (100 µg/ml ampicillin).

2.2.2   Plasmid and construct preparation

All expression plasmids used in this thesis were kindly generated by Dr Rachel Toth at the Division of Signal Transduction Therapy (DSTT) of the University of Dundee.

Table 2.7 List of plasmids

Plasmid name	DSTT number
EGFP-C1 VASP	DU1556
EGFP-C1 HA RhoGef16	DU1595
pcDNA5 FRT/TO GFP RhoA	DU11862
pcDNA5 FRT/TO GFP PANK2	DU31932
pcDNA5 FRT/TO GFP LMO7	DU31944
pcDNA5 FRT/TO GFP Rac3	DU40610
pcDNA5 FRT/TO GFP ARHGD1A	DU40632
pcDNA5 FRT/TO GFP ARHGD1B	DU40633
pcDNA5 FRT/TO GFP CDC42	DU40634
pcDNA5 FRT/TO GFP ARHGAP17	DU40635
pcDNA5 FRT/TO GFP ARHGAP29	DU40636
pcDNA5 FRT/TO GFP EPN2	DU40672
pcDNA5 FRT/TO GFP SCFD1	DU40684
pcDNA5 FRT/TO GFP DOCK10	DU45027
pcDNA5 FRT/TO GFP DOCK10 T1440A	DU45089

A starter culture of transformed *E. coli* was prepared by inoculating 15 ml LB containing antibiotic for selection (ampicillin or kanamycin) with a single colony from an LB agar plate and incubated for 6 h at 37°C.

From the starter culture, 10 ml was used to inoculate 200 ml of LB containing antibiotic for selection, and incubated for up to 16 h at 37°C. Bacterial cells were pelleted at 5500 g in a Sorvall RC5C centrifuge (Rotor SLA-1500) for 15 min and the bacterial pellets were either stored at -20°C or purified immediately.

2.2.3   Purification of plasmid DNA

The bacterial pellet was purified using the Qiagen HiSpeed Maxiprep kit, according to the manufacturer's instructions, at room temperature. The bacterial pellet was resuspended in 10 ml of cold Buffer P1 (50 mM Tris-HCl, pH 8.0, 10 mM EDTA, 100 μg/ml RNase A). After complete resuspension, 10 ml lysis buffer P2 (200 mM NaOH, 1% SDS) was added and the suspension mixed gently. The solution was neutralised after 5 min with 10 ml of cold neutralisation buffer P3 (3.0 M potassium acetate, pH 5.5), mixed thoroughly and poured into the QIAfilter Cartridge. During a 10 min incubation, the HiSpeed Maxi Tip was equilibrated by applying 10 ml Buffer QBT (750 mM NaCl, 50 mM MOPS, pH 7.0, 15% isopropanol, 0.15% Triton X-100). Cell debris was separated from the soluble lysate by filtering through a QIAfilter Cartridge into a HiSpeed Maxi Tip. The cleared lysate was left to filter through the tip by gravity, and the bound DNA was washed by the addition of 60 ml QC wash buffer (1.0 M NaCl, 50 mM MOPS, pH 7.0, 15% isopropanol) to the tip. The DNA was eluted with 15 ml Buffer QF (1.25 M NaCl, 50 mM Tris-HCl, pH 8.5, 15% isopropanol), and precipitated by the addition of 10.5 ml isopropanol. Following a 5 min incubation, the DNA was concentrated by filtering the solution through the QIAprecipitator Maxi Module, and washed by passing 2 ml of 70% ethanol through the Module. After air-drying the QIAprecipitator membrane by pressing air through it with a dry syringe, the DNA was eluted by filtering 1 ml Tris-EDTA (TE) buffer (10 mM Tris-HCl, pH 8.0, 1 mM EDTA) through the Module. To ensure a high yield of DNA, the elution step was repeated using the eluted 1 ml TE buffer. The DNA concentration was then measured, and samples were stored at -20°C.

2.2.4   Measurement of DNA concentration

DNA concentration was determined spectrophotometrically using a Nano-Drop system (ND-1000, www.nanodrop.com). The sample (1 µl) was pipetted onto the end of a fibre optic cable, and the optical density (OD) was measured at 260 nm. The DNA concentration was automatically determined using the following formula: concentration of DNA = OD_{260} x 50 µg/ml.

2.3   Methods: Cell biology

2.3.1   Cell culture

Pooled primary human umbilical vein endothelial cells (HUVECs) (Lonza or PromoCell) were grown on flasks, plates and glass coverslips coated with 10 µg/ml fibronectin (FN). FN was diluted in PBS ($+Ca^{2+}$, $+Mg^{2+}$), plastic-ware was coated for at least 1 h and glass coverslips were coated overnight in a humidified incubator at 37°C with 5% CO_2. HUVECs were grown in Endothelial Cell Basal Medium-2 (EBM-2), supplemented with endothelial cell growth supplement (EGM-2) containing 2% heat-inactivated foetal bovine serum (FBS), growth factors and antibiotics (see Table 2.1). Cells reached 80% confluence between 3 to 4 days after thawing, medium was changed every 2 days and cells sub-cultured 1:3 or 1:4 depending on their growth. Cells were only used up to passage 4, as cell growth slowed, cell area increased and cell morphology became irregular beyond this.

The human bone marrow endothelial cell line (HBMECs) was kindly obtained from Babette Weksler of Cornell University (Schweitzer et al., 1997). Cells were grown on flasks and plates coated with 0.2% (w/v) gelatin in Dulbecco's Modified Eagle's Medium (DMEM; Gibco), supplemented with 10% (v/v) heat-inactivated FBS, 2 mM glutamine, 10 mM HEPES, 10 000 U/ml penicillin, 10 000 µg/ml streptomycin (pen/strep) and RPMI vitamin mix. Cells were passaged at least twice after thawing before being used for experiments and used until passage 25. Medium was changed every 2 days and cells were sub-cultured 1:5.

Adherent human embryonic kidney 293 cells (HEK293) were cultured in DMEM supplemented with 10% (v/v) heat-inactivated FBS, 2 mM glutamine, 10 mM HEPES, 10 000 U/ml penicillin, 10 000 µg/ml streptomycin. Medium was changed every 2 days and cells were sub-cultured 1:5.

All cells were maintained at 37°C with 5% CO_2.

2.3.2   Thawing and freezing of cells

Frozen cryovials in liquid nitrogen were thawed rapidly in a 37°C waterbath, and cells were slowly diluted up to 10 ml with their respective medium, in a drop-wise manner. Cells were centrifuged at 200 g for 4 min, supernatant aspirated and 10 ml complete medium added. The cells were then transferred to a 75 cm^2 tissue culture flask, incubated overnight at 37°C with 5% CO_2 and the medium was changed the next day.

To freeze cell lines, cells were washed with PBS (-Ca^{2+}, -Mg^{2+}), detached using trypsin and pelleted at 200 g for 4 min. Cells were resuspended in freezing solution (90% FBS, 10% dimethyl sulphoxide (DMSO)) and aliquoted into cryovials containing 1 ml each. Cryovials were inserted into a cryo freezing container and stored at -80°C to allow slow freezing of 1°C per hour, overnight. The cells were transferred to liquid nitrogen for long-term storage.

2.3.3   Treatment of cells with insulin, insulin like growth factor-I, and inhibitors

Prior to any stimulation, cells were serum starved. Due to their sensitivity as primary cells, HUVECs were serum starved in EBM-2 medium containing 1% FBS and pen/strep for either 4 h, for short-term experiments (less than 8 h); or for 2 h, for long-term experiments (16 to 24 h). HBMEC and HEK293 cells were starved for 16 h in serum free DMEM containing pen/strep. Cells were maintained in starving medium throughout the experiments, to which insulin, insulin like growth factor-I (IGF-I) and/or the inhibitors were added.

Insulin was prepared as a 10 mg/ml stock solution and stored at 4°C. The optimal concentration of insulin required to activate the cells was first determined in initial experiments, testing final concentrations of 0, 12.5, 25, 50, 100 and 200 nM. An optimal concentration of 100 nM was used in subsequent experiments. A time course analysis of 0, 5, 10, 15, 30 and 60 min was initially performed to identify optimal insulin stimulation times. Cells were stimulated for 10 min for subsequent biochemical analysis.

IGF-I was prepared as a 50 µg/ml stock solution in sterile water, aliquoted and stored a -20°C. HEK293 cells were treated at a final concentration of 50 ng/ml for 20 min.

The PI3K inhibitor, PI-103, was prepared as a 10 mM stock solution in DMSO, aliquoted and stored at -20°C. HEK293 cells were treated at a final concentration of 10 µM for 30 min, and then treated with IGF-I as described above.

2.3.4 DNA transfection of HUVECs using Amaxa nucleofection

HUVECs were transfected with plasmid DNA using the Amaxa HUVEC nucleofection kit. HUVECs were trypsinised and washed once with PBS ($+Ca^{2+}$, $+Mg^{2+}$) and resuspended in HUVEC electroporation buffer (Amaxa) (1 x 10^6 cells in 100 µl of buffer per condition). Plasmid DNA (4 µg) was mixed with the cell suspension and transferred to an electroporation cuvette. Nucleofection was carried out with an Amaxa Nucleofector^{TM} (Amaxa, Cologne, Germany) using program A-34 according to the manufacturer's instructions. After nucleofection, the cells were immediately diluted with 1 ml EGM-2 medium and transferred to two FN-coated glass coverslips (for confluent monolayers) or four coverslips (for sub-confluent monolayers). Following a 24 h incubation at 37°C with 5% CO_2, cells were fixed in 4% PFA at room temperature for 20 min and stained for immunofluorescence (see section 2.3.10). Transfection efficiencies of ≈20 − 30% were achieved.

2.3.5   Transfection of mammalian cells using PEI

HEK293 cells were grown in complete DMEM medium. An 80% confluent T75 flask was split into six 10 cm-diameter dishes containing 10 ml media, and incubated for 24 h. For each dish, a DNA/PEI solution of 10 μg of plasmid DNA and 40 μl of PEI (polyethylenimine) was mixed into 1 ml of serum-free DMEM and incubated at room temperature for 20 min. The cells were then transfected by slowly adding 1 ml DNA/PEI solution in a drop-wise manner, and incubated at 37°C for 24 h. Transfection efficiencies of ≈75 - 90% were achieved.

2.3.6   siRNA transfection of HUVECs using Oligofectamine

HUVECs were seeded for siRNA transfection in a 6-well plate at a density of 1×10^5 cells per well, 24 h before transfection. On the day of transfection, growth medium in each well was replaced with 800 μl of Opti-MEM. Individual siRNAs (20 μM stock) were diluted in Opti-MEM (2.5 μl siRNA in 182.5 μl Opti-MEM per condition) so as to reach a concentration of 50 nM in the final transfection mix. Oligofectamine was diluted in Opti-MEM (4 μl in 15 μl) and the two prepared solutions were incubated at room temperature for 5 min. The two solutions were then mixed and lipid-siRNA complexes allowed to form for 20 min at room temperature. This mixture (200 μl) was then added drop-wise to the cells in each well (in 800 μl of medium) and incubated at 37°C with 5% CO_2. After 5 to 6 h, 500 μl of EGM-2 medium containing 12% FBS was added to each well (for a final FBS concentration of 4%). The following day, medium was changed to EGM-2 containing 2% FBS and the cells used for subsequent experiments. Mock transfections in all experiments were performed by replacing siRNA with growth medium in the transfection mixes.

2.3.7   ORIS^TM cell migration assay

The ORIS^TM cell migration assay (Platypus Technologies) (Figure 2.1) is a migration assay in which stoppers are introduced into a well of a 96-well plate preventing cells from seeding onto a central 'wound'. Stoppers are removed after cells have adhered following which migration is monitored. The percentage area of the central wound that cells had migrated into after 24 h was used to quantify the extent of migration.

| Apply stopper in FN-coated well and seed HUVECs | Incubate for 24 h at 37 °C to allow cell attachment | Remove stopper to create central wound | Image wound and save positions | Image cells migrated into wound |
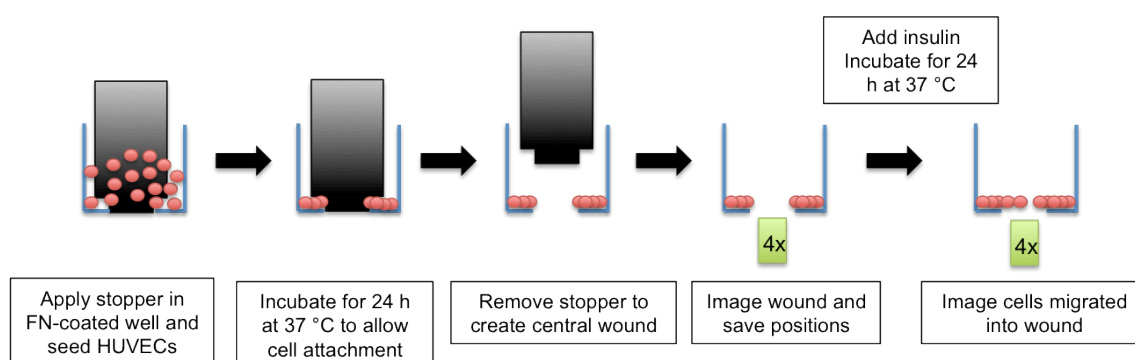
Figure 2.1 Schematic of the ORIS^TM Migration assay
A central stopper creates a wound in the HUVEC monolayer. The migration capacity of the cells is analysed when the stopper is removed and imaged before and after incubation, with or without the presence of insulin.

HUVECs were stained with Cell-Tracker Orange fluorescent dye, seeded (5 x 10^4 cells/well, 4 wells per condition) on FN-coated wells containing a central stopper and incubated overnight at 37°C in EGM-2 (Figure 2.1). siRNA-transfected HUVECs were seeded 48 h after transfection and maintained in growth medium throughout the experiment. For the insulin studies, cells were washed with PBS and starved in EBM-2 medium containing 1% FBS for 4 h. The stopper was then removed to create a central 'wound' in the monolayer. Images were acquired in the TRITC channel (excitation 548 nm, emission 576 nm), using a Nikon TE2000-E microscope with a Plan Fluor 4x objective (Nikon) and a Hamamatsu Orca-ER digital camera. Stage positions were saved using Velocity or Metamorph software and following a 24 h

incubation at 37°C, the stage file was reloaded and wells were imaged again at the identical position.

Cell migration was quantified by thresholding images using the auto thresholder applet in the ImageJ software and subtracting the percentage area of the 24 h wound from the initial wound (Figure 2.2). The mean of quadruplicate readings was expressed as a ratio of control versus untreated wells in insulin studies or siControl in knockdown analyses.
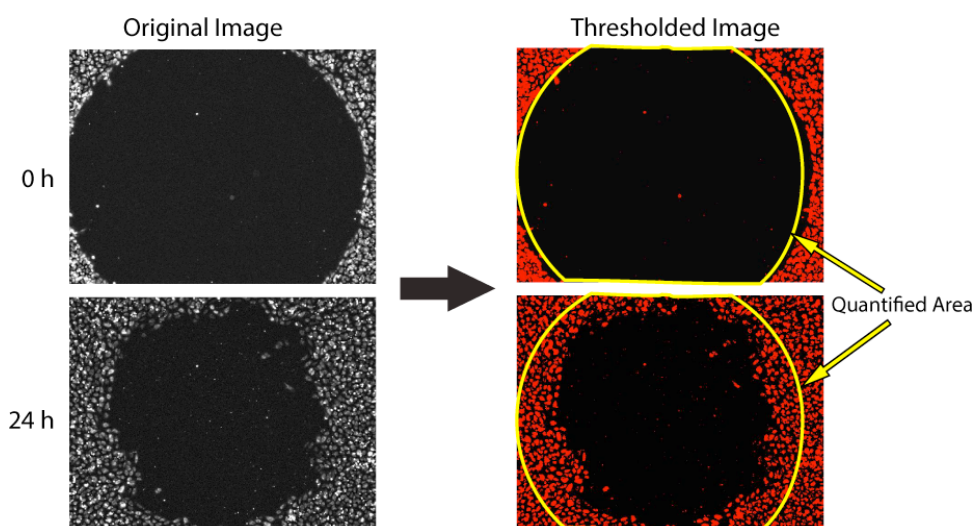
Figure 2.2 Cell migration quantification method

Images of monolayer wounds were thresholded using the auto thresholder applet in the ImageJ software. Cell migration was quantified by subtracting the percentage area of cells migrated into the wound after 24 h from the wound at 0 h, expressed as a ratio of control cells.

2.3.8   Permeability assay

In order to quantify junctional strength and permeability, FITC-dextran permeability assays were performed (Figure 2.3) (Monaghan-Benson and Wittchen, 2011; Siflinger-Birnboim et al., 1987). HUVECs were plated at confluency (1.2 x 10^5 cells/well) on FN-coated 0.4 µm Transwell™ filters (Thermo Fisher Scientific). siRNA-transfected HUVECs were seeded 48 h after transfection and maintained in EGM-2 throughout the experiment. For insulin studies, monolayers were starved in EBM-2 containing 1% FBS for 4 h and then treated with various concentrations of insulin (0 to 200 nM) for 30 min. For the analysis of HUVEC junctional permeability over time, cells were serum starved for 2 h and then treated with 100 nM insulin for 0, 10, 30, 60, 90 min and 4, 8 and 24 h.

FITC-dextran (0.1 mg/ml, molecular weight, 42 kDa) was added to the upper chamber and incubated at 37°C for 60 min. Therefore, in insulin studies with time points longer than 60 min, FITC-dextran was added in the final 60 min of incubation; and for shorter time-points, FITC-dextran was added to all wells prior to insulin stimulation to allow for equilibration before stimulation. A sample of medium (200 µl) was removed from the lower chamber to measure permeability to FITC-dextran and added to wells in a black 96 well plate with clear bottom (Nunc™). Fluorescence was measured using a microplate analyser (Fusion-FA; PerkinElmer; excitation, 492 nm; detection, 520 nm).
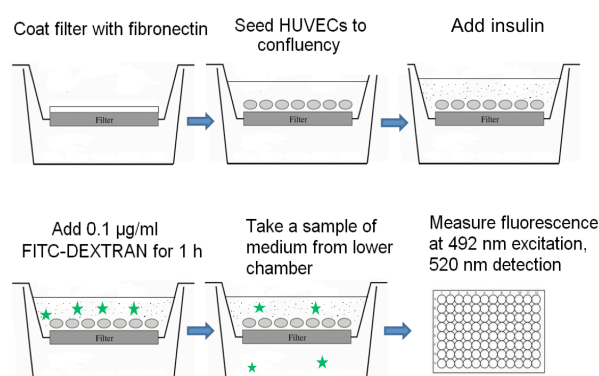
Figure 2.3 Schematic of the Transwell® permeability assay with FITC-dextran
HUVEC barrier function was analysed by permeability to FITC-dextran in a transwell assay. Fluorescence of the medium in lower chamber was used as a measure of permeability.

2.3.9   Loop-formation angiogenesis assay

When ECs are seeded onto the surface of a three-dimensional gel of Matrigel matrix they undergo morphogenic changes and form tube-like structures. The gel layer was prepared by thawing growth factor reduced Matrigel overnight at 4°C and diluted to a concentration of 4.5 mg/ml with cold PBS ($+Ca^{2+}$, $+Mg^{2+}$). This mixture (300 µl) was spread out onto each well of a 6-well dish and allowed to polymerise at room temperature for 1.5 h. For the insulin studies, HUVECs were incubated in EBM2 containing 1% FBS for 2 h, harvested with trypsin and seeded onto the Matrigel layer at a density of 2×10^5 cells per well in low serum medium. The cells were then treated with various concentrations of insulin. For the protein knockdown studies, HUVECs were transfected with siRNAs and seeded onto the Matrigel after 48 h, at a density of 2×10^5 cells per well in EGM-2. Loops were allowed to form for 24 h and monitored by phase-contrast time-lapse microscopy using a Nikon TE2000-E microscope with a Plan Fluor 4X objective and a Hamamatsu Orca-ER digital camera, at 37°C and 5% CO_2. Images were captured using Metamorph software. A frame rate of 1 frame/20 min was used for 24 h and movies were initiated 1 h after seeding cells onto Matrigel. Loop formation was quantified by counting the number of loops formed per field of the final frame (24 h, Figure 2.4). The mean value for at least 5 fields of each condition was used for statistical analysis.
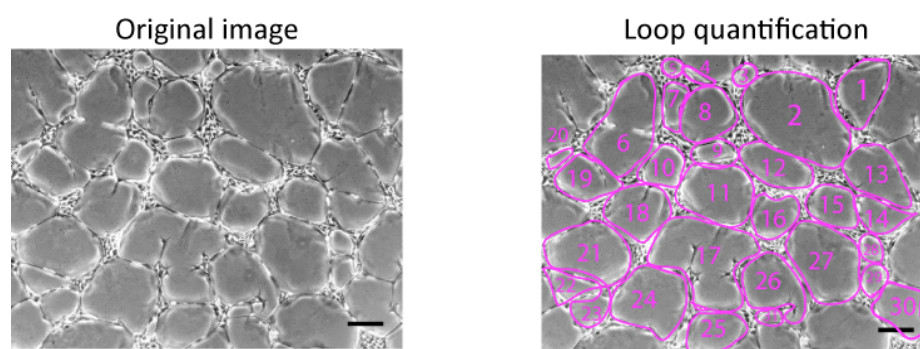
Figure 2.4 Quantification of the number of loops formed in the angiogenesis assay
The final image from time-lapse movies of angiogenic loops formed by HUVECs after 24 h is shown on the left; loops were quantified by counting the total number of complete loops as shown in pink on the right. Scale bar is 200 µm.

2.3.10 Immunofluorescence

Sterile glass coverslips (13 mm in diameter) were placed in a 24-well plate and coated with 10 µg/ml FN overnight at 37°C. For insulin studies, 1.5 x 10^5 HUVECs/well were seeded onto the coverslips and incubated overnight at 37°C. Cells were starved for 4 h in EBM-2 containing 1% FBS and then treated with various concentrations of insulin (0 – 200 nM) for 1 h or 100 nM insulin for 1, 4, 16 and 24 h.

In over-expression studies, 1 x 10^6 HUVECs were transfected with 4 µg DNA coding for GFP-fusion proteins of interest (RICH-1, Parg1, Epsin2 and LMO7) by nucleofection (see section 2.3.4). These cells were then seeded onto two coverslips and incubated for 24 h at 37°C. Cells transfected with siRNA targeting RICH-1, Parg1, Epsin2 and LMO7 were seeded onto coverslips 48 h after transfection and incubated for 24 h at 37°C.

Cells were fixed in 4% paraformaldehyde (PFA) at RT, washed twice with PBS (+Ca^{2+}, +Mg^{2+}), and stored overnight at 4°C in PBS (+Ca^{2+}, +Mg^{2+}). Cells were permeabilised with 0.2% Triton-X 100 (v/v) in PBS, at 4°C for 5 min and blocked with 3% bovine serum albumin (BSA) in PBS at RT for 30 min, to reduce non-specific binding of antibodies. Coverslips were stained with primary antibodies diluted in 3% BSA/PBS for 2 h at RT or overnight at 4°C. Coverslips were washed 3 times with PBS and incubated with fluorophore-conjugated secondary antibodies and phalloidin (1:400, to label F-actin) for 60 min at RT. Cells were then washed once in PBS containing DAPI (1:10 000) (for DNA staining), followed by 3 washes with PBS and 2 washes with H_2O. Coverslips were mounted onto glass slides using an anti-fade fluorescent mounting medium. Slides were stored in the dark at RT overnight for mounting medium to dry and then stored at 4°C until images were acquired.

2.3.11 Confocal microscopy

A Zeiss LSM510 confocal laser-scanning microscope with an EC Plan-Neofluar 40x/1.30 Oil DIC M27 or a Plan-Apochromat 63x/1.40 Oil DIC M27 objective, and ZEN software was used to take images of fluorescently stained cells. Images were taken at a resolution of 512 x 512 pixels using an average of 2 or 4 frames. Maximum intensity projections of HUVEC monolayers were generated from 10 z-stacks, spanning 4 µm with 0.4 µm intervals between each image.

The range finder function in the ZEN software was used to adjust the gain and offset to avoid saturation and high background in images. Images in each experiment were acquired using the same gain and offset settings if comparison between images was required. Lasers and filters used are shown in Table 2.8.

Table 2.8 Lasers and filters used for confocal microscopy

Fluorophore	Laser	Excitation (nm)	Emission (nm)	Filter (nm)
Alexa 488	Argon	488/494	520/517	Bandpass 505-530
Alexa 546	Helium/Neon	556	573	Bandpass 560-615
Alexa 647	Helium/Neon	650	668	Longpass 650
DAPI	Diode 405-30	405	430	Bandpass 420-480

2.4   Methods: Biochemistry

2.4.1   Preparation of cell lysates

Cells in 6-well plates or 10-cm dishes were placed on ice and washed with ice-cold PBS ($+Ca^{2+}$, $+Mg^{2+}$). Cells were lysed in 120 µl lysis buffer per well for 6-well plates, or 350 µl lysis buffer for each 10-cm dish. Cells were scraped into microfuge tubes, and incubated on ice for 10 min. Samples were cleared by centrifugation at 13 000 g at 4°C for 20 min, and the supernatant transferred to new tubes.

An appropriate volume of 4x sample buffer was added to the lysates to be analysed by Western blotting, samples were boiled at 72°C for 10 min and stored at -20°C.

For 14-3-3 overlay samples, a bicinchoninic acid (BCA) protein determination (Thermo Scientific) was performed according to the manufacturer's instructions, and equal quantities of protein were added to pre-clearing beads (see section 2.5.5).

2.4.2   SDS-PAGE and Western blotting

Prepared cell lysates were loaded into NuPAGE 4-12% Bis-Tris gels and resolved using an initial voltage of 75 V for 30 min, followed by a voltage of 150 V for 60 min in either NuPAGE MES buffer (for low molecular weight proteins 10 to 50 kDa) or MOPS buffer (for high molecular weight proteins 50 to 250 kDa). After gel electrophoresis, proteins were transferred onto a nitrocellulose membrane (0.45 µm) (Millipore) by Western blotting. The gel and membrane were equilibrated in 1X transfer buffer and sandwiched between 2 layers of Whatman paper, 2 sponges and inserted into a transfer cassette. The cassette was placed in a Mini-Protean transfer system (Bio-Rad) filled with 1X transfer buffer. Electrophoretic transfer of proteins onto the membrane was achieved at a constant voltage of 100 V for 1 h, for smaller proteins, or 90 min for high molecular weight proteins, at 4°C. After electrophoresis, membranes were blocked in blocking buffer (5% skimmed milk powder in TBST or 5% BSA in TBST) for 1 h at room temperature. Membranes were then incubated with primary antibodies (in BSA blocking buffer at the appropriate

dilution, see Table 2.3) overnight at 4°C. Membranes were washed 3 times with TBST for 10 min each and incubated with the secondary antibody (in BSA blocking buffer) at room temperature for 1 h. Unbound antibody was removed by washing 3 times with TBST and the HRP signal determined using an enhanced chemiluminescence (ECL) detection kit (GE Healthcare) according to the manufacturer's instructions and X-ray film (Fujifilm). Bands on X-ray films of immunoblots were quantified by densitometric analysis of the scanned films using ImageJ software.

2.4.3   Stripping of Western blots

To allow reprobing, nitrocellulose membranes were stripped by incubating in stripping buffer (70 mM Tris, 20 mM NaCl, pH 2.3), twice for 20 min each at 65°C. Membranes were subsequently washed 3 times with TBST and re-blocked in 5% skimmed milk powder in TBST or 5% BSA in TBST for 1 h at room temperature. Membranes were then reprobed with primary and secondary antibodies and developed according to the described Western blotting protocol.

2.5   Methods: 14-3-3 chromatography and 14-3-3 overlays

2.5.1   Expression and purification of the *S. cerevisiae* 14-3-3 isoforms BMH1 and BMH2

The 6-His tagged BMH1 and BMH2 14-3-3 isoforms from *Saccharomyces cerevisiae* were produced by staff at the Division of Signal Transduction Therapy (DSTT) of the University of Dundee. The methods have been previously described in (Moorhead et al., 1996). Briefly, plasmids expressing N-terminal 6-His tagged BMH1 and BMH2 were generated from the trc promoter in plasmid pTrcHisA as follows: polymerase chain reaction (PCR) mixes (0.1 ml) contained 10 mM Tris (pH 8.5), 50 mM KCl, 2 mM $MgCl_2$, 0.1 mg/ml gelatin, 0.2 mM each dNTP, 100 pmol each primer, 100 ng DNA and 1.25 units Taq polymerase which was added when the reaction mix was at 94°C. Conditions for each cycle were 94°C for 1 min to denature the DNA; 55°C for 1 min to anneal the primers; and 72°C for 1 min of DNA chain extension. The primers (synthesized by the NIMR sequencing service) were for BMH1, 5'CGCGGATCCATGGTCAACCAGTCGTGAAGATTC (which carries a *Bam*H1 site) and 5'CCCAAGCTTTTACTTTGGTGCTTCACCTTCGGCGGCAGC (which carries a *Hind*III site); and for BMH2 5'CGCGGATCCATGTCCCAAACTCGTGAAGATTC and 5'CCCAAGCTTTTATTTGGTTGGTTCACCTTGAG. Products were electrophoresed on a 1% (w/w) TAE agarose gel and DNA fragments were purified using a Gene-clean kit from Bio101. After ligation into the plasmid, the PCR products were sequenced by the dideoxy chain termination method using the Sequenase kit (USB).

LB containing 50 µg ampicillin/ml was inoculated with *E. coli* DH5α cells overexpressing 6-His tagged BMH1 or BMH2, and grown at 37°C until the absorbance at 600 nm reached 0.6. Expression was induced for 3 h with 0.5 mM isopropyl-thio-β-D-galactopyranoside and cells were harvested by centrifugation. The bacterial pellet was resuspended in buffer B (1.5 mM Na_2HPO_4, 5 mM KH_2PO_4 (pH 7.2), 137 mM NaCl, 5 mM KCl, 1 mM dithiothreitol (DTT), 1 mM EDTA, 5% glycerol and 1 mM PMSF) and sonicated at 12 microns for 7 cycles of 30 sec sonication and 30 sec cooling. The sonicate was clarified by centrifugation, and

applied to a Ni^{2+}-nitrilotriacetic acid–agarose column equilibrated and washed in buffer B. Fusion proteins (6-His BMH1 and 6-His BMH2) were eluted in buffer B containing 100 mM imidazole, concentrated in a Centricon-10 (Amicon), dialysed into storage buffer (25 mM Tris-HCl (pH 8), 90 mM NaCl, 1 mM EDTA, 1 mM DTT and 50% (v/v) glycerol) and stored at -20°C.

2.5.2   Coupling BMH1 and BMH2 to activated CH-Sepharose 4B

The recombinant 14-3-3 proteins were coupled to NHS-activated Sepharose (CH Sepharose 4B), which forms covalent bonds with lysine residues and other primary amine groups. Dry matrix (5 g) was poured onto the glass sinter of a filtering system and swelled to 15 ml in 500 ml of cold 1 mM HCl for 30 min with occasional stirring. The solution was removed under vacuum, insuring that the Sepharose always remained moist. The matrix was washed twice with 200 ml coupling buffer (0.1 M $NaHCO_3$, 0.5 M NaCl pH 8.0). Purified BMH1 and BMH2 (15 mg each, for a final concentration of 2 mg/ml) were added to the matrix, the volume was made up to 40 ml with coupling buffer and left to crosslink for 4 h at 4°C. The matrix was centrifuged at 400 g at 4°C for 5 min and the supernatant was removed. A 5 μl sample of the supernatant was used for a Bradford assay (A_{595}) to assess the efficiency of protein coupling to the matrix. Any remaining reactive groups of the matrix were blocked in 40 ml 0.1 M Tris-HCl pH 8.0 at 4°C for 1 h, mixing end-over-end. The matrix was washed by pouring onto a glass sinter under vacuum and washed alternately with 50 ml high pH buffer (50 mM Tris-HCl, 0.5 M NaCl, pH 8.0) followed by 50 ml low pH buffer (50 mM sodium acetate, 0.5 M NaCl, pH 4.0) for a total of 5 washes for each buffer. The 14-3-3-Sepharose was stored in 50 mM Tris-HCl, pH 7.5 and 0.05% sodium azide at 4°C until use. Before using, 14-3-3 Sepharose was washed twice with 20 ml Buffer A (25 mM Tris-HCl pH 7.5 (4°C), 100 mM NaCl, 25 mM NaF).

2.5.3   14-3-3-affinity chromatography of human cell extracts

Confluent HBMECs were incubated in low serum conditions (DMEM containing 1% FBS, 2 mM glutamine, 10 000 U/ml penicillin, 10 000 µg/ml streptomycin) for 16 h. Fifty 15-cm dishes were stimulated with 100 nM insulin for 10 min and fifty 15-cm dishes were left untreated as control cells. Cells were washed with cold PBS and lysed in 500 µl lysis buffer per dish, on ice and centrifuged at 15000 g for 30 min at 4°C. Samples of the supernatants were collected for biochemical and protein analysis. The remaining clarified supernatants (control and insulin-stimulated) were mixed end-over-end with 5 ml 14-3-3-Sepharose each, overnight at 4°C. The mixture was poured into two Econo-columns, the flow throughs collected, and the columns washed with 500 ml Buffer B (25 mM Tris-HCl pH 7.5, 500 mM NaCl, 25 mM NaF). Proteins that bound to the phosphopeptide binding site of 14-3-3 proteins were eluted by the competitive phosphopeptide ARAApSAPA. The protein/Sepharose mixture was incubated with 12 ml of 2 mM ARAApSAPA peptide in Buffer A for 2 h at 4°C. A second elution was performed with a further 12 ml of 2 mM phosphopeptide for 1 h at 4°C. The eluates were combined with a final wash of 12 ml Buffer A and concentrated to 40 µl and desalted in Vivaspin concentrators (10 000 MWcut-off). Samples were then alkylated and separated by SDS-PAGE electrophoresis (see section 2.6.1). This protocol is summarised in Figure 2.5.
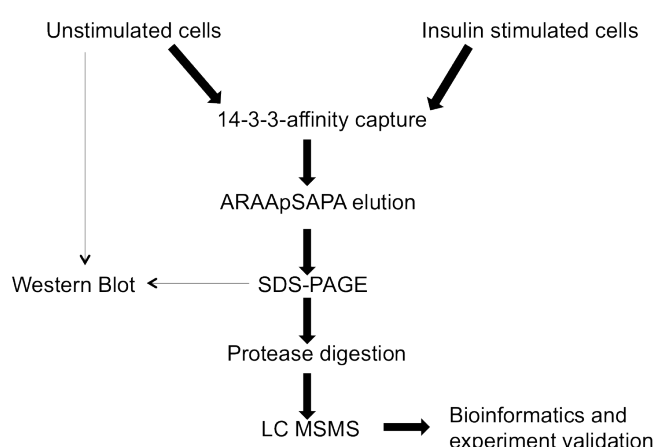
Figure 2.5 14-3-3-affinity capture and identification of proteins whose phosphorylation and binding to 14-3-3s is stimulated by insulin

2.5.4   Preparation of DIG-labelled 14-3-3 probe for 14-3-3 overlays

The DIG-labelled 14-3-3 probe was prepared by Dr Catherine Johnson in the MacKintosh laboratory (University of Dundee). 14-3-3 protein (usually 50 µg each of the 6-His-tagged BMH1 and BMH2 isoforms) was incubated for 2 h at room temperature with 8 µg digoxygenin-Omethylcarbonyl-ε-aminocaproic acid-N-hydroxysuccinimide (DIG-NHS) ester, added from a 2 mg/ml stock solution in DMSO, and 400 µl PBS, pH 8.5, with occasional mixing. The mixture was dialysed extensively in PBS pH 7.2 at 4°C to remove unreacted DIG ester, and diluted to a final protein concentration of 1 µg/ml in 25 mM Tris-HCl pH 7.5, 500 mM NaCl, 2 mg/ml BSA. The resulting DIG-14-3-3 probe was stored at 4°C with 0.05% sodium azide.

2.5.5   GFP-Trap pull-downs

GFP-fusion proteins of the candidate insulin-regulated protein hits identified in the 14-3-3-affinity purification were overexpressed in HEK293 cells (as described in section 2.3.5). These proteins were enriched by GFP-Trap pull downs for 14-3-3 overlay analysis (described in the section 2.5.6). GFP-Trap (DSTT, University of Dundee) is a GFP-binding protein coupled to Sepharose beads for biochemical analysis of GFP fusion proteins and their interacting partners (Rothbauer et al., 2008). All procedures were carried out at 4°C. Cell lysates with equal quantities of total protein (between 1 and 3 mg) were pre-cleared to remove proteins that bound specifically or non-specifically to Protein G Sepharose. Cell lysates were incubated with 20 µl of washed Protein G-Sepharose beads on a rotating wheel for 30 min, followed by centrifugation at 5500 g at 2 min. The pre-cleared lysates were added to GFP-Trap coupled to Sepharose beads (produced by DSTT) and incubated on a rotating wheel for 2 h. Following centrifugation at 5500 g for 2 min, the supernatant was removed and the beads washed twice with high salt buffer (50 mM Tris-HCl pH 7.5, 250 mM NaCl) and a further two times with no salt buffer (50 mM Tris-HCl pH 7.5). Sample buffer containing 500 mM DTT was then added to the beads, and the proteins were dissociated and denatured by boiling the samples at 72°C for 10 min. Samples were stored at -20°C.

2.5.6   DIG-14-3-3 overlays

Proteins enriched by GFP-Trap pull downs were separated by SDS-PAGE, transferred to nitrocellulose, and the membrane was blocked with 5% (w/v) non-fat milk powder as previously described for Western blotting (see section 2.4.2). The membrane was washed in TBST, and incubated with 1 ng/ml DIG-labelled 14-3-3 protein in 5% BSA blocking buffer, overnight at 4°C. The membrane was washed three times for 10 min in TBST, and incubated with HRP-conjugated anti-DIG antibody diluted 1:5000 in TBST containing 5% BSA for 1 h. Following another washing step to remove any unbound probe, the overlay was developed with ECL reagent as described in the manufacturer's instructions and X-ray film.

2.6   Methods: Protein chemistry

2.6.1   Proteolytic digestion of proteins 'in gel'

Concentrated proteins eluted from the 14-3-3-affinity column were prepared for SDS-PAGE by adding 4X LDS sample buffer containing DTT (10 mM final concentration), and boiled at 72°C for 10 min. After cooling, iodoacetamide was added to a concentration of 50 mM, and the samples incubated at room temperature for 30 min on a shaking platform in the dark to alkylate cysteine residues. Samples were then subjected to electrophoresis with a NuPAGE 4-12% Bis-Tris gel and resolved at a constant voltage of 150 V for 90 min in NuPAGE MES buffer. The gels were stained overnight with Colloidal Coomassie blue using the Novex® Colloidal Coomassie Blue Staining Kit (Invitrogen). Stained protein bands were excised, and the proteins digested 'in gel' with trypsin. The proteins in the elution lanes were excised with a razor blade; cut into 6 small pieces each and placed in microfuge tubes. The gel pieces were destained for 15 min at room temperature on a vibrating platform in a solution of 200 µl methanol (MeOH) and 100 mM ammonium bicarbonate (AmBic), 50% (v/v). Gel pieces were then alternately incubated three times in 100% MeOH for 15 min, followed by 100 mM triethylammonium bicarbonate (TEAB). A final wash in MeOH was performed to

completely dehydrate the gel, the MeOH was removed and samples were left to air dry. Trypsin was diluted to a final concentration of 5 ng/μl in TEAB, pH 7.8, and 30 μl was added to each gel piece (150 ng trypsin each). Samples were placed on ice for 10 min, followed by the addition of 30 μl TEAB to cover gel pieces and incubated overnight on a vibrating platform at 30°C. After 16 h, the supernatant was transferred to new tubes, 60 μl MeOH/TEAB/formic acid (50%, 45%, 5%, v/v/v) was added to the gel pieces and incubated for 15 min at room temperature. The supernatant was then added to the previous extraction, evaporated to complete dryness and stored at -20°C.

2.6.2   Protein mass fingerprinting analysis for protein identification

All the mass spectrometry (MS) analyses were performed by staff at the MRC Protein Phosphorylation Unit (College of Life Sciences, University of Dundee). Mass fingerprinting for protein identification was performed on the tryptic peptides by LC-MS-MS (liquid chromatography mass spectrometry mass spectrometry) on a Thermo LTQ-Orbitrap system (Thermo Fisher Scientific, Schwerte, Germany) coupled to a Proxeon Easy-LC HPLC system. The peptide mixtures were loaded onto a nanoseparations C_{18} guard column (0.1 x 20 mm) equilibrated in 0.1% formic acid/water at 5 ml/min and then separated on a 0.075 x 150 mm PepMap C_{18} column, equilibrated in 0.1% formic acid/water (LC Packings, Amsterdam, Netherlands). RAW files from Excalibur (Thermo) were processed by Raw2msm (Olsen et al., 2005) to generate peak lists that were analysed using the Mascot search engine (www.matrixscience.com) against the UniProt database (release 2012 03 (consisting of 535 248 sequences and 189 901 164 residues)). For each protein match, Mascot calculates an overall Protein Score. This number reflects the combined scores of all observed mass spectra that can be matched to amino acid sequences within that protein. A higher score indicates a more confident match. The significance threshold was $p < 0.05$; only peptides with ion scores over 20 were considered and only proteins with at least one unique peptide (red bold in Mascot) were considered.

2.7   Statistical analysis

Statistical analysis was carried out where indicated using data from three or more independent experiments. Statistical significance was calculated with SigmaPlot Version 12.0 (http://www.sigmaplot.com) using statistical tests chosen as a result of data meeting specific criteria using Normality (Shaprio-Wilk) and Equal of Variance tests.   Statistical significance was determined by using an unpaired Student's t-test, or where specified using the Mann-Whitney U test or one-way ANOVA (analysis of variance) (Holm-Sidak method).

3   Effects of insulin on endothelial cells

3.1   Introduction

Endothelial cells (ECs) are the first cells to come into contact with chemical stimuli, such as cytokines and hormones that pass through the systemic circulation. The endothelium rapidly responds to these stimuli, activating many physiological processes and thus acts as a key regulator of haemostasis, vascular tone, and immune and inflammatory responses (Sumpio et al., 2002) (see section 1.2). The endothelium is an important insulin target. Previous studies have shown that besides its metabolic effects, insulin acts as an anti-inflammatory agent that suppresses leucocyte adhesion molecules and NF-κB (Dandona et al., 2009).

The balance between the two main signalling pathways in ECs determines the vascular response to insulin (see section 1.3.2). The PI3K/Akt pathway results in vasodilation via nitric oxide production, whereas endothelin-1 dependent vasoconstriction occurs through MAPK/ERK-dependent signalling. The regulation of insulin signalling in ECs is essential since impaired PI3K/Akt signalling observed in obese and type 2 diabetic animal models attenuates insulin-induced capillary recruitment and insulin delivery, resulting in reduced glucose uptake by the skeletal muscle (Kubota et al., 2013). Moreover, the impaired PI3K-dependent signalling causes an imbalance between the production of nitric oxide and endothelin-1 and leads to a proflammatory and prothrombic state with defective vasodilation, known as endothelial dysfunction (Endemann and Schiffrin, 2004). Insulin resistance, a decrease in insulin sensitivity, is frequently associated with endothelial dysfunction that results in cardiovascular disease (Muniyappa and Sowers, 2013).

A loss of endothelial barrier function is one of the earliest indications of inflammation and atherosclerosis (Libby, 2012). The integrity of the endothelial barrier is highly dependent on actomyosin-based contractility and cell-cell junctions (see section 1.2.3), however the role of insulin in the regulation of endothelial barrier function is not well described. This chapter focuses on identifying the effect of insulin on endothelial junctions and the cytoskeleton.

3.2   Insulin activates Akt in endothelial cells

Insulin signalling is mediated by a complex network of signalling pathways that regulate diverse cellular functions and include multiple feedback loops, cross-talk between major signalling branches, and intersect signalling pathways of heterologous receptors (Muniyappa et al., 2007; Nystrom and Quon, 1999; Taniguchi et al., 2006). Of the two main insulin signalling pathways the PI3K/Akt pathway is responsible for most of the metabolic actions of insulin and regulating cardiovascular homeostasis (Muniyappa et al., 2007) (see section 1.3.2).

Experimentally, the optimal conditions required to stimulate ECs with insulin were firstly determined. Insulin activates the PI3K pathway inducing a conformational change in Akt that makes it accessible to phosphorylation at threonine 308. Full activation occurs by the subsequent phosphorylation of serine 473 (Alessi et al., 1996a). In this study, Ser473 phosphorylation of Akt was analysed to quantify the degree of insulin-stimulated endothelial activation. Initially, cells were stimulated with physiological concentrations of insulin (100 – 500 pmol/L), however, no changes in Akt phosphorylation were observed (data not shown). The majority of studies of insulin action on ECs have used unphysiologically high concentrations of insulin to stimulate phosphorylation of Akt, eNOS and other insulin-activated pathways (Hermann et al., 2000; Zeng et al., 2000). As per previous studies, HUVECs were stimulated with insulin at concentrations of 0 – 200 nM (Figure 3.1) and for different stimulation times (0 – 60 min) with 100 nM insulin (Figure 3.2).

Initially, primary human umbilical vein endothelial cells (HUVECs) and a human bone marrow endothelial cell line (HBMECs) were incubated in low serum conditions (growth factor free EBM2 containing 1% FCS) for 4 h followed by insulin stimulation. However, basal levels of Akt phosphorylation levels were high and increases could not be observed when compared to untreated control cells. When these same conditions were used to treat HeLa cells, a four-fold increase in Akt phosphorylation was observed in response to insulin (data not shown). ECs were too sensitive for complete serum starvation, as a high level of cell death was observed. It was also noted that the PI3K/Akt pathway could also be activated by

shear stress during the washing steps in the cell lysate preparation. Thus, basal levels of pAkt were reduced by incubating the cells in low serum conditions for 16 h and handled gently to ensure that cell activation was as a result of insulin stimulation.

Insulin induced a strong dose-dependent Akt activation in both HUVECs (Figure 3.1A) and HBMECs (Figure 3.1B). Maximal increases of 1.55- and 2.9-fold were observed in the HUVECs and HBMECs, respectively, after incubation with 200 nM insulin for 10 min (Figure 3.1). An optimal concentration of 100 nM was chosen for subsequent experiments, as this concentration produced the most reproducible response in the ECs.

Insulin activated Akt within the first 5 min of stimulation and phosphorylation was maintained for 30 min in HUVECs (Figure 3.2A) and for the whole period of observation (60 min) in HBMECs (Figure 3.2B).
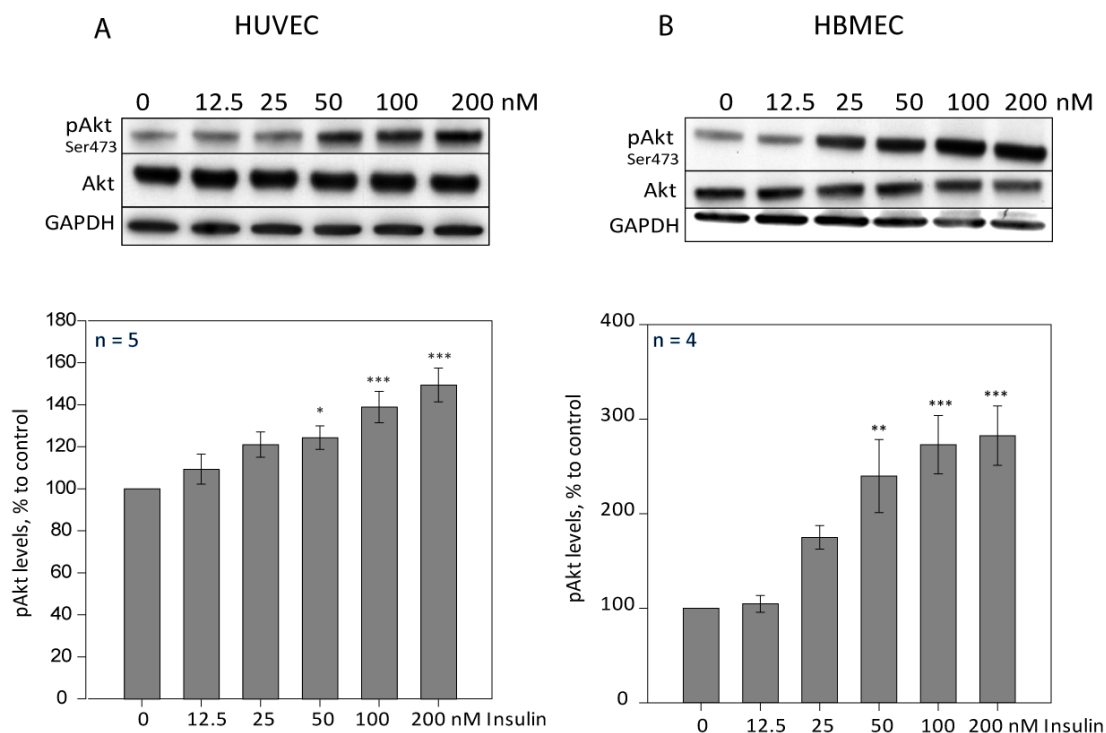
Figure 3.1 Insulin stimulates the phosphorylation of Akt in endothelial cells

HUVECs (A) and HBMECs (B) were stimulated with increasing concentrations of insulin (0 – 200 nM) for 10 min, following low serum conditions (EBM2 + 1% FCS) for 16 h. Top panels show representative Western blots. Graphs in the lower panel were generated from data analysed by densitometric scanning of Western blots, normalised to total Akt and GAPDH levels, relative to control. Data shown are the mean of five (A) and four (B) independent experiments ± SEM. *p<0.05, **p<0.005, ***p<0.001; One-way ANOVA (Holm-Sidak method).
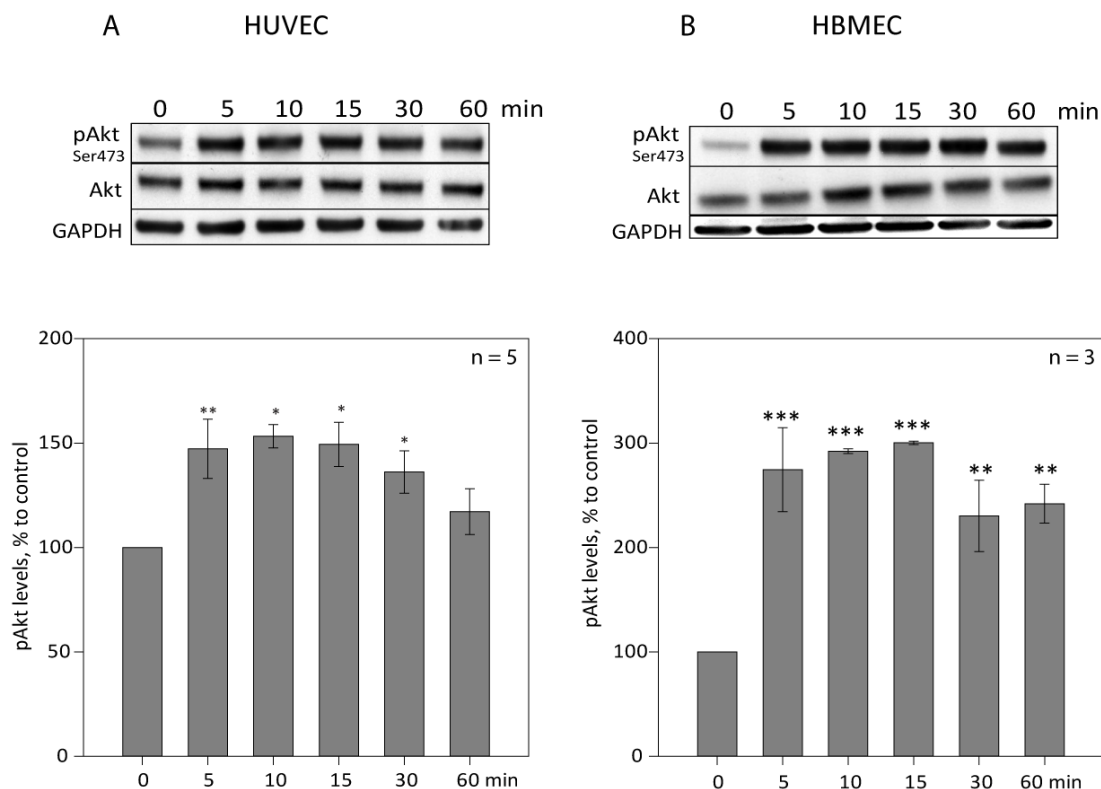
Figure 3.2 Insulin stimulates the phosphorylation of Akt within 5 minutes

HUVECs (A) and HBMEC s (B) were stimulated with insulin (100 nM) at various time points (0 – 60 min), following low serum conditions (EBM2 + 1% FCS) for 16 h. Top panels show representative Western blots. Graphs in the lower panel were generated from data analysed by densitometric scanning of Western blots, normalised to total Akt and GAPDH levels, relative to control. Data shown are the mean of five (A) and three (B) independent experiments ± SEM. *$p<0.05$, **$p<0.005$, ***$p<0.001$; One-way ANOVA (Holm-Sidak method).

3.3   Effect of insulin on endothelial cell-cell junctions

3.3.1   Insulin decreases basal endothelial cell permeability

ECs provide a semi-selective permeable barrier between the blood and the interstitial space. The degree of permeability depends on the structural integrity of inter-endothelial junctions, as well as actomyosin-based cell contractility, and can be modified by a variety of circulating vasoactive inflammatory stimuli and hormones such as insulin, derived from blood or surrounding tissues (Gunduz et al., 2010; Vandenbroucke et al., 2008). The effect of insulin on endothelial permeability was investigated in a permeability assay using a tracer flux assay, quantifying the movement of a 40 kDa fluorescent marker fluorescein isothiocyanate (FITC) – dextran in a Transwell™ system (Monaghan-Benson and Wittchen, 2011; Siflinger-Birnboim et al., 1987). Confluent HUVEC monolayers on FN-coated Transwell™ filters were treated with insulin (0 – 200 nM) for 30 min, following incubation in low serum conditions (EBM2 containing 1% FCS) for 4 h. FITC-Dextran was added to the upper chamber for 60 min, and the fluorescence was measured from samples taken from the lower chamber.

Insulin induced a small but significant decrease of approximately 20% in endothelial permeability that was not concentration dependent (Figure 3.3). This reduction was observed after 60 min of insulin stimulation (Figure 3.4), following an initial variable increase in permeability seen at earlier time-points (10 and 30 min). A maximum reduction of 40% in permeability to FITC-dextran was observed after stimulating HUVECs with insulin for 4 h.
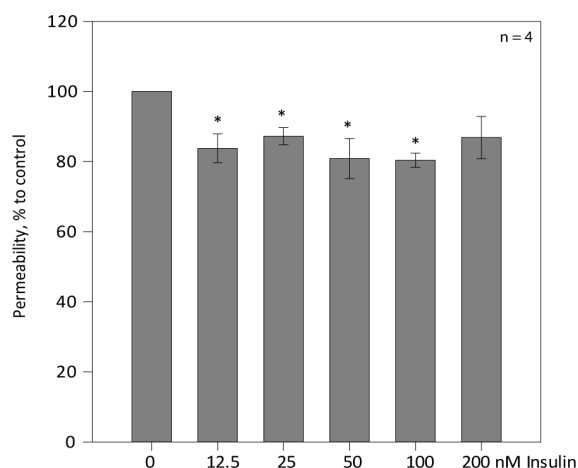
Figure 3.3 Insulin decreases basal endothelial cell permeability to FITC-dextran

HUVECs were seeded on Transwell™ filters (0.4 µm pore size) and incubated overnight at 37 °C. Cells were incubated in medium containing 1% FCS for 4 h and then treated with various insulin concentrations (0 – 200 nM) for 30 min. FITC-dextran (0.1 mg/ml) was added to the upper chamber and the lower chamber fluorescence was measured after 60 min. Fluorescence was measured for triplicate wells and quantified as a percentage relative to control. Data shown are the mean of four independent experiments ± SEM. * $p < 0.05$; One-way ANOVA (Holm-Sidak method).
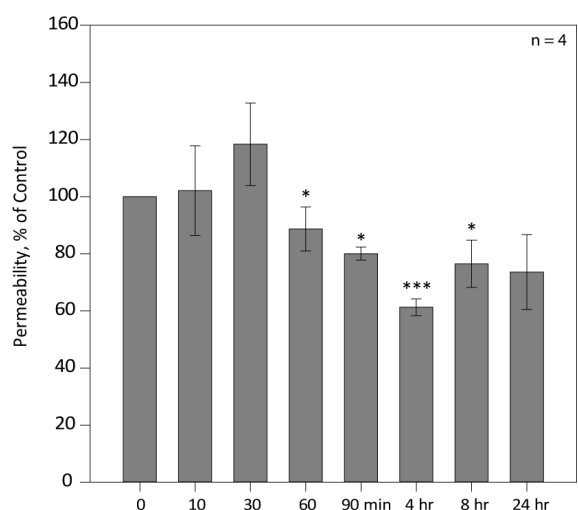
Figure 3.4 Effect of insulin on endothelial cell permeability over 24 hours

HUVECs were seeded on Transwell™ filters (0.4 µm pore size) and incubated overnight at 37 °C. Cells were incubated in medium containing 1% FCS for 2 h prior to being treated with insulin (100 nM) for the various time-points. For early time-points (0, 10, 30, 60 min) FITC-dextran (0.1 mg/ml) was added to the upper chamber 60 min before measuring fluorescence in the lower chamber. For time-points up to 90 min, and from 4 to 24 h; FITC-dextran was added to the upper chamber in the final 60 min. Fluorescence was measured for triplicate wells and quantified as a percentage relative to control. Data shown are the mean of four independent experiments ± SEM. * $p < 0.05$, ***$p < 0.001$; 2-way-paired t-test.

3.3.2   Effect of insulin on HUVEC morphology

The distribution of F-actin within ECs as well as the cell-cell junctions can be altered by a number of inflammatory mediators resulting in changes in endothelial morphology (Dejana and Giampietro, 2012; Esser et al., 1998; McKenzie and Ridley, 2007). After observing insulin-induced permeability changes in ECs (Figure 3.3 and Figure 3.4), the effects of insulin stimulation on cell morphology were investigated by immunofluorescent staining. Confluent HUVEC monolayers were incubated in EBM2 medium containing 1% FCS for 4 h and stimulated with various concentrations (0 to 200 nM) of insulin for 10 min (Figure 3.5). HUVECs were also stimulated with insulin (100 nM) over a period of time (0, 1, 4, 16 and 24 h) (Figure 3.6). Unstimulated control HUVECs displayed a round cobblestone-like morphology with bundles of actin filaments enriched along the cell-cell boundaries (yellow asterisk, Figure 3.6). VE-cadherin staining was localized linearly along cell–cell borders and with a wider reticular distribution where adjacent cells overlapped (white arrows, Figure 3.5). No noticeable changes were observed in HUVEC morphology after 10 min of insulin stimulation at various insulin concentrations (Figure 3.5). This time-point was optimal for Akt phosphorylation (Figure 3.2), however may not have been long enough to induce cytoskeletal changes. When cells were stimulated for longer periods of time (1 to 24 h), insulin induced an increase in peripheral F-actin bundles (red boxes, Figure 3.6), with the greatest increase observed at 4 h of stimulation, however this increase was not quantitatively assessed.
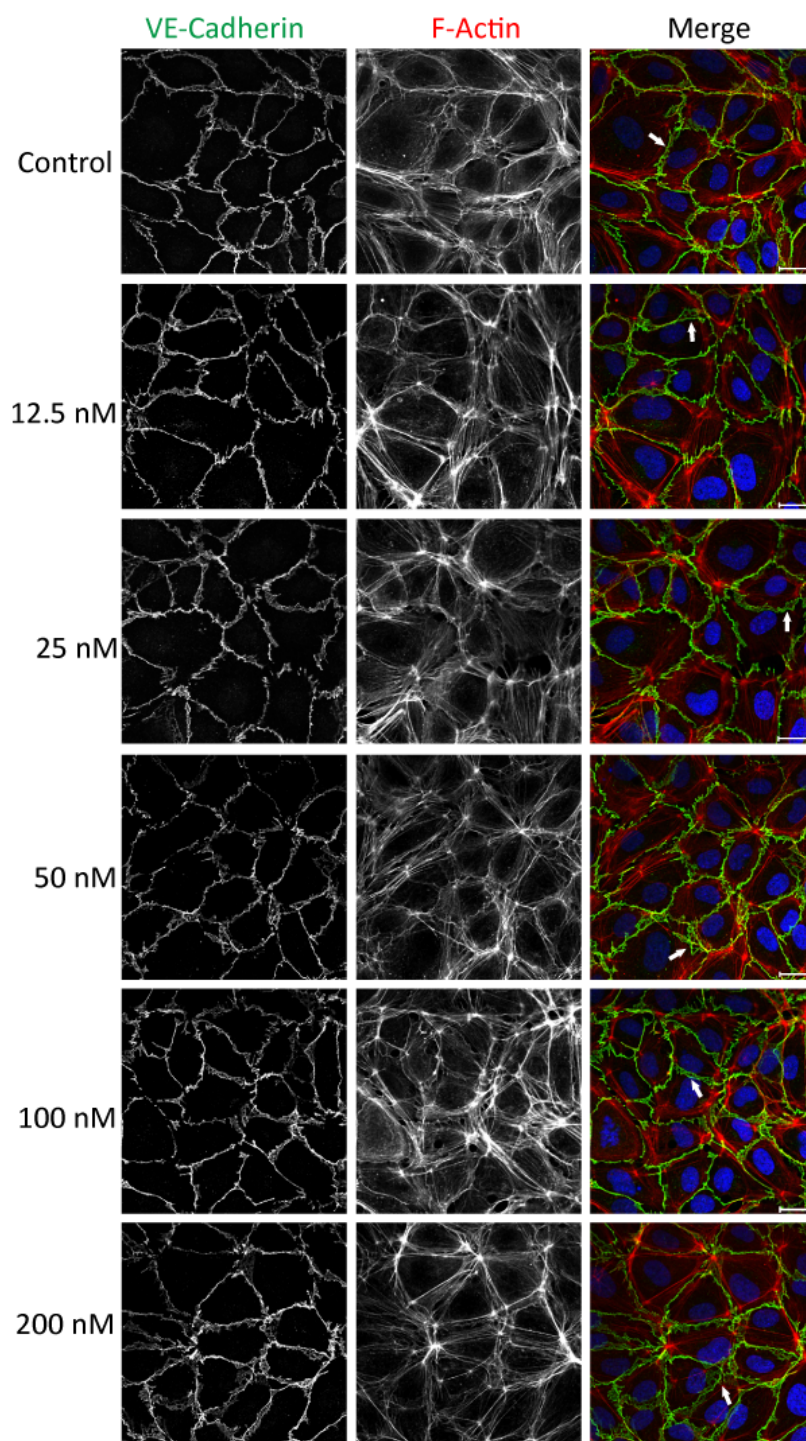
Figure 3.5 Insulin does not induce any major changes in HUVEC morphology at early time-points

Immunofluorescence micrographs of confluent HUVECs treated with insulin (0 to 200 nM) for 10 min after incubation in low serum conditions (EBM-2 containing 1% FBS, 4 h). Cells were stained with VE-cadherin for adherens junctions (green in merge), Alexa Fluor 546-conjugated phalloidin for F-actin (red in merge), and DAPI for nuclei (blue in merge). White arrows indicate reticular junctions. Images were acquired by confocal microscopy with a 63x oil immersion objective and are representative of random fields from three independent experiments. Scale bars are 20 μm.
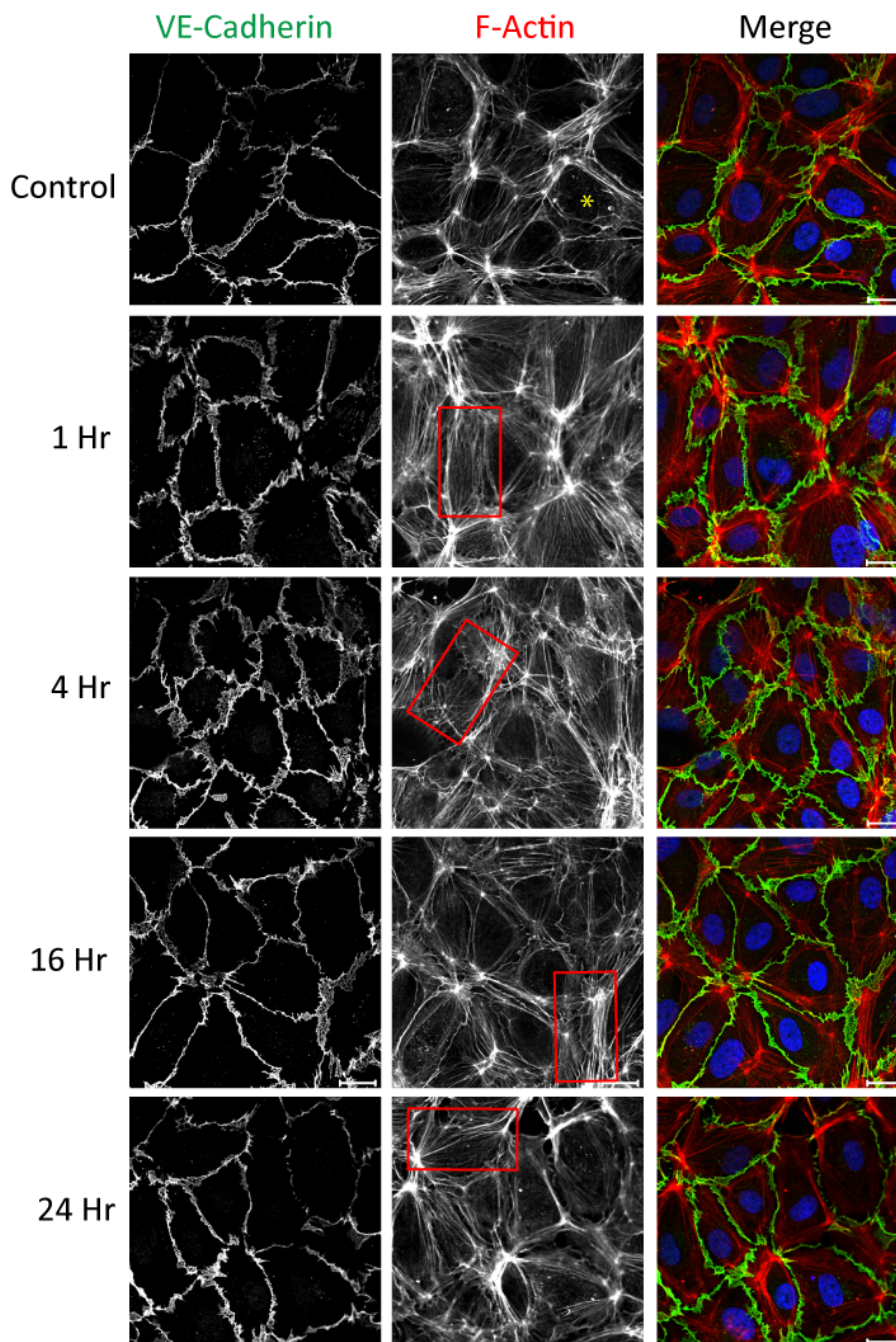
Figure 3.6 Insulin increases peripheral F-actin in HUVECs

Immunofluorescence micrographs of confluent HUVECs treated with insulin (100 nM) at various time points (0 to 24 h), following incubation in low serum conditions (EBM2 containing 1% FCS) for 4 h. Cells were stained with VE-cadherin for adherens junctions (green in merge), Alexa Fluor 546-conjugated phalloidin for F-actin (red in merge), and DAPI for nuclei (blue in merge). Yellow asterisk shows regular F-actin arrangement in untreated control cells, with actin filaments enriched along the cell-cell boundaries. Red boxes indicate increased peripheral F-actin in insulin-treated cells. Images were acquired by confocal microscopy with a 63x oil immersion objective and are maximum intensity projections of 10 confocal z-stacks, spanning 4 μm with 0.4 μm intervals between each image. Images are representative of random fields from three independent experiments. Scale bars are 20 μm.

3.4   Insulin increases cell migration in a wound healing assay

Cell migration is essential for a variety of physiologic processes such as tissue repair and regeneration. Wound healing is a dynamic, interactive process that consists of three phases: inflammation, tissue formation and tissue remodelling (Chen et al., 2012). The inflammatory phase is composed of a series of events including coagulation, release of vasoactive substances, chemokines, and cytokines that are important for regulating the consequential phases of proliferation and remodelling (Schreml et al., 2010). PI3K/Akt signalling is activated during these phases, and is also required for cell migration and survival.

A commonly used method to assess cell migration *in vitro* is the scratch assay, which measures the movement of cells into a wound made by a physical scratch through the confluent endothelial monolayer. However, results can be highly variable due to the inconsistency of the wounds created and the scratch could damage the underlying extracellular matrix affecting cell migration. The Oris™ Cell Migration Assay creates a reproducible cell-free area with uniform dimensions with the use silicone stoppers that act as barriers when cells are seeded into the well (Gough et al., 2011). It is a particularly useful assay for studying EC migration, as these cells tend to migrate collectively rather than as individual cells, for which random migration assays are primarily used. The ORIS™ cell migration assay was performed in order to investigate whether insulin would have an effect on EC migration. HUVECs were seeded onto wells in a FN-coated 96-well plate containing the central stoppers. After the cells attached and formed confluent monolayers, they were incubated in EBM2 medium containing 1% FCS for 4 h and treated with various concentrations of insulin (0 to 200 nM). The stoppers were removed to create a central cell-free area, the wells were imaged and the cells were incubated for 24 h and imaged again. More insulin-treated HUVECs migrated into the cell-free area than untreated control cells. Both the 50 nM and 100 nM insulin concentrations resulted in a 46% increase in cell migration, compared to untreated cells. These results suggest that insulin increases HUVEC migration in a dose-dependent manner (Figure 3.7).
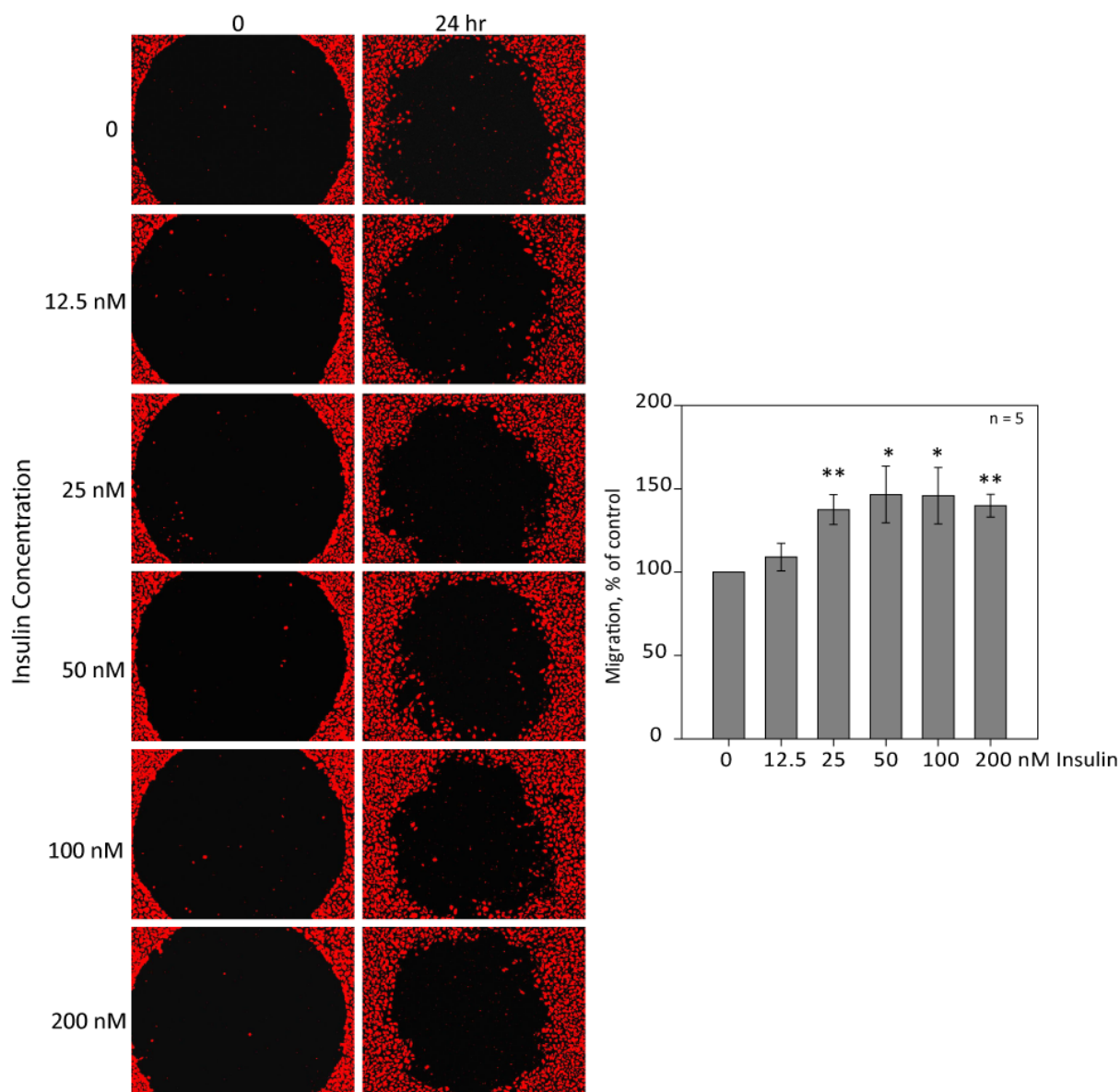
Figure 3.7 Insulin increases cell migration in a wound-healing assay

HUVECs were stained with Cell-Tracker Orange fluorescent dye, seeded in wells containing a central insert, and incubated for 16 to 18 h at 37°C. The cells were washed and incubated in low serum medium, EBM2 containing 1% FCS for 4 h. The insert was then removed to create a central wound in the monolayer, and imaged at 4x magnification (0 h). Insulin was added (0 to 200 nM) and cells incubated for 24 hours at 37°C. The wells were imaged again (24 h) using the saved locations of 0 h and the area of the wound closure was calculated using ImageJ software, as a percentage relative to unstimulated control cells. Data shown are the mean of five independent experiments ± SEM. *p<0.05, **p<0.005; 2-way-paired t-test.

3.5   Insulin stimulates angiogenic tube formation

Angiogenesis is the development of new blood vessels from pre-existing vessels that requires the proliferation, migration and remodelling of ECs (Lamalice et al., 2007). Neoangiogenesis is an essential process in wound healing (Schreml et al., 2010) and agents that stimulate angiogenesis can improve blood flow in patients with ischaemic diseases (Goodwin, 2007). When ECs are plated on a three-dimensional scaffold of extracellular matrix, they self-organise and differentiate into capillary-like networks (Ingber and Folkman, 1989; Risau, 1997). In order to study the effects of insulin on angiogenesis, an *in vitro* Matrigel-based assay was performed. HUVECs were incubated in EBM2 medium containing 1% FCS for 2 h before insulin stimulation and plating on Matrigel. When the HUVECs attach to the Matrigel they elongate and extend cellular processes to actively find other cells and form a well-organised network of loops. This requires many cytoskeletal changes as well as migratory mechanisms and the HUVECs were not able to cope with these demands for long periods of time in starving media. Therefore, a shorter starvation period of 2 h was required for this assay compared to other assays that are usually incubated in low serum conditions for 4 h. Insulin stimulation increased the number of angiogenic loops formed by the HUVECs in a dose-dependent manner, compared to unstimulated control cells in 24 h (Figure 3.8, Movies S1 and S2).

Previous studies have shown that insulin does not stimulate endothelial cell proliferation in 24 h (Liu et al., 2009), and therefore this increase is attributed to an increase in cell migration, which is consistent with the findings from the ORIS™ migration assay (Figure 3.7).
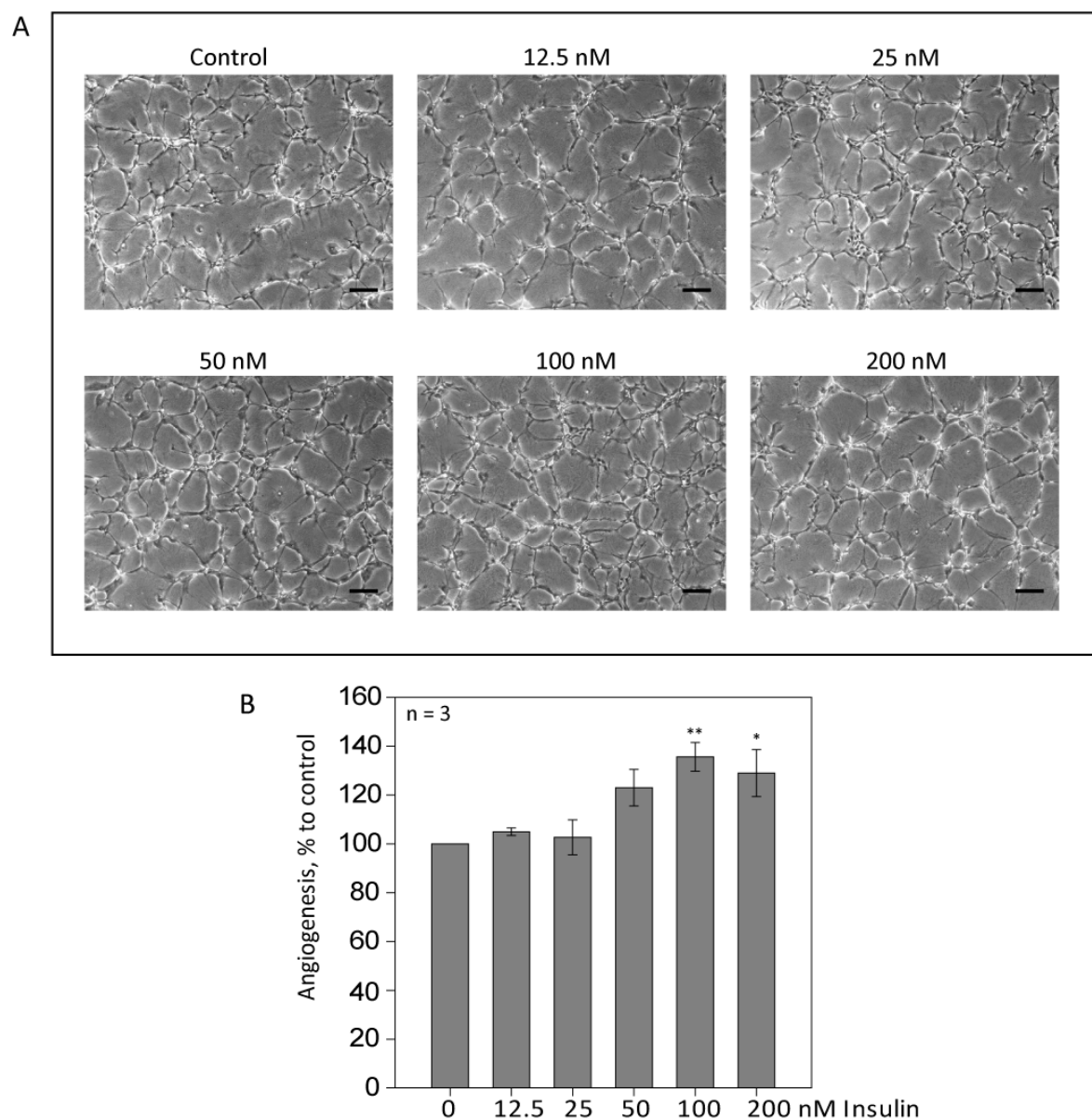
Figure 3.8 Insulin stimulates angiogenic loop formation

HUVECs were incubated in EBM2 medium containing 1% FCS for 2 h, and seeded onto polymerised Matrigel (4.5 mg/ml) in medium containing increasing concentrations of insulin (0 – 200 nM). Cells were incubated for 1 h and loop formation was monitored by time-lapse microscopy using a 4x objective, acquiring images every 20 min for 24 h. Representative images (A) are the final frames of angiogenic loops formed after 24 h. Quantification was performed by counting the total number of complete loops in the final frame of the movies, as a percentage relative to unstimulated control cells (B). Data shown are the mean of three independent experiments ± SEM. *p<0.05, **p<0.005; One-way ANOVA (Holm-Sidak method). Scale bar is 200 μm.

3.6   Discussion

Results in this chapter indicate that insulin affects endothelium barrier function and cell migration, which might be a consequence of changes to the actin cytoskeleton.

3.6.1   Insulin activates Akt in endothelial cells

Insulin mediates its effects by binding to its cell surface receptor, the insulin receptor (IR) (Nitert et al., 2005). ECs from different vascular beds are heterogeneous and differ in the surface receptor concentration and affinity for insulin. For example, arterial ECs have 2.5 times more insulin receptors than ECs isolated from veins (Bar et al., 1980). HUVECs are often used as a primary model for studies of the human endothelium and were chosen for this study because they were easily available and have been shown to specifically bind insulin (Bar et al., 1978). Large quantities of cells were required for the subsequent protein phosphorylation screen (see Chapter 4), and these levels were not attainable using primary cells. Therefore, HBMECs were used for the screen and included in the Akt activation biochemical analyses.

It was firstly necessary to establish the optimal conditions required to stimulate ECs with insulin. As most of the metabolic actions of insulin are mediated through the PI3K/Akt pathway (Hermann et al., 2000; Zeng et al., 2000), phosphorylated Akt (pAkt) was used as a read out. The limited insulin response detected in HUVECs compared to HBMECs could be attributed to lower levels of IR, described above. The variation between the response of the primary cells and the established cell line is interesting, and further investigation into the IR gene expression, ligand binding and receptor protein expression in HBMECs is required to determine if these differences could be attributed to IR levels. In a study that compared the expression of chemokine receptors and adhesion molecules in endothelia derived from different human tissues, levels of chemokine receptors varied according to the endothelial cell type with differences observed between HUVECs and HBMECs (Hillyer et al., 2003). Therefore, differences in the IR levels between the two cell types could also be possible, contributing to their variable response to insulin stimulation.

3.6.2 Insulin decreases endothelial permeability and induces cortical actin filament remodelling

Cultured ECs are often used to model the endothelium and elucidate the molecular mechanisms involved in regulating endothelial barrier function. Although these models show limited resemblance to real physiological structures and functions, they provide insight for testing mechanistic hypotheses related to cell signalling that regulate barrier function. The addition of insulin to endothelial monolayers demonstrates the ability of the endothelium to respond rapidly to chemical stimuli. Insulin stimulation initially resulted in a variable response in permeability. This increase in permeability might be attributable to the enhanced vesicle (caveolae) transcellular transport of insulin across the endothelium (King and Johnson, 1985; Wang et al., 2006). Although the exact transit pathway that transports insulin across ECs is not fully elucidated, it has been suggested that insulin remains within a vesicular compartment, that buds off from the luminal plasma membrane of the EC and moves to the abluminal side to subsequently fuse and release its content (reviewed in (Tuma and Hubbard, 2003). FITC-dextran molecules could have been incorporated in the vesicles and actively transported across the endothelial monolayer, until insulin equilibrium was achieved. It would be interesting to analyse endothelial permeability at these earlier time points using a more sensitive technique, such as measuring transendothelial electrical resistance, to fully investigate the initial permeability dynamics. Following this initial variability, stimulation with insulin resulted in a small, but significant decrease in endothelial permeability. The vasoprotective actions of insulin could be as a result of decreasing endothelial permeability induced by pro-inflammatory mediators, such as TNF-α (McKenzie and Ridley, 2007).

The permeability effects of insulin on the endothelium are usually associated with an increase in endothelial NO production through the PI3K pathway (Zeng and Quon, 1996). In smooth muscle cells, insulin inhibits Rho/ROCK-mediated actin-myosin contraction via a mechanism dependent on the presence of NO (Begum et al., 2002; Sandu et al., 2001). However, the role of NO in the regulation of endothelial barrier function is controversial (reviewed in (Yuan, 2006)). The debate

emerged from the observations that manipulation of endothelial NO production has biphasic characteristics and could be either beneficial (cardioprotective (Johnson et al., 1991; Ozaki et al., 2002; Rath et al., 2006)) or detrimental (cytotoxic (Bucci et al., 2005)) to vascular barrier properties depending on the stimulus, experimental conditions, vascular bed, time window and local concentration of NO (Yuan, 2006). Furthermore, eNOS activity is regulated by many other factors such as its intracellular localisation (Shaul, 2002), post-translational modifications as well as protein-protein interactions with other effector molecules (Sessa, 2005). These differences illustrate that the effect of NO is context dependent and can be influenced by other signalling pathways that are activated simultaneously by growth factors or inflammatory mediators (Murohara et al., 1998). Thus, the insulin-mediated changes in endothelial permeability are unlikely to be due solely to an increase in NO production.

A previous study has demonstrated that insulin increases endothelial barrier function in rat coronary microvascular ECs (Gunduz et al., 2010). This study observed that insulin induced an increase in the formation of the peripheral F-actin bundling along the edges of ECs and reduced stress fibre formation after 5 min of exposure. No actin cytoskeletal changes were observed when HUVECs were stimulated with insulin for 10 min, however increases in peripheral F-actin bundles was detected after 1 h. ECs are morphologically and functionally heterogeneous with greatest differences between those from the macro- and microcirculation in a variety of tissues (reviewed in (Garlanda and Dejana, 1997). These differences could result in the different kinetics reported for the microvascular cells and observed here with HUVECs, although both cell types would have to be simultaneously compared to confirm this. A recent study has shown that cortical actin filament remodelling occurs to facilitate the caveola-mediated trans-endothelial transport of insulin (Wang et al., 2012).

The Rho GTPase Rac1 is known to control F-actin organisation (Aspenstrom et al., 2004; Hall, 1998). Moreover, Rac1 is required for endothelial cell-cell junctional assembly and maturation (Lampugnani et al., 2002; Wojciak-Stothard et al., 2001).

Rac1 appears to be a critical component in insulin signalling. Insulin induced a 3-fold increase in Rac1 activation in microvascular ECs, and insulin-induced endothelial barrier stabilization was abolished when Rac1 was inhibited (Gunduz et al., 2010). Furthermore, genetic deletion of Rac1 in mouse lung ECs causes defective cell-cell contact organisation compared to control cells (Tan et al., 2008). Endothelia from different tissues vary considerably in their permeability characteristics (Simionescu et al., 2002). It would therefore be interesting to measure Rac1 activity in HUVECs, for example by pull downs using the region of Pak1 that binds to activated Rac1, as well as observing localised changes at the EC junctions using FRET analysis.

Stimulating microvascular ECs with insulin resulted a prominent increase in VE-cadherin staining at cell-cell junctions (Gunduz et al., 2010). No observable difference in the VE-cadherin staining was detected in the HUVECs, although VE-cadherin staining was not quantitatively assessed and subtle changes could be present.

In conclusion, insulin-induced actin cytoskeleton reorganisation could be linked to a decrease in basal endothelial permeability, however further experiments are needed to further examine this association. These cytoskeletal rearrangements could contribute to the anti-inflammatory actions of insulin.

3.6.3   Insulin increases EC migration in a wound healing assay and angiogenic tube formation

One of the hallmarks of diabetes is impaired wound healing (Brem and Tomic-Canic, 2007). Various animal models have demonstrated the importance of insulin for healing, with systematic insulin treatment accelerating healing in fractures, skin incision wounds and skin ulcers (Gregory, 1965; Hanam et al., 1983; Pierre et al., 1998; Rosenthal, 1968). Moreover, severe impairment of insulin signalling is observed in the wounds of diabetic mouse models (Goren et al., 2006). In correspondence with these findings, insulin dose-dependently increased HUVEC migration in an *in vitro* 'wound-healing' assay. Wound healing *in vivo* requires three phases: inflammation, tissue formation and tissue remodelling (Singer and Clark,

1999). Insulin has been shown to improve healing by contributing to both the inflammatory and tissue formation phases. Topical insulin application regulates the wound inflammatory response in a mouse excision model by inducing accelerated macrophage infiltration and inflammation resolution (Chen et al., 2012). However, the *in vitro* experiments performed in this study utilised Transwell assays without the presence of ECs. It would be interesting to investigate whether insulin treatment of ECs affects leucocyte transendothelial migration.

Once the inflammatory phase is controlled, the healing proceeds with granulation tissue development to generate new connective tissue and blood vessels within the wound (Liu et al., 2009). Angiogenesis provides oxygen and nutrients to the wounded area and is a critical process for optimal healing (Li et al., 2007). It requires the proliferation and migration of ECs (Hoeben et al., 2004). *In vitro* insulin stimulation of ECs on an extracellular matrix increased in angiogenic loop formation, suggesting that insulin is a stimulator of angiogenesis. This was similarly observed in a human microvascular endothelial cell line (HMEC-1) with insulin stimulating endothelial tube formation by increased cell migration and not proliferation (Liu et al., 2009). The *in vivo* model in this study further showed that the presence of insulin increased the vessel length as well as the number of branches present, which indicates vessel maturation. The authors found that insulin stimulated Rac1 translocation from the cytosol to the membrane where it localised to membrane ruffles in subconfluent cells. Furthermore, transfecting HMEC-1 with a dominant-negative form of Rac1 (Rac1-DN) abolished insulin-induced microvascular EC migration and angiogenesis (Liu et al., 2009). Interestingly, genetic deletion of Rac1 in mouse lung ECs causes reduced migration, tube formation and adhesion, compared to control cells (Tan et al., 2008). The importance of Rac1 in the cardiovascular system including its critical role in ECs is reviewed in (Sawada et al., 2010). Further analysis is required to establish if Rac1 contributes to HUVEC insulin-induced migration and angiogenic loop formation.

In conclusion, insulin induces EC migration and increases angiogenic tube formation. It would be interesting to test if these processes are dependent on the activation of Rac1.

4   Insulin stimulated binding of 14-3-3s to proteins in endothelial cells

4.1   Introduction

Protein kinase cascades provide the regulatory mechanisms for many essential processes. Insulin signals through phosphorylation cascades with most of its metabolic actions mediated via the highly conserved, tightly regulated PI3K/Akt pathway (Muniyappa et al., 2007) (see Chapter 1.3.2.1). The serine/threonine protein kinase Akt acts as a central regulator in insulin signalling through the phosphorylation of a wide variety of downstream substrates (Taniguchi et al., 2006). Akt has been identified as a critical node in insulin signalling (Taniguchi et al., 2006), and plays an important role in human physiology and disease (Manning and Cantley, 2007). Furthermore, the activation of PI3K and the subsequent generation of PIP_3 also activates other AGC family protein kinases, including PKA, PKG, PKC, ROCKs; serum and glucocorticoid-regulated kinase (SGK), p90RSK, and AMP-activated protein kinase (AMPK) (Tinti et al., 2012; Yaffe et al., 1997). The AGC kinases phosphorylate many downstream substrates at specific sites, which in some cases can create binding motifs for the phosphoprotein-binding 14-3-3 proteins (see section 1.6.2). Screening phosphopeptide libraries for sequences that display optimal binding to 14-3-3 revealed two high-affinity 14-3-3 binding motifs (Yaffe et al., 1997) (see section 1.6.2), with mode I motifs dominating in physiological 14-3-3-binding proteins. These motifs overlap with the substrate specificity of AGC kinases including Akt. This specificity means that the 14-3-3 proteins can be used to capture and identify new substrates of these protein kinases in cellular responses to growth factors and other stimuli (Dubois et al., 2009; Pozuelo Rubio et al., 2004).

Proteins that are phosphorylated in response to insulin can be purified using 14-3-3 affinity capture (Pozuelo Rubio et al., 2004). Not only does this technique identify new downstream targets of insulin signalling, but it also provides insight into the biological effects of 14-3-3s (Chen et al., 2011). Binding of 14-3-3s to their targets can trigger conformational changes, and can also alter how the binding proteins

interact with other proteins (see section 1.6.3). Therefore, identifying targets that bind to 14-3-3 proteins provides a good starting point for determining the mechanisms that are responsible for translating insulin-stimulated phosphorylation events into physiological actions and for mediating many of the actions of insulin (Chen et al., 2011).

4.2   Identification of insulin-induced 14-3-3 binding proteins in HBMECs

A large-scale 14-3-3 affinity purification was performed to identify phosphorylated targets of insulin signalling in ECs, using a method developed in the MacKintosh laboratory (Pozuelo Rubio et al., 2004). HBMECs were incubated in low serum conditions for 16 h (as previous described in sections 2.5.3 and 3.2) and either stimulated with insulin (100 nM) for 10 min or left unstimulated. Cells were lysed and extracts run through 14-3-3-Sepharose columns. Proteins that bound to 14-3-3s were eluted from the column by competition with a 14-3-3-binding phosphopeptide ARAApSAPA (see Figure 2.5). Figure 4.1 shows these eluted proteins after concentration of approximately 90 fold, SDS-PAGE separation and visualisation with colloidal Coomassie blue. 14-3-3-capture chromatography enriched several proteins compared to total cell extracts, however major differences between insulin-stimulated and control samples were not noticeable by eye. This is not uncommon as the sensitivity required to detect these changes is not achievable with Coomassie staining (Weiss et al., 2009). The lanes containing 14-3-3 column eluates were each excised from the gel in six segments for tryptic digestion and mass spectral analysis. Mass fingerprinting for protein identification was performed on the tryptic peptides by LC-MS-MS on a Thermo LTQ-Orbitrap system by staff at the MRC Protein Phosphorylation Unit mass spectrometry service (College of Life Sciences, University of Dundee). RAW files from Excalibur (Thermo) were processed by Raw2msm (Olsen et al., 2005) to generate peak lists that were analysed using the Mascot search engine (www.matrixscience.com) against the UniProt database (release 2012 03 (consisting of 535 248 sequences and 189 901

164 residues). The significance threshold was $p < 0.05$, only peptides with ion scores over 20 were considered and only proteins with at least one unique peptide (red bold in Mascot) were considered (see section 2.6.2). In total, 299 proteins were identified from the unstimulated control extract, and 390 proteins identified from the insulin-stimulated HBMEC extract. Supplementary Table 1 provides the full dataset of proteins identified in the screen. 14-3-3-binding proteins for which 14-3-3-binding sites have been established in the literature are known as 'gold standard' proteins. Seven 'gold standard' proteins were identified in this study (highlighted in red in Supplementary Table S1), as well as 26 established insulin mediators (highlighted in blue in Supplementary Table S1), such as Mitogen-activated protein kinase 1 and Insulin-degrading enzyme.
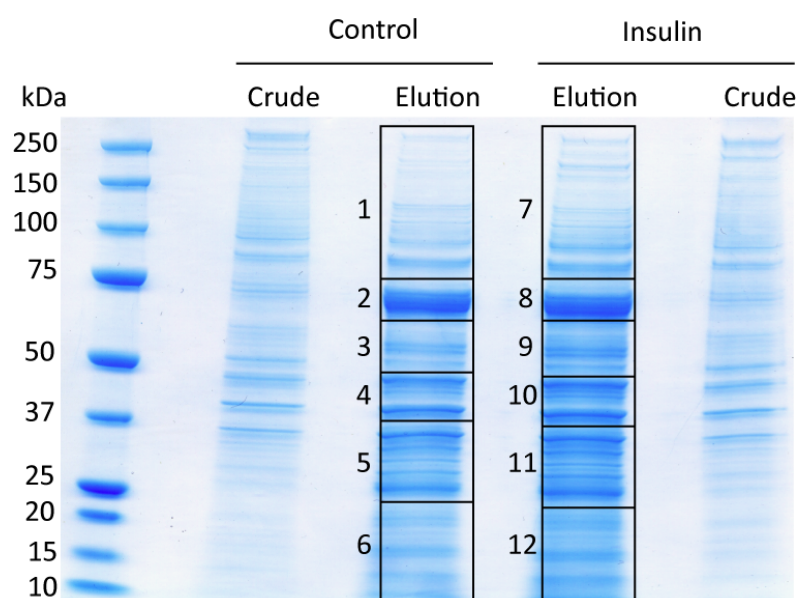
Figure 4.1 Coomassie-stained SDS-polyacrylamide gel of HBMEC proteins eluted from the 14-3-3-affinity chromatography columns
HBMECs were stimulated with insulin (100 nM) for 10 min, or left unstimulated (control) after incubation in DMEM containing 1% FCS for 16 h. Small aliquots of the protein lysates were stored for crude sample, and proteins in cell lysates were captured on 14-3-3-Sepharose. After washing, parallel elutions with 2 mM of the competitive phosphopeptide ARAApSAPA were performed. Following concentration in Vivaspin concentrators (10 000 MW cut-off), the eluted samples were separated on a 4–12% Bis-Tris SDS-polyacryamide gel and proteins were visualised using colloidal Coomassie blue. The two lanes were cut into six horizontal fragments (labelled 1-12) for tryptic digestion and mass spectral analysis.

In order to investigate how the 14-3-3-binding proteins isolated from ECs relate to all the currently known 14-3-3 partners, the data were compared to the 14-3-3 interactome of all known 14-3-3-binding partners to date (Figure 4.2). This interactome was created by Johnson *et al.* (2011), with data collated from publications that described one-interaction at a time, as well as high-throughput 14-3-3-affinity and mass spectrometry-based studies. Proteins identified in the present study were added to the database and transcribed into a VisANT graph (Hu et al., 2009) to identify the commonalities and differences among experiments. Each study was assigned a node (red), connected to all the proteins identified (green) in that study by grey lines. If identical proteins were identified in other studies, another grey line connects to it from that particular node, and orientates the protein between the two studies. Using the 'relaxed elegant' VisANT rule (Hu et al., 2004) proteins that were identified in at least 3 studies were placed in the centre of the figure, whereas proteins on the outer edges were unique to each of the individual studies. All known gold standard proteins are depicted in magenta (GD, Figure 4.2). Of the 433 14-3-3-binding proteins identified in this study (blue), 234 proteins were previously identified in other studies, and 199 proteins were unique (Figure 4.2).
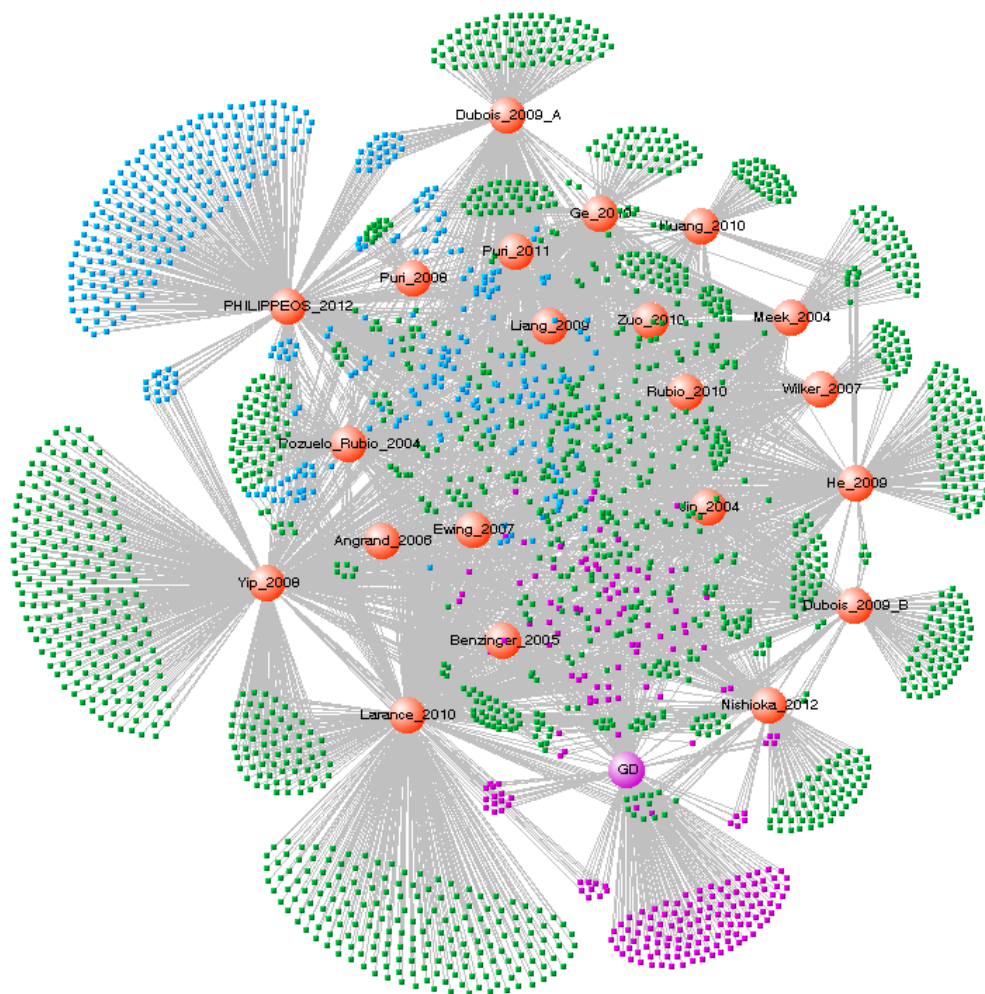
Figure 4.2 HBMEC 14-3-3-Binding partners in the relation to 14-3-3 interactome

A VisANT graph showing overlap between 14-3-3-captured proteins identified in HBMECs (Figure 4.1) and proteins identified for their affinity for 14-3-3s in proteomics screens reported in the literature (Johnson et al., 2011). Each study is assigned a node in red and grey lines connect the same proteins between studies, which are assigned as green nodes. Gold standard proteins (GD), for which 14-3-3-binding sites have been established, are depicted in magenta. Blue nodes are proteins identified in this HBMEC study. The 14-3-3-binding partners database was downloaded from the MacKintosh laboratory website: http://www.ppu.mrc.ac.uk/research/?pid=5&sub1=14-3-3%2BPartners

Changes in endothelial cell-cell junctions and the endothelial cytoskeleton are essential for vascular repair and inflammatory responses (see section 1.2.5). Since insulin stimulation decreased basal endothelial permeability, and increased EC migration and angiogenic loop formation (see Chapter 3), the next aim of the study was to identify proteins that regulate the effects of insulin on cell-cell junctions and cell migration. Among the 14-3-3-binding proteins identified in HBMECs, those involved in cytoskeletal regulation were therefore of particular interest, especially Rho family signalling components, as these proteins regulate actin cytoskeletal organization and intercellular junction integrity (Ridley, 2006). Twelve of the 14-3-3-binding proteins identified in HBMECs were shortlisted for further analysis based on their predicted roles in endothelial cytoskeletal regulation (Table 4.1). Proteins highlighted in blue were isolated in both insulin-stimulated and control lysates, and proteins highlighted in yellow were isolated from the insulin-stimulated cells only (Table 4.1). Transforming protein RhoA (RhoA), Ras-related C3 botulinum toxin substrate 3 (Rac3) and Cell division control protein 42 (Cdc42) are Rho GTPases. Rho guanine nucleotide exchange factor 16 (ARHGEF16) and Dedicator of cytokinesis protein 10 (DOK10) are guanine nucleotide exchange factors (GEFs, GTPase activators). RICH-1 and Parg1 are GTPase-activating proteins (GAPs, down regulators of GTPases); and Rho GDP-dissociation inhibitor 1 and 2 (GDIR1 and GDIR2) are Rho GDP dissociation inhibitors (RhoGDIs, sequestering GTPases in the cytoplasm). See section 1.4.1 for regulation of Rho GTPase activity. Epsin2 (EPN2) and Sec1 family domain-containing protein 1 (SCFD1) are proteins involved in clathrin-mediated endocytosis, and EPN2 has previously been shown to regulate Cdc42 signalling (Aguilar et al., 2006). LIM domain only protein 7 (LMO7) is a regulator of the myocardin-related transcription factors (MRTFs), and has recently been shown to play an important role in cell migration, requiring Rho GTPases (Hu et al., 2011).

		Protein Name	Abbreviation	
1		Transforming protein RhoA	RHOA	RhoGTPase
2		Ras-related C3 botulinum toxin substrate 3	RAC3	
3		Cell division control protein 42	CDC42	
4		Rho guanine nucleotide exchange factor 16	ARHGEF16	RhoGEF
5		Dedicator of cytokinesis protein 10	DOC10	
6		Rho GDP-dissociation inhibitor 1	GDIR1	RhoGDI
7		Rho GDP-dissociation inhibitor 2	GDIR2	
8		Rho GTPase-activating protein 17	RICH-1	RhoGAP
9		Rho GTPase-activating protein 29	PARG1	
10		Epsin2	EPN2	
11		Sec1 family domain-containing protein 1	SCFD1	
12		LIM domain only protein 7	LMO7	

Table 4.1 HBMEC 14-3-3-binding proteins shortlisted for further analysis

Mass spectral analysis identified 299 proteins in the control sample, and 390 proteins in the insulin-stimulated sample from the phosphopeptide elution of the 14-3-3-affinity chromatography. From these, 12 proteins were chosen for further analysis based on their predicted roles in endothelial cytoskeletal regulation. Proteins highlighted in blue were isolated in both insulin-stimulated and control lysates, and proteins highlighted in yellow were isolated from the insulin-stimulated cells only.

4.3   Validation of protein hits

Proteins isolated by 14-3-3 affinity capture include phosphoproteins that bind 14-3-3s directly, as well as proteins that bind 14-3-3s indirectly as components of multiprotein complexes. In order to test which of the twelve selected proteins bind directly to 14-3-3s and are regulated by insulin signalling, 14-3-3 far-Western overlay assays were performed (Moorhead et al., 1999). Validation analysis in HBMECs with insulin stimulation would have been ideal, however this was precluded by the low transfection rates and subtle insulin responses observed in HBMECs (see section 3.2). As the interaction between 14-3-3 proteins and their possible binding partners was the focus of these experiments, human embryonic kidney cells (HEK293) were chosen for their high transfection efficiency rates and ability to generate functional, mature proteins from plasmid vectors (Thomas and Smart, 2005). HEK293 cells express both IR and IGF-IR, which share a high similarity of structure and intracellular signalling events (Dupont and LeRoith, 2001). However, HEK293 cells are more sensitive to IGF-I stimulation (Beitner-Johnson and LeRoith, 1995; El-Shewy et al., 2007) and thus IGF-I was used for 14-3-3 binding validation analyses. A PI3K inhibitor (PI-103) (Knight et al., 2006) was included in these experiments to determine whether protein phosphorylation, and hence 14-3-3 binding, was stimulated via the PI3K/Akt pathway. GFP-fusion proteins for each of the proteins in Table 4.1 were over-expressed in HEK293 cells, which were serum starved for 16 to 18 h, and either treated with IGF-I, or PI-103 and then with IGF-I. The cells were lysed and proteins isolated by GFP immunoprecipitation, separated by SDS-PAGE, and transferred onto nitrocellulose membranes. Compared with conventional Western blots, Far-Westerns use digoxigenin (DIG)-labelled 14-3-3s in place of the primary antibody, followed by a horseradish peroxidase-conjugated anti-DIG antibody (Moorhead et al., 1999).

Vasodilator-stimulated phosphoprotein (VASP) was identified in this study (see Supplementary Table S1) and was included as a negative control in the 14-3-3 far-Western overlays, as it has been previously reported that VASP binding to 14-3-3 is not regulated by insulin (Dubois et al., 2009). Similarly, Pantothenate kinase 2

(PANK2) was included as a positive control (Figure 4.4), as it is an insulin-regulated 14-3-3-binding protein (MacKintosh laboratory, unpublished data). Of the twelve proteins selected from the 14-3-3-affinity purification, RhoA and ARHGEF16 did not bind to DIG-14-3-3 above background levels (Figure 4.3) and therefore most likely came down in multiprotein complexes or they bound non-specifically to the Sepharose. SCFD1, Rac3, GDIR1, GDIR2, Cdc42 and Dok10 were shown to bind directly to 14-3-3 proteins, but these interactions were not regulated by IGF-1 (Figure 4.3).

RICH-1, Parg1, EPN2 and LMO7 all bound directly to 14-3-3s and these interactions were increased by IGF-I stimulation and decreased by PI-103 (Figure 4.4). A small increase in 14-3-3 binding to RICH-1 and Parg1 in the Far-Western assay was observed when cells were stimulated with IGF-I, and so too was an increase in the co-immunoprecipitation of endogenous 14-3-3s with the test protein. 14-3-3 binding to EPN2 was increased when cells were stimulated by IGF-I, however this was not decreased when PI3K signalling was inhibited with PI-103. There are fifteen members of the PI3K family, and although PI-103 is a potent inhibitor of PI3K family members, it has selectivity toward PI3K class I isoforms (particularly p110α) and mTOR (Knight et al., 2006). Therefore it may be that the 14-3-3-binding sites of EPN2 are phosphorylated by PI3K-independent kinases stimulated by IGF-I. LMO7 binding to 14-3-3 was increased by IGF-I stimulation, and this was inhibited by PI-103 (Figure 4.4).
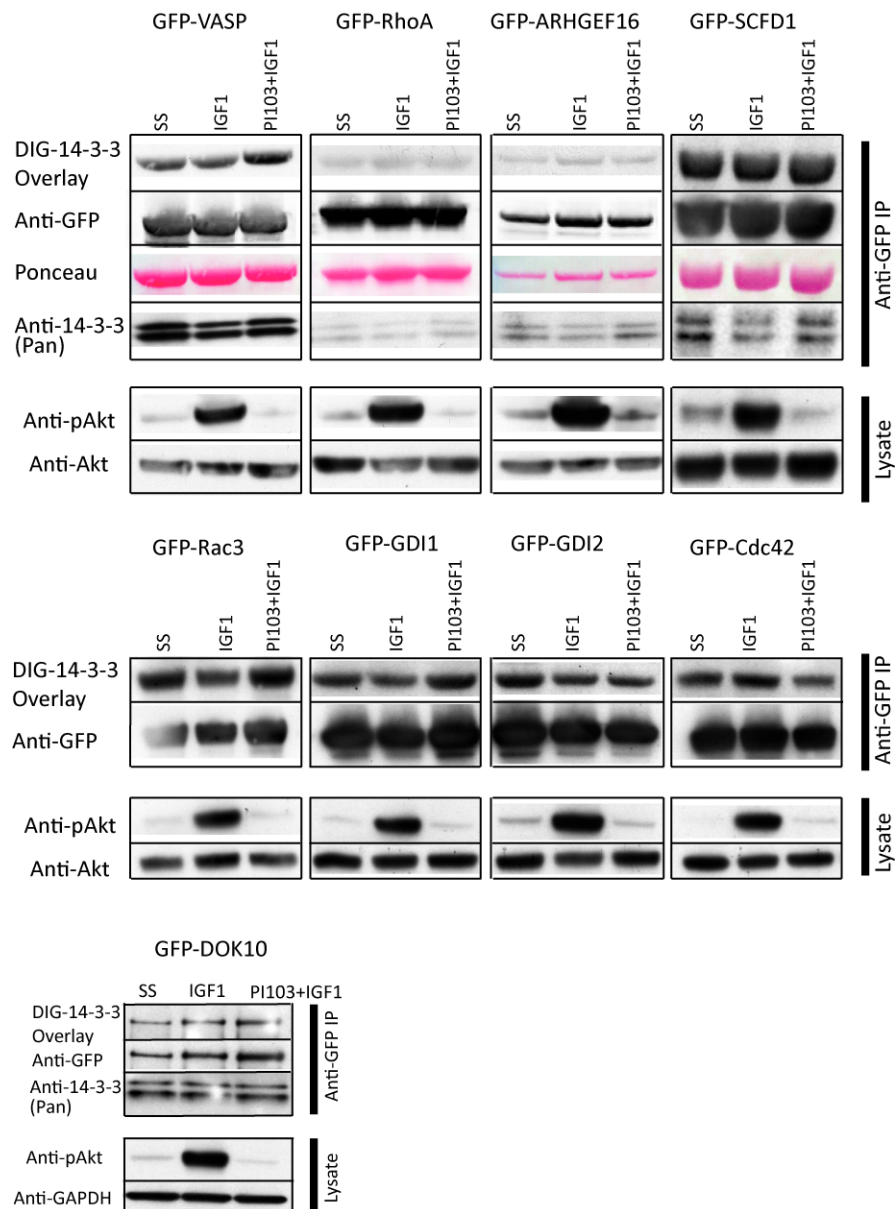
Figure 4.3 Proteins whose binding to 14-3-3 is not regulated by IGF-I in HEK293 cells

HEK293 cells were transfected to express GFP-fusions of proteins identified in the HBMEC 14-3-3-affinity capture experiment. After 24 h, cells were serum starved (ss) overnight and then treated with IGF-I for 20 min, or PI-103 and IGF-I for 30 min and 20 min, respectively. Cells were lysed and proteins enriched by anti-GFP immunoprecipitation. Samples were electrophoresed on 4–12% Bis-Tris SDS-polyacryamide gels and 14-3-3-overlays performed to observe direct binding of proteins to 14-3-3 in response to IGF-I stimulation. In some cases, immunoprecipitated proteins were also immunoblotted with a pan-14-3-3 antibody (Santa Cruz K-19) to detect endogenous 14-3-3-proteins that were pulled down with the overexpressed proteins of interest. Cell stimulation was confirmed by immunobloting with an antibody to pAkt. VASP was used as a negative control, as it is a known 14-3-3 binding protein, whose interaction is not regulated by insulin. Images are representative blots from three independent experiments.
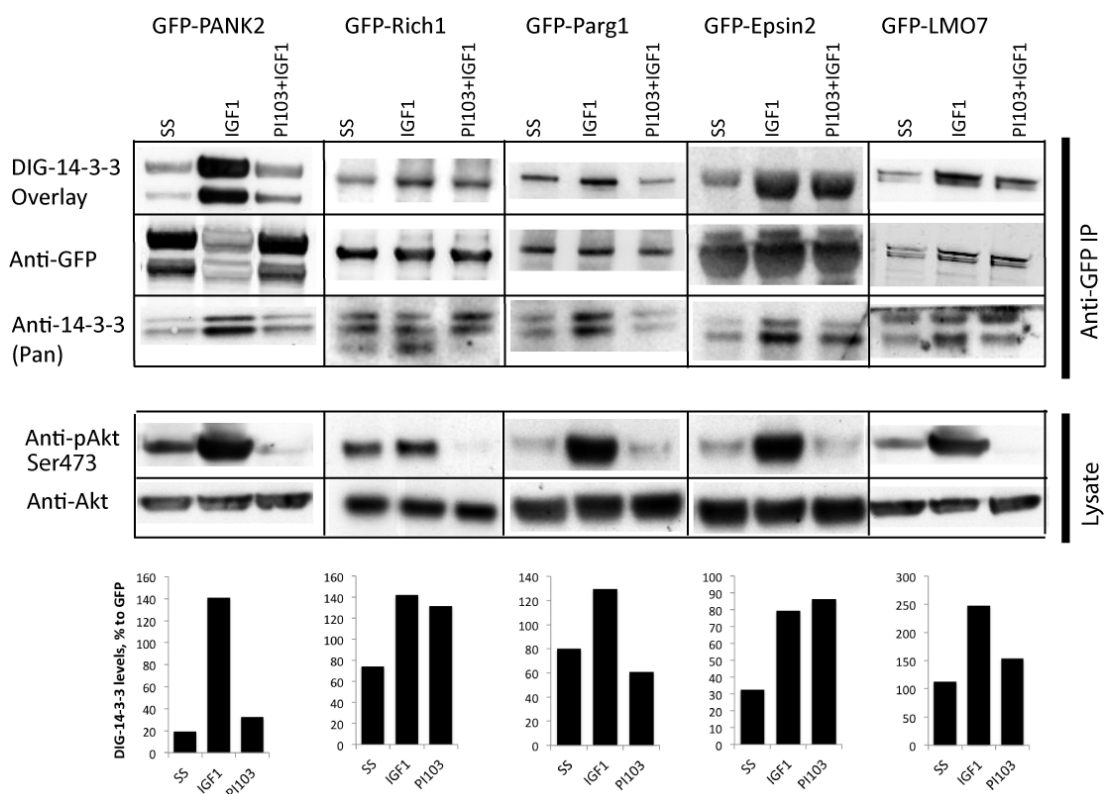
Figure 4.4 Proteins whose binding to 14-3-3 is stimulated by IGF-I

HEK293 cells were transfected to express GFP-fusions of proteins identified in the HBMEC 14-3-3-affinity capture. After 24 h, cells were serum starved (ss) overnight and then treated with IGF-1 for 20 min, or PI-103 followed by IGF-1 for 30 min and 20 min, respectively. Cells were lysed and proteins enriched by anti-GFP immunoprecipitation. Samples were run on SDS-PAGE gels and 14-3-3-overlays were performed to observe protein binding to 14-3-3 in response to IGF-1 stimulation. Immunoprecipitated proteins were also probed with a pan-14-3-3 antibody (Santa Cruz K-19) to detect endogenous 14-3-3-proteins that were pulled down with the overexpressed proteins of interest. Cell stimulation was confirmed by immunoblotting with an antibody to pAkt. PANK2 was used as a positive control, as it is a known insulin-regulated 14-3-3 binding protein. Graphs were generated from data analysed by densitometric scanning of DIG-14-3-3 from each representative Western blot above, normalised to GFP. Images and their respective quantitation are representative from three independent experiments.

4.4   Bioinformatic prediction of 14-3-3 binding sites

Much is already known about the sequences of 14-3-3-binding motifs in proteins, which can be translated into algorithms to predict potential phosphorylation sites. Together with the high affinity binding motifs (see section 1.6.2), there are other structural restrictions that have been identified. Generally 14-3-3-binding phosphosites must have at least one basic residue in the -3 to -5 positions relative to the phosphorylated serine or threonine, and never a +1 proline (Tinti et al., 2012; Yaffe et al., 1997). Several in silico methods are available to predict phosphosites on linear motifs ranging from simple consensus patterns and position-specific scoring matrix (PSSM) to more advanced machine-learning algorithms such as artificial neuronal networks (NetPhosK, (Hjerrild et al., 2004)) (reviewed in (Miller and Blom, 2009) and (Krogh, 2008)). PSSM is a sequence profile that represents the preference of particular amino acids surrounding the residue of interest (Miller and Blom, 2009).

Recently, Tinti *et al.* (2012) demonstrated that most well-defined human 14-3-3-binding proteins are 2R-ohnologues, which are protein-coding genes in families that were produced by two rounds of whole genome duplication at the origin of vertebrates, and usually consist of two to four members in a family. Aligning 14-3-3-binding proteins with their pro-orthologues from the invertebrate chordates identified lynchpins: 14-3-3-binding phosphosites that are conserved across members of a given family. Current experiments in the MacKintosh laboratory indicate that aligning the sequences of 14-3-3-binding proteins with other members of their 2R-ohnologue family and searching for potential lynchpins provides a better method of predicting 14-3-3-binding sites, compared with motif-based profile scanning alone. The search for lynchpins also takes account of physiological phosphorylation sites that are recorded in Phosphosite (www.phosphosite.org*)* *(Hornbeck et al., 2012)*. While these bioinformatics predictions are accelerating experimental identification of regulatory sites, they are not intended to substitute for experimental analyses. With this caution, Michele Tinti (University of Dundee) performed this method of sequence alignment for RICH-1, Parg1, Epsin2 and LMO7 to predict their candidate 14-3-3 phosphosites (Table 4.2).

Protein ID	Description	Abbreviation	Candidate phosphorylation site(s)				
Q68EM7	ARHGAP17/RICH-1	RHG17_HUMAN	S595	T808			
Q52LW3	ARHGAP29/Parg1	RHG29_HUMAN	S607	S1019	S1144/ S1146		
O95208	Epsin2	EPN2_HUMAN	T272				
Q8WWI1	LIM domain only 7	LMO7_HUMAN	S300	T753	T780	S1493	S1510

Table 4.2 Summary of candidate 14-3-3-binding phosphosites for IGF-I-responsive 14-3-3-binding proteins

RICH-1 is predicted to have two potential 14-3-3-binding phosphosites, S595 and T808 (Figure 4.5). These were predicted by aligning sequences from ARHGAP44 (RICH-2), SH3 domain-binding protein 1, and from the genome sequence of amphioxus (lancelet, *Branchiostoma*), the least-derived living invertebrate relative of the vertebrates within the phylum Chordata (Tinti et al., 2012). Neither of these sites match the Akt consensus, and therefore could be phosphorylated by other AGC kinases activated by insulin.

The putative 14-3-3 binding phosphosites for Parg1 (S607; S1019; S1144/1146) were identified by aligning sequences from GEM-interacting protein, Minor histocompatibility protein HA-1 and sequences from invertebrates *Caenorhabditis, Cintestinalis, Branchiostoma floridae*, and *Trichoplax adhaerens* (Figure 4.6). S1019 and S1146 are identified to conform to Akt consensus sites when analysed on ScanSite 2.0 (Obenauer et al., 2003) using a medium stringency threshold, which indicates that the motif identified is within the top 1% of all matching sequences contained in the SwissProt vertebrate database.

Epsins are a conserved family of endocytic adapter proteins. When EPN2 was aligned with other members of the epsin family, as well as thirteen chordates, only T272 was identified as a potential 14-3-3-binding phosphosite (Figure 4.7). This site is highly conserved throughout the sequences, however is not a predicted Akt consensus site.

LMO7 has been identified in five previous high-throughput 14-3-3-binding studies (Benzinger et al., 2005; Dubois et al., 2009; Johnson et al., 2010; Larance et al., 2010; Meek et al., 2004). There are five putative 14-3-3-binding phosphosites (S300; T753; T780; S1493 and S1510), predicted by sequence alignment with LIM and calponin homology domains-containing protein 1, and four different chordates (Figure 4.8). S1493 is identified as an Akt consensus site using a high stringency threshold, which indicates that the motif identified is within the top 0.2% of all matching sequences contained in the SwissProt vertebrate database. S1510 matches Akt consensus under medium stringency.
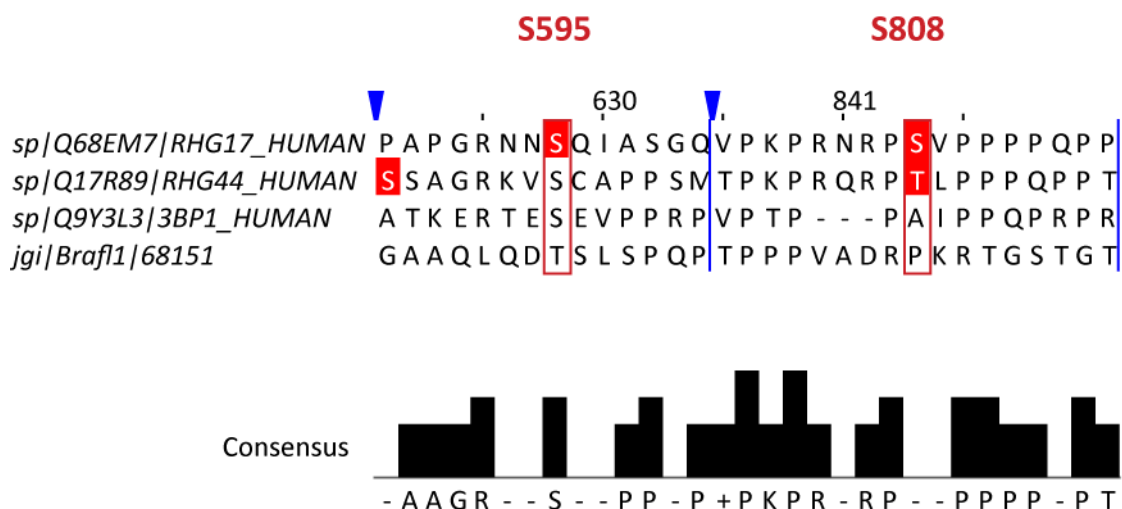
Figure 4.5 Bioinformatic prediction of 14-3-3 phosphorylation sites for ARHGAP17 (RICH-1)

The sequence of ARHGAP17 (RICH-1; RHG17) was aligned with ARHGAP44 (RICH-2), SH3 domain-binding protein 1 (3BP1), and amphioxus (lancelet, *Branchiostoma,* the last-derived living invertebrate relative of the vertebrates within the phylum Chordata) using Jalview (version 2.8, http://www.jalview.org/). Figure only depicts regions of the sequence that contain predicted 14-3-3-binding phosphosites (highlighted in red boxes, predicted by both neural network and position specific scoring matrix), with the alignment column number depicted above the sequences. Blue lines and arrows indicate where regions in the sequences were condensed. Full sequence alignments are provided on the compact disc (CD) in the supplementary.

Figure 4.6 Bioinformatic prediction of 14-3-3 phosphorylation sites for ARHGAP29 (Parg1)

The sequence of ARHGAP29 (Parg1, RHG29) was aligned with GEM-interacting protein (GMIP), Minor histocompatibility protein HA-1 (HMHA1) and homologous sequences from invertebrates *Caenorhabditis, Cintestinalis, Branchiostoma floridae*, and *Trichoplax adhaerens* using Jalview (version 2.8, http://www.jalview.org/). 14-3-3-binding phosphosites (red boxes) highlighted in light blue are predicted by either neural network or position specific scoring matrix; residues highlighted in red are predicted by both. Figure only depicts regions of the sequence that contain predicted 14-3-3-binding phosphosites, with the alignment column number depicted above the sequences. Blue lines and arrows indicate where regions in the sequences were condensed. Full sequence alignments are provided on the CD in the supplementary.

Figure 4.7 Bioinformatic prediction of 14-3-3 phosphorylation sites for Epsin2 (EPN2)
The sequence of EPN2 was aligned with other members of the human Epsin family as homologous sequences from 13 chordates using Jalview (version 2.8, http://www.jalview.org/). the putative 14-3-3-binding phosphosite highlighted in red, based on predictions from both network and position specific scoring matrix. The alignment column number is depicted ab sequences. Full sequence alignment is provided on the CD in the supplementary.
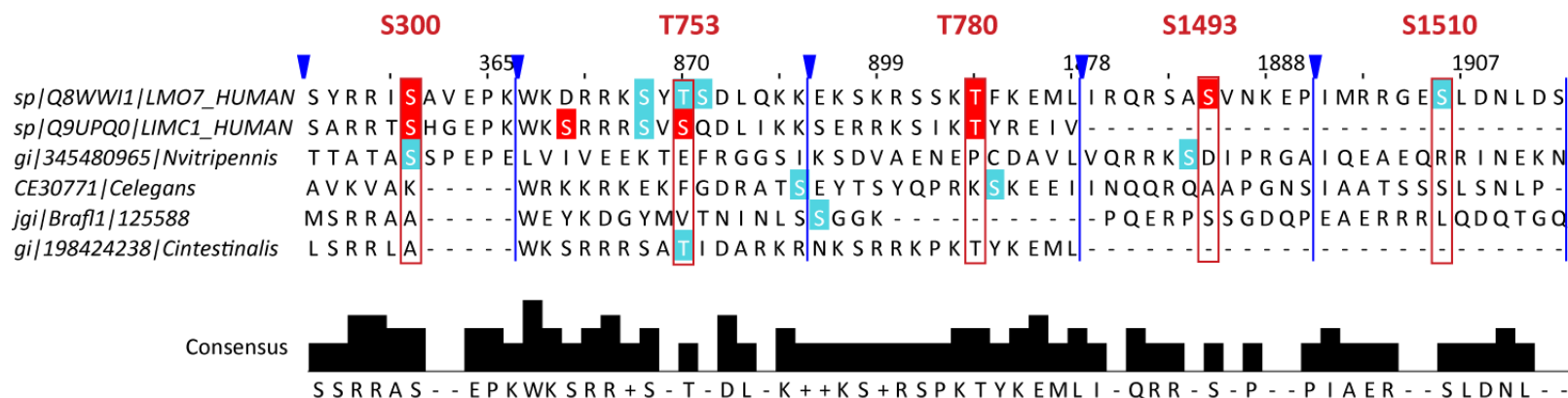
Figure 4.8 Bioinformatic prediction of 14-3-3 phosphorylation sites for LIM domain only 7 (LMO7)

The sequence of LMO7 was aligned with LIM and calponin homology domains-containing protein 1, and homologous sequences from four different chordates using Jalview (version 2.8, http://www.jalview.org/). The putative 14-3-3-binding phosphosites are highlighted in red boxes; blue residues are predicted by neural network or position specific scoring matrix and red residues predicted by both. Figure only depicts regions of the sequence that contain predicted 14-3-3-binding phosphosites, with the alignment column number depicted above the sequences. Blue lines and arrows indicate where regions in the sequences were condensed. Full sequence alignments are provided on the CD in the supplementary.

4.5   Discussion

Insulin exerts most of its metabolic actions by protein phosphorylation cascades through the PI3K/Akt pathway, which plays an essential role in regulating many biological processes. Most metabolic pathways are mapped using a reverse discovery method, whereby the metabolic action is identified and used as the end point to determine the upstream signalling. However, a forward method of discovery is possible by using 14-3-3 proteins as bait to identify novel insulin-responsive proteins (Larance et al., 2010). The phosphorylation of many AGC protein kinase substrates creates a docking site for 14-3-3 protein family members (Johnson et al., 2010) and this high affinity binding specificity was used to identify insulin-stimulated protein phosphorylation changes in ECs. Although 14-3-3 proteins do not bind to phosphorylated tyrosines or to phosphorylated serines and threonines that are followed by proline residues (Chen et al., 2011), this method captures many of the phosphorylation changes stimulated by insulin. Whilst the raw data from the screen is likely to contain false positives/negatives, the use of 14-3-3-phosphoproteomics has been used previously to identify many proteins that bind to 14-3-3 proteins in response to signalling pathways that are activated by insulin (Dubois et al., 2009; Larance et al., 2010). The screen provides a good starting point to identify several candidates, which can then be validated with biochemical techniques as novel targets of the insulin PI3K/Akt signalling pathway.

A visual representation of the 14-3-3 binding proteins isolated from ECs in relation to other published 14-3-3-phosphoproteomics screens best demonstrates the similarities and differences observed between 14-3-3 screens (see Figure 4.2). Each study identifies new proteins, but sometimes also fails to recognise proteins discovered in other studies. Interestingly, this even occurs when studies are compared using the same experimental conditions (Johnson et al., 2010). These discrepancies are to be expected as a consequence of all the variables involved in proteomic methods and mass spectrometry. Therefore 14-3-3 binding proteins only identified in this study and not others may not necessarily be unique to ECs, but the screen provided interesting candidates to study functionally in ECs. The

identification of seven known 14-3-3 'gold standard' proteins, such as Yorkie, Cofilin and Myosin phosphatase-targeting subunit 1 (MYPT1), in the screen was encouraging and added a level of confidence to the protein hits identified. The positioning of a specific protein in the VisANT graph does not increase its prediction as a valid 14-3-3 binding protein, as 'gold standard' proteins are distributed both in the centre and periphery of the graph (Johnson et al., 2010).

4.5.1 **Selection of potential actin cytoskeleton regulators**

After observing that insulin was able to induce some cytoskeletal changes in ECs and to enhance barrier function (see section 3.3.1), increase cell migration (see section 3.4) and increase angiogenic loop formation (see section 3.5), particular interest was placed on the Rho family small GTPases and their effectors. It is well established that members of the Rho GTPase family are key regulators of the actin cytoskeleton (reviewed in (Heasman and Ridley, 2008) that can also contribute to cell survival (see section 1.4). Thus, these molecular switches could mediate the anti-inflammatory and protective effects of insulin on the endothelium. Furthermore, protein phosphorylation and the subsequent binding of 14-3-3s could regulate the activity of Rho GTPase signalling pathways.

Biochemical validation of the potential 14-3-3 binding proteins identified in the screen revealed that insulin signalling was more likely to affect regulators of the typical Rho GTPases (particularly the GAPs), rather than the Rho GTPases themselves. This does not appear to be the case with the atypical members of the Rho GTPase family, as it was recently demonstrated that 14-3-3 proteins regulate the activity of the constitutively GTP-bound Rnd3 when phosphorylated by ROCK and PKC (Riou et al., 2013). RhoA, Rac3 and Cdc42 were identified in the screen, however 14-3-3 binding was not affected by IGF-I stimulation and PI3K inhibition. This was particularly surprising for Rac3, which had previously been identified in a high throughput 14-3-3 screen in HeLa cells +/- insulin. Rac3 had a high isotope differential (d_0/d_4) ratio, suggesting that insulin enhanced Rac3 binding to 14-3-3 when compared to unstimulated cells (Dubois et al., 2009). However, this

prediction was not further validated in that study, and changes in 14-3-3 binding were not observed in Far-Western overlays when HEK293 cells were stimulated with IGF-I or when PI3K was inhibited in this study. It would be interesting to investigate whether differences in 14-3-3 binding to Rac3 occur in 14-3-3 Far-Western overlays using HeLa cells stimulated with insulin.

As described in Chapter 1.4.1, there are two types of RhoGEFs, Dbl family and DOCK family GEFs. It is interesting that members of both classes were identified as potential 14-3-3-binding proteins in ECs. ARHGEF16, also known as Ephexin4, has been identified as a Dbl family GEF for RhoG and has been shown to play a role in cell migration in breast cancer (Hiramoto-Yamaki et al., 2010). DOCK10, a member of the other family of RhoGEFs, was also previously shown to play a role in cancer cell migration through the activation of Cdc42 (Gadea et al., 2008). Both GEFs were selected to identify if they were involved in the pathways that increased cell migration when ECs are stimulated with insulin (see section 3.4). ARHGEF16 had previously been identified in other high throughput 14-3-3 affinity studies (Ewing et al., 2007; Meek et al., 2004; Pozuelo Rubio et al., 2004) in HeLa and HEK293 cell lines without insulin stimulation. However, those studies did not further validate this interaction. In my hands, ARHGEF16 did not interact directly with 14-3-3 in 14-3-3 Far Western overlays. In contrast to ARHGEF16, DOCK10 directly interacted with 14-3-3; however this interaction was not regulated by insulin via the PI3K/Akt pathway, and therefore neither protein was investigated further.

4.5.2 **IGF-I responsive 14-3-3 binding**

The two RhoGAPs identified in this study, RICH-1 and Parg1, have never previously been identified as 14-3-3 binding partners. Although there was only a subtle increase in 14-3-3 binding with IGF-I stimulation, these changes could possibly contribute to the cytoskeletal changes observed in Chapter 3, and were therefore selected for further functional analysis (see Chapter 5). The interaction of RhoGAPs with 14-3-3 proteins was previously shown to play a key role in regulating cell motility (Rowland et al., 2011). RhoGAP22 was identified as an Akt substrate that

binds to 14-3-3 proteins when stimulated by insulin. This insulin-responsive 14-3-3-RhoGAP22 interaction negatively regulates the GAP activity of RhoGAP22, modulating the GTP loading of Rac1 and thereby affecting actin turnover and cell motility (Rowland et al., 2011).

Phosphorylation of Epsin2 and LMO7 by IGF-I also resulted in an increase in 14-3-3 binding. Epsin2 had previously been identified in a 14-3-3 phosphoproteome screen of muscle cells stimulated with insulin (Larance et al., 2010), as well as in a proteomic analysis of insulin-regulated 14-3-3-interacting proteins in insulin-sensitive tissues (Yip et al., 2008). Neither of these studies pursued the functional role of Epsin2 in insulin signalling.

Similarly, LMO7 was previously identified in five high-throughput studies (Benzinger et al., 2005; Dubois et al., 2009; Johnson et al., 2010; Larance et al., 2010; Meek et al., 2004). Moreover, LMO7 had a high isotope differential (d_0/d_4) ratio between HeLa cells stimulated with insulin and unstimulated control cells, suggesting that insulin enhances LMO7 binding to 14-3-3 (Dubois et al., 2009). Biochemical validation confirmed this prediction and thus further analysis of the functional role of LMO7 in insulin signalling in ECs was investigated (see Chapter 5.4).

In summary, 14-3-3-affinity purification is an effective method to identify novel insulin-responsive proteins. RICH-1, Parg1, LMO7 and Epsin2 were positively validated as insulin-sensitive 14-3-3-binding proteins, and their functional roles in ECs are described in Chapter 5. It would be interesting to investigate the specific roles of 14-3-3 proteins in these insulin signalling pathways, through mutagenesis of the candidate 14-3-3-binding phosphosites identified by bioinformatic analysis.

5   Investigating the roles of insulin-stimulated 14-3-3 binding protein hits in endothelial cells

5.1   Introduction

The number of proteins isolated from insulin-stimulated endothelial cells in the 14-3-3-affinity screen in Chapter 4 attests to the many proteins that insulin regulates. Of the 12 proteins short-listed for further validation, RICH-1, Parg1, LMO7 and Epsin2 showed increased direct binding to 14-3-3 proteins when stimulated with IGF-I, and this effect was PI3K dependent. This chapter describes a number of functional assays performed with these proteins in order to gain further insight into their roles in endothelial cells.

5.2   ARHGAP17 / RICH-1

Rho GTPases are critical regulators of dynamic cytoskeletal changes (reviewed in Ridley, 2006). The ability of these proteins to function as molecular switches is due to their capacity to cycle between an active GTP-bound and inactive GDP-bound state. Three protein families tightly regulate this cycling: GEFs (guanine nucleotide-exchange factors), GAPs (GTPase-activating proteins) and GDIs (guanine nucleotide-dissociation inhibitors) (see section 1.4.1). The GAPs inactivate Rho GTPases by stimulating their intrinsic GTPase activity, leading to the hydrolysis of the γ -GTP and consequently to the inactivation of the protein (Lamarche and Hall, 1994; Moon and Zheng, 2003). It has been predicted that there are approximately 2- to 3-fold more GAPs compared to the GTPases they regulate, with the human genome encoding between 59 and 70 proteins with a RhoGAP domain (Tcherkezian and Lamarche-Vane, 2007). It has been suggested that this abundance is due to several reasons: i) some GAPs are preferentially expressed in specific tissues, and/or localised at specific sites within the cell; ii) GAPs could act specifically on a single GTPase or in specific signalling complexes; iii) GAPs could selectively regulate specific Rho GTPase signalling pathways; or iv) GAPs could act as effectors or

scaffold proteins that mediate cross-talk between Rho GTPases and other signalling pathways (Tcherkezian and Lamarche-Vane, 2007).

ARHGAP17 was identified in a two-hybrid screen for cDNAs encoding proteins that bound to the Src homology 3 domain of Cdc42-interacting protein 4 (CIP4) (Richnau and Aspenstrom, 2001). It was named RICH-1 (*R*hoGAP *i*nteracting with *C*IP4 *h*omologues) and found to have homology with KIAA0672 (RICH-2, ARHGAP44), the rat protein Nadrin (neuron-associated developmentally regulated protein) and mouse Abl-binding protein 3BP-1 (SH3-binding protein 1, (Cicchetti et al., 1992; Harada et al., 2000; Richnau and Aspenstrom, 2001)). All four proteins contain an N-terminal Bin/amphiphysin/Rvs (BAR) domain (first recognised as a conserved domain in BIN1, amphiphysins and the yeast proteins Rvs167p and Rvs161p (David et al., 1994)), followed by a RhoGAP domain and C-terminal proline-rich region (Figure 5.1). These similarities suggest that RICH-1, RICH-2, Nadrin and 3BP-1 form a closely related family of RhoGAPs (Richnau and Aspenstrom, 2001). The GAP domains of all four proteins have been shown to be functionally similar by stimulating the GTP hydrolysis of Cdc42 and Rac1, *in vitro*, and Nadrin also has some activity towards RhoA (Harada et al., 2000).
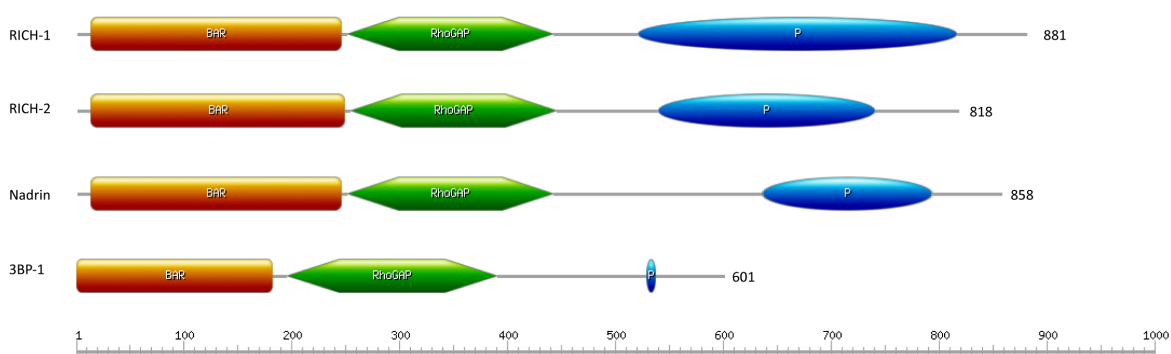
Figure 5.1 Protein homology between RICH-1, RICH-2, Nadrin and 3BP-1.
Functional domain similarities group RICH-1, RICH-2, Nadrin and 3BP-1 into a RhoGAP subfamily. Each contain a BAR (Bin/amphiphysin/Rvs) domain (orange), a RhoGAP domain (green) and a proline-rich region (p, blue).

RICH-1 is expressed in many tissues, but has particularly high expression levels in the heart, placenta and skeletal muscle (Richnau and Aspenstrom, 2001). Initial GTPase activation and nucleotide exchange assays revealed that the RhoGAP domain of RICH-1 stimulated the GTP hydrolysis of both Rac1 and Cdc42, but had no effect on RhoA. This observation was confirmed in GTPase binding domain pull-down assays, following expression of the RhoGAP domain or a catalytically inactive mutant of RICH-1 in PAE/PDGFRβ cells (Richnau and Aspenstrom, 2001). However, when RICH-1 GAP activity was measured in epithelial cells using Raichu FRET probes and GTPase binding domain pull-down assays, RICH-1 was only able to reduce the levels of Cdc42-GTP, but had no effect on Rac1 or RhoA (Wells et al., 2006). This observation suggests that RICH-1 may have cell specific functionality. The role of RICH-1 in endothelial cells has yet to be determined.

5.2.1 GFP-RICH-1 over-expression localises at the membrane in migrating endothelial cells

Investigating the localisation of proteins at the sub-cellular level leads to a better understanding of protein function, interaction networks and cellular signalling pathways (Stadler et al., 2013). The localisation of RICH-1 in endothelial cells was determined by transiently transfecting HUVECs with an expression plasmid encoding GFP-tagged RICH-1, then seeding onto fibronectin (FN)-coated glass coverslips. Cells were fixed and stained for F-actin and cell-cell junction proteins at 24 h. GFP-RICH-1 displayed a cytoplasmic distribution (Figure 5.2, Figure 5.3 and Figure 5.4) with no obvious effect on the organisation of the actin cytoskeleton, when compared to GFP-transfected HUVECs. RICH-1 localised at the plasma membrane in lamellipodia (indicated by the blue arrows in Figure 5.2) in sub-confluent HUVECs. However, it did not localise to cell-cell junctions in confluent monolayers (Figure 5.3 and Figure 5.4) suggesting that RICH-1 might be required at the membrane to regulate lamellipodial protrusion. Over-expression of GFP-RICH-1 did not disrupt cell-cell adherens junctions visualised by continuous vascular-endothelial cadherin (VE-cadherin) staining linearly along cell-cell borders (indicated by yellow arrow-heads in Figure 5.3). Tight junctions were also maintained, as shown by linear ZO-1 staining along the cell-cell boundaries (blue arrows, Figure 5.3). However, tight junctions were slightly disrupted at the apical and basolateral regions of the unstimulated cells (red arrowheads, Figure 5.4B).

Stimulating GFP-RICH-1-expressing HUVECs with insulin increased the number of vesicles in the cell compared to unstimulated cells, with GFP-RICH-1 localising on the vesicle structures (yellow arrows, Figure 5.4). ZO-1 staining appeared to be less disrupted when GFP-RICH-1 HUVECs were stimulated with insulin (red arrowheads, Figure 5.4B).
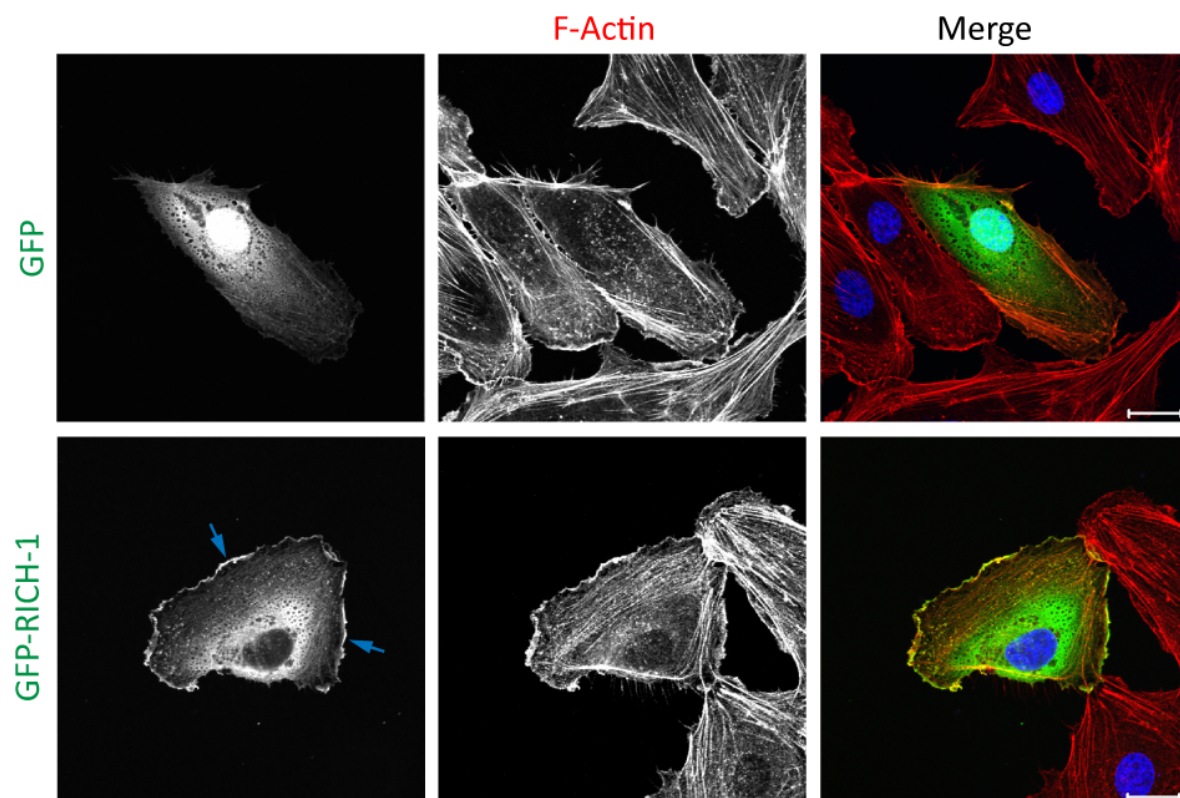
Figure 5.2 RICH-1 localises at the plasma membrane in subconfluent endothelial cells

HUVECs were transfected with pcDNA5 FRT/TO GFP ARHGAP17 (GFP-RICH-1), seeded onto FN-coated glass coverslips and fixed after 24 h. Cells were stained with Alexa Fluor 546-conjugated phalloidin for F-actin (red in merge), and DAPI for nuclei (blue in merge). Blue arrows indicate RICH-1 localisation at the membrane. Images were acquired by confocal microscopy with a 63x oil immersion objective and are maximum intensity projections of 10 confocal z-stacks, spanning 4 µm with 0.4 µm intervals between each image. Images are representative fields from three independent experiments. Scale bars are 20 µm.
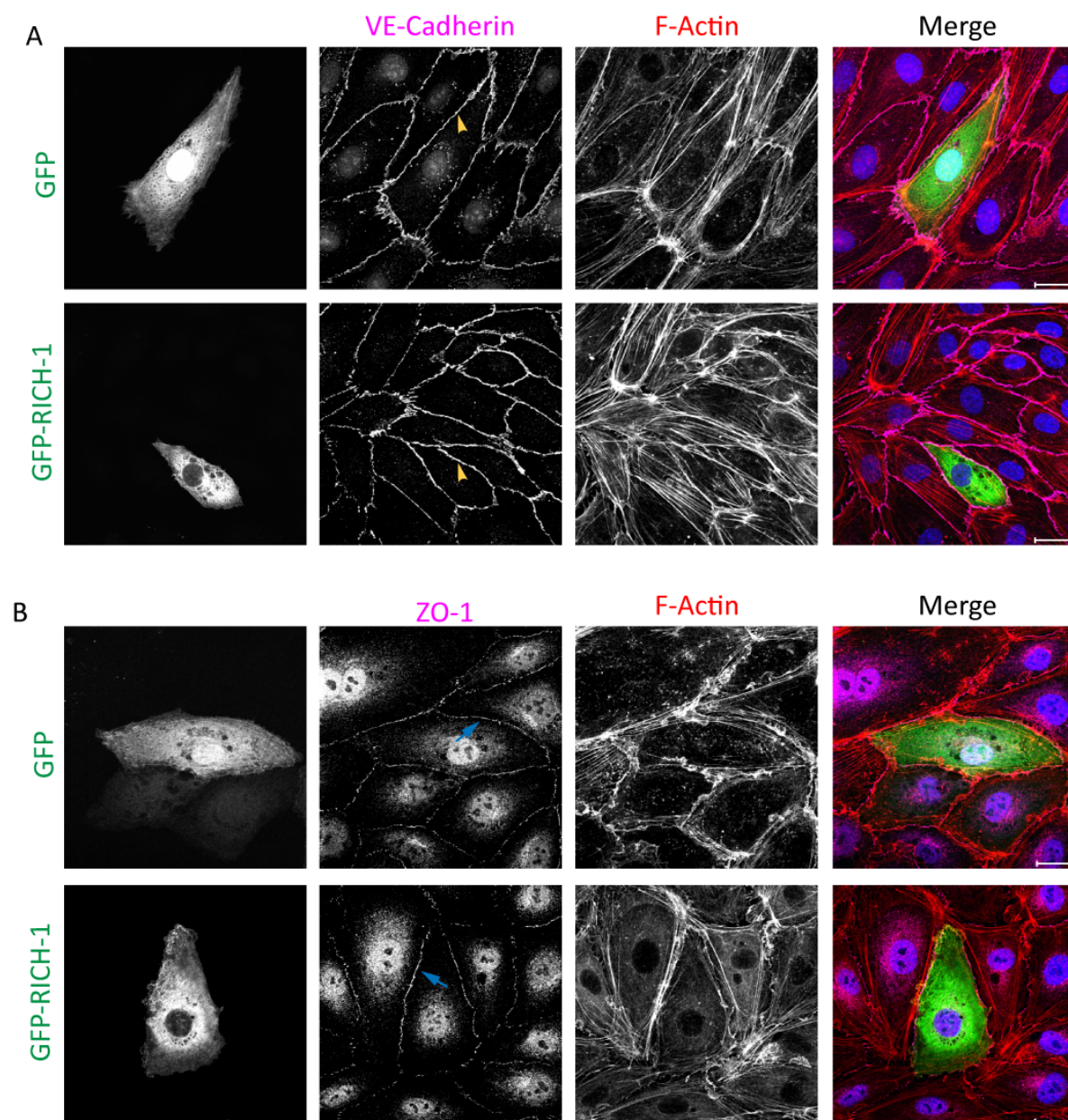
Figure 5.3 Endothelial cell-cell junctions are maintained when RICH-1 is overexpressed

HUVECs were transfected with pcDNA5 FRT/TO GFP ARHGAP17 (GFP-RICH-1), seeded onto FN-coated glass coverslips and fixed after 24 h. Cells were stained with Alexa Fluor 546-conjugated phalloidin for F-actin (red in merge), DAPI for nuclei (blue in merge), VE-cadherin (A) or ZO-1 (B) for adherens and tight junctions, respectively (magenta in merge). Yellow arrowheads indicate continuous adherens junctions, and blue arrows indicate uninterrupted tight junctions. Images were acquired by confocal microscopy with a 63x oil immersion objective and are maximum intensity projections of 10 confocal z-stacks, spanning 4 μm with 0.4 μm intervals between each image. Images are representative from three independent experiments. Scale bars are 20 μm.
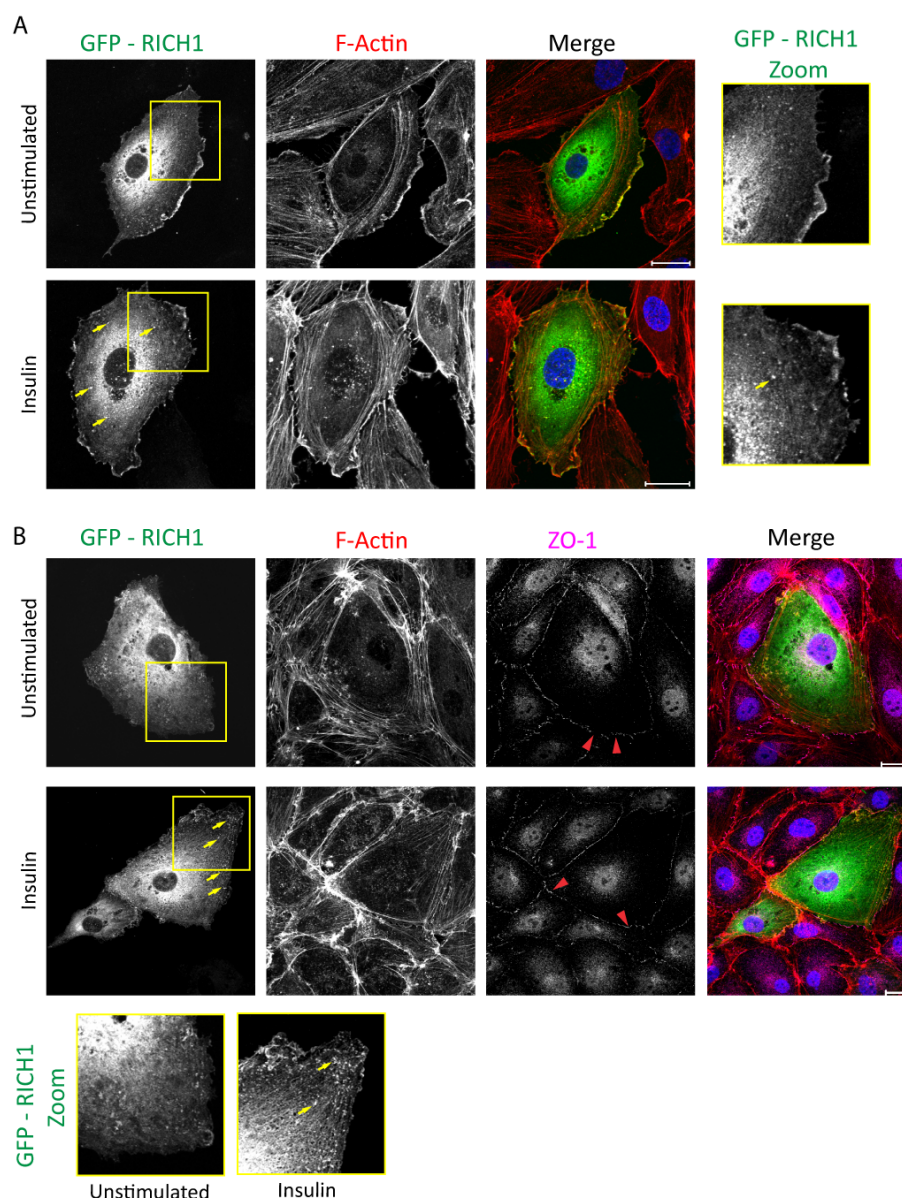
Figure 5.4 RICH-1 localises on vesicle structures when ECs are stimulated by insulin

HUVECs were transfected with pcDNA5 FRT/TO GFP ARHGAP17 (GFP-RICH-1) and seeded onto FN-coated glass coverslips. Cells were incubated for 24 h and then incubated in EBM2 medium containing 1% FCS for 4 h, stimulated with 100 nM insulin for 1 h and fixed. Subconfluent cells (A) were stained with Alexa Fluor 546-conjugated phalloidin for F-actin (red in merge), and DAPI for nuclei (blue in merge), and confluent cells (B) were also stained with ZO-1 for tight junctions (magenta in merge). Yellow arrows indicate RICH-1 localisation on the vesicles in insulin-stimulated cells. Red arrowheads indicate differences in tight junctions. Yellow-boxed areas are shown at higher magnification on the right of A and below B. Images were acquired by confocal microscopy with a 63x oil immersion objective and are maximum intensity projections of 10 confocal z-stacks, spanning 4 μm with 0.4 μm intervals between each image. Images are representative fields from three independent experiments. Scale bars are 20 μm.

5.2.2   siRNA-mediated knock-down of RICH-1 in endothelial cells

In order to gain more insight into the functional role of RICH-1 in endothelial cells, an RNA interference approach was chosen to knock down protein expression. Four oligonucleotides (siRNAs) were tested for their ability to transiently decrease RICH-1 expression in endothelial cells. All four siRNAs knocked down RICH-1 levels after 72 h following transfection, compared to cells treated with oligofectamine only (mock) and control cells transfected with a non-targeting siRNA (siControl), with an efficiency of between 55 and 70%, when analysed by immunoblotting (Figure 5.5). Oligos 1 and 2 were then chosen for use in subsequent experiments, and are represented as siRICH1-1 and siRICH1-2, respectively.
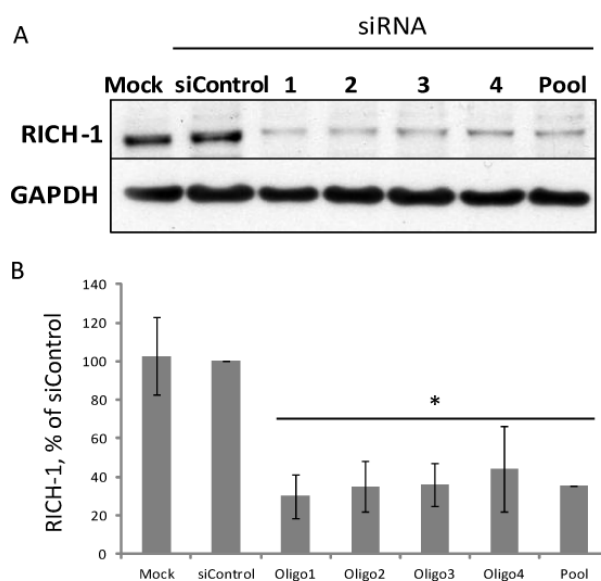
Figure 5.5 siRNA mediated knockdown of RICH-1 in HUVECs
Representative immunoblot (A) of HUVECs transfected with 4 different siRNA oligonucleotides targeting RICH-1. Mock represents cells treated with oligofectamine only, and Pool represents an equal mixture of oligos 1 – 4. Cells were transfected with 20 nM of siRNA using Oligofectamine^{TM}, and incubated for 72 h at 37°C, 5% CO_2. Cells were lysed and protein analysed by immunoblotting with an anti-RICH-1 antibody. Blots were re-probed for GAPDH as a loading control. (B) Data were generated by densitometric scanning of the Western blots, normalised to total GAPDH levels, relative to siControl. Data shown are the mean of three independent experiments ± SEM. Statistical significance was assessed by an unpaired Student's t-test; *$p < 0.05$.

5.2.3   RICH-1 depletion disrupts tight junctions in endothelial cells

siControl treated HUVECs had a round cobblestone-like morphology with bundles of actin filaments enriched along the cell-cell boundaries (Figure 5.6). Although RICH-1-depleted HUVECs maintained their cobblestone-like morphology, cells exhibited slightly more disorganised bundles of actin filaments, with some stress fibres traversing the length of the cell (Figure 5.6). At some areas, bright 'knots' of F-actin were present usually in the area between three or more ECs (red arrows, Figure 5.6). The most noticeable change in cell morphology, as a result of RICH-1 knockdown, was the disruption of tight junctions, visualised by altered ZO-1 staining (highlighted by yellow arrowheads, and zoomed area in Figure 5.6). siControl cells maintained linear, continuous junctions along cell–cell borders (blue arrow), whereas RICH-1-depleted HUVECs exhibited fragmented ZO-1 staining, perpendicular to the cell-cell borders. ZO-1 staining was particularly disjointed or absent in the F-actin 'knot' regions.
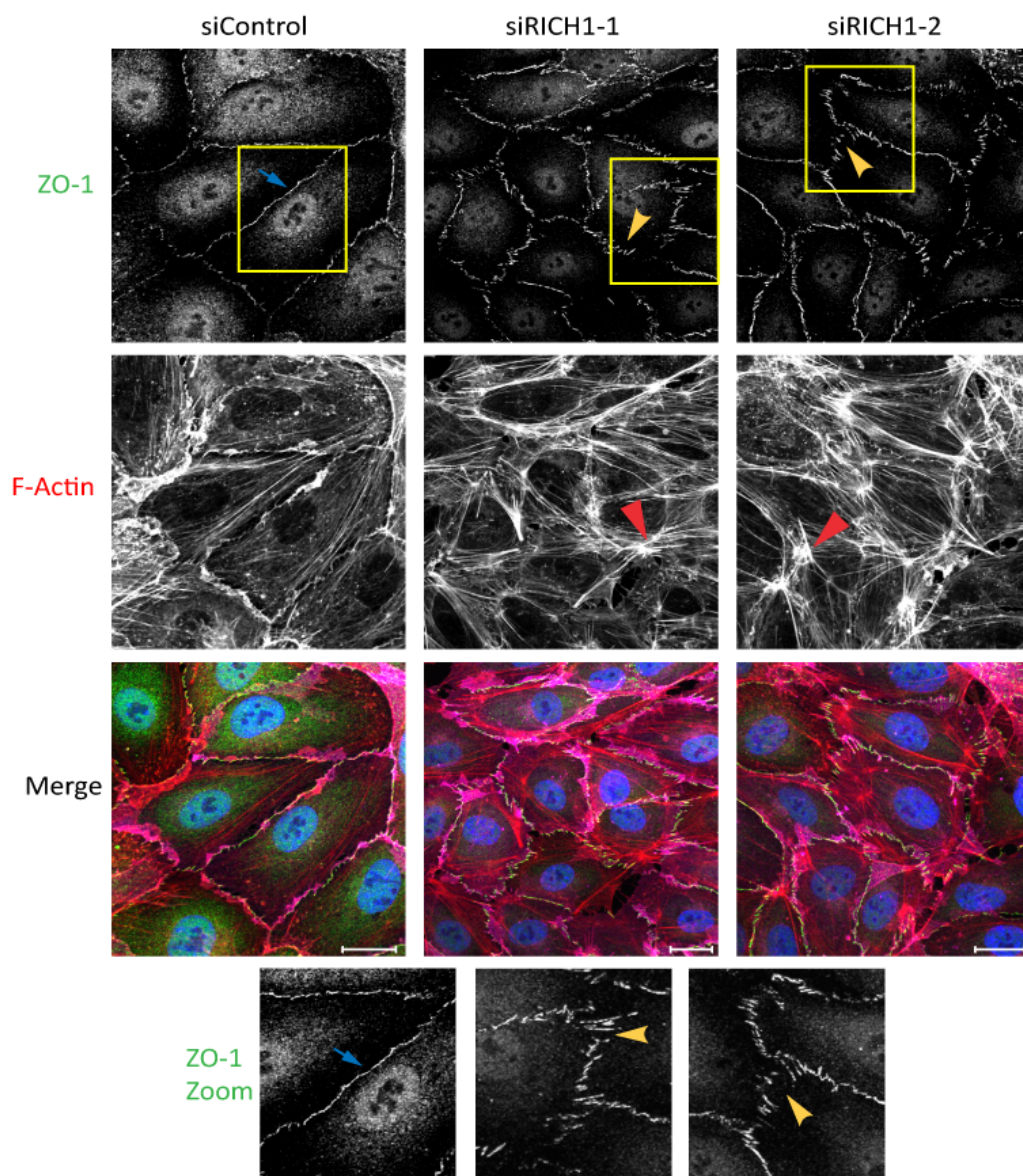
Figure 5.6 RICH-1 depletion disrupts tight junctions in endothelial cells

Immunofluorescence micrographs of HUVECs transfected with siRNA targeting RICH-1. Cells were seeded on FN-coated coverslips 48 h after transfection, and fixed after a further 24 h. Cells were stained with zonula occludens protein 1 (ZO-1) for tight junctions (green in merge), Alexa Fluor 546-conjugated phalloidin for F-actin (red in merge), anti CD31 (PECAM-1) antibody (magenta in merge), and DAPI for nuclei (blue in merge). Yellow-boxed areas are shown at higher magnification below. Images were acquired by confocal microscopy with a 63x oil immersion objective and are maximum intensity projections of 10 confocal z-stacks, spanning 4 μm with 0.4 μm intervals between each image. Images are representative from three independent experiments. Scale bars are 20 μm.

5.2.4   **RICH-1 knock-down decreases cell migration in a wound healing assay**

Insulin stimulated EC migration in the ORIS^{TM} migration assay (see section 3.4). In order to investigate whether RICH-1 plays a role in migration, RICH-1-depleted cells were assessed for their ability to migrate in this assay.

HUVECs were transfected with siRNAs targeting RICH-1. After 24 h cells were stained with CellTracker^{TM} Orange and seeded onto FN-coated wells containing a central stopper. Cells were incubated for a further 24 h and the central stopper removed. Images of the wound were taken, and cells were left to migrate into the central area for 24 h, and a second set of images were taken of the same locations. RICH-1 depletion significantly reduced cell migration compared to cells treated with oligofectamine only (mock), and non-targeting siControl transfected cells at 24 h (Figure 5.7). Due to time limitations, this assay was only performed using one oligo, and would require validation by another. When the experiment was repeated in the presence of insulin, the migration of mock and siControl-treated cells significantly increased (as seen in section 3.4). However, insulin stimulation had no effect on migration of the RICH-1-depleted cells (Figure 5.7).
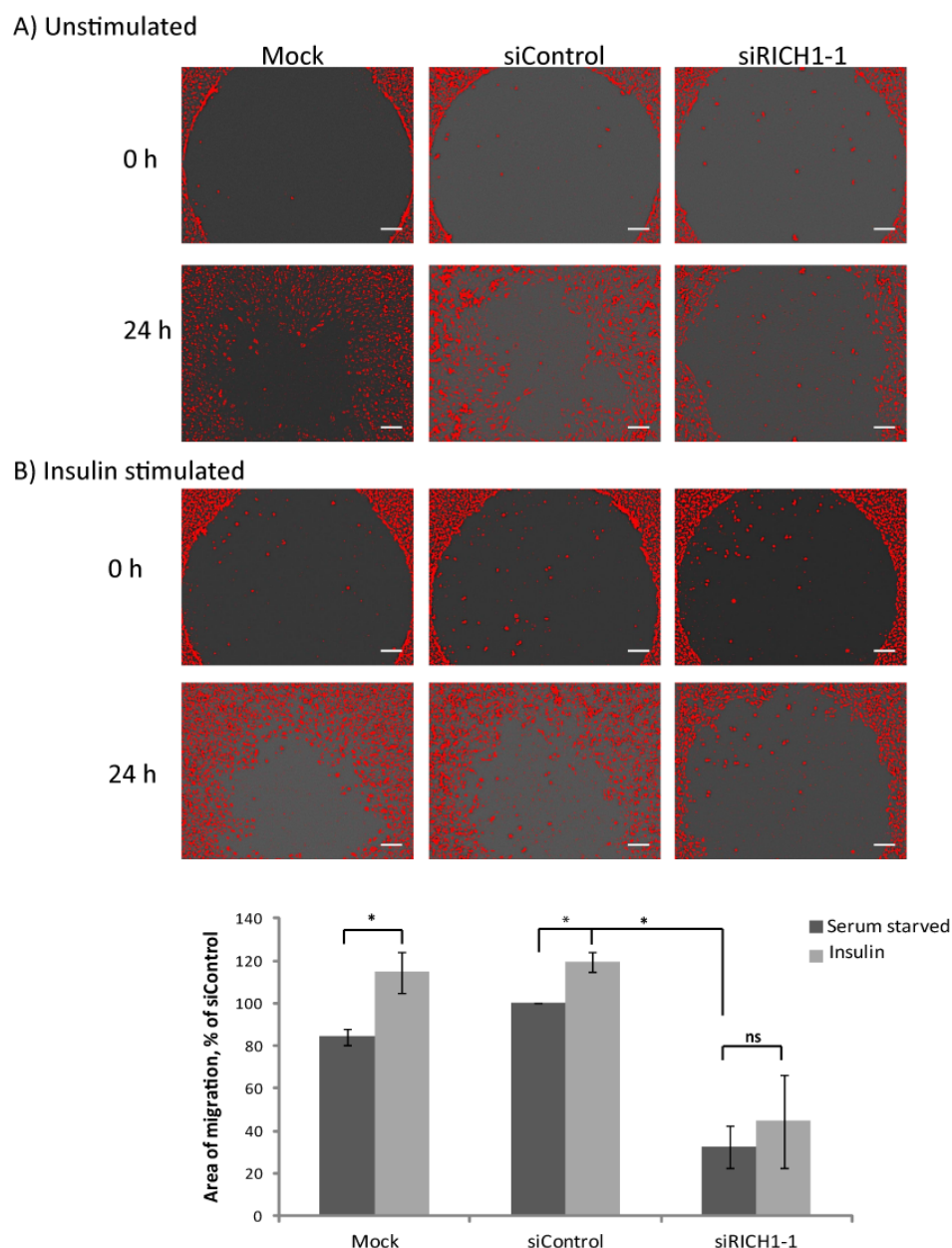
Figure 5.7 RICH-1 depletion decreases cell migration in the ORIS assay

HUVECs were transfected with siRNA targeting RICH-1 or control siRNA. After 24 h cells were stained with Cell-Tracker Orange fluorescent dye, seeded in wells containing a central insert, and incubated for 24 h at 37°C. The inserts were then removed to create a central wound in the monolayer, and imaged at 4x magnification (0 h). For the insulin studies (B), cells were serum starved for 2 h prior to removing the inserts, imaged and then stimulated with 100 nM insulin. Cells were incubated for 24 hours at 37°C and imaged again (24 h) using the saved locations of 0 h. The migratory capacity of the cells was quantified by measuring the percentage area of the central wound that cells had migrated into after 24 h using ImageJ software, as a percentage relative to siControl cells. Data shown are the mean of four (A) and three (B) independent experiments ± SEM. Statistical significance was assessed by an unpaired Student's t-test; *p<0.05, ns = not significant. Scale bars are 200 µm.

5.2.5   RICH-1 depletion does not affect loop formation in an angiogenesis assay

Endothelial cells undergo morphogenic processes to form new vessels in response to various stimuli (see Chapter 1.5). Lumen and tube development involves the formation of intracellular vacuoles, which is mediated by the establishment and coalescence of pinocytic intracellular vacuoles (Bayless et al., 2000). Rho GTPases regulate endothelial morphogenesis with Cdc42 and Rac1 specifically being shown as critical regulators of endothelial cell lumen formation during the early stages of angiogenesis (Bayless and Davis, 2002; Koh et al., 2008). As RICH-1 is a known Cdc42 GAP, its role in angiogenesis was investigated by siRNA knockdown in HUVECs. The *in vitro* loop formation assay provides a simplified imitation of angiogenesis and is considered to mimic the cord formation step in sprouting angiogenesis (Goodwin, 2007). RICH-1-depleted HUVECs were plated on Matrigel to investigate their ability to form loops in the *in vitro* angiogenesis assay. HUVECs were transfected with siRNAs targeting RICH-1, and seeded on the Matrigel after 48 h. Cells were left to form loops for 24 h, recorded by time-lapse movies.

Initially, siRICH1-1 knockdown cells appeared to self-organise faster than siControl treated cells at the 4 h time-point, elongating and forming the protrusions that become the cords of a loop (Figure 5.8, Movies S3 and S4). Although there was a slight increase in the number of angiogenic loops formed after 24 h, compared to siControl cells, this was not statistically significant when repeated in three independent experiments (Figure 5.8B).
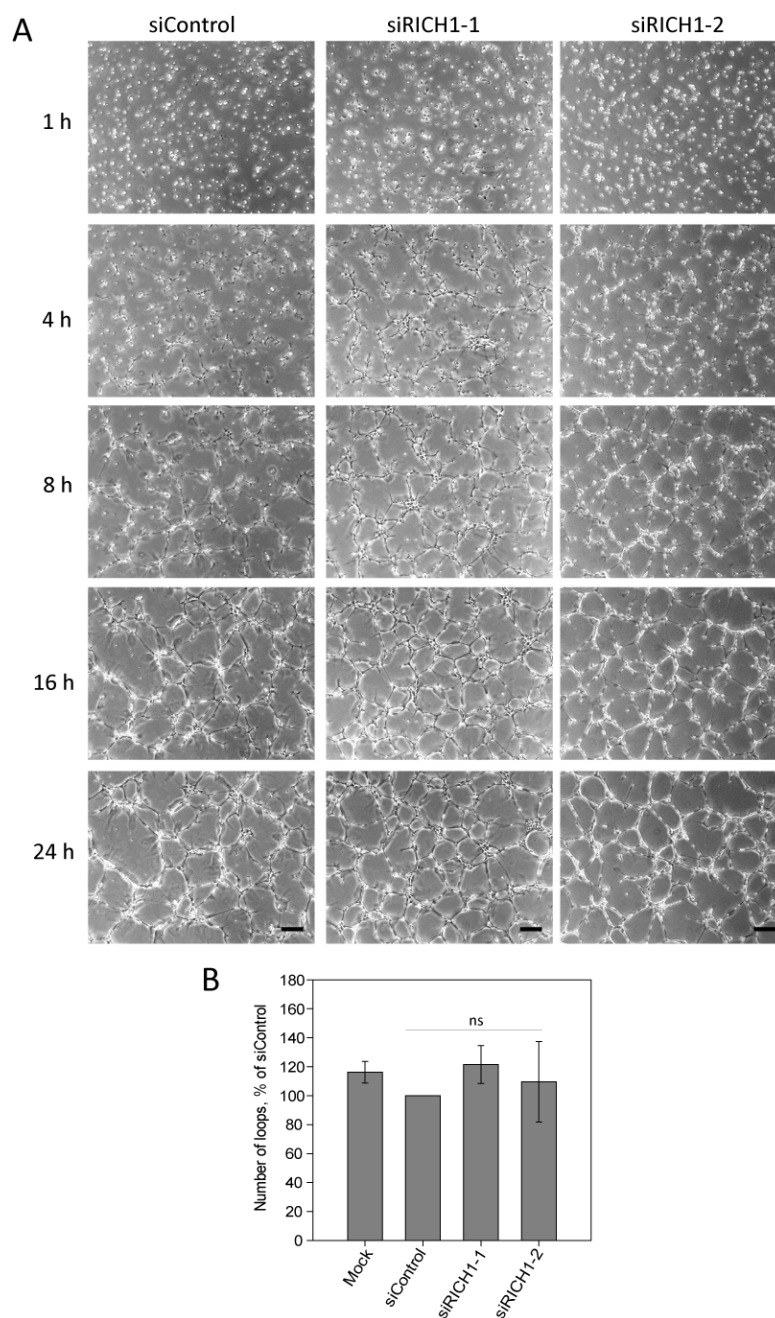
Figure 5.8 RICH-1 depletion does not affect loop formation in the angiogenesis assay

HUVECs were transfected with siRNAs targeting RICH-1 or control siRNA. Cells were seeded onto polymerised Matrigel (4.5 mg/ml) 48 h after transfection, incubated for 1 h at 37 °C and loop formation was monitored by time-lapse microscopy using a 4x objective, acquiring images every 20 min for 24 h (A). Quantification was performed by counting the total number of complete loops per field, as a percentage relative to siControl-transfected cells (B). At least 5 fields were scored per condition in each experiment and data shown are the mean of four and three independent experiments for siRICH1-1 and siRICH1-2, respectively, normalised to siControl ± SEM (siControl = 100 %). No significant differences were observed between siRICH-1 knockdown and siControl cells. Statistical significance was assessed by a Mann-Whitney *U* test; ns = not significant. Scale bars are 200 μm.

5.2.6   Effect of RICH-1 depletion on the permeability of endothelial monolayers

Endothelial cell-cell junctions have significant roles in mediating endothelial permeability (see section 1.2.3). Since the depletion of RICH-1 disrupted endothelial tight junctions (see section 5.2.3), its role on basal cell permeability was investigated using the FITC-dextran Transwell^{TM} assay described in Chapter 2.3.8 and 3.3.1. RICH-1 depletion appeared to increase endothelial cell permeability compared to siControl treated cells (Figure 5.9), however this was not statistically significant when repeated in three independent experiments, due to the variability between repeats. This variability could be due to differences in RICH-1 knockdown efficiency, or differences between HUVECs such as cell passage number. The experiment would be need to be repeated to determine whether RICH-1 plays a role in maintaining cell-cell junctions in endothelial cells.
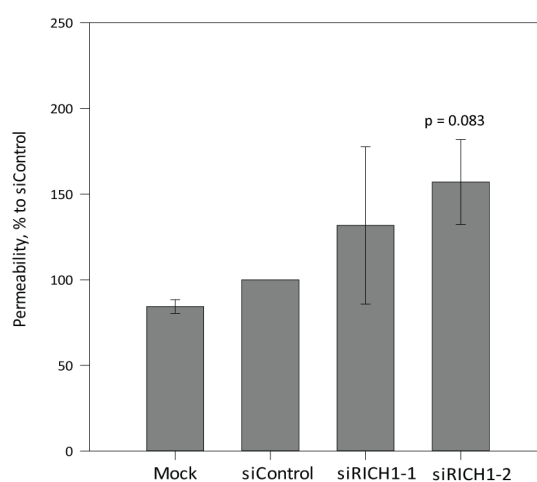
Figure 5.9 Effect of RICH-1 depletion on endothelial cell permeability

HUVECs were transfected with siRNAs targeting RICH-1 or control siRNA. Cells were seeded onto Transwell™ filters (0.4 µm pore size) 48 h after transfection and incubated for 24 h at 37 °C. FITC-dextran (0.1 mg/ml) was added to the upper chamber and the lower chamber fluorescence was measured after 60 min. Fluorescence was measured for duplicate wells and quantified as a percentage relative to control. Data shown are the mean of three independent experiments ± SEM. Statistical significance was assessed by an unpaired Student's t-test.

5.3   ARHGAP29 / Parg1

ARHGAP29 was first identified by a yeast two-hybrid screen in the search for proteins that interact with protein-tyrosine phosphatase PTPL1 (Saras et al., 1997). This intracellular protein has a cysteine-rich domain, with homology to a regulatory phorbol ester/diaclyglycerol-binding domain, followed by a RhoGAP domain. It was therefore named *P*TPL1-*a*ssociated *R*hoGA*P 1* (Parg1) (Figure 5.10) (Saras et al., 1997; Tcherkezian and Lamarche-Vane, 2007). Parg1 is expressed at higher levels in skeletal muscle and the heart than in other tissues. The RhoGAP domain was shown to be active with a strong GAP activity on RhoA (Myagmar et al., 2005; Saras et al., 1997). Parg1 inhibited Rho-mediated stress fibres in in NIH3T3 cells (Myagmar et al., 2005). Interestingly, Parg1 interacts with the Ras-related protein Rap2 in a GTP-dependent manner, and this interaction suppresses the stress fibre inhibitory effects of Parg1 (Myagmar et al., 2005).

Parg1 was shown to play a critical role in blood vessel tubulogenesis *in vitro* (Xu et al., 2011). Parg1 binds to Ras interacting protein 1 (Rasip1), and both proteins are required for blood vessel formation by endothelial cells. When either Rasip1 or Parg1 were depleted, RhoA activation increased, resulting in increased actomyosin contractility and cell polarity disruption that resulted in failed lumen morphogenesis *in vitro* (Xu et al., 2011).

A very recent study provided a link between Rap1 and Rasip1, and demonstrated the importance of Parg1 in regulating the endothelial cytoskeleton (Post et al., 2013). This study showed that Rasip1 is a Rap1 effector, as Rap1-induced cell spreading and stabilisation of endothelial barrier function requires the Rasip-Parg1 complex.

These studies demonstrate the critical role of Parg1 in regulating the endothelial actin cytoskeleton and barrier function.

1261 aa

Figure 5.10 Domain structure of Parg1

Parg1 has a zinc finger (612 – 657) that contains a cysteine-rich phorbol ester domain (C), followed by a RhoGAP domain (671 – 886). The last 4 residues (1258 – 1261) provide a binding site for PTPL1 (orange).

5.3.1   GFP-Parg1 expression decreases endothelial F-actin levels

The cellular localisation of GFP-Parg1 was determined by transiently transfecting HUVECs with an expression plasmid encoding GFP-Parg1. Parg1 displayed a uniform diffuse localisation in the cytoplasm (Figure 5.11). Expression of GFP-Parg1 resulted in a striking decrease of endothelial F-actin, with a complete loss of radial stress fibres (Figure 5.11, yellow asterisks). This finding was consistent with Parg1 overexpression in NIH3T3 fibroblasts (Myagmar et al., 2005) and very recently in HUVECs (Post et al., 2013). In confluent monolayers (Figure 5.11A) adherens junctions were well maintained, as visualised by the linear reticular distribution of β-catenin (reticular adherens junctions, yellow arrowhead). When β-catenin is released and stabilized in the cytosol, it is translocated to the nucleus and modulates gene transcription (Gumbiner, 1995). GFP-Parg1 expression cells appeared to have less nuclear β-catenin staining compared to GFP-expressing HUVECs. When cells were sub-confluent (Figure 5.11B) GFP-Parg1 expressing cells were able to form junctions at the contact between adjacent cells (blue arrows).

Insulin stimulation of GFP-Parg1 expressing cells did not induce any discernable morphological changes. The diffuse cytoplasmic distribution was still observed, although GFP-Parg1 expression appeared more granular with less localisation occurring in the perinuclear area (Figure 5.12). This finding, however, needs to be investigated further for greater confidence.
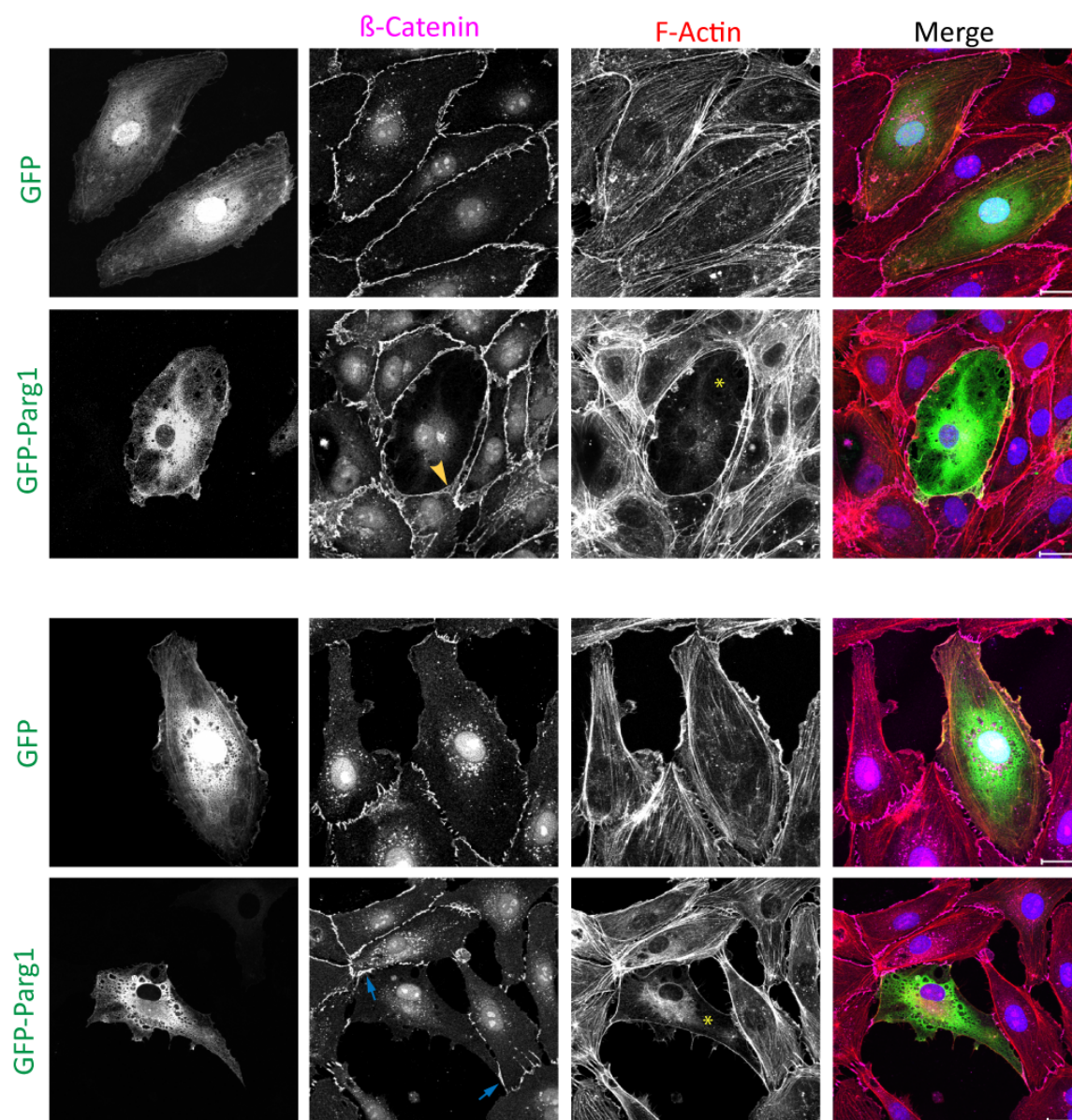
Figure 5.11 GFP-Parg1 expression decreases endothelial F-actin levels

HUVECs were transfected with pcDNA5 FRT/TO GFP ARHGAP29 (GFP-Parg1), seeded onto FN-coated glass coverslips and fixed after 24 h. Cells were stained with Alexa Fluor 546-conjugated phalloidin for F-actin (red in merge), anti-ß-catenin for adherens junctions (magenta in merge) and DAPI for nuclei (blue in merge). Yellow asterisk highlight overall decrease F-actin in the cell compared to untransfected neighbouring cells. Yellow arrow depicts reticular adherens junctions; blue arrows show cell-cell junctions are formed in adjacent cells. Images were acquired by confocal microscopy with a 63x oil immersion objective and are maximum intensity projections of 10 confocal z-stacks, spanning 4 µm with 0.4 µm intervals between each image. Images are representative of random fields from three independent experiments. Scale bars are 20 µm.
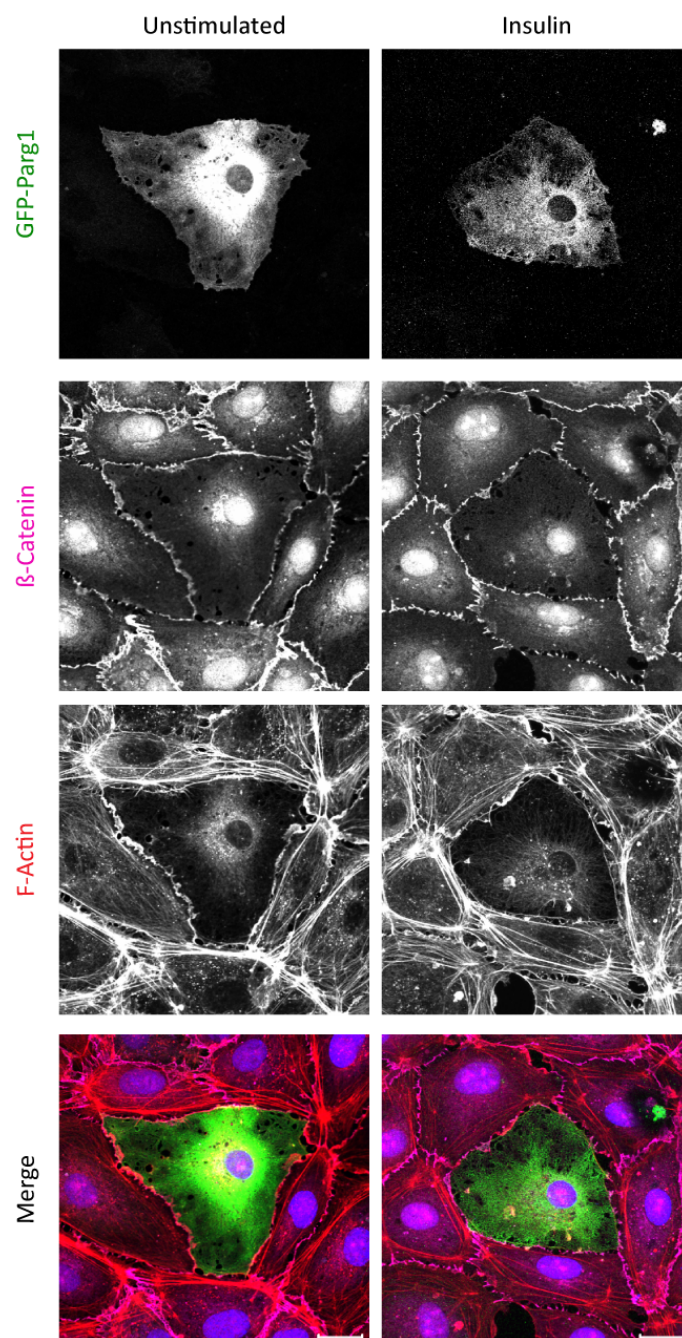
Figure 5.12 Insulin does not affect Parg1 localisation in endothelial cells

HUVECs were transfected with pcDNA5 FRT/TO GFP ARHGAP29 (GFP-Parg1) and seeded onto FN-coated glass coverslips. Cells were incubated for 24 h and then serum starved for 4 h in EBM2 medium containing 1% FCS. Cells were stimulated with 100 nM insulin for 1 h, fixed and stained with Alexa Fluor 546-conjugated phalloidin for F-actin (red in merge), anti-β-catenin for adherens junctions (magenta in merge), and DAPI for nuclei (blue in merge). Images were acquired by confocal microscopy with a 63x oil immersion objective and are maximum intensity projections of 10 confocal z-stacks, spanning 4 μm with 0.4 μm intervals between each image. Images are representative of random fields from three independent experiments. Scale bars are 20 μm.

5.3.2   siRNA mediated knock-down of Parg1 in endothelial cells

An RNA interference approach to knock down Parg1 expression was chosen to evaluate its functional role in endothelial cells. Parg1 expression was down regulated in HUVECs using four siRNA oligonucleotides (siRNAs), and a knock down efficiency of between 75 to 95% was achieved after 72 h, determined by immunoblotting, when compared to a non-targeting control siRNA (Figure 5.13). Oligonucleotides 2 and 3 were chosen for functional assays, as they provided good knock down efficiencies and exhibited similar morphological phenotypes when visualised by phase contrast microscopy (data not shown). These siRNAs are referred to as siParg1-2 and siParg1-3.
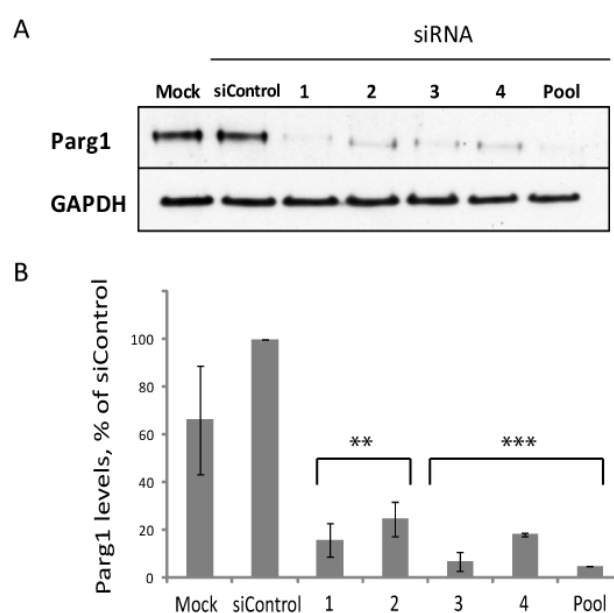
Figure 5.13 siRNA-mediated knockdown of Parg1 in HUVECs
Representative immunoblot (A) of lysates from HUVECs transfected with 4 different siRNA oligonucleotides targeting Parg1. Mock represents cells treated with oligofectamine only, and Pool represents an equal mixture of oligos 1 – 4. Cells were transfected with 20 nM of siRNA using Oligofectamine^{TM}, and incubated for 72 h at 37°C, 5% CO_2. Cells were lysed and protein analysed by immunoblotting with an anti-Parg1 antibody. Blots were re-probed for GAPDH as a loading control. (B) Data were generated by densitometric scanning of the Western blots, normalised to total GAPDH levels, relative to siControl. Data shown are the mean of three independent experiments ± SEM. Statistical significance was assessed by an unpaired Student's t-test; ** $p < 0.005$, *** $p < 0.001$.

5.3.3   Parg1 depletion induces stress fibres

HUVECs were transfected with siRNAs targeting Parg1 and stained for F-actin and β-catenin (Figure 5.14). Control cells maintain their cobblestone-like morphology (as observed in Chapter 3), with β-catenin localizing linearly along cell–cell borders (continuous adherens junctions) and with a wider reticular distribution where adjacent cells overlapped (reticular adherens junctions; Figure 5.14, yellow arrowheads) (Fernandez-Martin et al., 2012). Depletion of Parg1 resulted in cell elongation and a dramatic increase in stress fibres that traversed the length of the cell (Figure 5.14, red arrows). Linear continuous adherens junctions along the cell-cell borders (parallel to the stress fibres) were maintained in Parg1 knockdown cells, however junctions perpendicular to the stress fibres were discontinuous (blue arrows in Figure 5.14), indicative of impaired barrier function (Millan et al., 2010).

In summary, these results indicate that Parg1 regulates stress fibres in endothelial cells.
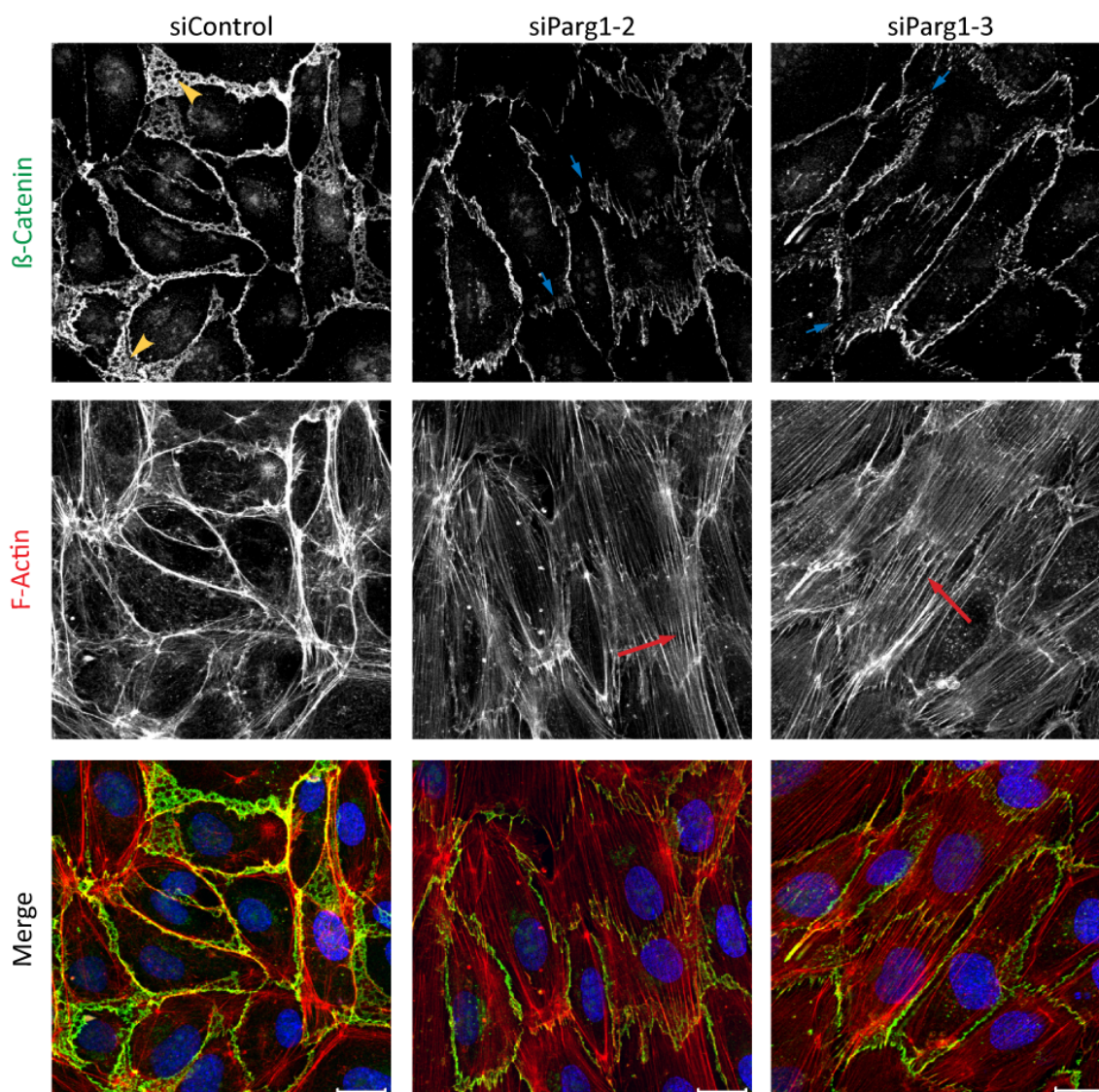
Figure 5.14 Parg1 depletion induces stress fibres

Immunofluorescence micrographs of HUVECs transfected with siRNA targeting Parg1. Cells were seeded on FN-coated coverslips 48 h after transfection, and fixed after a further 24 h. Cells were stained with β-catenin for adherens junctions (green in merge), Alexa Fluor 546-conjugated phalloidin for F-actin (red in merge), and DAPI for nuclei (blue in merge). Images were acquired by confocal microscopy with a 63x oil immersion objective and are maximum intensity projections of 10 confocal z-stacks, spanning 4 μm with 0.4 μm intervals between each image. Images are representative fields from three independent experiments. Scale bars are 20 μm.

5.3.4   Parg1 knock-down decreases cell migration in a wound healing assay

Parg1 has a profound effect on the actin cytoskeleton, and therefore could be involved in regulating cell migration. The ORIS^{TM} migration was performed using Parg1-depleted HUVECs to investigate the role of Parg1 in endothelial cell migration. The experiment was performed as described for RICH-1-depleted cells (see section 5.2.4) using siRNAs targeting Parg1.

Parg1-depleted HUVECs had a significant reduction in cell migration compared to untreated (mock) cells and siControl treated cells (Figure 5.15). When the experiments were repeated in the presence of insulin, untransfected and siControl-transfected cells responded with an increase in migration (as observed in section 3.4), however insulin stimulation had no effect on the migration of Parg1-depleted cells (Figure 5.15). Due to time limitations, the effect of insulin on Parg1-depleted HUVECs was only investigated using one oligo (siParg1-2), and further analysis is required for siParg1-3.
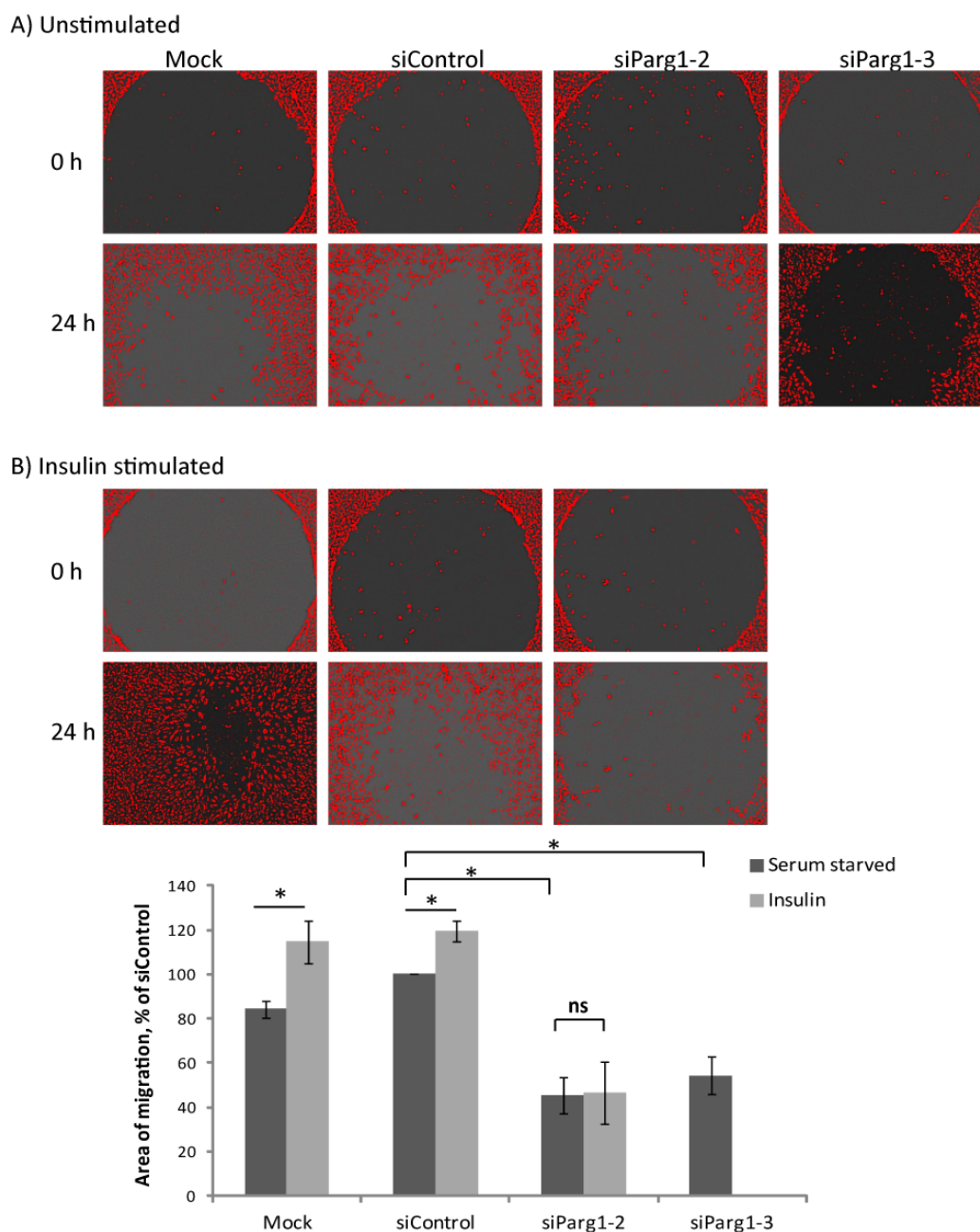
Figure 5.15 Parg1 knockdown decreases cell migration

HUVECs were transfected with siRNAs targeting Parg1 or control siRNA. After 24 h cells were stained with Cell-Tracker Orange fluorescent dye, seeded in wells containing a central insert, and incubated for 24 h at 37°C. The inserts were then removed to create a central wound in the monolayer, and imaged at 4x magnification. For the insulin studies, cells were serum starved for 2 h prior to removing the inserts, imaged and then stimulated with 100 nM insulin. Cells were incubated for 24 hours at 37°C and imaged again using the saved locations of initial wounds. The migratory capacity of the cells was quantified by measuring the percentage area of the central wound that cells had migrated into after 24 h using ImageJ software, as a percentage relative to siControl cells. Data shown are the mean of four and three independent experiments ± SEM of unstimulated and insulin studies, respectively. Statistical significance was assessed by an unpaired Student's t-test; *p<0.05, ns = not significant.

5.3.5   Parg1 depletion disrupts loop formation in an angiogenesis assay

The role of Parg1 was investigated in an *in vitro* angiogenesis assay as it has previously been shown to be a central regulator in developmental tubulogenesis (Xu et al., 2011) and it affects endothelial F-actin distribution (see Figure 5.14). HUVECs were transfected with siRNAs targeting Parg1, and seeded onto polymerised Matrigel after 48 h. Angiogenic loop formation was monitored by time-lapse microscopy for 24 h. siControl treated cells elongated and extended cellular processes leading to cell-cell adhesion, forming a well organised network of cells (Figure 5.16). These cells were able to interact with each other and form closed loops. Parg1-depleted HUVECs were able to extend cellular processes, and interact with other cells, but these connections were not maintained and frequently collapsed (Figure 5.16A, Movies S3 and S5). There was a significant decrease in maintained loop formation in Parg1-depleted cells at 24 h (Figure 5.16B). Interestingly, deformation of the Matrigel was observed during the retraction of the collapsed loops (see Movie S5 on supplementary CD).
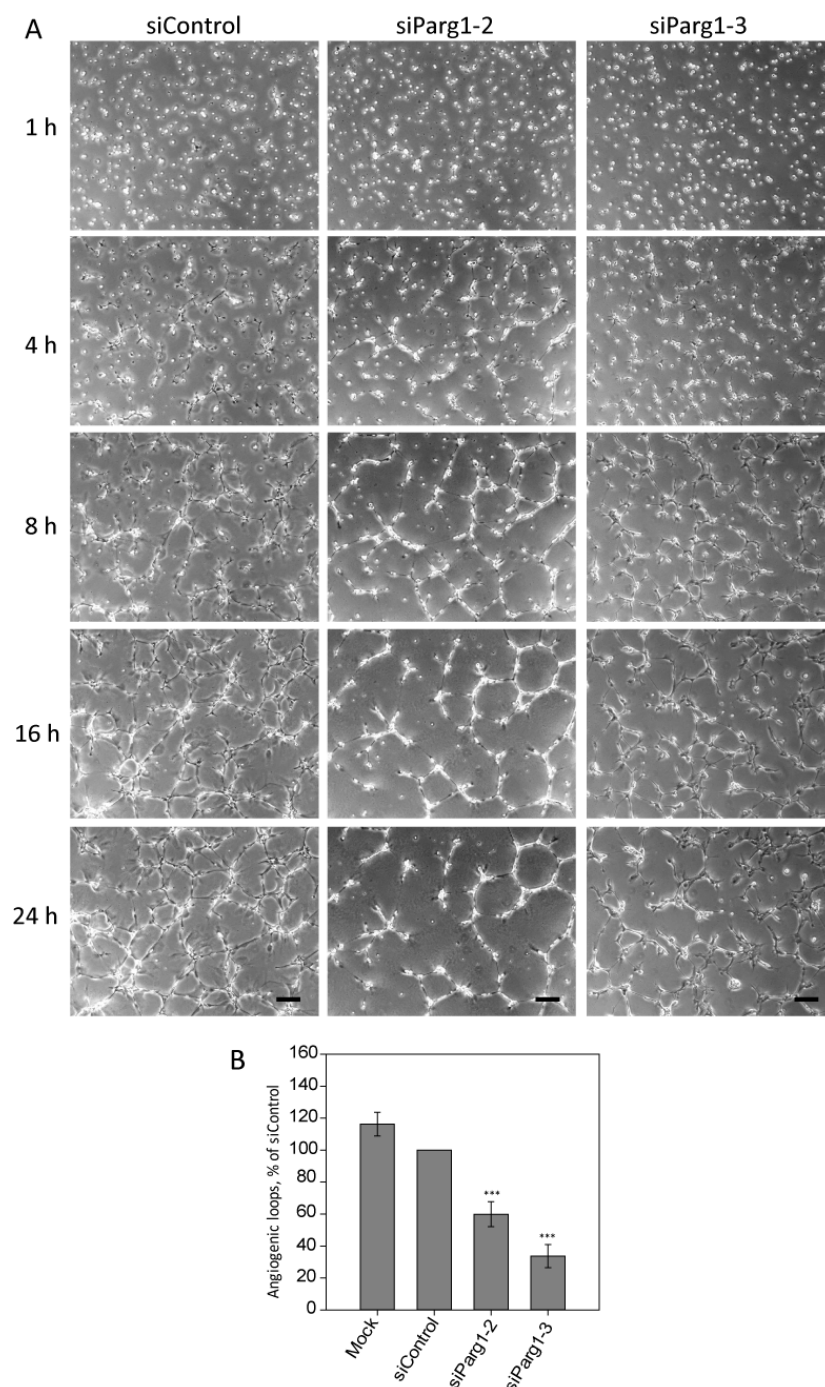
Figure 5.16 Parg1 depletion disrupts angiogenic loop formation

HUVECs were transfected with siRNAs targeting Parg1. Cells were seeded onto polymerised Matrigel (4.5 mg/ml) 48 h after transfection, incubated for 1 h at 37 °C and loop formation was monitored by time-lapse microscopy using a 4x objective, acquiring images every 20 min for 24 h (A). Quantification was performed by counting the total number of complete loops per field, as a percentage relative to siControl cells (B). At least 5 fields were scored per condition in each experiment and data shown are the mean of four and three independent experiments for siParg1-1 and siParg1-2, respectively, normalised to siControl ± SEM (siControl = 100 %). ***p<0.001, One-way ANOVA (Holm-Sidak method). Scale bars are 200 μm.

5.3.6   siRNA knock down of Parg1 increases basal endothelial cell permeability

Depleting HUVECs of Parg1 results in dramatic morphology changes (see section 5.3.3). Cells appear to elongate with stress fibres, accompanied by the disruption of cell-cell junctions. This could lead to leaky cell-cell junctions and thus a FITC-dextran permeability assay was performed to measure the effect of Parg1 knockdown on endothelial barrier function. Parg1 knockdown resulted in an increase in cell permeability when compared to siControl treated cells (Figure 5.17). siParg1-3-treated HUVECs had a significant increase in cell permeability (Figure 5.17), suggesting that Parg1 is essential for maintaining cell-cell junctions. Cells treated with siParg1-2 had a lot of variability between experimental repeats, and therefore did not result in a statistically significant increase in permeability. Due to the variable nature of this assay, further repeats are required to confirm that both siRNA oligonucleotides produce similar phenotypes.
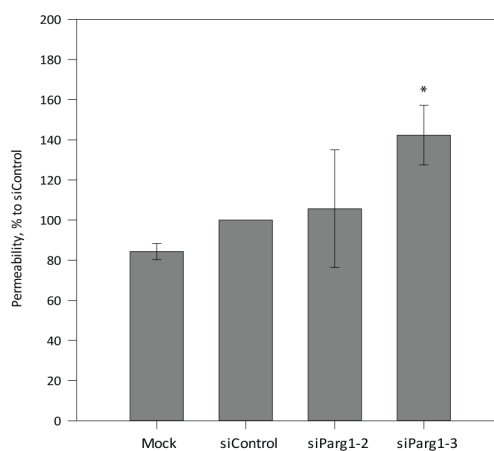
Figure 5.17 Parg1 depletion increases basal endothelial cell permeability

HUVECs were transfected with siRNAs targeting Parg1. Cells were seeded onto Transwell™ filters (0.4 μm pore size) 48 h after transfection and incubated for 24 h at 37 °C. FITC-dextran (0.1 mg/ml) was added to the upper chamber and the lower chamber fluorescence was measured after 60 min. Fluorescence was measured for duplicate wells and quantified as a percentage relative to control. Data shown are the mean of three independent experiments ± SEM. Statistical significance was assessed by a Mann-Whitney U test; *p<0.05.

5.4   LIM domain only 7 (LMO7)

LIM domain only 7 (LMO7) is an interesting hit identified from the 14-3-3-binding screen, as it had previously been identified in the MacKintosh laboratory for its potential role in regulating insulin signalling (Dubois et al., 2009). Moreover, LMO7 was previously shown to co-localise with F-actin and play an important role in cell migration, requiring Rho GTPases (Hu et al., 2011). LMO7 is a multifunctional protein that belongs to the PDZ and LIM domain-containing protein family, which function as protein-protein recognition modules that are essential for integrating diverse cellular networks (Kadrmas and Beckerle, 2004). The protein comprises of a LIM domain, Calponin Homology (CH) domain and a PDZ domain (Figure 5.18). Interestingly, LMO7 shuttles between the cell surface and the nucleus, indicating it has two different functions.

Figure 5.18 Domain structure of LMO7
LMO7 consists of 1683 amino acids with a Calponin Homology (CH) domain, a PDZ domain and an LIM domain.

For its nuclear function, LMO7 localises at the nuclear envelope binding a nuclear membrane protein called emerin. Mutations in emerin result in X-linked Emery-Dreifuss muscular dystrophy (EMED), and LMO7 appears to also play a role in this disease due to its ability to transcriptionally regulate emerin by mutual feedback regulation (Holaska et al., 2006). LMO7 is highly expressed in muscle and heart and has been found to regulate a large number of genes, including forty-six muscle and heart genes (Holaska et al., 2006; Ott et al., 2008; Putilina et al., 1998). Its importance in the heart was further established in zebrafish, where LMO7 knockdown resulted in severe defects in heart development (Ott et al., 2008).

LMO7 has been shown to localise at adherens junctions in epithelial cells by binding to two F-actin binding proteins, afadin and α-actinin (Ooshio et al., 2004). In doing so, LMO7 acts as an adapter protein connecting the two adherens proteins, nectin and E-cadherin (see chapter 1.2.2) (Ooshio et al., 2004). However, it was postulated that LMO7 is not necessary during the formation of cell-cell junctions but rather acts as a stabilizer of the junctional complexes after they are recruited.

Although multifunctional roles of LMO7 have been identified, its role in endothelial cells is yet to be determined.

5.4.1   **GFP-LMO7 localises in both the cytoplasm and the nucleus**

GFP-tagged LMO7 localised diffusely in the nucleus and cytoplasm, consistent with its dual role as a transcription factor and adaptor protein (Figure 5.19). Strong localisation at the plasma membrane was not observed, in contrast to previous reports in epithelial cells (Ooshio et al., 2004). Linear VE-cadherin staining suggests that GFP-LMO7 expression does not affect adherens junctions (Figure 5.19). LMO7 did not appear to affect F-actin levels, as normal bundles of actin filaments were present enriched along the cell-cell boundaries (Figure 5.19).
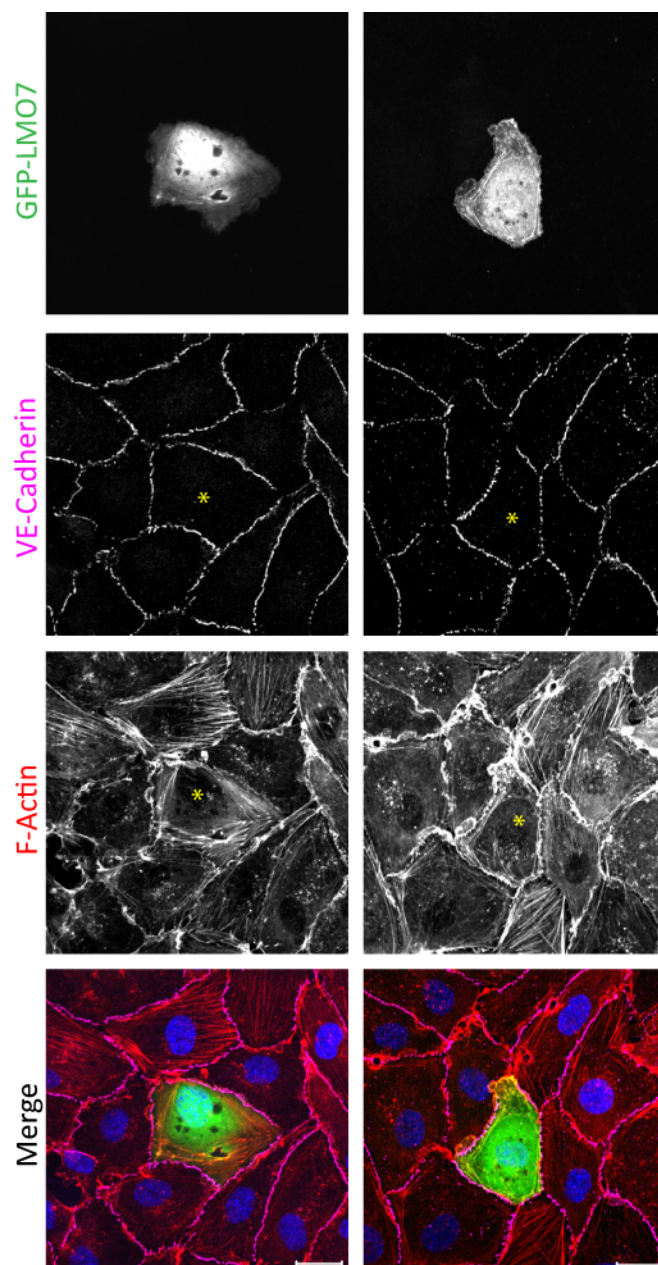
Figure 5.19 LMO7 localises in both the cytoplasm and nucleus in endothelial cells
HUVECs were transfected with pcDNA5 FRT/TO GFP LMO7, seeded onto FN-coated glass coverslips and fixed after 24 h. Cells were stained with Alexa Fluor 546-conjugated phalloidin for F-actin (red in merge), VE-cadherin for adherens junctions (magenta in merge) and DAPI for nuclei (blue in merge). Yellow asterisks indicate transfected cells. Images were acquired by confocal microscopy with a 63x oil immersion objective and are maximum intensity projections of 10 confocal z-stacks, spanning 4 μm with 0.4 μm intervals between each image. Images are representative of random fields from three independent experiments. Scale bars are 20 μm.

5.4.2 siRNA mediated knock-down of LMO7 in endothelial cells

LMO7 protein was down regulated in HUVECs using four siRNA oligonucleotides, and a knock-down efficiency of between 30 – 67% was achieved after 72 h, determined by immunoblotting, when compared to a non-targeting control siRNA (Figure 5.20). Oligonucleotides 1 and 3 were chosen for functional assays, as they provided higher and more consistent knock down efficiencies with a mean of 67% and 50%, respectively. These siRNAs are referred to as siLMO7-1 and siLMO7-3.
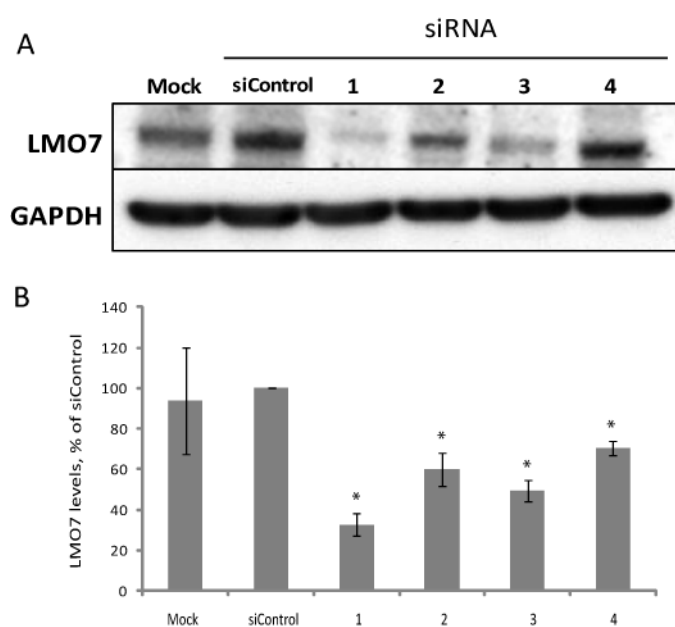
Figure 5.20 siRNA mediated knock down of LMO7 in HUVECs
Representative immunoblot (A) of HUVECs transfected with 4 different siRNA oligonucleotides targeting LMO7. Mock represents cells treated with oligofectamine only. Cells were transfected with 20 nM of siRNA using Oligofectamine[TM], and incubated for 72 h at 37°C, 5% CO_2. Cells were lysed and protein analysed by immunoblotting with an anti-LMO7 antibody. Blots were re-probed for GAPDH as a loading control. (B) Data were generated by densitometric scanning of the Western blots, normalised to total GAPDH levels, relative to siControl. Data shown are the mean of three independent experiments ± SEM. Statistical significance was assessed by an unpaired Student's t-test; *$p < 0.05$.

5.4.3 **LMO7 depletion affects tight junctions in endothelial cells**

LMO7 binds two F-actin binding proteins afadin and α-actinin and stabilises epithelial junctions by connecting the nectin-afadin and E-cadherin-catenin complexes (Ooshio et al., 2004). No obvious cell morphology changes were observed in LMO7-depleted HUVECs. β-catenin localised linearly along the cell-cell boundaries and adherens reticular junctions were maintained. Depleting LMO7 appeared to slightly increase the number of stress fibres present in the cells and disorganise F-actin; however these did not affect cell shape or cell-cell junctions (Figure 5.21).

When confluent monolayers of siLMO7-depleted HUVECs were stained for TJs, the localization of the tight junctional protein ZO-1 was altered (Figure 5.22). siControl treated cells displayed a linear localisation of ZO-1 along most cell-cell boundaries, however depleting LMO7 resulted in ZO-1 proteins extending perpendicularly into the neighbouring cells (yellow boxed area in Figure 5.22). PECAM-1 staining also suggested that cells overlapped less when LMO7 was absent; with thinner areas of PECAM-1 present between neighbouring cells, when compared to siControl cells (yellow boxed area in Figure 5.22).

In summary, LMO7 depletion alters TJs, but did not appear to affect AJs in HUVECs. Further quantification of the junctions is required to identify if any subtle changes are occurring.
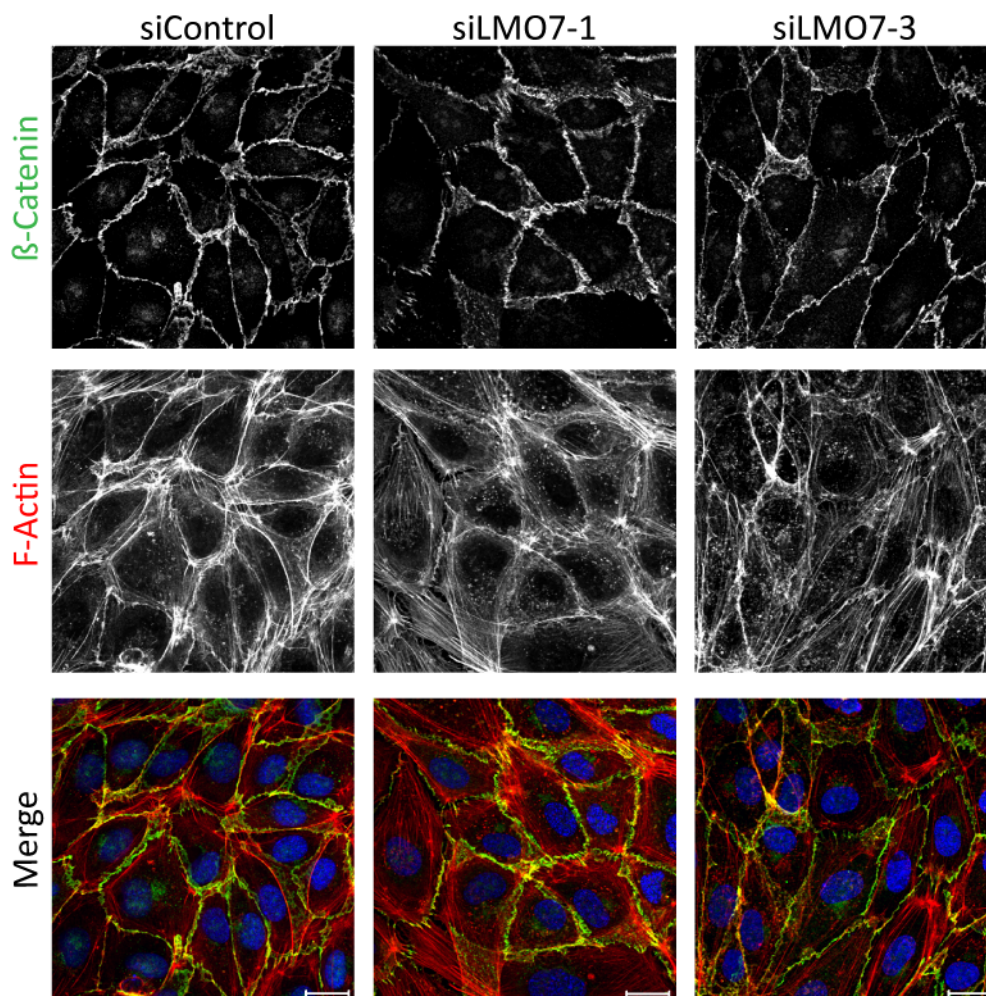
Figure 5.21 LMO7 depletion does not appear to affect adherens junctions in HUVECs

Immunofluorescence micrographs of HUVECs transfected with siRNA targeting LMO7. Cells were seeded on FN-coated coverslips 48 h after transfection, and fixed after a further 24 h. Cells were stained with β-catenin for adherens junctions (green in merge), Alexa Fluor 546-conjugated phalloidin for F-actin (red in merge), and DAPI for nuclei (blue in merge). Images were acquired by confocal microscopy with a 63x oil immersion objective and are maximum intensity projections of 10 confocal z-stacks, spanning 4 μm with 0.4 μm intervals between each image. Images are representative of random fields from three independent experiments. Scale bars are 20 μm.

Figure 5.22 LMO7 depletion alters tight junctional proteins

Immunofluorescence micrographs of HUVECs transfected with siRNA targeting LMO7 or control siRNA. Cells were seeded on FN-coated coverslips 48 h after transfection, and fixed after a further 24 h. Cells were stained with antibodies to ZO-1 for tight junctions (green in merge), Alexa Fluor 546-conjugated phalloidin for F-actin (red in merge), anti CD31 (PECAM-1) antibody (magenta in merge), and DAPI for nuclei (blue in merge). Yellow-boxed areas are shown at higher magnification to the right. Images were acquired by confocal microscopy with a 63x oil immersion objective and are maximum intensity projections of 10 confocal z-stacks, spanning 4 µm with 0.4 µm intervals between each image. Images are representative from three independent experiments. Scale bars are 20 µm.

5.4.4   LMO7 knock-down does not affect cell motility in a wound healing assay

LMO7 was shown to play an important role in breast cancer migration by relieving actin-mediated inhibition through Rho-dependent myocardin-related transcription factors (MRTFs) (Hu et al., 2011). In order to investigate the role of LMO7 in endothelial cell migration, LMO7-depleted cells were assessed for their ability to migrate in the ORIS^{TM} migration assay. The experiment was performed as described for RICH-1-depleted cells (see section 5.2.4) using siRNAs targeting LMO7.

Depleting cells of LMO7 did not significantly increase cell migration compared to siControl-transfected cells (Figure 5.23). When the experiment was repeated in the presence of insulin, the migration of LMO7-depleted cells slightly increased when compared to unstimulated cells, however this effect was not statistically significant as observed with mock and siControl-treated cells (Figure 5.23). Due to time limitations, the effect of insulin on LMO7-depleted HUVECs was only investigated using one oligo (siLMO7-1), and further analysis is required for siLMO7-3.
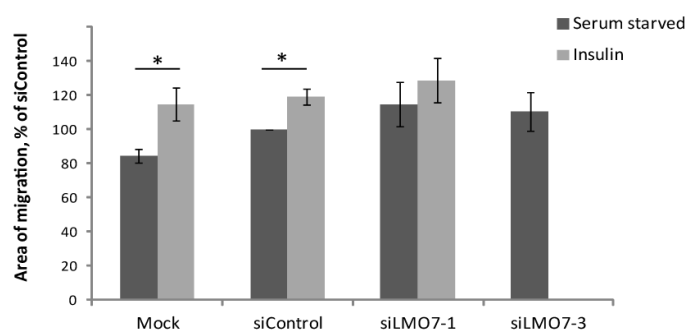
Figure 5.23 LMO7 knock-down does not affect endothelial cell migration

HUVECs were transfected with siRNAs targeting LMO7 or control siRNA. After 24 h cells were stained with Cell-Tracker Orange fluorescent dye, seeded in wells containing a central insert, and incubated for 24 h at 37°C. The inserts were then removed to create a central wound in the monolayer, and imaged at 4x magnification. For the insulin studies, cells were serum starved for 2 h prior to removing the inserts, imaged and then stimulated with 100 nM insulin. Cells were incubated for 24 hours at 37°C and imaged again using the saved locations of initial wounds. The migratory capacity of the cells was quantified by measuring the percentage area of the central wound that cells had migrated into after 24 h using ImageJ software, as a percentage relative to siControl cells. Data shown are the mean of four and three independent experiments ± SEM of unstimulated and insulin studies, respectively. Statistical significance was assessed by an unpaired Student's t-test; *p<0.05.

5.4.5   LMO7 depletion might increase loop formation in an in vitro angiogenesis assay

LMO7 gene knockdown experiments in zebrafish embryos resulted in severe defects in heart development (Ott et al., 2008). The role of LMO7 in an angiogenesis assay was investigated. Depleting cells of LMO7 resulted in a significant increase in loop formation after 24 h, when compared to siControl treated cells (Figure 5.24, Movies S3 and S6), only with one of the two siRNA oligos. siLMO7-1 had a greater knockdown efficiency than siLMO7-3 (see Figure 5.20), and this could account for the lack of effect of siLMO7-3. However, siLMO7-3 treated HUVECs appeared to form loops faster than siControl treated cells (see 4 h time-point in Figure 5.24), and thus quantification at time-points earlier than 24 h might result in a different quantitative outcome.
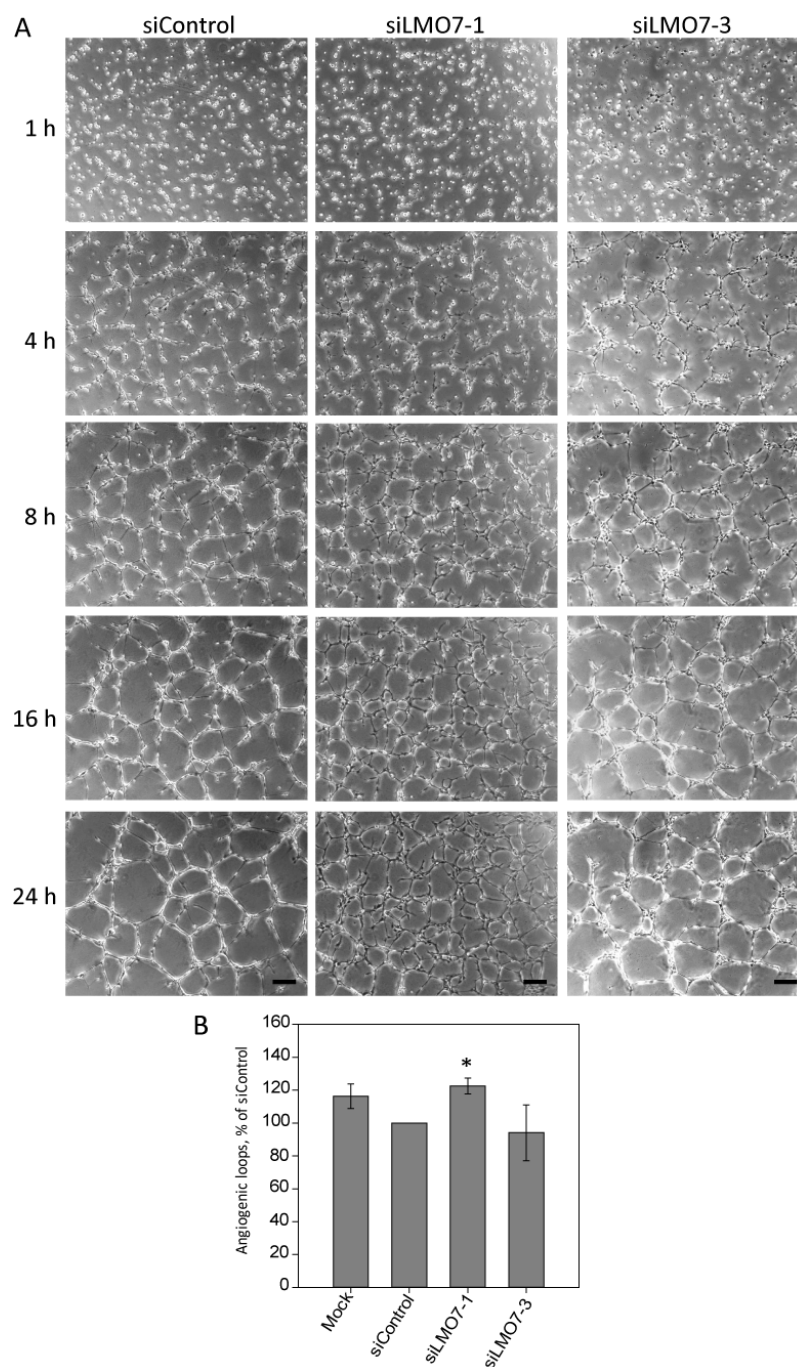
Figure 5.24 LMO7 depletion might increase loop formation in an angiogenesis assay

HUVECs were transfected with siRNAs targeting LMO7. Cells were seeded onto polymerised Matrigel (4.5 mg/ml) 48 h after transfection, incubated for 1 h at 37 °C and loop formation was monitored by time-lapse microscopy using a 4x objective, acquiring images every 20 min for 24 h (A). Quantification was performed by counting the total number of complete loops per field at 24 h, as a percentage relative to siControl cells (B). At least 5 fields were scored per condition in each experiment and data shown are the mean of four and three independent experiments for siLMO7-1 and siLMO7-3, respectively, normalised to siControl ± SEM (siControl = 100%). Statistical significance was assessed by the Mann-Whitney U test; *$p < 0.05$. Scale bars are 200 µm.

5.4.6   LMO7 depletion does not affect basal endothelial cell permeability

LMO7 has been shown to stabilise epithelial adherens junctions by binding to α-actinin and afadin and linking the nectin-afadin and cadherin–catenin complexes (Ooshio et al., 2004). A FITC-dextran permeability assay was performed with LMO7-depleted cells to determine if LMO7 plays a role in endothelial barrier function. Depleting HUVECs of LMO7 did not affect endothelial permeability, as no significant change was observed between LMO7-depleted and siControl-treated cells (Figure 5.25).

Together with immunostaining data (section 5.4.3), this suggests that endothelial barrier function is maintained without the presence of LMO7, even though ZO-1 localisation was altered.
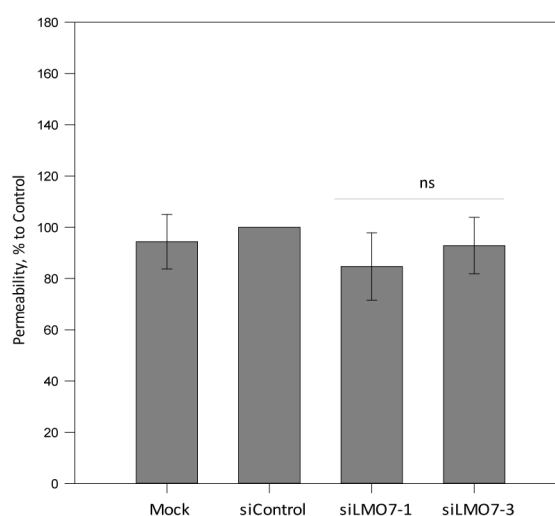
Figure 5.25 LMO7 depletion does not affect endothelial cell permeability

HUVECs were transfected with siRNAs targeting LMO7. Cells were seeded onto Transwell™ filters (0.4 µm pore size) 48 h after transfection and incubated for 24 h at 37 °C. FITC-dextran (0.1 mg/ml) was added to the upper chamber and the lower chamber fluorescence was measured after 60 min. Fluorescence was measured for duplicate wells and quantified as a percentage relative to control. Data shown are the mean of three and four independent experiments for siLMO7-1 and siLMO7-3, respectively, ± SEM. Statistical significance was assessed by the Mann-Whitney *U* test; ns = not significant.

5.5 Epsin2

Epsins were first discovered as interacting partners of the endocytic accessory protein Eps15 (and therefore named *Eps*15-*in*teracting protein, Epsin) (Chen et al., 1998), and were found to be necessary for endocytosis (Wendland et al., 1999). Endocytosis is an essential cellular process in which cells internalise sections of the plasma membrane to (i) actively take up extracellular materials (such as nutrients), and (ii) to control the composition of their membrane and surface area (Sen et al., 2012). It is also crucial for cell homeostasis, as internalising activated ligand-receptor complexes from the cell surface regulates multiple signalling pathways and downstream signal transduction. There are several forms of endocytosis (reviewed in Conner and Schmid, 2003); however this section will focus on the clathrin-mediated pathway as Epsin2 belongs to a family of endocytic clathrin adapters (Rosenthal et al., 1999). Clathrin is a self-assembling protein that forms a coated pit on the inner surface of the plasma membrane that then buds into the cell to form a coated vesicle in the cytoplasm of the cell (Brodsky, 2012). This highly coordinated process requires adaptor proteins that bind to clathrin, as it cannot bind directly to membranes and cargo. The adaptor proteins select transmembrane cargos that have been monoubiquitinated at the plasma membrane, induce invagination, scission and release of the newly formed endocytic vesicle into the cytosol (Wendland, 2002). Adaptor proteins also interact with accessory proteins, which bind phospholipids and stimulate the assembly of clathrin into polymerised baskets (Wendland, 2002).

Mammals express three epsins: Epsin 1, Epsin 2, and Epsin 3 encoded by different genes (EPN1, EPN2, and EPN3, respectively). EPN1 and 2 are highly expressed in the brain, but are broadly expressed in all tissues tested (Chen et al., 1998; Chen et al., 2009; Rosenthal et al., 1999), whereas EPN3 is highly expressed in the stomach compared to other tissues (Ko et al., 2010). Epsins contain an epsin N-terminal homology (ENTH) domain, which directly interacts with PIP_2 in the plasma membrane and also has membrane-deforming properties (Ford et al., 2002), followed by two ubiquitin-interacting motifs (UIM) and an unstructured region

containing motifs for clathrin binding, EPS15 binding and adapter protein-2 (AP-2) binding (Chen et al., 1998; Itoh et al., 2001; Polo et al., 2002; Reider and Wendland, 2011; Rosenthal et al., 1999) (Figure 5.26). Epsins are recruited at the early stages of endocytosis via the binding of its ENTH domain to PIP_2, and its interactions with other coat components (Itoh et al., 2001).
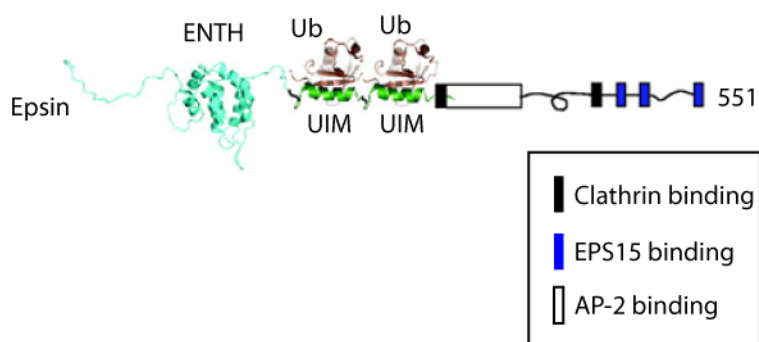
Figure 5.26 Representation of the molecular architecture of Epsin 1 and 2

Epsins 1 and 2 consist of an epsin N-terminal homology (ENTH) domain followed by two ubiquitin (Ub)-interacting motifs (UIM) and an unstructured region containing motifs for clathrin binding (black blocks), EPS15 binding (blue blocks) and AP-2 binding (white block). Figure adapted from Reider and Wendland, 2011.

Epsin plays an important role in signalling regulation. Mice lacking either EPN1 or EPN2 did not display any obvious phenotypic defects, suggesting redundant functions. However, double knockout of EPN1 and EPN2 in mice resulted in embryonic lethality at the beginning of organogenesis (embryonic day 10), due to the disruption of Notch signalling, with embryos exhibiting major angiogenesis defects (Chen et al., 2009). However, in mouse models with constitutive or inducible deletions of EPN1 and EPN2 specifically in endothelial cells, adult mice did not exhibit any abnormal phenotypes (Pasula et al., 2012). This suggests that a lack of EPN1 and EPN2 after the vasculature has developed has little impact on established vessels in normal tissues. Interestingly, a lack of epsin in the vasculature in a tumour environment resulted in highly disorganized vascular structures, leaky

vessels and a reduction in tumour growth, due to excessive vascular endothelial growth factor (VEGF) signalling (Pasula et al., 2012). VEGF promotes epsin binding to ubiquitinated vascular endothelial growth factor receptor 2 (VEGFR2), for endocytosis to occur, and subsequent degradation of VEGFR2. Endothelial epsins therefore negatively regulate VEGF signalling and in their absence this signalling cannot be attenuated, resulting in non-productive leaky angiogenesis (Pasula et al., 2012).

Aguilar et al. (2006) report that epsins are an important link between the endocytic and cell polarity machineries as the ENTH domain regulates specific Cdc42 signalling pathways in yeast cells. Epsins bind to Cdc42 GAPs and sequester their activity, thereby relieving the GAP-induced Cdc42 inhibition (Aguilar et al., 2006). Epsins interact via their ENTH domain with the Cdc42/Rac1 GAP and Ral effector, Ral-binding protein 1 (RalBP1) and this interaction was shown to be essential for cell migration (Coon et al., 2010). In mammalian cells the ENTH domain localises to filopodia and lamellipodia, processes that require precise spatial and temporal fine-tuning of Cdc42 and Rac1 to form (Aguilar et al., 2006).

These studies together indicate the importance of epsins in signal regulation.

5.5.1 GFP-Epsin2 has a punctate cytoplasmic distribution in endothelial cells

The role of epsins in endothelial cells has recently been investigated *in vivo* focusing on the global mechanism of epsins in angiogenesis (Pasula et al., 2012). My study focuses on the role of Epsin2 in endothelial cells in an attempt to elucidate its role in insulin signalling.

GFP-Epsin2 displayed punctate cytoplasmic distribution in HUVECs. This was expected as epsin1 was previously shown to accumulate in puncta in chinese hamster ovary (CHO) cells (Chen et al., 1998) and COS7 cells (Ford et al., 2002). GFP-Epsin2 had no obvious effect on the organisation of the actin cytoskeleton, when compared to GFP-transfected HUVECs (Figure 5.27). Adherens junctions were not affected by GFP-Epsin2 in confluent monolayers, visualised by linear VE-cadherin staining along the cell boundaries (Figure 5.27A). Sub-confluent GFP-Epsin2 expressing cells appeared to exhibit slight membrane ruffling, compared to control GFP-transfected HUVECS (Figure 5.27B). Insulin stimulation of GFP-Epsin2-expressing cells induced lamellipodium formation (Figure 5.28, red arrows), which was not observed in unstimulated cells or cells expressing control GFP. This would need to be quantified to determine if this is a specific response to Epsin2 overexpression.
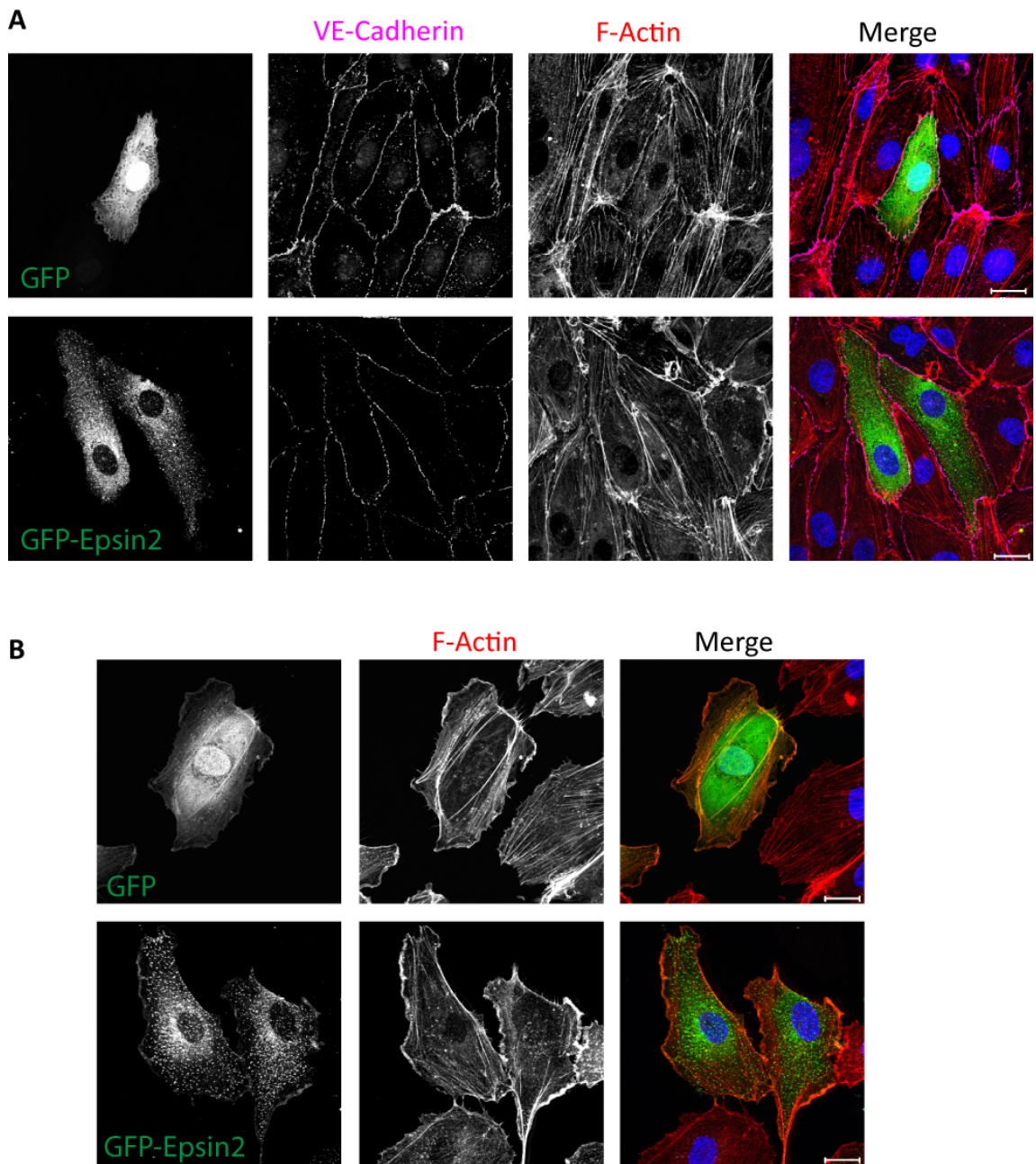
Figure 5.27 GFP-Epsin2 is localised in puncta in the cytoplasm in endothelial cells
HUVECs were transfected with pcDNA5 FRT/TO GFP Epsin2 seeded onto FN-coated glass coverslips and fixed after 24 h. Confluent monolayers (A) and sub-confluent (B) cells were stained with Alexa Fluor 546-conjugated phalloidin for F-actin (red in merge), anti-β-catenin for adherens junctions in confluent monolayers (A, magenta in merge) and DAPI for nuclei (blue in merge). Images were acquired by confocal microscopy with a 63x oil immersion objective and are maximum intensity projections of 10 confocal z-stacks, spanning 4 μm with 0.4 μm intervals between each image. Images are representative fields from three independent experiments. Scale bars are 20 μm.
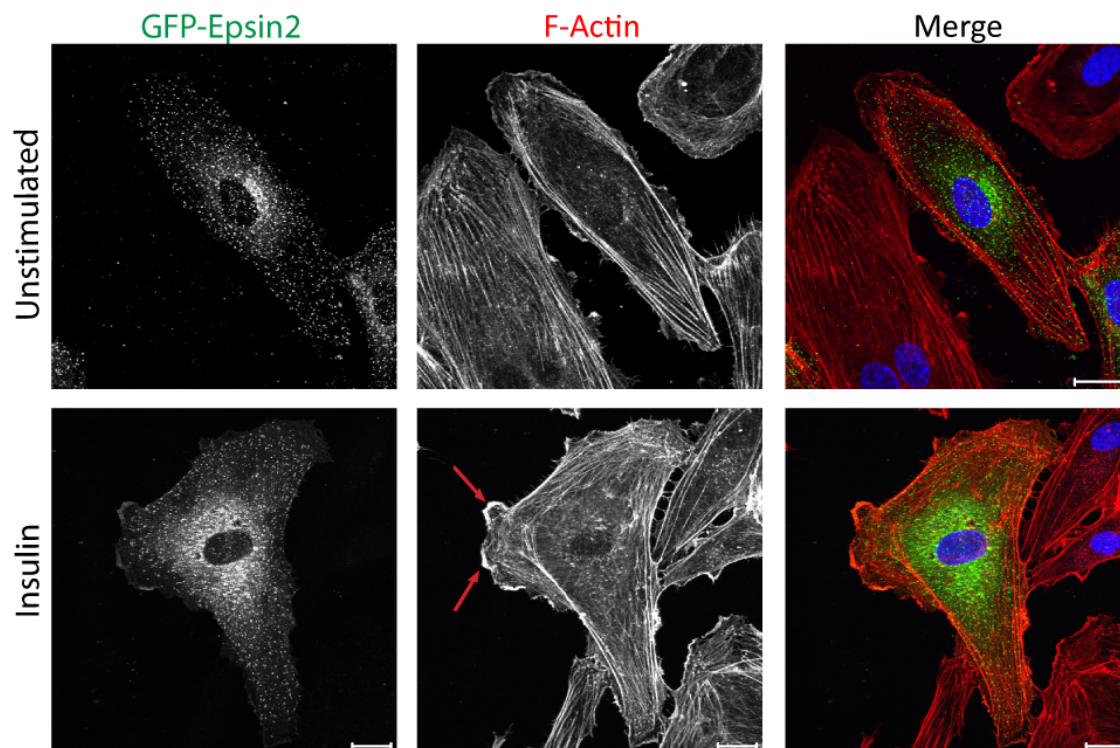
Figure 5.28 Insulin stimulation induces lamellipodia in GFP-Epsin2-expressing ECs
HUVECs were transfected with pcDNA5 FRT/TO GFP Epsin2 and seeded onto FN-coated glass coverslips. Cells were incubated for 24 h and then serum starved for 4 h in EBM2 medium containing 1% FCS. Cells were stimulated with 100 nM insulin for 1 h, fixed and stained with Alexa Fluor 546-conjugated phalloidin for F-actin (red in merge), and DAPI for nuclei (blue in merge). Red arrows indicate lamellipodia. Images were acquired by confocal microscopy with a 63x oil immersion objective and are maximum intensity projections of 10 confocal z-stacks, spanning 4 µm with 0.4 µm intervals between each image. Images are representative fields from three independent experiments. Scale bars are 20 µm.

5.5.2   siRNA mediated knock-down of Epsin2 in endothelial cells

To investigate the functional role of Epsin2 in endothelial cells, Epsin2 expression was down regulated in HUVECs using four siRNA oligonucleotides. A knock-down efficiency of between 78 – 90% was achieved after 72 h, determined by immunoblotting, when compared to a non-targeting control siRNA (Figure 5.29B). Oligonucleotides 4 and 17 were chosen for functional assays, as they provided good knock-down efficiencies and exhibited similar morphological phenotypes when visualised with phase contrast microscopy (data not shown). These siRNAs are referred to as siEpsin2-4 and siEpsin2-17.
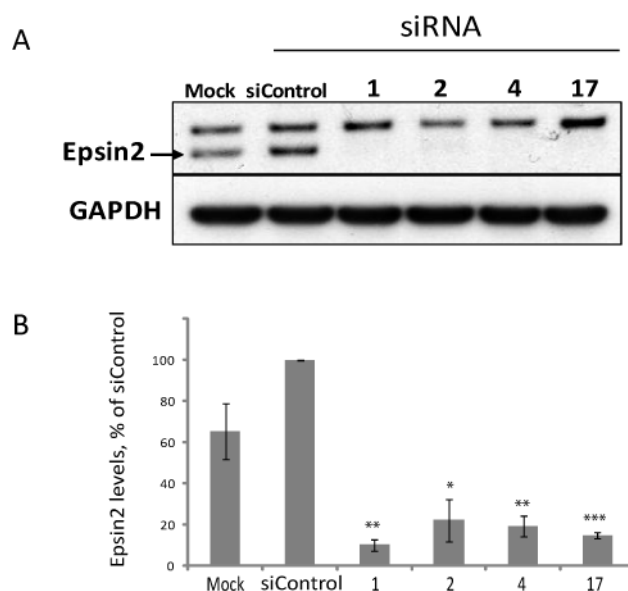
Figure 5.29 siRNA mediated knock down of Epsin2 in HUVECs

Representative immunoblot (A) of HUVECs transfected with 4 different siRNA oligonucleotides targeting Epsin2. Mock represents cells treated with oligofectamine only. Cells were transfected with 20 nM of siRNA using Oligofectamine™, and incubated for 72 h at 37°C, 5% CO_2. Cells were lysed and protein analysed by immunoblotting with an anti-Epsin2 antibody. Blots were re-probed for GAPDH. (B) Data were generated by densitometric scanning of the Western blots, normalised to total GAPDH levels, relative to siControl. Data shown are the mean of three independent experiments ± SEM. Statistical significance was assessed by an unpaired Student's t-test; *$p<0.05$, ** $p<0.005$, ***$p<0.001$

5.5.3 Epsin2 depletion does not induce any morphological changes in ECs

HUVECs were transfected with siRNAs targeting Epsin2 and stained for F-actin and β-catenin (Figure 5.30). Depletion of Epsin2 had no apparent effect on HUVEC morphology (Figure 5.30). Nuclear β-catenin appeared to increase in Epsin2-depleted cells, especially in cells treated with siEpsin2-17.
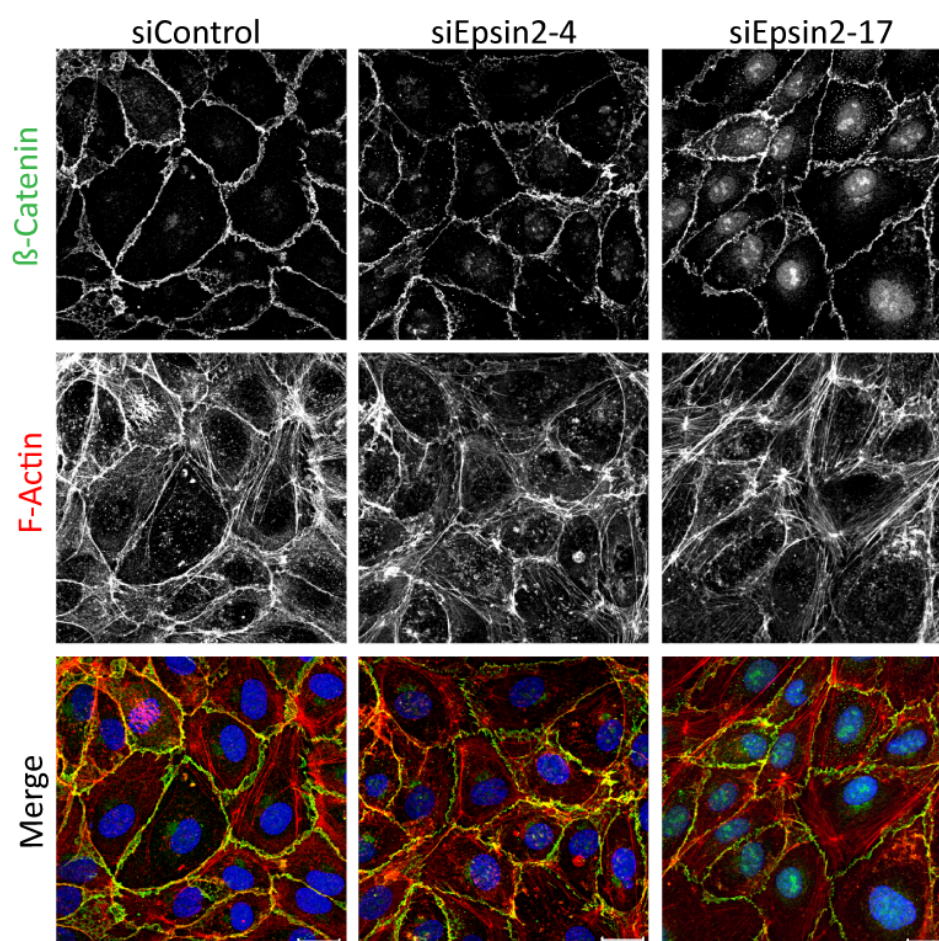
Figure 5.30 Epsin2 depletion does not induce any major morphological changes in HUVECs

Immunofluorescence micrographs of HUVECs transfected with siRNAs targeting siControl and Epsin2. Cells were seeded on FN-coated coverslips 48 h after transfection, and fixed after a further 24 h. Cells were stained with β-catenin for adherens junctions (green in merge), Alexa Fluor 546-conjugated phalloidin for F-actin (red in merge), and DAPI for nuclei (blue in merge). Images were acquired by confocal microscopy with a 63x oil immersion objective and are maximum intensity projections of 10 confocal z-stacks, spanning 4 μm with 0.4 μm intervals between each image. Images are representative fields from three independent experiments. Scale bars are 20 μm.

5.5.4   **Epsin2 depletion does not affect cell motility or permeability**

It has been previously shown that epsins are required for the cell polarity-dependent process of cell migration and invasion in NIH3T3 fibroblasts and HT1080 fibrosarcoma cells, through interaction with the Cdc42/Rac1 GAP and signalling molecule RalBP1 (Coon et al., 2010). This defect in migration was observed in epsin1- and epsin2-double knockdown cells. In order to investigate if Epsin2 has a specific role in endothelial cell migration, the ORIS wound healing migration assay was performed. The experiment was performed as described for RICH-1-depleted cells (see section 5.2.4) using siRNAs targeting Epsin2.

Epsin2 depletion had no significant on cell migration compared to untreated (mock) cells, and non-targeting siControl transfected cells at 24 h, either with or without insulin stimulation (Figure 5.31). Due to time limitations, the effect of insulin on Epsin2-depleted HUVECs was only investigated using one oligo (siEpsin2-4), and further analysis is required for siEpsin2-17.

Epsins have also been shown to be involved in the regulation of Cdc42 signalling (Aguilar et al., 2006), which contributes to stabilising endothelial adherens junctions (Broman et al., 2006). However, Epsin2 deletion did not affect endothelial permeability (Figure 5.32).
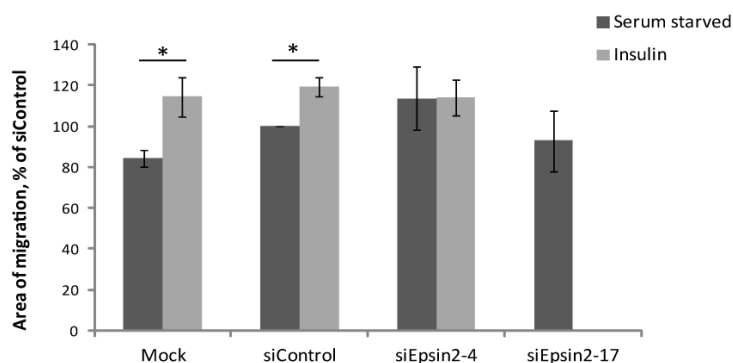
Figure 5.31 Epsin2 knock down does not affect endothelial cell migration in a wound-healing assay

HUVECs were transfected with siRNAs targeting Epsin2 or control siRNA. After 24 h cells were stained with Cell-Tracker Orange fluorescent dye, seeded in wells containing a central insert, and incubated for 24 h at 37°C. The inserts were then removed to create a central wound in the monolayer, and imaged at 4x magnification. For the insulin studies, cells were serum starved for 2 h prior to removing the inserts, imaged and then stimulated with 100 nM insulin. Cells were incubated for 24 hours at 37°C and imaged again using the saved locations of initial wounds. The migratory capacity of the cells was quantified by measuring the percentage area of the central wound that cells had migrated into after 24 h using ImageJ software, as a percentage relative to siControl cells. Data shown are the mean of four and three independent experiments ± SEM of unstimulated and insulin studies, respectively. Statistical significance was assessed by an unpaired Student's t-test; *p<0.05.

Figure 5.32 Epsin2 knock down does not affect endothelial cell permeability

HUVECs were transfected with siRNAs targeting Epsin2. Cells were seeded onto Transwell™ filters (0.4 µm pore size) 48 h after transfection and incubated for 24 h at 37 °C. FITC-dextran (0.1 mg/ml) was added to the upper chamber and the lower chamber fluorescence was measured after 60 min. Fluorescence was measured for duplicate wells and quantified as a percentage relative to control. Data shown are the mean of three independent experiments ± SEM. Statistical significance was assessed by the Mann-Whitney *U* test; ns = not significant.

5.5.5   Epsin2 depletion increases loop formation during angiogenesis

Mice lacking both epsin1 and 2 exhibited major angiogenesis defects and died at E10 (Chen et al., 2009). However, epsin1 and epsin2 deletion specifically in endothelial cells did not show any obvious phenotypic defects in mice (Pasula et al., 2012). In an angiogenesis loop assay Epsin2-depleted-HUVECs attached to Matrigel, elongated, extended cellular processes and established closed loops faster than control cells (see Movies S3 and S7). Cells appeared to be more dynamic, and formed islands of cells from loops merging together. HUVECs depleted of Epsin2 formed significantly more loops than siControl-treated cells (Figure 5.33, Movies S3 and S7).
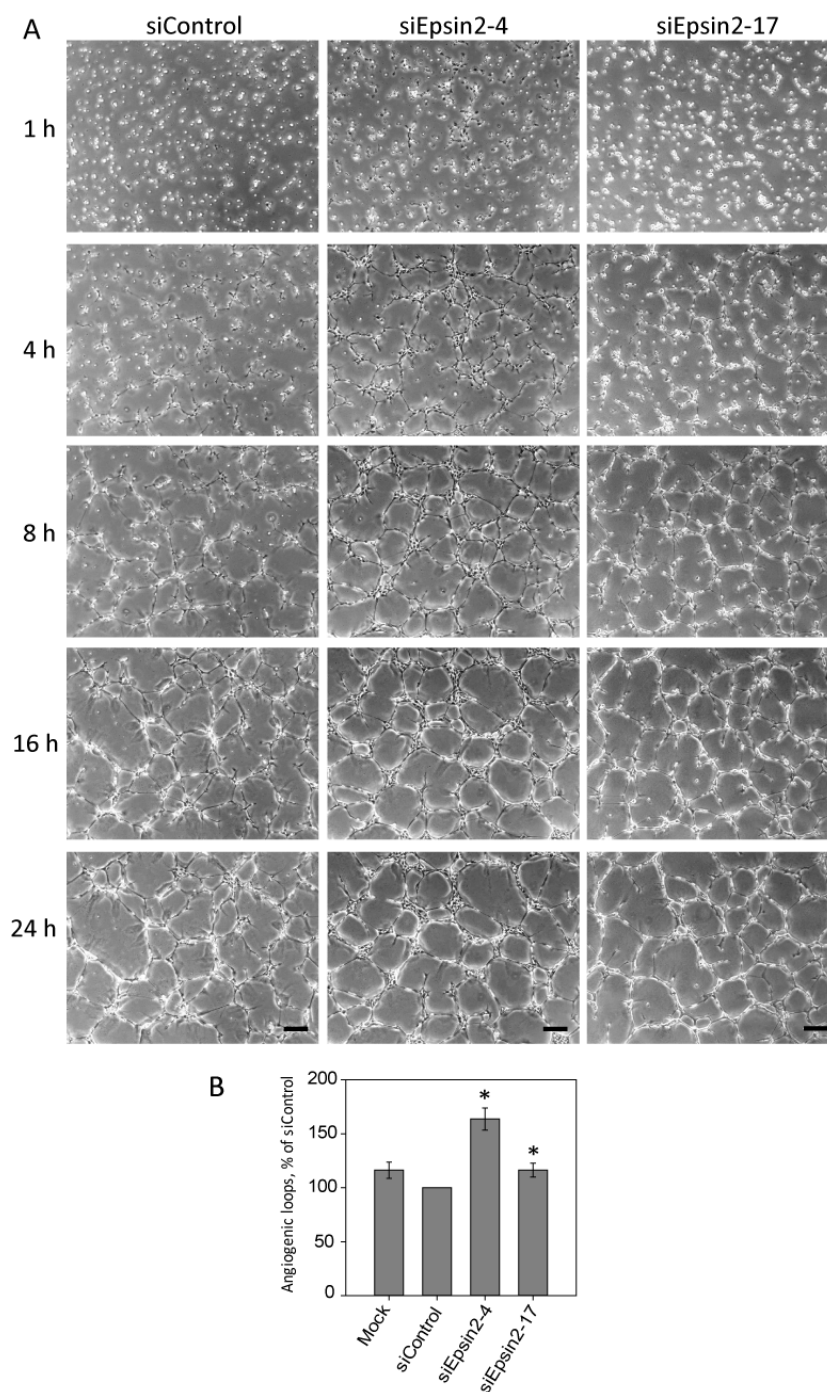
Figure 5.33 Epsin2 depletion increases loop formation in the angiogenesis assay

HUVECs were transfected with siRNAs targeting Epsin2. Cells were seeded onto polymerised Matrigel (4.5 mg/ml) 48 h after transfection, incubated for 1 h at 37 °C and loop formation was monitored by time-lapse microscopy using a 4x objective, acquiring images every 20 min for 24 h (A). Quantification was performed by counting the total number of complete loops per field at 24 h, as a percentage relative to siControl cells (B). At least 5 fields were scored per condition in each experiment and data shown are the mean of four and three independent experiments for siEpsin-4 and siEpsin2-17, respectively, normalised to siControl ± SEM (siControl = 100 %). Statistical significance was assessed by the Mann-Whitney *U* test; *p<0.05. Scale bars are 200 µm.

5.6   Summary

Over-expression and RNA interference analysis of RICH-1, Parg1, LMO7 and Epsin2 were performed in order to elucidate their role in endothelial insulin signalling. A summary of these findings is presented in Table 5.1.

	RICH-1	Parg1	LMO7	Epsin2
Over-expression				
Localisation	Cytoplasm & Membrane	Cytoplasm	Nucleus & Cytoplasm	Cytoplasm (puncta)
Effect on actin cytoskeleton	↑Lamellipodia?	↓ F-Actin		↑Lamellipodia with insulin?
siRNA-mediated knockdown				
Cell-cell junctions				
Adherens junctions		Disrupted		
Tight junctions	Disrupted		Mislocalised	
Cell Migration	↓	↓	→	→
Angiogenesis	→	↓	↑?	↑
Cell Permeability	↑?	↑	→	→

Table 5.1 Summary of characterisation of the insulin-stimulated 14-3-3 binding protein hits in endothelial cells.

Functional assays were performed with insulin-stimulated 14-3-3 binding proteins to elucidate their roles in endothelial cells. All four proteins are important regulators of the endothelial cytoskeleton, as over-expression and RNA interference analysis resulted in morphologic and functional changes. Down arrows (blue) indicate a decrease in the assay, up arrows (red) show an increase, and right arrow indicates no change was observed.

5.7 Discussion

The functional roles of the selected insulin-sensitive 14-3-3 binding proteins RICH-1, Parg1, LMO7 and Epsin2 are not well known in ECs. Overexpression analysis and an RNAi approach were primarily used to assess these roles, and the analyses presented in this chapter provides insight into their involvement in the anti-inflammatory effects of insulin.

5.7.1 Possible roles of RICH-1 at the plasma membrane

In sub-confluent HUVECs, GFP-RICH-1 localised in the cytoplasm and at the plasma membrane in lamellipodial protrusions. BAR domain proteins have emerged as central regulators of dynamic membrane remodelling (reviewed in (Mim and Unger, 2012)). The mechanisms involved in membrane curvature are not fully elucidated, however it has been proposed that BAR domain proteins act as scaffold proteins that recruit different binding partners and coordinate the different events during the endocytic process (Qualmann et al., 2011). The well-established roles of the endocytic system involve sorting, processing and degradation of internalized cargo using a series of compartments including early and recycling endosomes, multivesicular bodies, late endosomes and lysosomes. However, recent evidence suggests that endosomes have key roles in other processes such as cellular signalling, cytokinesis, cell polarization and migration (reviewed in (Gould and Lippincott-Schwartz, 2009). BAR proteins bind to phospholipids and spherical liposomes, transforming them into long tubes. This tubulating activity was firstly observed with the endocytic proteins dynamin 1, amphiphysin-1 (Takei et al., 1999), endophilin (Farsad et al., 2001) and Epsin1 (Ford et al., 2002). The BAR domain of RICH-1 binds to membrane phospholipids and is capable of deforming liposomes into tubular structures (Richnau et al., 2004). Interestingly, RICH-1 localised on vesicular structures when cells were stimulated with insulin. Does this finding suggest that RICH-1 could play a role in vesicle formation or membrane transport? Aspenström and colleagues (Richnau and Aspenstrom, 2001; Richnau et al., 2004) have demonstrated that RICH-1 interacts with endophilin and amphiphysin through

its proline-rich motif. Moreover, a pulldown of RICH-1 identified two endocytic adapter proteins CIN85 (cognate adaptor cbl-interacting protein of 85 kDa) and CD2AP (CD2-associated protein) (Wells et al., 2006), which form a complex with endophilin that targets epidermal growth factor (EGF) (Dikic, 2002; Kowanetz et al., 2004; Soubeyran et al., 2002) and hepatocyte growth factor (HGF) (Petrelli et al., 2002) receptors for endocytosis. It would be interesting to investigate whether RICH-1 modulates insulin signalling via IR recycling, and whether 14-3-3 proteins facilitate this mechanism.

5.7.2   RICH-1 is important for tight junctional integrity in endothelial cells

The most striking effect of RICH-1 depletion by RNAi in ECs was the disruption of tight junctions. This has previously been observed in epithelial cells, in which the GAP activity of RICH-1 was required for proper TJ maintenance and long-term stability (Wells et al., 2006). Furthermore, that study identified that RICH-1 binds through a scaffold protein angiomotin (Amot) to the polarity proteins Pals1 (Proteins Associated with Lin Seven 1) (Straight et al., 2004), Patj (PALS1-Associated Tight Junction protein) (or its paralogue Mupp1) (Shin et al., 2005) and Par3 that are all necessary for proper TJ integrity in epithelial cells (Wells et al., 2006). It has been proposed that the association of the PDZ-binding motif with scaffolding proteins could be a general mechanism of confining GTPase activity to distinct subcellular compartments (Garcia-Mata and Burridge, 2007). Amot contains a PDZ-domain binding motif that interacts with Patj that also binds TJ components ZO-3 and claudin (Roh et al., 2002), thereby recruiting Amot and RICH-1 to the tight junctions (Wells et al., 2006). Amot and RICH-1 interact through BAR/coiled-coil domains and both proteins fail to localise at the TJs without these domains with RICH-1 shifting from the membrane to the cytoplasm (Wells et al., 2006). Interestingly, expression of Amot inhibits RICH-1 GAP activity against Cdc42. The effect of protein phosphorylation on this interaction is yet to be determined. Further studies are required to investigate whether the phosphorylation of RICH-1

by insulin, and the subsequent binding of 14-3-3 proteins, affects the interaction of Amot and RICH-1.

Apical and basolateral polarity in epithelial cells is controlled by the precise temporal and spatial localization of a conserved set of polarity proteins that form complexes. The apical Par3/Par6/aPKC complex is fundamental for epithelial polarity (recently reviewed in (Chen and Zhang, 2013). Par3 is known to interact at epithelial cellular junctions (Izumi et al., 1998), while Par6 and aPKC maintains the integrity of the apical domain (Martin-Belmonte et al., 2007). Protein phosphorylation is emerging as a key mechanism by which polarity proteins are regulated (Nagai-Tamai et al., 2002). It has previously been shown that the Par3/Par6/aPKC polarity complex is regulated in a phosphorylation-dependent mechanism through 14-3-3 binding (Hurd et al., 2003). Par3 directly interacts with 14-3-3 and this interaction requires the phosphorylation of Par3 at serine 144 (Hurd et al., 2003). Interestingly, aPKC and Par3 have been shown to interact with RICH-1 in Flag-RICH-1 immunoprecipitates, but no interaction was observed between Par6 and RICH-1 (Wells et al., 2006). Further analysis is required to investigate if there is a direct interaction between RICH-1 and Par3 or if 14-3-3 proteins act as a scaffold for the polarity complex to form upon protein phosphorylation. If the latter is true, insulin stimulation could possibly phosphorylate both proteins, inducing 14-3-3 binding and formation of a complex that could regulate cell polarity and barrier control.

Transmembrane proteins of the tight junctions are delivered to the plasma membrane in vesicles and are constitutively recycled into endosomes to maintain functional tight junctions (Fletcher and Rappoport, 2014). Further studies investigating the involvement of RICH-1 in vesicle formation could elucidate if this mechanism contributes to trafficking of transmembrane proteins and maintaining the endothelial barrier.

5.7.3 RICH-1 regulates endothelial cell migration

Amot was initially recognized for roles in the migration of ECs, localising to lamellipodia at the leading edge of migrating cells (Troyanovsky et al., 2001). Amot-deficient ECs exhibited a loss of polarity, assessed by Golgi orientation, and had impaired directional migration in response to chemotactic factors (Aase et al., 2007). Furthermore, RICH-1 failed to localise to lamellipodia in Amot-deficient immortal ECs (Aase et al., 2007). It would be interesting to further investigate if the decrease in cell migration was due to the mislocalisation of RICH-1 rather than Amot alone, as RICH-1 depleted HUVECs also exhibit a significant defect in cell migration in a wound-healing assay.

The RICH-1 interacting protein CD2AP has also recently been shown to interact with cortactin and capping protein at the cell periphery, facilitating lamellipodial formation (Zhao et al., 2013). As an increase in membrane ruffling was observed in GFP-RICH-1 overexpressing HUVECs and cell migration was impaired in RICH-1 depleted cells, it would be interesting to investigate whether RICH-1 is involved in this complex.

5.7.4 Parg1 is an endothelial cytoskeletal regulator

Altering the expression of Parg1 induced striking cytoskeletal changes in HUVECs. Expression of GFP-Parg1 resulted in a decrease of endothelial F-actin levels with a noticeable loss of radial stress fibres. Moreover, depletion of Parg1 produced a distinct morphological phenotype in which cells appeared to elongate, induce stress fibres that traverse the length of the cell and have disrupted cell-cell junctions. Multiple signalling pathways are involved in the formation of stress fibres in ECs (Beckers et al., 2010) and the Rho-ROCK signalling pathway is fundamental in the regulation of stress fibres (Naumanen et al., 2008). Parg1 has been shown to have preferential GAP activity towards RhoA over Rac1 and Cdc42 (Saras et al., 1997). Previous studies have shown that silencing Parg1 in HUVECs decreased activated Cdc42 and Rac1 levels and upregulated RhoA activation (Xu et al., 2011). Activation of Rho results in increased activity of its effector ROCK, which phosphorylates MLC2

and MYPT1, resulting in increased actomyosin contraction (Kimura et al., 1996) (see Chapter 1.4.2). Thus, overexpression of Parg1 results in RhoA down regulation, preventing stress fibre formation. HA-Parg1 expression in fibroblasts resulted in a distinct morphological phenotype whereby cells rounded up and extended long beaded dendritic processes with no actin stress fibres (Myagmar et al., 2005). Conversely, Parg1 depletion activates RhoA, resulting in MLC2 phosphorylation and stress fibre formation.

5.7.5   Parg1 is required to maintain endothelial barrier function

Perturbations to the actin cytoskeleton can affect the integrity of endothelial monolayers. Stress fibres in confluent endothelial cells are predominantly linked to adherens junctions (Millan et al., 2010) and stress fibre induction can lead to a physical disruption of cell-cell junctions as a result of an increase tensile force. Parg1 depletion resulted in an increase in endothelial permeability, suggesting that cell-cell junctions were disrupted. This was supported by discontinuous β-catenin staining of confluent HUVEC monolayers upon Parg1 depletion. Furthermore, it has recently been shown that depletion of Parg1 decreased basal electrical impedance in HUVECs, indicative of junction disruption (Post et al., 2013).

The small GTPase Rap1 regulates endothelial barrier function and cell spreading by coordinating both integrin-mediated and cadherin-mediated adhesions (reviewed in (Jeyaraj et al., 2011). This dynamic modulation is regulated by the cAMP activation of Rap1 through the GEF Epac1 (exchange factor directly activated by cAMP) (Borland et al., 2009). In cultured HUVECs, activation of Epac1–Rap1 by cAMP enhances endothelial barrier function through the recruitment of β-catenin, resulting in the stabilization of VE-cadherin at cell-cell junctions (Fukuhra et al., 2006), altering actin cytoskeleton organization and activating microtubule growth (Jeyaraj et al., 2011). Recently, Parg1 has been shown to mediate Rap1 regulation in endothelial barrier function by interacting with the Rap1 effector, ras-interacting protein 1 (Rasip1) and the Rasip1 homologue, Radil (Post et al., 2013). Parg1 is required as part of the effector complex for Rap1-mediated cell spreading and

endothelial barrier control. Epac1-Rap1 signalling disrupts radial stress fibres and induces cortical actin bundles resulting in a switch from discontinuous, motile junctions into linear, stable junctions (Cullere et al., 2005; Kooistra et al., 2005; Pannekoek et al., 2011). Epac-Rap1 signalling is involved in insulin exocytosis in β-cells (Leech et al., 2010). As GFP-Parg1 expressing HUVECs exhibited less radial stress fibres and stable reticular cell-cell junctions, further analysis into the effect of insulin on the Rap1 signalling pathway in ECs is warranted to investigate whether the enhanced endothelial barrier function induced by insulin occurs through this signalling cascade.

5.7.6   Parg1 is required for EC migration and angiogenic loop formation

An *in vitro* angiogenesis assay was used to determine whether Parg1 is involved in regulating angiogenesis. This assay simulates angiogenesis by testing the capacity of ECs to organise into stable networks that result in the formation of loop-like structures when plated onto polymerised Matrigel. Although this assay represents only a part of the angiogenic process, it provides insight into the mechanisms involved for the initial stages of cord sprouting angiogenesis (Goodwin, 2007). HUVECs initially extended cellular processes within the first 8 h, however in Parg1-depleted cells there were fewer extensions made and those that were able to connect with other cells eventually collapsed. A decrease in loop formation was observed in Parg1-depleted HUVECs, as cells were unable to maintain these connections. Previous *in vitro* studies have shown that Cdc42 and Rac1 mediate endothelial lumen formation, while RhoA activation suppresses it (Bayless and Davis, 2002, 2004; Koh et al., 2009). Silencing Parg1 in HUVECs decreased levels of activated Cdc42 and Rac1, and upregulated RhoA levels (Xu et al., 2011), which could contribute to the defect in angiogenesis observed. Furthermore, depleting HUVECs of Parg1 significantly reduced their ability to migrate in the wound-healing assay. For effective angiogenic sprout formation, ECs need to migrate and this defect could result in the limited ability of Parg1-depleted HUVECs to sprout.

5.7.7   **LMO7 and endothelial tight junction regulation**

LMO7 localises diffusely in the nucleus and cytoplasm of ECs as observed in other cell types, MDCK (Yamada et al., 2004), MTD-1A (Ooshio et al., 2004), C2C12 myoblasts (Dedeic et al., 2011) and HeLa cells (Holaska et al., 2006). Although GFP-LMO7 did not localise at endothelial AJs as previously described in epithelial cells (Ooshio et al., 2004), the importance of LMO7 in TJ regulation appears to be consistent across cell types. LMO7 transduces signals from the cell surface to the nucleus and it has been previously proposed that specific signals could release LMO7 from its sequestered position at the plasma membrane, allowing it to translocate to the nucleus to enhance the expression of emerin and other LMO7-dependent genes (Holaska et al., 2006). Could insulin trigger this shift by phosphorylating LMO7 and inducing 14-3-3 binding? This is plausible, as 14-3-3-mediated conformational changes can facilitate subcellular relocalization by deforming and/or masking a nuclear localization signal (Muslin and Xing, 2000).

Many reports have suggested that AJs and TJs are functionally and structurally linked and while EC AJs were not visibly affected by the overexpression or depletion of LMO7, AJs could influence TJ organization (Ikenouchi et al., 2007; Taddei et al., 2008). Similar to LMO7, the AJ protein β-catenin is also a transcription factor that is tethered to the plasma membrane by cadherins and α-catenin (Liebner et al., 2006; Wheelock and Johnson, 2003) (see Chapter 1.2.2.1). When β-catenin translocates to the nucleus it modulates cell transcription. Not much is known about the genes modulated by β-catenin specifically in ECs; however, β-catenin can stabilize Forkhead-box protein-O1 (FoxO1) at the promoter of the TJ protein claudin-5 (Taddei et al., 2008). β-catenin forms a complex with the T-cell factor (TCF), which is constitutively associated with the *claudin-5* promoter, and with FoxO1, this complex represses the expression of claudin-5 (Gavard and Gutkind, 2008). Interestingly, Akt phosphorylation of FoxO induces 14-3-3 binding, reducing its transcriptional activity (Brunet et al., 1999; Cahill et al., 2001). Binding of 14-3-3 masks the DNA binding domain of FoxO, as well as increasing nuclear export sequestering it in the cytoplasm (reviewed in (Tzivion et al., 2011). Previous studies have demonstrated that insulin is able to inhibit the transcriptional activity of FoxO (Perrot and Rechler, 2003; Tsai et al., 2003). If the phosphorylation of LMO7 and concomitant binding of 14-3-3 resulted in nuclear importation, emerin expression

would increase, because LMO7 positively regulates emerin (Holaska et al., 2006). Emerin binds directly to β-catenin and attenuates β-catenin activity by restricting its accumulation in the nucleus (Markiewicz et al., 2006). Moreover, 14-3-3 proteins have also been shown to sequester β-catenin in the cytoplasm when phosphorylated by Akt (Tian et al., 2004).

In summary, further studies are required to test if insulin enhances emerin levels by nuclear importation of LMO7. Hypothetically, insulin stimulation could upregulate claudin-5 indirectly, by releasing the inhibitory effect of FoxO1 and β-catenin through the induction of Akt and 14-3-3 binding.

5.7.8   Insulin stimulation of GFP-Epsin2-expressing HUVECs induces lamellipodium formation

Epsins were initially discovered as a result of their ability to bind components of the endocytic machinery and were identified as key adaptor proteins required for endocytosis (Chen et al., 1998; Wendland et al., 1999). However, recent studies are beginning to elucidate the critical roles that epsins play in signalling (reviewed in (Sen et al., 2012). Epsins are able to regulate Cdc42 by interacting with and sequestering Cdc42 GAPs in yeast (Aguilar et al., 2006), similar to the epsin-interacting protein, intersectin (Hussain et al., 2001; Jenna et al., 2002). Interestingly, epsins are also able to regulate Rac signalling through its interaction with RalBP1 (Coon et al., 2010). Epsin depletion led to decreased levels of activated Rac1, resulting in cell migration defects (Coon et al., 2010).

HUVECs expressing GFP-Epsin2 displayed a punctate cytoplasmic distribution as previously observed in other cell types, such as fibrosarcoma cells (Coon et al., 2010). Insulin stimulation appeared to increase lamellipodia in GFP-Epsin2-expressing cells. These extensions were not observed in unstimulated cells and thus it would be interesting to investigate whether insulin stimulation activates RalBP1 signalling, increasing localised active Rac1 that could induce these protrusions at the plasma membrane.

Espin2-depletion did not affect migration of unstimulated ECs, in contrast to what was observed in fibrosarcoma cells (Coon et al., 2010). Interestingly, insulin did not

increase cell migration in Epsin2-depleted HUVECs. This suggests that primary ECs require an external stimulus to recruit epsins to drive the migratory machinery, whilst cancer cells may secrete autocrine factors that act via epsins to promote cell migration.

5.7.9   Epsin2 is required to regulate angiogenesis

Epsin2 depletion in ECs resulted in an increase of loop formation in an *in vitro* angiogenesis assay. It has previously been demonstrated that silencing of Epsin1 and Epsin2 in HUVECs results in elevated VEGFR2 signalling (Pasula et al., 2012). VEGF signalling is crucial for angiogenesis, initiating signal cascades required for EC migration and proliferation (reviewed in (Olsson et al., 2006); see Chapter 1.5). VEGF induces epsin binding to ubiquitinated VEGFR2, promoting endocytosis and degradation of the receptor (Pasula et al., 2012). In the absence of epsin, VEGF signalling is constitutively active leading to increased proliferation of ECs.

Interestingly, an increase in cell migration was observed in HUVECs depleted of both Epsin1 and Epsin2 (Pasula et al., 2012), whereas no significant change in cell migration was observed with Epsin2-depleted HUVECs in the ORIS wound-healing assay. Mice lacking either epsin grew normally and did not exhibit any phenotypic defects, whereas double knockout mice died at E10 (Chen et al., 2009). The authors suggest that Epsin1 and Epsin2 function redundantly, and that isoform-specific functions are not essential for life. However, these findings do not exclude specific and unique roles of either isoform, for example specifically in ECs. So although Epsin2-depletion increases angiogenic loop formation, it may be that Epsin1 is able to compensate for Epsin2 depletion during cell migration. This suggests that the increase in loop formation could be due to an increase in proliferation due to excessive VEGF signalling, however further studies are required to confirm this.

As insulin stimulates angiogenic loop formation (see Chapter 3.5), it would be interesting to investigate whether the insulin-stimulated phosphorylation of Epsin2, and subsequent binding of 14-3-3, sequesters the ability Epsin2 to bind to ubiquitylated   VEGFR2   thus   enhancing   VEGF/VEGFR2   signalling.

6   Concluding Remarks

Insulin elicits metabolism-independent, anti-inflammatory protection against myocardial ischaemic injury and the development of atherosclerosis (Yu et al., 2011). However, the mechanisms through which insulin exerts this protection are not fully understood. Although a loss of endothelial barrier function is one of the earliest indications of inflammation (Libby, 2012), the roles of insulin in endothelial barrier regulation are not well described. This thesis provides some insight into the effect of insulin on the endothelial cytoskeleton and cell-cell junctions.

Results presented in this thesis suggest that insulin could possibly mediate its protective action by activating proteins that stabilise the cell-cell junctions. This study was performed in a non-diseased cell model with functional insulin signalling pathways. However, these findings may not be evident or beneficial in certain pathological states, such as insulin resistance or cancer. This study focused on the role of insulin as a cardioprotective agent in the context of CVD.

Insulin was shown to decrease basal HUVEC permeability, increase angiogenesis loop formation and increase cell migration in a wound-healing model *in vitro*, compared to untreated cells. EC morphology and responses to cytokines vary substantially between different vascular beds (Aird, 2012), and it is therefore possible that ECs from different parts of the vasculature might respond differently to insulin (Woth et al., 2013). It would be interesting to compare the effects of insulin on ECs from different vascular beds.

Using phospho-specific 14-3-3 proteins as bait, 4 insulin-sensitive proteins were identified in a proteomic screen. Although 14-3-3 proteins were used as a tool in this study to identify protein phosphorylation changes stimulated by insulin in ECs, it would be important to investigate the specific roles of the 14-3-3 proteins in these signalling cascades. These roles could be elucidated by mutagenesis of the candidate 14-3-3-binding phosphosites identified by bioinformatic analysis. Further analysis is required to confirm that insulin stimulates the phosphorylation of these

proteins and to elucidate the specific kinase responsible for phosphorylating the 14-3-3 phosphosites.

All four insulin-sensitive 14-3-3-binding proteins identified in this study are important for the normal function of ECs. As described in Chapter 5, altering the expression of these proteins in ECs induced major cytoskeletal and/or cell-cell junctional changes, indicating that they participate in EC signalling pathways. Further experiments are required to elucidate the exact mechanisms of their actions. Firstly, Rho GTPase activity assays would determine if the target proteins induce the observed changes via these molecular switches. The hypothesized working model suggests that insulin stimulation results in phosphorylation of the target proteins, creating a docking site for 14-3-3 protein family members (Johnson et al., 2010). For RICH-1, this interaction could induce a conformational change that disrupts the association with Amot, alleviating its inhibitory action on the RICH-1 GAP activity (Wells et al., 2006), resulting in decreased Rac activity at the TJs (Figure 6.1). Active Rac1 has previously been shown to disrupt EC TJs (Wojciak-Stothard et al., 2001), and thus RICH-1 could act to stabilise EC TJs via Rac1 regulation. For Parg1, it would be necessary to investigate if insulin stimulation activates Parg1, resulting in a decrease in RhoA activity. A decrease in RhoA activation would prevent MLC phosphorylation required for stress fibre formation (Amano et al., 1996; Kimura et al., 1996) and thus ensure AJs are not subjected to centripetal tension (Dejana and Orsenigo, 2013), resulting in more stable AJs (Figure 6.1).

One possible way LMO7 could affect endothelial cell-cell junctions is by regulating the expression of TJ proteins. LMO7 has previously been shown to exert signal-dependent transcription by regulating actin dynamics via the Rho-dependent MRTF-SRF signalling pathway (Hu et al., 2011). Further studies are required to investigate whether insulin is able to act as a stimulus that releases LMO7 from its association with cell-cell junctional proteins (Ooshio et al., 2004). These studies should also include constructs of LMO7 with mutated 14-3-3 binding sites, in order to establish if 14-3-3 proteins are required to shuttle LMO7 into the nucleus (Figure 6.1). LMO7 is a transcription factor that regulates the transcription of emerin, as well as many

other genes (Holaska et al., 2006) and has been shown to bind directly to β-catenin and attenuate β-catenin activity in the nucleus (Markiewicz et al., 2006). β-catenin stabilises FoxO1 at the promoter of the TJ protein claudin-5 (Taddei et al., 2008) and together with TCF, this complex represses the expression of claudin-5 (Gavard and Gutkind, 2008). Thus, further studies are required to elucidate if insulin stimulation results in an increase of claudin-5 expression required for TJ stability, via LMO7/emerin sequestering of β-catenin.

Apart from the possibility that insulin induces changes to EC junctions via Rho GTPases, insulin signalling could also be regulated by endocytosis (Figure 6.2). RICH-1 has been previously shown to associate with two endocytic adapter proteins, CIN85 and CD2AP (Wells et al., 2006), which form a complex with endophilin that targets receptors for endocytosis (Petrelli et al., 2002). Moreover, an increase in vesicle-like structures was observed when GFP-RICH-1-expressing HUVECs were stimulated with insulin. Further studies are required to investigate whether RICH-1 modulates insulin signalling via IR recycling.

The epsin family of proteins are essential for clathrin-mediated endocytosis, however they have also be described to play roles in cell migration (Coon et al., 2010) and angiogenesis (Pasula et al., 2012). IGF-I stimulation of Epsin2 induced 14-3-3-binding, however bioinformatic prediction only indicates one candidate 14-3-3 binding site on Epsin2 (Chapter 4.4). It has previously been shown than Epsin binds and inhibits the Rac1 and Cdc42 GAP activity of RalBP1 (Coon et al., 2010). Could the 14-3-3-dimer act as a scaffold protein to facilitate this interaction (Figure 6.2)? Further analyses are required to establish whether Epsin2 contributes to insulin-stimulated cell migration by driving lamellipodium extension and whether this is via an increase in Rac1 activity.

The following hypothetical models present the proposed functions of RICH-1, Parg1, LMO7 and Epsin2 in ECs and summarises results presented in this thesis.
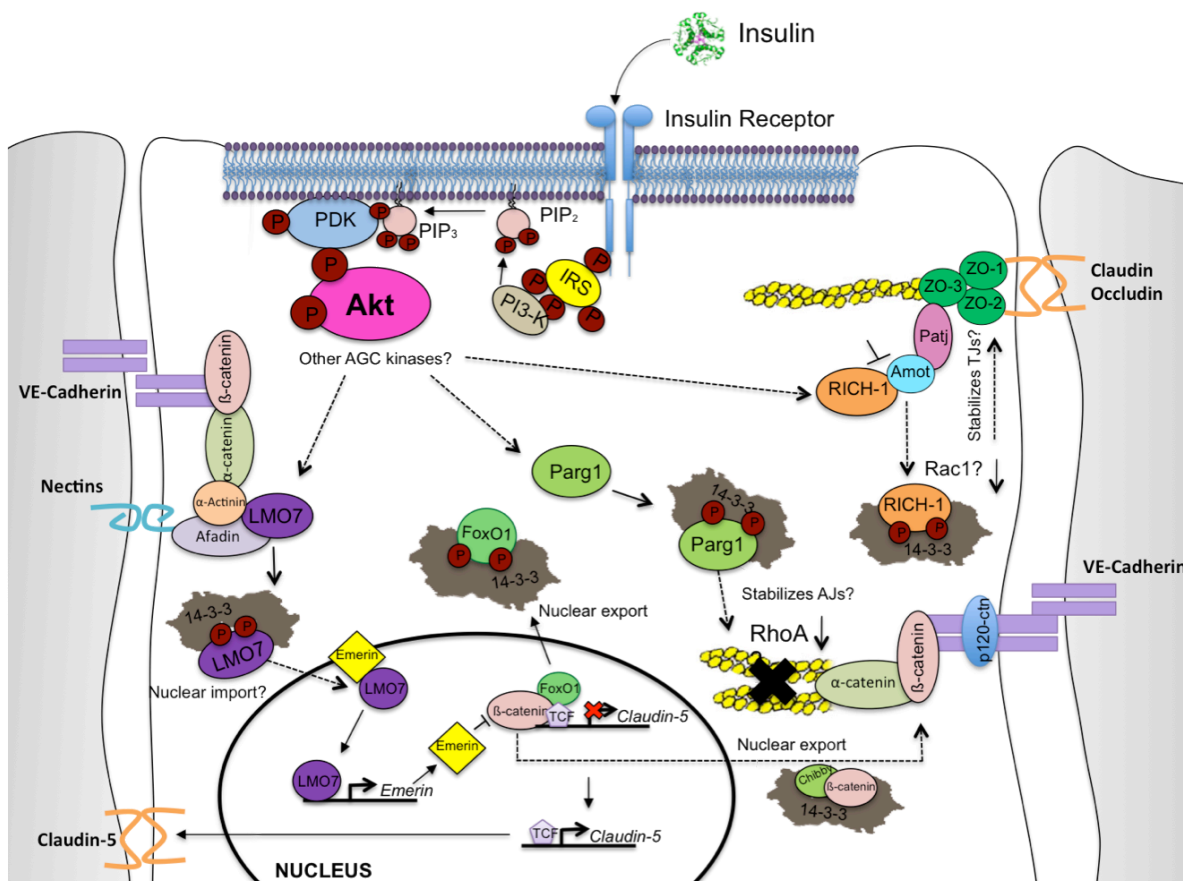
Figure 6.1 Schematic of proposed roles of RICH-1, Parg1 and LMO7 on endothelial cell-cell junctions

Insulin stimulation of ECs results in the activation of Akt and other AGC kinases that phosphorylate many down-stream substrates. Phosphorylation of RICH-1 by one of these kinases induces 14-3-3 binding, which could disrupt the association of RICH-1 from Amot, alleviating its inhibitory action on the RICH-1 GAP activity and thus possibly reduce Rac1 levels. Reduced Rac1 activity could stabilize TJs. LMO7 could also contribute to TJ stabilization by regulating the expression of the TJ protein Claudin-5. 14-3-3-binding could induce nuclear import of LMO7, enhancing levels of emerin in the nucleus. Emerin inhibits β-catenin, which is required to stabilize FoxO1 on the *Claudin-5* promoter with TCF. 14-3-3 proteins export FoxO1 and β-catenin out of the nucleus, relieving the inhibition of *Claudin-5* gene expression. Phosphorylation of Parg1 and subsequent 14-3-3 binding could enhance its Rho GAP activity for RhoA, reducing the levels of active RhoA at AJs and preventing stress fibre formation. The resulting decrease in centripetal tension could result in stable AJs. Solid lines indicate direct known signalling mechanisms and direct protein-protein interactions, broken lines indicate proposed mechanisms that require further analysis to be fully characterised.
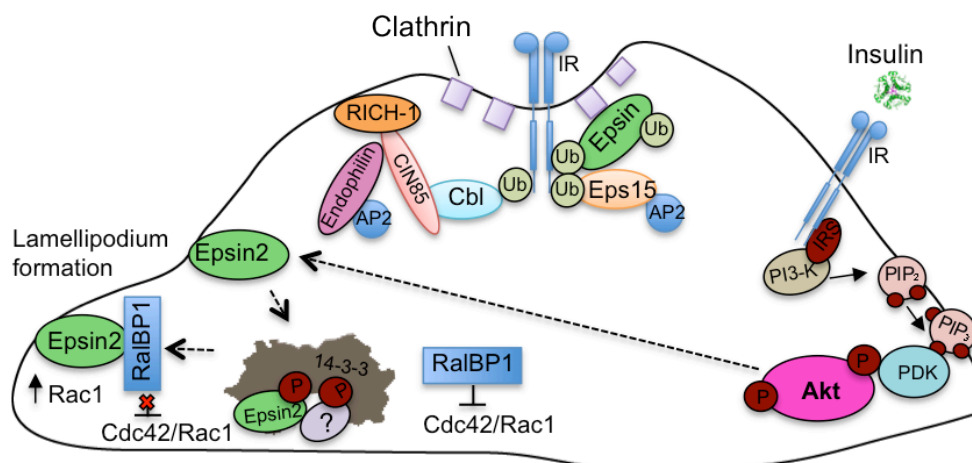
Figure 6.2 Schematic model of the roles of Epsin2 in insulin signalling in ECs

Epsins are essential for clathrin-mediated endocytosis. Further analyses are required to investigate if Epsin2 and RICH-1 are involved in the recycling of the insulin receptor (IR). Insulin-stimulated phosphorylation of Epsin2 is proposed to increase lamellipodium formation. The interaction of Epsins and RalBP1 has been shown to alleviate the Rac1/Cdc42 GAP activity inhibition of RalBP1, resulting in increased levels of active Rac1. Further studies are required to investigate whether 14-3-3 proteins facilitate this interaction upon insulin-stimulated Epsin2 phosphorylation. Solid lines indicate direct known signalling mechanisms and direct protein-protein interactions, broken lines indicate proposed mechanisms that require further analysis to be fully characterised.

6.1   Study limitations

This study encountered a number of limitations, which need to be considered.

Due to the scale required to perform the proteomic screen, the study used immortalised ECs from human bone marrow (HBMECs), whereas all functional analyses were performed with primary ECs isolated from human umbilical veins (HUVECs). Similarities between HBMECs and HUVECs have previously been demonstrated (Hillyer et al., 2003), and proteins identified in the HBMEC screen were expressed in HUVECs, as demonstrated in Chapter 5. However, differences may exist between ECs from difference vascular beds as well as between immortalised and primary cells, and it is worth noting that performing the screen in another cell model could have identified other insulin-stimulated 14-3-3-proteins.

The insulin concentrations investigated in the study were widely used in other *in vitro* studies (Hermann et al., 2000; Zeng et al., 2000). However, it must be acknowledged that these levels are unphysiologically high and at these concentrations other receptors, such as IGF-IR and insulin/IGF-I hybrid receptors, may also be activated (Nitert et al., 2005). Further studies could incorporate the use of inhibitors to identify the exact receptors and signalling pathways required for insulin to stimulate 14-3-3-binding to RICH-1, Parg1, LMO7 and Epsin2. These studies would also provide evidence that these proteins mediate the effects of insulin.

GFP-fusion proteins were utilised in this study to investigate temporal protein localisation in HUVECs. This common technique is useful to study the distribution of the protein in its natural environment, however any such engineering of a native protein carries the risk of affecting its localization. Moreover, as the HUVECs continue to express endogenous levels of these proteins, effects arising from overexpression also need to be taken into consideration. Analysing endogenous proteins, by the use of specific antibodies and immunofluorescence in fixed cells, is an alternative method that could be utilised. However, this method also comes with limitations, such as artefacts generated from cell fixation and permeabilization

methods or off-target binding due to antibody cross-reactivity with other proteins (Stadler et al., 2013). Ideally, both methods should be incorporated and the complementary data used to determine the subcellular protein localisation.

In conclusion, this thesis has described a 14-3-3-based proteomic screen that identified novel insulin-stimulated regulators of endothelial function. Understanding the molecular basis for insulin signalling on endothelial functions is vital for identifying new targets for treating cardiovascular disease in the future.

Supplementary

Table S1 List of proteins identified from 14-3-3-affinity purification of HBMEC lysates ± insulin

HBMECs were stimulated with insulin (100 nM) for 10 min, or left unstimulated after incubation in DMEM containing 1% FCS for 16 h. Proteins in cell lysates were captured on 14-3-3-Sepharose and eluted with 2 mM of the competitive phosphopeptide ARAApSAPA. Following concentration in Vivaspin concentrators (10 000 MW cut-off), the eluted samples were separated on a 4–12% Bis-Tris SDS-polyacryamide gel and proteins were visualised using colloidal Coomassie blue (see Figure 4.1). The separated proteins were excised from the gel in six segments (unstimulated labelled segment 1-6, insulin stimulated labelled 7-12) for tryptic digestion and mass spectral analysis. Proteins ranked in alphabetical order. Proteins highlighted in red are Gold standard proteins, for which 14-3-3-binding sites have been established. Proteins highlighted in blue are known insulin signalling mediators.

Accession No.	Protein Description	Accession Name	Mass (Da)	Excised segment
Q04446	1,4-alpha-glucan-branching enzyme	GLGB_HUMAN	80879	2 & 8
P61604	10 kDa heat shock protein, mitochondrial	CH10_HUMAN	10925	6 & 12
Q9NRX4	14 kDa phosphohistidine phosphatase	PHP14_HUMAN	13995	12
P31946	14-3-3 protein beta/alpha	1433B_HUMAN	28179	5 & 11
P62258	14-3-3 protein epsilon	1433E_HUMAN	29326	5 & 11
Q04917	14-3-3 protein eta	1433F_HUMAN	28372	5
P61981	14-3-3 protein gamma	1433G_HUMAN	28456	5 & 11
P27348	14-3-3 protein theta	1433T_HUMAN	28032	5 & 11
P63104	14-3-3 protein zeta/delta	1433Z_HUMAN	27899	5 & 11
P62191	26S protease regulatory subunit 4	PRS4_HUMAN	49325	9
P51665	26S proteasome non-ATPase regulatory subunit 7	PSD7_HUMAN	37060	10
P49189	4-trimethylaminobutyraldehyde dehydrogenase	AL9A1_HUMAN	54679	3 & 9
P63220	40S ribosomal protein S21	RS21_HUMAN	9220	6 & 12
P08865	40S ribosomal protein SA	RSSA_HUMAN	32947	5 & 11
P52209	6-phosphogluconate dehydrogenase, decarboxylating	6PGD_HUMAN	53619	4 & 10
P10809	60 kDa heat shock protein, mitochondrial	CH60_HUMAN	61187	3 & 9
P11021	78 kDa glucose-regulated protein	GRP78_HUMAN	72402	2 & 8
Q9BWD1	Acetyl-CoA acetyltransferase, cytosolic	THIC_HUMAN	41838	4 & 10
P24752	Acetyl-CoA acetyltransferase, mitochondrial	THIL_HUMAN	45456	4 & 10
Q99798	Aconitate hydratase, mitochondrial	ACON_HUMAN	86113	7
O14639	Actin-binding LIM protein 1	ABLM1_HUMAN	89513	5
O96019	Actin-like protein 6A	ACL6A_HUMAN	47944	4
P61160	Actin-related protein 2	ARP2_HUMAN	45017	4 & 10
O15143	Actin-related protein 2/3 complex subunit 1B	ARC1B_HUMAN	41722	4 & 10
O15145	Actin-related protein 2/3 complex subunit 3	ARPC3_HUMAN	20761	6 & 12
P59998	Actin-related protein 2/3 complex subunit 4	ARPC4_HUMAN	19768	6 & 12

O15511	Actin-related protein 2/3 complex subunit 5	ARPC5_HUMAN	16367	6 & 12
Q9BPX5	Actin-related protein 2/3 complex subunit 5-like protein	ARP5L_HUMAN	16931	6 & 12
P61158	Actin-related protein 3	ARP3_HUMAN	47797	4 & 10
P68032	Actin, alpha cardiac muscle 1	ACTC_HUMAN	42334	4 & 10
P62736	Actin, aortic smooth muscle	ACTA_HUMAN	42381	11
P60709	Actin, cytoplasmic 1	ACTB_HUMAN	42052	4 & 10
O95433	Activator of 90 kDa heat shock protein ATPase homolog 1	AHSA1_HUMAN	38421	10
P07741	Adenine phosphoribosyltransferase	APT_HUMAN	19766	6 & 12
P23526	Adenosylhomocysteinase	SAHH_HUMAN	48255	4 & 10
P54819	Adenylate kinase 2, mitochondrial	KAD2_HUMAN	26689	5 & 11
P00568	Adenylate kinase isoenzyme 1	KAD1_HUMAN	21735	6 & 12
P30520	Adenylosuccinate synthetase isozyme 2	PURA2_HUMAN	50465	10
Q01518	Adenylyl cyclase-associated protein 1	CAP1_HUMAN	52325	3 & 9
P36405	ADP-ribosylation factor-like protein 3	ARL3_HUMAN	20614	12
P49588	Alanine--tRNA ligase, cytoplasmic	SYAC_HUMAN	107484	1 & 7
P14550	Alcohol dehydrogenase [NADP(+)]	AK1A1_HUMAN	36892	5 & 11
P15121	Aldose reductase	ALDR_HUMAN	36230	5 & 11
P12814	Alpha-actinin-1	ACTN1_HUMAN	103563	1 & 7
O43707	Alpha-actinin-4	ACTN4_HUMAN	105245	1 & 7
P49419	Alpha-aminoadipic semialdehyde dehydrogenase	AL7A1_HUMAN	59020	3 & 9
P06733	Alpha-enolase	ENOA_HUMAN	47481	4 & 10
P04083	Annexin A1	ANXA1_HUMAN	38918	5 & 11
P07355	Annexin A2	ANXA2_HUMAN	38808	5 & 11
P12429	Annexin A3	ANXA3_HUMAN	36524	5 & 11
P09525	Annexin A4	ANXA4_HUMAN	36088	5 & 11
P08758	Annexin A5	ANXA5_HUMAN	35971	5 & 11
P08133	Annexin A6	ANXA6_HUMAN	76168	2 & 8
Q9NQ90	Anoctamin-2	ANO2_HUMAN	114695	9
Q9BZZ5	Apoptosis inhibitor 5	API5_HUMAN	59310	9
O95831	Apoptosis-inducing factor 1, mitochondrial	AIFM1_HUMAN	67144	3 & 9
O43776	Asparagine--tRNA ligase, cytoplasmic	SYNC_HUMAN	63758	9
P17174	Aspartate aminotransferase, cytoplasmic	AATC_HUMAN	46447	4 & 10
P00505	Aspartate aminotransferase, mitochondrial	AATM_HUMAN	47886	4 & 10
Q15121	Astrocytic phosphoprotein PEA-15	PEA15_HUMAN	15088	6
P06576	ATP synthase subunit beta, mitochondrial	ATPB_HUMAN	56525	3 & 9
O00148	ATP-dependent RNA helicase DDX39A	DDX39_HUMAN	49611	4 & 10
Q8NHQ9	ATP-dependent RNA helicase DDX55	DDX55_HUMAN	69073	2
P51572	B-cell receptor-associated protein 31	BAP31_HUMAN	28031	5
Q9Y2J2	Band 4.1-like protein 3	E41L3_HUMAN	121458	5 & 12
Q562R1	Beta-actin-like protein 2	ACTBL_HUMAN	42318	10
P06865	Beta-hexosaminidase subunit alpha	HEXA_HUMAN	61120	9
P07686	Beta-hexosaminidase subunit beta	HEXB_HUMAN	63527	11
P31939	Bifunctional purine biosynthesis protein PURH	PUR9_HUMAN	65089	2 & 8
Q13867	Bleomycin hydrolase	BLMH_HUMAN	53155	9
O60885	Bromodomain-containing protein 4	BRD4_HUMAN	152580	5

P62158	Calmodulin	CALM_HUMAN	16827	6 & 12
P27797	Calreticulin	CALR_HUMAN	48283	3 & 9
P10644	cAMP-dependent protein kinase type I-alpha regulatory subunit	KAP0_HUMAN	43183	10
P16152	Carbonyl reductase [NADPH] 1	CBR1_HUMAN	30641	5 & 11
O75828	Carbonyl reductase [NADPH] 3	CBR3_HUMAN	31230	5
P07339	Cathepsin D	CATD_HUMAN	45037	5 & 11
P60953	Cell division control protein 42 homolog	CDC42_HUMAN	21587	12
Q99741	Cell division control protein 6 homolog	CDC6_HUMAN	63650	5
P49454	Centromere protein F	CENPF_HUMAN	370844	8
Q5SW79	Centrosomal protein of 170 kDa	CE170_HUMAN	175586	6 & 12
O00299	Chloride intracellular channel protein 1	CLIC1_HUMAN	27248	5 & 11
Q9Y696	Chloride intracellular channel protein 4	CLIC4_HUMAN	28982	5 & 11
Q13185	Chromobox protein homolog 3	CBX3_HUMAN	20969	6 & 12
O75390	Citrate synthase, mitochondrial	CISY_HUMAN	51908	10
Q00610	Clathrin heavy chain 1	CLH1_HUMAN	193260	1 & 7
Q14019	Coactosin-like protein	COTL1_HUMAN	16049	6 & 12
P53618	Coatomer subunit beta	COPB_HUMAN	108214	4
P23528	Cofilin-1	COF1_HUMAN	18719	6 & 12
Q9Y281	Cofilin-2	COF2_HUMAN	18839	12
Q99829	Copine-1	CPNE1_HUMAN	59649	9
Q8IYJ1	Copine-9	CPNE9_HUMAN	62281	9
Q13951	Core-binding factor subunit beta	PEBB_HUMAN	21723	12
Q9ULV4	Coronin-1C	COR1C_HUMAN	53899	4 & 10
P42771	Cyclin-dependent kinase inhibitor 2A, isoforms 1/2/3	CD2A1_HUMAN	16579	6 & 12
P21291	Cysteine and glycine-rich protein 1	CSRP1_HUMAN	21409	12
P99999	Cytochrome c	CYC_HUMAN	11855	6
P28838	Cytosol aminopeptidase	AMPL_HUMAN	56530	3 & 9
O00154	Cytosolic acyl coenzyme A thioester hydrolase	BACH_HUMAN	42454	4 & 10
Q96KP4	Cytosolic non-specific dipeptidase	CNDP2_HUMAN	53187	3 & 9
Q96BY6	Dedicator of cytokinesis protein 10	DOC10_HUMAN	251825	2 & 8
P30038	Delta-1-pyrroline-5-carboxylate dehydrogenase, mitochondrial	AL4A1_HUMAN	62137	9
Q13011	Delta(3,5)-Delta(2,4)-dienoyl-CoA isomerase, mitochondrial	ECH1_HUMAN	36136	5
P33316	Deoxyuridine 5~-triphosphate nucleotidohydrolase, mitochondrial	DUT_HUMAN	26832	6 & 12
P60981	Destrin	DEST_HUMAN	18950	6 & 12
Q9NR28	Diablo homolog, mitochondrial	DBLOH_HUMAN	27342	6 & 12
P09622	Dihydrolipoyl dehydrogenase, mitochondrial	DLDH_HUMAN	54713	3 & 9
P36957	Dihydrolipoyllysine-residue succinyltransferase component of 2-oxoglutarate dehydrogenase complex	ODO2_HUMAN	49067	9
Q16555	Dihydropyrimidinase-related protein 2	DPYL2_HUMAN	62711	9
Q14195	Dihydropyrimidinase-related protein 3	DPYL3_HUMAN	62323	3 & 9
Q9NY33	Dipeptidyl peptidase 3	DPP3_HUMAN	82880	7
Q9UKJ8	Disintegrin and metalloproteinase domain-containing protein 21	ADA21_HUMAN	83403	1

O14490	Disks large-associated protein 1	DLGP1_HUMAN	110117	6
Q16531	DNA damage-binding protein 1	DDB1_HUMAN	128142	1 & 7
P49736	DNA replication licensing factor MCM2	MCM2_HUMAN	102516	7
Q14566	DNA replication licensing factor MCM6	MCM6_HUMAN	93801	7
P27695	DNA-(apurinic or apyrimidinic site) lyase	APEX1_HUMAN	35931	5 & 11
Q9UBS4	DnaJ homolog subfamily B member 11	DJB11_HUMAN	40774	4 & 10
Q96FJ2	Dynein light chain 2, cytoplasmic	DYL2_HUMAN	10457	6
Q32P44	Echinoderm microtubule-associated protein-like 3	EMAL3_HUMAN	96221	7
P29692	Elongation factor 1-delta	EF1D_HUMAN	31217	12
P26641	Elongation factor 1-gamma	EF1G_HUMAN	50429	4 & 10
P13639	Elongation factor 2	EF2_HUMAN	96246	1 & 7
P30040	Endoplasmic reticulum resident protein 29	ERP29_HUMAN	29032	5 & 11
P14625	Endoplasmin OS=Homo sapiens	ENPL_HUMAN	92696	1 & 7
P84090	Enhancer of rudimentary homolog	ERH_HUMAN	12422	6 & 12
P30084	Enoyl-CoA hydratase, mitochondrial	ECHM_HUMAN	31823	11
O95208	Epsin-2	EPN2_HUMAN	68667	5 & 12
P60842	Eukaryotic initiation factor 4A-I	IF4A1_HUMAN	46353	4 & 10
P62495	Eukaryotic peptide chain release factor subunit 1	ERF1_HUMAN	49228	9
P05198	Eukaryotic translation initiation factor 2 subunit 1	IF2A_HUMAN	36374	11
P06730	Eukaryotic translation initiation factor 4E	IF4E_HUMAN	25310	5
A6NMX2	Eukaryotic translation initiation factor 4E type 1B	I4E1B_HUMAN	27750	11
P55010	Eukaryotic translation initiation factor 5	IF5_HUMAN	49648	3 & 9
Q6IS14	Eukaryotic translation initiation factor 5A-1-like	IF5AL_HUMAN	16990	6 & 12
P15311	Ezrin	EZRI_HUMAN	69484	2 & 8
P47755	F-actin-capping protein subunit alpha-2	CAZA2_HUMAN	33157	5
P14324	Farnesyl pyrophosphate synthase	FPPS_HUMAN	48758	5 & 11
Q16658	Fascin	FSCN1_HUMAN	55123	3 & 9
Q01469	Fatty acid-binding protein, epidermal	FABP5_HUMAN	15497	12
Q53RD9	Fibulin-7	FBLN7_HUMAN	49055	4 & 10
P21333	Filamin-A	FLNA_HUMAN	283301	1 & 7
O75369	Filamin-B	FLNB_HUMAN	280157	1 & 7
Q14315	Filamin-C	FLNC_HUMAN	293407	1 & 7
P30043	Flavin reductase (NADPH)	BLVRB_HUMAN	22219	6
P04075	Fructose-bisphosphate aldolase A	ALDOA_HUMAN	39851	4 & 10
P09972	Fructose-bisphosphate aldolase C	ALDOC_HUMAN	39830	4
P07954	Fumarate hydratase, mitochondrial	FUMH_HUMAN	54773	4 & 10
P09382	Galectin-1	LEG1_HUMAN	15048	6 & 12
P17931	Galectin-3	LEG3_HUMAN	26193	5 & 11
P09104	Gamma-enolase	ENOG_HUMAN	47581	10
P11413	Glucose-6-phosphate 1-dehydrogenase	G6PD_HUMAN	59675	3 & 9
P06744	Glucose-6-phosphate isomerase	G6PI_HUMAN	63335	3 & 9
P14314	Glucosidase 2 subunit beta	GLU2B_HUMAN	60357	11
P00390	Glutathione reductase, mitochondrial	GSHR_HUMAN	56791	3 & 9
P78417	Glutathione S-transferase omega-1	GSTO1_HUMAN	27833	5 & 11

P09211	Glutathione S-transferase P	GSTP1_HUMAN	23569	6 & 12
P48637	Glutathione synthetase	GSHB_HUMAN	52523	3 & 9
P04406	Glyceraldehyde-3-phosphate dehydrogenase	G3P_HUMAN	36201	5 & 11
Q8WTR4	Glycerophosphodiester phosphodiesterase domain-containing protein 5	GDPD5_HUMAN	69112	6 & 12
P30419	Glycylpeptide N-tetradecanoyltransferase 1	NMT1_HUMAN	57112	3 & 9
Q9HC38	Glyoxalase domain-containing protein 4	GLOD4_HUMAN	35170	5 & 11
Q9HAV7	GrpE protein homolog 1, mitochondrial	GRPE1_HUMAN	24492	11
P62826	GTP-binding nuclear protein Ran	RAN_HUMAN	24579	5 & 11
P47224	Guanine nucleotide exchange factor MSS4	MSS4_HUMAN	14115	6 & 12
P63244	Guanine nucleotide-binding protein subunit beta-2-like 1	GBLP_HUMAN	35511	5 & 11
P08107	Heat shock 70 kDa protein 1A/1B	HSP71_HUMAN	70294	2 & 8
P34932	Heat shock 70 kDa protein 4	HSP74_HUMAN	95127	1 & 7
P11142	Heat shock cognate 71 kDa protein	HSP7C_HUMAN	71082	2 & 8
Q92598	Heat shock protein 105 kDa	HS105_HUMAN	97716	7
P04792	Heat shock protein beta-1	HSPB1_HUMAN	22826	5
P07900	Heat shock protein HSP 90-alpha	HS90A_HUMAN	85006	1 & 7
P08238	Heat shock protein HSP 90-beta	HS90B_HUMAN	83554	1 & 7
Q9UK76	Hematological and neurological expressed 1 protein	HN1_HUMAN	16005	6 & 12
P52597	Heterogeneous nuclear ribonucleoprotein F	HNRPF_HUMAN	45985	12
P61978	Heterogeneous nuclear ribonucleoprotein K	HNRPK_HUMAN	51230	9
P19367	Hexokinase-1	HXK1_HUMAN	103561	1
P09429	High mobility group protein B1	HMGB1_HUMAN	25049	5 & 11
P26583	High mobility group protein B2	HMGB2_HUMAN	24190	5 & 11
P49773	Histidine triad nucleotide-binding protein 1	HINT1_HUMAN	13907	6 & 12
Q9BX68	Histidine triad nucleotide-binding protein 2, mitochondrial	HINT2_HUMAN	17208	6 & 12
P12081	Histidine--tRNA ligase, cytoplasmic	SYHC_HUMAN	57944	3 & 9
O15047	Histone-lysine N-methyltransferase SETD1A	SET1A_HUMAN	186718	2
Q16543	Hsp90 co-chaperone Cdc37	CDC37_HUMAN	44953	4 & 10
Q16836	Hydroxyacyl-coenzyme A dehydrogenase, mitochondrial	HCDH_HUMAN	34329	11
P52292	Importin subunit alpha-2	IMA2_HUMAN	58168	9
Q15181	Inorganic pyrophosphatase	IPYR_HUMAN	33095	5 & 11
P14735	Insulin-degrading enzyme	IDE_HUMAN	118692	7
O75874	Isocitrate dehydrogenase [NADP] cytoplasmic	IDHC_HUMAN	46915	4
P48735	Isocitrate dehydrogenase [NADP], mitochondrial	IDHP_HUMAN	51333	4 & 10
Q13907	Isopentenyl-diphosphate Delta-isomerase 1	IDI1_HUMAN	26645	5
Q12840	Kinesin heavy chain isoform 5A	KIF5A_HUMAN	118161	1 & 7
P00338	L-lactate dehydrogenase A chain	LDHA_HUMAN	36950	5 & 11
P07195	L-lactate dehydrogenase B chain	LDHB_HUMAN	36900	5 & 11
Q04760	Lactoylglutathione lyase	LGUL_HUMAN	20992	6 & 12
P09960	Leukotriene A-4 hydrolase	LKHA4_HUMAN	69868	2 & 8
Q14847	LIM and SH3 domain protein 1	LASP1_HUMAN	30097	6 & 12
Q8WWI1	LIM domain only protein 7	LMO7_HUMAN	194002	12

P31025	Lipocalin-1	LCN1_HUMAN	19409	6 & 12
P24666	Low molecular weight phosphotyrosine protein phosphatase	PPAC_HUMAN	18487	6 & 12
Q12912	Lymphoid-restricted membrane protein	LRMP_HUMAN	62767	8
Q15046	Lysine--tRNA ligase	SYK_HUMAN	68461	3 & 9
P42785	Lysosomal Pro-X carboxypeptidase	PCP_HUMAN	56277	9
P14174	Macrophage migration inhibitory factor	MIF_HUMAN	12639	6 & 12
P40121	Macrophage-capping protein	CAPG_HUMAN	38760	4 & 10
Q14764	Major vault protein	MVP_HUMAN	99551	1 & 7
P40925	Malate dehydrogenase, cytoplasmic	MDHC_HUMAN	36631	5 & 11
P40926	Malate dehydrogenase, mitochondrial	MDHM_HUMAN	35937	5 & 11
Q9Y5P6	Mannose-1-phosphate guanyltransferase beta	GMPPB_HUMAN	40379	4 & 10
P11310	Medium-chain specific acyl-CoA dehydrogenase, mitochondrial	ACADM_HUMAN	47015	4 & 10
Q9NZL9	Methionine adenosyltransferase 2 subunit beta	MAT2B_HUMAN	37870	5
P50579	Methionine aminopeptidase 2	AMPM2_HUMAN	53713	9
Q15691	Microtubule-associated protein RP/EB family member 1	MARE1_HUMAN	30151	5 & 11
Q10713	Mitochondrial-processing peptidase subunit alpha	MPPA_HUMAN	58729	3 & 9
P28482	Mitogen-activated protein kinase 1	MK01_HUMAN	41762	10
P26038	Moesin	MOES_HUMAN	67892	2 & 8
Q9UKD2	mRNA turnover protein 4 homolog	MRT4_HUMAN	27657	2 & 8
P14649	Myosin light chain 6B	MYL6B_HUMAN	22864	6 & 12
P58546	Myotrophin	MTPN_HUMAN	13058	6 & 12
Q9NXD2	Myotubularin-related protein 10	MTMRA_HUMAN	89186	7
P15586	N-acetylglucosamine-6-sulfatase	GNS_HUMAN	62840	3 & 7
O95865	N(G),N(G)-dimethylarginine dimethylaminohydrolase 2	DDAH2_HUMAN	29911	5 & 11
Q9Y6E7	NAD-dependent ADP-ribosyltransferase sirtuin-4	SIRT4_HUMAN	35678	8
Q13765	Nascent polypeptide-associated complex subunit alpha	NACA_HUMAN	23370	5 & 12
Q8NF91	Nesprin-1	SYNE1_HUMAN	1017069	6 & 12
Q14697	Neutral alpha-glucosidase AB	GANAB_HUMAN	107263	1 & 7
P55769	NHP2-like protein 1	NH2L1_HUMAN	14393	12
P22307	Non-specific lipid-transfer protein	NLTP_HUMAN	59640	12
P61970	Nuclear transport factor 2	NTF2_HUMAN	14640	6 & 12
P15531	Nucleoside diphosphate kinase A	NDKA_HUMAN	17309	6
P22392	Nucleoside diphosphate kinase B	NDKB_HUMAN	17401	12
Q9NTK5	Obg-like ATPase 1	OLA1_HUMAN	44943	10
P04181	Ornithine aminotransferase, mitochondrial	OAT_HUMAN	48846	4 & 10
Q9BZ23	Pantothenate kinase 2, mitochondrial	PANK2_HUMAN	63268	4 & 10
P20962	Parathymosin	PTMS_HUMAN	11523	6 & 12
O00151	PDZ and LIM domain protein 1	PDLI1_HUMAN	36505	12
Q9NR12	PDZ and LIM domain protein 7	PDLI7_HUMAN	50896	12
P62937	Peptidyl-prolyl cis-trans isomerase A	PPIA_HUMAN	18229	6 & 12
P23284	Peptidyl-prolyl cis-trans isomerase B	PPIB_HUMAN	23785	6 & 12
Q96AY3	Peptidyl-prolyl cis-trans isomerase FKBP10	FKB10_HUMAN	64717	3 & 9

P62942	Peptidyl-prolyl cis-trans isomerase FKBP1A	FKB1A_HUMAN	12000	6 & 12
P26885	Peptidyl-prolyl cis-trans isomerase FKBP2	FKBP2_HUMAN	15810	6 & 12
Q00688	Peptidyl-prolyl cis-trans isomerase FKBP3	FKBP3_HUMAN	25218	5
Q02790	Peptidyl-prolyl cis-trans isomerase FKBP4	FKBP4_HUMAN	52057	3 & 9
O43447	Peptidyl-prolyl cis-trans isomerase H	PPIH_HUMAN	19481	6 & 12
Q13526	Peptidyl-prolyl cis-trans isomerase NIMA-interacting 1	PIN1_HUMAN	18346	12
O60437	Periplakin	PEPL_HUMAN	205193	11
Q06830	Peroxiredoxin-1	PRDX1_HUMAN	22324	6 & 12
P32119	Peroxiredoxin-2	PRDX2_HUMAN	22049	6 & 12
P30044	Peroxiredoxin-5, mitochondrial	PRDX5_HUMAN	22301	12
P30041	Peroxiredoxin-6	PRDX6_HUMAN	25133	12
P30086	Phosphatidylethanolamine-binding protein 1	PEBP1_HUMAN	21158	6 & 12
P00558	Phosphoglycerate kinase 1	PGK1_HUMAN	44985	4 & 10
P07205	Phosphoglycerate kinase 2	PGK2_HUMAN	45166	4
P18669	Phosphoglycerate mutase 1	PGAM1_HUMAN	28900	5 & 11
Q8IV08	Phospholipase D3	PLD3_HUMAN	55127	9
Q9Y617	Phosphoserine aminotransferase	SERC_HUMAN	40796	10
P13797	Plastin-3	PLST_HUMAN	71279	3 & 9
P07359	Platelet glycoprotein Ib alpha chain	GP1BA_HUMAN	69425	5 & 11
P68402	Platelet-activating factor acetylhydrolase IB subunit beta	PA1B2_HUMAN	25724	5 & 11
Q15102	Platelet-activating factor acetylhydrolase IB subunit gamma	PA1B3_HUMAN	25832	5 & 11
Q15149	Plectin	PLEC_HUMAN	533462	9
Q9UHX1	Poly(U)-binding-splicing factor PUF60	PUF60_HUMAN	60009	11
Q9Y2S7	Polymerase delta-interacting protein 2	PDIP2_HUMAN	42235	5 & 11
P26599	Polypyrimidine tract-binding protein 1	PTBP1_HUMAN	57357	12
P02545	Prelamin-A/C	LMNA_HUMAN	74380	2 & 8
A2PYH4	Probable ATP-dependent DNA helicase HFM1	HFM1_HUMAN	163705	8
Q13206	Probable ATP-dependent RNA helicase DDX10	DDX10_HUMAN	101168	10
Q6PRD1	Probable G-protein coupled receptor 179	GP179_HUMAN	260623	11
O00469	Procollagen-lysine,2-oxoglutarate 5-dioxygenase 2	PLOD2_HUMAN	85373	1 & 7
P07737	Profilin-1	PROF1_HUMAN	15216	6 & 12
P35080	Profilin-2	PROF2_HUMAN	15378	12
O14737	Programmed cell death protein 5	PDCD5_HUMAN	14276	6
P12004	Proliferating cell nuclear antigen	PCNA_HUMAN	29092	5 & 11
Q9UQ80	Proliferation-associated protein 2G4	PA2G4_HUMAN	44101	4 & 10
Q15185	Prostaglandin E synthase 3	TEBP_HUMAN	18971	6 & 12
Q14914	Prostaglandin reductase 1	PTGR1_HUMAN	36075	5
P25786	Proteasome subunit alpha type-1	PSA1_HUMAN	29822	5 & 11
P25787	Proteasome subunit alpha type-2	PSA2_HUMAN	25996	6 & 12
P25788	Proteasome subunit alpha type-3	PSA3_HUMAN	28643	5 & 11
P25789	Proteasome subunit alpha type-4	PSA4_HUMAN	29750	5 & 11
P28066	Proteasome subunit alpha type-5	PSA5_HUMAN	26565	11
P60900	Proteasome subunit alpha type-6	PSA6_HUMAN	27838	5 & 11
Q8TAA3	Proteasome subunit alpha type-7-like	PSA7L_HUMAN	28683	5 & 11

P49721	Proteasome subunit beta type-2	PSB2_HUMAN	22993	6 & 12
P28070	Proteasome subunit beta type-4	PSB4_HUMAN	29242	6 & 12
P28072	Proteasome subunit beta type-6	PSB6_HUMAN	25570	6 & 12
Q99622	Protein C10	C10_HUMAN	13284	12
Q9Y2B0	Protein canopy homolog 2	CNPY2_HUMAN	20981	6 & 12
O60888	Protein CutA	CUTA_HUMAN	19218	12
P07237	Protein disulfide-isomerase	PDIA1_HUMAN	57480	3 & 9
P30101	Protein disulfide-isomerase A3	PDIA3_HUMAN	57146	3 & 9
P13667	Protein disulfide-isomerase A4	PDIA4_HUMAN	73229	2 & 8
Q15084	Protein disulfide-isomerase A6	PDIA6_HUMAN	48490	4 & 10
Q99497	Protein DJ-1	PARK7_HUMAN	20050	6 & 12
O95571	Protein ETHE1, mitochondrial	ETHE1_HUMAN	28368	5
Q8N485	Protein limb expression 1 homolog	LIX1_HUMAN	32213	4
O14974	Protein phosphatase 1 regulatory subunit 12A	MYPT1_HUMAN	115610	6 & 12
P49593	Protein phosphatase 1F	PPM1F_HUMAN	49971	3
P31949	Protein S100-A11	S10AB_HUMAN	11847	12
P06703	Protein S100-A6	S10A6_HUMAN	10230	6 & 12
P55735	Protein SEC13 homolog	SEC13_HUMAN	36031	11
Q92734	Protein TFG	TFG_HUMAN	43478	6 & 12
Q15436	Protein transport protein Sec23A	SC23A_HUMAN	87018	7
P53992	Protein transport protein Sec24C	SC24C_HUMAN	119789	7
O94979	Protein transport protein Sec31A	SC31A_HUMAN	133900	12
P21980	Protein-glutamine gamma-glutamyltransferase 2	TGM2_HUMAN	78420	7
P06454	Prothymosin alpha	PTMA_HUMAN	12196	6 & 12
P61457	Pterin-4-alpha-carbinolamine dehydratase	PHS_HUMAN	12049	6 & 12
P00491	Purine nucleoside phosphorylase	PNPH_HUMAN	32325	5 & 11
A6NMY6	Putative annexin A2-like protein	AXA2L_HUMAN	38806	10
Q5VTE0	Putative elongation factor 1-alpha-like 3	EF1A3_HUMAN	50495	5 & 10
Q8IZP2	Putative protein FAM10A4	F10A4_HUMAN	27561	10
Q2M238	Putative RRN3-like protein FLJ77916	RRN3L_HUMAN	17529	10
Q5JXB2	Putative ubiquitin-conjugating enzyme E2 N-like	UE2NL_HUMAN	17366	12
P11177	Pyruvate dehydrogenase E1 component subunit beta, mitochondrial	ODPB_HUMAN	39550	11
P14618	Pyruvate kinase isozymes M1/M2	KPYM_HUMAN	58470	3 & 9
Q9BXR0	Queuine tRNA-ribosyltransferase	TGT_HUMAN	44703	10
Q53FA7	Quinone oxidoreductase PIG3	QORX_HUMAN	35685	11
P31150	Rab GDP dissociation inhibitor alpha	GDIA_HUMAN	51177	3 & 9
P50395	Rab GDP dissociation inhibitor beta	GDIB_HUMAN	51087	4 & 10
Q15404	Ras suppressor protein 1	RSU1_HUMAN	31521	5
P15153	Ras-related C3 botulinum toxin substrate 2	RAC2_HUMAN	21814	6
P60763	Ras-related C3 botulinum toxin substrate 3	RAC3_HUMAN	21764	12
P62491	Ras-related protein Rab-11A	RB11A_HUMAN	24492	12
O43353	Receptor-interacting serine/threonine-protein kinase 2	RIPK2_HUMAN	61726	2
P18754	Regulator of chromosome condensation	RCC1_HUMAN	45397	4 & 10
P52565	Rho GDP-dissociation inhibitor 1	GDIR1_HUMAN	23250	5 & 11

P52566	Rho GDP-dissociation inhibitor 2	GDIR2_HUMAN	23031	5 & 12
Q68EM7	Rho GTPase-activating protein 17	RHG17_HUMAN	95776	9
Q52LW3	Rho GTPase-activating protein 29	RHG29_HUMAN	143514	7
Q5VV41	Rho guanine nucleotide exchange factor 16	ARHGG_HUMAN	80340	9
Q96AT9	Ribulose-phosphate 3-epimerase	RPE_HUMAN	25139	6
Q9Y5S9	RNA-binding protein 8A	RBM8A_HUMAN	19934	6 & 12
P10768	S-formylglutathione hydrolase	ESTD_HUMAN	31956	11
Q8WVM8	Sec1 family domain-containing protein 1	SCFD1_HUMAN	72676	9
Q12765	Secernin-1	SCRN1_HUMAN	46980	3 & 9
Q9NVA2	Septin-11	SEP11_HUMAN	49652	9
Q15019	Septin-2	SEPT2_HUMAN	41689	4 & 10
Q16181	Septin-7	SEPT7_HUMAN	50933	4 & 10
P34897	Serine hydroxymethyltransferase, mitochondrial	GLYM_HUMAN	56414	3 & 9
O43464	Serine protease HTRA2, mitochondrial	HTRA2_HUMAN	48868	5 & 11
P49591	Serine--tRNA ligase, cytoplasmic	SYSC_HUMAN	59253	9
Q9BXM7	Serine/threonine-protein kinase PINK1, mitochondrial	PINK1_HUMAN	63641	1
Q9H0K1	Serine/threonine-protein kinase SIK2	SIK2_HUMAN	104705	12
P30153	Serine/threonine-protein phosphatase 2A 65 kDa regulatory subunit A alpha isoform	2AAA_HUMAN	66065	3 & 9
P62714	Serine/threonine-protein phosphatase 2A catalytic subunit beta isoform	PP2AB_HUMAN	36123	5 & 11
P62140	Serine/threonine-protein phosphatase PP1-beta catalytic subunit	PP1B_HUMAN	37961	11
P35237	Serpin B6	SPB6_HUMAN	42936	9
P02768	Serum albumin	ALBU_HUMAN	71317	2 & 8
O75368	SH3 domain-binding glutamic acid-rich-like protein	SH3L1_HUMAN	12766	12
Q9H299	SH3 domain-binding glutamic acid-rich-like protein 3	SH3L3_HUMAN	10488	6 & 12
Q7L8J4	SH3 domain-binding protein 5-like	3BP5L_HUMAN	43701	9
Q9NR45	Sialic acid synthase	SIAS_HUMAN	40738	4 & 10
Q8IUH8	Signal peptide peptidase-like 2C	IMP5_HUMAN	75538	10
Q96FS4	Signal-induced proliferation-associated protein 1	SIPA1_HUMAN	112821	6
Q04837	Single-stranded DNA-binding protein, mitochondrial	SSBP_HUMAN	17249	6 & 12
Q6EEV6	Small ubiquitin-related modifier 4	SUMO4_HUMAN	10735	6 & 12
Q86UG4	Solute carrier organic anion transporter family member 6A1	SO6A1_HUMAN	81176	12
Q13813	Spectrin alpha chain, brain	SPTA2_HUMAN	285163	7
Q01082	Spectrin beta chain, brain 1	SPTB2_HUMAN	275237	7
Q7KZF4	Staphylococcal nuclease domain-containing protein 1	SND1_HUMAN	102618	1 & 7
P16949	Stathmin	STMN1_HUMAN	17292	6 & 12
P38646	Stress-70 protein, mitochondrial	GRP75_HUMAN	73920	2 & 8
P31948	Stress-induced-phosphoprotein 1	STIP1_HUMAN	63227	2 & 8
Q9HCN8	Stromal cell-derived factor 2-like protein 1	SDF2L_HUMAN	23812	6
Q96I99	Succinyl-CoA ligase [GDP-forming] subunit beta,	SUCB2_HUMAN	46824	10

	mitochondrial			
Q8NBJ7	Sulfatase-modifying factor 2	SUMF2_HUMAN	33936	11
Q9UBE0	SUMO-activating enzyme subunit 1	SAE1_HUMAN	38882	10
Q9UBT2	SUMO-activating enzyme subunit 2	SAE2_HUMAN	71749	7
P00441	Superoxide dismutase [Cu-Zn]	SODC_HUMAN	16154	6 & 12
O60264	SWI/SNF-related matrix-associated actin-dependent regulator of chromatin subfamily A member 5	SMCA5_HUMAN	122513	3
Q96C24	Synaptotagmin-like protein 4	SYTL4_HUMAN	76603	10
P17987	T-complex protein 1 subunit alpha	TCPA_HUMAN	60819	9
P50991	T-complex protein 1 subunit delta	TCPD_HUMAN	58401	9
P48643	T-complex protein 1 subunit epsilon	TCPE_HUMAN	60089	9
P49368	T-complex protein 1 subunit gamma	TCPG_HUMAN	61066	3 & 9
P50990	T-complex protein 1 subunit theta	TCPQ_HUMAN	60153	3 & 9
P40227	T-complex protein 1 subunit zeta	TCPZ_HUMAN	58444	9
Q9Y490	Talin-1	TLN1_HUMAN	271766	1 & 7
P10599	Thioredoxin	THIO_HUMAN	12015	12
O95881	Thioredoxin domain-containing protein 12	TXD12_HUMAN	19365	6 & 12
Q9BRA2	Thioredoxin domain-containing protein 17	TXD17_HUMAN	14217	6 & 12
Q8NBS9	Thioredoxin domain-containing protein 5	TXND5_HUMAN	48283	4 & 10
Q16881	Thioredoxin reductase 1, cytoplasmic	TRXR1_HUMAN	71832	9
P30048	Thioredoxin-dependent peroxide reductase, mitochondrial	PRDX3_HUMAN	28017	6 & 12
O43396	Thioredoxin-like protein 1	TXNL1_HUMAN	32630	5 & 11
P26639	Threonine--tRNA ligase, cytoplasmic	SYTC_HUMAN	84294	7
P04818	Thymidylate synthase	TYSY_HUMAN	35978	11
Q9UDY2	Tight junction protein ZO-2	ZO2_HUMAN	134104	12
P37837	Transaldolase	TALDO_HUMAN	37688	5 & 11
P20290	Transcription factor BTF3	BTF3_HUMAN	22211	12
Q13263	Transcription intermediary factor 1-beta	TIF1B_HUMAN	90261	11
P61586	Transforming protein RhoA	RHOA_HUMAN	22096	6 & 12
Q01995	Transgelin	TAGL_HUMAN	22653	6 & 12
P37802	Transgelin-2	TAGL2_HUMAN	22548	6 & 12
P55072	Transitional endoplasmic reticulum ATPase	TERA_HUMAN	89950	1 & 7
P29401	Transketolase	TKT_HUMAN	68519	2 & 8
P13693	Translationally-controlled tumor protein	TCTP_HUMAN	19697	6 & 12
P60174	Triosephosphate isomerase	TPIS_HUMAN	31057	5 & 11
P67936	Tropomyosin alpha-4 chain	TPM4_HUMAN	28619	5 & 11
P07951	Tropomyosin beta chain	TPM2_HUMAN	32945	5 & 11
P23381	Tryptophan--tRNA ligase, cytoplasmic	SYWC_HUMAN	53474	3 & 9
O75347	Tubulin-specific chaperone A	TBCA_HUMAN	12904	6 & 12
P62310	U6 snRNA-associated Sm-like protein LSm3	LSM3_HUMAN	11838	12
P54578	Ubiquitin carboxyl-terminal hydrolase 14	UBP14_HUMAN	56489	3 & 9
P40818	Ubiquitin carboxyl-terminal hydrolase 8	UBP8_HUMAN	128413	9
P09936	Ubiquitin carboxyl-terminal hydrolase isozyme L1	UCHL1_HUMAN	25151	6 & 12
P62979	Ubiquitin-40S ribosomal protein S27a	RS27A_HUMAN	18296	6 & 12
Q13404	Ubiquitin-conjugating enzyme E2 variant 1	UB2V1_HUMAN	16598	6 & 12

P22314	Ubiquitin-like modifier-activating enzyme 1	UBA1_HUMAN	118858	1 & 7
O60701	UDP-glucose 6-dehydrogenase	UGDH_HUMAN	55674	9
Q16222	UDP-N-acetylhexosamine pyrophosphorylase	UAP1_HUMAN	59131	3 & 9
P30085	UMP-CMP kinase	KCY_HUMAN	22436	6 & 12
Q5NDL2	Uncharacterized glycosyltransferase AER61	AER61_HUMAN	62826	9
Q8TDB4	Uncharacterized protein C4orf49	CD049_HUMAN	25431	11
Q9BY89	Uncharacterized protein KIAA1671	K1671_HUMAN	197617	11
Q9HB07	UPF0160 protein MYG1, mitochondrial	MYG1_HUMAN	42765	10
Q9H7C9	UPF0366 protein C11orf67	CK067_HUMAN	13438	6 & 12
Q969H8	UPF0556 protein C19orf10	CS010_HUMAN	18897	6
P06132	Uroporphyrinogen decarboxylase	DCUP_HUMAN	41103	4
Q16851	UTP--glucose-1-phosphate uridylyltransferase	UGPA_HUMAN	57076	3 & 9
P21281	V-type proton ATPase subunit B, brain isoform	VATB2_HUMAN	56807	9
Q96QK1	Vacuolar protein sorting-associated protein 35	VPS35_HUMAN	92447	7
P50552	Vasodilator-stimulated phosphoprotein	VASP_HUMAN	39976	5 & 12
P13611	Versican core protein	CSPG2_HUMAN	374585	12
P18206	Vinculin	VINC_HUMAN	124292	1 & 7
O75083	WD repeat-containing protein 1	WDR1_HUMAN	66836	2 & 8
P12955	Xaa-Pro dipeptidase	PEPD_HUMAN	55311	9
P46937	Yorkie homolog	YAP1_HUMAN	54484	6 & 12
Q5T200	Zinc finger CCCH domain-containing protein 13	ZC3HD_HUMAN	197203	4
Q5BKZ1	Zinc finger protein 326	ZN326_HUMAN	65955	11
Q15942	Zyxin	ZYX_HUMAN	62436	11

References

Aase, K., Ernkvist, M., Ebarasi, L., Jakobsson, L., Majumdar, A., Yi, C., Birot, O., Ming, Y., Kvanta, A., Edholm, D., *et al.* (2007). Angiomotin regulates endothelial cell migration during embryonic angiogenesis. Genes & Development *21*, 2055-2068.

Abe, K., and Takeichi, M. (2008). EPLIN mediates linkage of the cadherin catenin complex to F-actin and stabilizes the circumferential actin belt. Proc Natl Acad Sci U S A *105*, 13-19.

Abraham, S., Yeo, M., Montero-Balaguer, M., Paterson, H., Dejana, E., Marshall, C.J., and Mavria, G. (2009). VE-Cadherin-mediated cell-cell interaction suppresses sprouting via signaling to MLC2 phosphorylation. Curr Biol *19*, 668-674.

Adam, A.P., Sharenko, A.L., Pumiglia, K., and Vincent, P.A. (2010). Src-induced tyrosine phosphorylation of VE-cadherin is not sufficient to decrease barrier function of endothelial monolayers. J Biol Chem *285*, 7045-7055.

Aguilar, R.C., Longhi, S.A., Shaw, J.D., Yeh, L.-Y., Kim, S., Schön, A., Freire, E., Hsu, A., McCormick, W.K., Watson, H.A., *et al.* (2006). Epsin N-terminal homology domains perform an essential function regulating Cdc42 through binding Cdc42 GTPase-activating proteins. Proceedings of the National Academy of Sciences of the United States of America *103*, 4116-4121.

Aird, W.C. (2012). Endothelial Cell Heterogeneity. Cold Spring Harbor perspectives in medicine *2*.

Aitken, A. (2006). 14-3-3 proteins: a historic overview. Semin Cancer Biol *16*, 162-172.

Alessi, D.R., Andjelkovic, M., Caudwell, B., Cron, P., Morrice, N., Cohen, P., and Hemmings, B.A. (1996a). Mechanism of activation of protein kinase B by insulin and IGF-1. EMBO J *15*, 6541-6551.

Alessi, D.R., Caudwell, F.B., Andjelkovic, M., Hemmings, B.A., and Cohen, P. (1996b). Molecular basis for the substrate specificity of protein kinase B; comparison with MAPKAP kinase-1 and p70 S6 kinase. FEBS Lett *399*, 333-338.

Alessi, D.R., James, S.R., Downes, C.P., Holmes, A.B., Gaffney, P.R., Reese, C.B., and Cohen, P. (1997). Characterization of a 3-phosphoinositide-dependent protein kinase which phosphorylates and activates protein kinase Balpha. Curr Biol *7*, 261-269.

Allingham, M.J., van Buul, J.D., and Burridge, K. (2007). ICAM-1-mediated, Src- and Pyk2-dependent vascular endothelial cadherin tyrosine phosphorylation is required for leukocyte transendothelial migration. Journal of immunology (Baltimore, Md : 1950) *179*, 4053-4064.

Allport, J.R., Muller, W.A., and Luscinskas, F.W. (2000). Monocytes induce reversible focal changes in vascular endothelial cadherin complex during transendothelial migration under flow. J Cell Biol *148*, 203-216.

Alwan, A. (2011). Global status report on noncommunicable diseases 2010 (World Health Organization).

Amano, M., Ito, M., Kimura, K., Fukata, Y., Chihara, K., Nakano, T., Matsuura, Y., and Kaibuchi, K. (1996). Phosphorylation and activation of myosin by Rho-associated kinase (Rho-kinase). J Biol Chem *271*, 20246-20249.

Asakura, S. (1961). The interaction between G-actin and ATP. Archives of Biochemistry and Biophysics *92*, 140-149.

Aspenstrom, P., Fransson, A., and Saras, J. (2004). Rho GTPases have diverse effects on the organization of the actin filament system. Biochem J *377*, 327-337.

Aspenstrom, P., Ruusala, A., and Pacholsky, D. (2007). Taking Rho GTPases to the next level: the cellular functions of atypical Rho GTPases. Experimental cell research *313*, 3673-3679.

Aurrand-Lions, M., Duncan, L., Ballestrem, C., and Imhof, B.A. (2001). JAM-2, a novel immunoglobulin superfamily molecule, expressed by endothelial and lymphatic cells. J Biol Chem *276*, 2733-2741.

Banting, F.G., Best, C.H., Collip, J.B., Campbell, W.R., and Fletcher, A.A. (1922). Pancreatic Extracts in the Treatment of Diabetes Mellitus. Canadian Medical Association journal *12*, 141-146.

Bar, R.S., Hoak, J.C., and Peacock, M.L. (1978). Insulin receptors in human endothelial cells: identification and characterization. J Clin Endocrinol Metab *47*, 699-702.

Bar, R.S., Peacock, M.L., Spanheimer, R.G., Veenstra, R., and Hoak, J.C. (1980). Differential Binding of Insulin to Human Arterial and Venous Endothelial Cells in Primary Culture. Diabetes *29*, 991-995.

Bayless, K.J., and Davis, G.E. (2002). The Cdc42 and Rac1 GTPases are required for capillary lumen formation in three-dimensional extracellular matrices. J Cell Sci *115*, 1123-1136.

Bayless, K.J., and Davis, G.E. (2004). Microtubule depolymerization rapidly collapses capillary tube networks in vitro and angiogenic vessels in vivo through the small GTPase Rho. J Biol Chem *279*, 11686-11695.

Bayless, K.J., and Johnson, G.A. (2011). Role of the cytoskeleton in formation and maintenance of angiogenic sprouts. Journal of vascular research *48*, 369-385.

Bayless, K.J., Salazar, R., and Davis, G.E. (2000). RGD-dependent vacuolation and lumen formation observed during endothelial cell morphogenesis in three-dimensional fibrin matrices involves the alpha(v)beta(3) and alpha(5)beta(1) integrins. Am J Pathol *156*, 1673-1683.

Bazzoni, G. (2006). Endothelial tight junctions: permeable barriers of the vessel wall. Thromb Haemost *95*, 36-42.

Bazzoni, G., and Dejana, E. (2001). Pores in the sieve and channels in the wall: control of paracellular permeability by junctional proteins in endothelial cells. Microcirculation *8*, 143-152.

Bazzoni, G., and Dejana, E. (2004). Endothelial cell-to-cell junctions: molecular organization and role in vascular homeostasis. Physiol Rev *84*, 869-901.

Beckers, C.M., van Hinsbergh, V.W., and van Nieuw Amerongen, G.P. (2010). Driving Rho GTPase activity in endothelial cells regulates barrier integrity. Thromb Haemost *103*, 40-55.

Begum, N., Sandu, O.A., and Duddy, N. (2002). Negative regulation of rho signaling by insulin and its impact on actin cytoskeleton organization in vascular smooth muscle cells: role of nitric oxide and cyclic guanosine monophosphate signaling pathways. Diabetes *51*, 2256-2263.

Beitner-Johnson, D., and LeRoith, D. (1995). Insulin-like Growth Factor-I Stimulates Tyrosine Phosphorylation of Endogenous c-Crk. Journal of Biological Chemistry *270*, 5187-5190.

Benz, P.M., Blume, C., Moebius, J., Oschatz, C., Schuh, K., Sickmann, A., Walter, U., Feller, S.M., and Renne, T. (2008). Cytoskeleton assembly at endothelial cell-cell contacts is regulated by alphaII-spectrin-VASP complexes. J Cell Biol *180*, 205-219.

Benzinger, A., Muster, N., Koch, H.B., Yates, J.R., 3rd, and Hermeking, H. (2005). Targeted proteomic analysis of 14-3-3 sigma, a p53 effector commonly silenced in cancer. Mol Cell Proteomics *4*, 785-795.

Blundell, T.L., Dodson, G.G., Dodson, E., Hodgkin, D.C., and Vijayan, M. (1971). X-ray analysis and the structure of insulin. Recent progress in hormone research *27*, 1-40.

Bogatcheva, N.V., and Verin, A.D. (2008). The role of cytoskeleton in the regulation of vascular endothelial barrier function. Microvascular research *76*, 202-207.

Booth, G.L., Kapral, M.K., Fung, K., and Tu, J.V. (2006). Relation between age and cardiovascular disease in men and women with diabetes compared with non-diabetic people: a population-based retrospective cohort study. Lancet *368*, 29-36.

Borland, G., Smith, B.O., and Yarwood, S.J. (2009). EPAC proteins transduce diverse cellular actions of cAMP. British journal of pharmacology *158*, 70-86.

Bos, J.L., Rehmann, H., and Wittinghofer, A. (2007). GEFs and GAPs: Critical Elements in the Control of Small G Proteins. Cell *129*, 865-877.

Boureux, A., Vignal, E., Faure, S., and Fort, P. (2007). Evolution of the Rho family of ras-like GTPases in eukaryotes. Molecular biology and evolution *24*, 203-216.

Brem, H., and Tomic-Canic, M. (2007). Cellular and molecular basis of wound healing in diabetes. J Clin Invest *117*, 1219-1222.

Bridges, D., and Moorhead, G.B. (2005). 14-3-3 proteins: a number of functions for a numbered protein. Science's STKE : signal transduction knowledge environment *2005*, re10.

Brodsky, F.M. (2012). Diversity of clathrin function: new tricks for an old protein. Annu Rev Cell Dev Biol *28*, 309-336.

Broman, M.T., Kouklis, P., Gao, X., Ramchandran, R., Neamu, R.F., Minshall, R.D., and Malik, A.B. (2006). Cdc42 Regulates Adherens Junction Stability and Endothelial Permeability by Inducing α-Catenin Interaction With the Vascular Endothelial Cadherin Complex. Circulation Research *98*, 73-80.

Brunet, A., Bonni, A., Zigmond, M.J., Lin, M.Z., Juo, P., Hu, L.S., Anderson, M.J., Arden, K.C., Blenis, J., and Greenberg, M.E. (1999). Akt promotes cell survival by phosphorylating and inhibiting a Forkhead transcription factor. Cell *96*, 857-868.

Bucci, M., Roviezzo, F., Posadas, I., Yu, J., Parente, L., Sessa, W.C., Ignarro, L.J., and Cirino, G. (2005). Endothelial nitric oxide synthase activation is critical for vascular leakage during acute inflammation in vivo. Proc Natl Acad Sci U S A *102*, 904-908.

Cahill, C.M., Tzivion, G., Nasrin, N., Ogg, S., Dore, J., Ruvkun, G., and Alexander-Bridges, M. (2001). Phosphatidylinositol 3-kinase signaling inhibits DAF-16 DNA binding and function via 14-3-3-dependent and 14-3-3-independent pathways. J Biol Chem *276*, 13402-13410.

Cantley, L.C. (2002). The Phosphoinositide 3-Kinase Pathway. Science *296*, 1655-1657.

Carlier, M.F., Laurent, V., Santolini, J., Melki, R., Didry, D., Xia, G.X., Hong, Y., Chua, N.H., and Pantaloni, D. (1997). Actin depolymerizing factor (ADF/cofilin) enhances the rate of filament turnover: implication in actin-based motility. J Cell Biol *136*, 1307-1322.

Carmeliet, P., and Jain, R.K. (2011). Molecular mechanisms and clinical applications of angiogenesis. Nature *473*, 298-307.

Cau, J., and Hall, A. (2005). Cdc42 controls the polarity of the actin and microtubule cytoskeletons through two distinct signal transduction pathways. J Cell Sci *118*, 2579-2587.

Chardin, P. (2003). GTPase regulation: getting aRnd Rock and Rho inhibition. Curr Biol *13*, R702-704.

Chaudhuri, A., Dandona, P., and Fonseca, V. (2012). Cardiovascular benefits of exogenous insulin. J Clin Endocrinol Metab *97*, 3079-3091.

Cheatham, B., and Kahn, C.R. (1995). Insulin action and the insulin signaling network. Endocr Rev *16*, 117-142.

Chen, H., Fre, S., Slepnev, V.I., Capua, M.R., Takei, K., Butler, M.H., Di Fiore, P.P., and De Camilli, P. (1998). Epsin is an EH-domain-binding protein implicated in clathrin-mediated endocytosis. Nature *394*, 793-797.

Chen, H., Ko, G., Zatti, A., Di Giacomo, G., Liu, L., Raiteri, E., Perucco, E., Collesi, C., Min, W., Zeiss, C.*, et al.* (2009). Embryonic arrest at midgestation and disruption of Notch signaling produced by the absence of both epsin 1 and epsin 2 in mice. Proc Natl Acad Sci U S A *106*, 13838-13843.

Chen, J., and Zhang, M. (2013). The Par3/Par6/aPKC complex and epithelial cell polarity. Experimental cell research *319*, 1357-1364.

Chen, S., Synowsky, S., Tinti, M., and MacKintosh, C. (2011). The capture of phosphoproteins by 14-3-3 proteins mediates actions of insulin. Trends Endocrinol Metab *22*, 429-436.

Chen, W.T. (1981). Mechanism of retraction of the trailing edge during fibroblast movement. The Journal of Cell Biology *90*, 187-200.

Chen, X., Liu, Y., and Zhang, X. (2012). Topical insulin application improves healing by regulating the wound inflammatory response. Wound repair and regeneration : official publication of the Wound Healing Society [and] the European Tissue Repair Society *20*, 425-434.

Cicchetti, P., Mayer, B.J., Thiel, G., and Baltimore, D. (1992). Identification of a protein that binds to the SH3 region of Abl and is similar to Bcr and GAP-rho. Science *257*, 803-806.

Coblitz, B., Shikano, S., Wu, M., Gabelli, S.B., Cockrell, L.M., Spieker, M., Hanyu, Y., Fu, H., Amzel, L.M., and Li, M. (2005). C-terminal recognition by 14-3-3 proteins for surface expression of membrane receptors. J Biol Chem *280*, 36263-36272.

Cohen, P. (2006). The twentieth century struggle to decipher insulin signalling. Nat Rev Mol Cell Biol *7*, 867-873.

Comerford, K.M., Lawrence, D.W., Synnestvedt, K., Levi, B.P., and Colgan, S.P. (2002). Role of vasodilator-stimulated phosphoprotein in PKA-induced changes in endothelial junctional permeability. FASEB journal : official publication of the Federation of American Societies for Experimental Biology *16*, 583-585.

Cook, D.R., Rossman, K.L., and Der, C.J. (2013). Rho guanine nucleotide exchange factors: regulators of Rho GTPase activity in development and disease. Oncogene.

Cook-Mills, J., Johnson, J., Deem, T., Ochi, A., Wang, L., and Zheng, Y. (2004). Calcium mobilization and Rac1 activation are required for VCAM-1 (vascular cell adhesion molecule-1) stimulation of NADPH oxidase activity. Biochem J *378*, 539-547.

Coon, B.G., Burgner, J., Camonis, J.H., and Aguilar, R.C. (2010). The epsin family of endocytic adaptors promotes fibrosarcoma migration and invasion. J Biol Chem *285*, 33073-33081.

Cullere, X., Shaw, S.K., Andersson, L., Hirahashi, J., Luscinskas, F.W., and Mayadas, T.N. (2005). Regulation of vascular endothelial barrier function by Epac, a cAMP-activated exchange factor for Rap GTPase. Blood *105*, 1950-1955.

Cummins, P.M. (2012). Occludin: one protein, many forms. Mol Cell Biol *32*, 242-250.

Dandona, P., Chaudhuri, A., Ghanim, H., and Mohanty, P. (2009). Insulin as an anti-inflammatory and antiatherogenic modulator. J Am Coll Cardiol *53*, S14-20.

Daughaday, W.H., and Rotwein, P. (1989). Insulin-like growth factors I and II. Peptide, messenger ribonucleic acid and gene structures, serum, and tissue concentrations. Endocr Rev *10*, 68-91.

David, C., Solimena, M., and De Camilli, P. (1994). Autoimmunity in stiff-Man syndrome with breast cancer is targeted to the C-terminal region of human amphiphysin, a protein similar to the yeast proteins, Rvs167 and Rvs161. FEBS Lett *351*, 73-79.

Davis, G.E., Black, S.M., and Bayless, K.J. (2000). Capillary morphogenesis during human endothelial cell invasion of three-dimensional collagen matrices. In vitro cellular & developmental biology Animal *36*, 513-519.

De Caterina, R., Libby, P., Peng, H.B., Thannickal, V.J., Rajavashisth, T.B., Gimbrone, M.A., Jr., Shin, W.S., and Liao, J.K. (1995). Nitric oxide decreases cytokine-induced endothelial activation. Nitric oxide selectively reduces endothelial expression of adhesion molecules and proinflammatory cytokines. J Clin Invest *96*, 60-68.

De Matteis, M.A., and Morrow, J.S. (2000). Spectrin tethers and mesh in the biosynthetic pathway. J Cell Sci *113 (Pt 13)*, 2331-2343.

Dedeic, Z., Cetera, M., Cohen, T.V., and Holaska, J.M. (2011). Emerin inhibits Lmo7 binding to the Pax3 and MyoD promoters and expression of myoblast proliferation genes. J Cell Sci *124*, 1691-1702.

Dejana, E. (2004). Endothelial cell-cell junctions: happy together. Nat Rev Mol Cell Biol *5*, 261-270.

Dejana, E., Bazzoni, G., and Lampugnani, M.G. (1999). Vascular endothelial (VE)-cadherin: only an intercellular glue? Experimental cell research *252*, 13-19.

Dejana, E., and Giampietro, C. (2012). Vascular endothelial-cadherin and vascular stability. Current opinion in hematology *19*, 218-223.

Dejana, E., and Orsenigo, F. (2013). Endothelial adherens junctions at a glance. J Cell Sci *126*, 2545-2549.

Dejana, E., Orsenigo, F., and Lampugnani, M.G. (2008). The role of adherens junctions and VE-cadherin in the control of vascular permeability. J Cell Sci *121*, 2115-2122.

Dejana, E., Orsenigo, F., Molendini, C., Baluk, P., and McDonald, D.M. (2009). Organization and signaling of endothelial cell-to-cell junctions in various regions of the blood and lymphatic vascular trees. Cell Tissue Res *335*, 17-25.

Diaz, R., Paolasso, E.A., Piegas, L.S., Tajer, C.D., Moreno, M.G., Corvalan, R., Isea, J.E., and Romero, G. (1998). Metabolic modulation of acute myocardial infarction. The ECLA (Estudios Cardiologicos Latinoamerica) Collaborative Group. Circulation *98*, 2227-2234.

Dikic, I. (2002). CIN85/CMS family of adaptor molecules. FEBS Lett *529*, 110-115.

Dimmeler, S., Fleming, I., Fisslthaler, B., Hermann, C., Busse, R., and Zeiher, A.M. (1999). Activation of nitric oxide synthase in endothelial cells by Akt-dependent phosphorylation. Nature *399*, 601-605.

Disanza, A., Bisi, S., Winterhoff, M., Milanesi, F., Ushakov, D.S., Kast, D., Marighetti, P., Romet-Lemonne, G., Muller, H.M., Nickel, W.*, et al.* (2013). CDC42 switches IRSp53 from inhibition of actin growth to elongation by clustering of VASP. EMBO J.

Dominguez, R. (2009). Actin filament nucleation and elongation factors--structure-function relationships. Critical reviews in biochemistry and molecular biology *44*, 351-366.

Dong, Z.M., and Wagner, D.D. (1998). Leukocyte-endothelium adhesion molecules in atherosclerosis. The Journal of laboratory and clinical medicine *132*, 369-375.

Du, Y.C., Zhang, Y.S., Lu, Z.X., and Tsou, C.L. (1961). Resynthesis of insulin from its glycyl and phenylalanyl chains. Scientia Sinica *10*, 84-104.

Dubois, F., Vandermoere, F., Gernez, A., Murphy, J., Toth, R., Chen, S., Geraghty, K.M., Morrice, N.A., and MacKintosh, C. (2009). Differential 14-3-3 affinity capture reveals new downstream targets of phosphatidylinositol 3-kinase signaling. Mol Cell Proteomics *8*, 2487-2499.

Dupont, J., and LeRoith, D. (2001). Insulin and Insulin-Like Growth Factor I Receptors: Similarities and Differences in Signal Transduction. Hormone Research in Paediatrics *55(suppl 2)*, 22-26.

Ebnet, K., Schulz, C.U., Meyer Zu Brickwedde, M.K., Pendl, G.G., and Vestweber, D. (2000). Junctional adhesion molecule interacts with the PDZ domain-containing proteins AF-6 and ZO-1. J Biol Chem *275*, 27979-27988.

Ehringer, W.D., Edwards, M.J., and Miller, F.N. (1996). Mechanisms of alpha-thrombin, histamine, and bradykinin induced endothelial permeability. J Cell Physiol *167*, 562-569.

El-Shewy, H.M., Lee, M.-H., Obeid, L.M., Jaffa, A.A., and Luttrell, L.M. (2007). The Insulin-like Growth Factor Type 1 and Insulin-like Growth Factor Type 2/Mannose-6-phosphate Receptors Independently Regulate ERK1/2 Activity in HEK293 Cells. Journal of Biological Chemistry *282*, 26150-26157.

Ellerbroek, S.M., Wennerberg, K., and Burridge, K. (2003). Serine phosphorylation negatively regulates RhoA in vivo. J Biol Chem *278*, 19023-19031.

Endemann, D.H., and Schiffrin, E.L. (2004). Endothelial dysfunction. Journal of the American Society of Nephrology : JASN *15*, 1983-1992.

Engelhardt, B. (2003). Development of the blood-brain barrier. Cell and tissue research *314*, 119-129.

Engelman, J.A., Luo, J., and Cantley, L.C. (2006). The evolution of phosphatidylinositol 3-kinases as regulators of growth and metabolism. Nat Rev Genet *7*, 606-619.

Esser, S., Lampugnani, M.G., Corada, M., Dejana, E., and Risau, W. (1998). Vascular endothelial growth factor induces VE-cadherin tyrosine phosphorylation in endothelial cells. J Cell Sci *111 (Pt 13)*, 1853-1865.

Ewing, R.M., Chu, P., Elisma, F., Li, H., Taylor, P., Climie, S., McBroom-Cerajewski, L., Robinson, M.D., O'Connor, L., Li, M.*, et al.* (2007). Large-scale mapping of human protein-protein interactions by mass spectrometry. Molecular systems biology *3*, 89.

Farsad, K., Ringstad, N., Takei, K., Floyd, S.R., Rose, K., and De Camilli, P. (2001). Generation of high curvature membranes mediated by direct endophilin bilayer interactions. J Cell Biol *155*, 193-200.

Félétou, M. (2011). The Endothelium: Part 1: Multiple Functions of the Endothelial Cells—Focus on Endothelium-Derived Vasoactive Mediators.

Feng, D., Nagy, J.A., Dvorak, H.F., and Dvorak, A.M. (2002). Ultrastructural studies define soluble macromolecular, particulate, and cellular transendothelial cell pathways in venules, lymphatic vessels, and tumor-associated microvessels in man and animals. Microscopy research and technique *57*, 289-326.

Feng, J., Park, J., Cron, P., Hess, D., and Hemmings, B.A. (2004). Identification of a PKB/Akt hydrophobic motif Ser-473 kinase as DNA-dependent protein kinase. J Biol Chem *279*, 41189-41196.

Fernandez-Martin, L., Marcos-Ramiro, B., Bigarella, C.L., Graupera, M., Cain, R.J., Reglero-Real, N., Jimenez, A., Cernuda-Morollon, E., Correas, I., Cox, S.*, et al.* (2012). Crosstalk between reticular adherens junctions and platelet endothelial cell adhesion molecule-1 regulates endothelial barrier function. Arterioscler Thromb Vasc Biol *32*, e90-102.

Ferri, N. (2013). Pharmacological Modulation of Small GTPases in Cardiovascular Diseases: From Statins to Selective Inhibitors. Journal of cardiovascular pharmacology *62*, 329-330.

Firat-Karalar, E.N., and Welch, M.D. (2011). New mechanisms and functions of actin nucleation. Curr Opin Cell Biol *23*, 4-13.

Fletcher, S.J., and Rappoport, J.Z. (2014). Tight junction regulation through vesicle trafficking: bringing cells together. Biochemical Society transactions *42*, 195-200.

Ford, M.G., Mills, I.G., Peter, B.J., Vallis, Y., Praefcke, G.J., Evans, P.R., and McMahon, H.T. (2002). Curvature of clathrin-coated pits driven by epsin. Nature *419*, 361-366.

Forget, M.A., Desrosiers, R.R., Gingras, D., and Beliveau, R. (2002). Phosphorylation states of Cdc42 and RhoA regulate their interactions with Rho GDP dissociation inhibitor and their extraction from biological membranes. Biochem J *361*, 243-254.

Frattali, A.L., Treadway, J.L., and Pessin, J.E. (1992). Transmembrane signaling by the human insulin receptor kinase. Relationship between intramolecular beta subunit trans- and cis-autophosphorylation and substrate kinase activation. J Biol Chem *267*, 19521-19528.

Fukata, M., Kuroda, S., Nakagawa, M., Kawajiri, A., Itoh, N., Shoji, I., Matsuura, Y., Yonehara, S., Fujisawa, H., Kikuchi, A.*, et al.* (1999). Cdc42 and Rac1 regulate the interaction of IQGAP1 with beta-catenin. J Biol Chem *274*, 26044-26050.

Fukuhra, S., Sakurai, A., Yamagishi, A., Sako, K., and Mochizuki, N. (2006). Vascular endothelial cadherin-mediated cell-cell adhesion regulated by a small GTPase, Rap1. Journal of biochemistry and molecular biology *39*, 132-139.

Gadea, G., Sanz-Moreno, V., Self, A., Godi, A., and Marshall, C.J. (2008). DOCK10-mediated Cdc42 activation is necessary for amoeboid invasion of melanoma cells. Curr Biol *18*, 1456-1465.

Gage, M.C., Yuldasheva, N.Y., Viswambharan, H., Sukumar, P., Cubbon, R.M., Galloway, S., Imrie, H., Skromna, A., Smith, J., Jackson, C.L.*, et al.* (2013). Endothelium-specific insulin resistance leads to accelerated atherosclerosis in areas with disturbed flow patterns: A role for reactive oxygen species. Atherosclerosis *230*, 131-139.

Gao, F., Gao, E., Yue, T.L., Ohlstein, E.H., Lopez, B.L., Christopher, T.A., and Ma, X.L. (2002). Nitric oxide mediates the antiapoptotic effect of insulin in myocardial ischemia-reperfusion: the roles of PI3-kinase, Akt, and endothelial nitric oxide synthase phosphorylation. Circulation *105*, 1497-1502.

Garcia-Mata, R., Boulter, E., and Burridge, K. (2011). The 'invisible hand': regulation of RHO GTPases by RHOGDIs. Nat Rev Mol Cell Biol *12*, 493-504.

Garcia-Mata, R., and Burridge, K. (2007). Catching a GEF by its tail. Trends Cell Biol *17*, 36-43.

Garlanda, C., and Dejana, E. (1997). Heterogeneity of endothelial cells. Specific markers. Arterioscler Thromb Vasc Biol *17*, 1193-1202.

Gavard, J. (2009). Breaking the VE-cadherin bonds. FEBS Letters *583*, 1-6.

Gavard, J., and Gutkind, J.S. (2006). VEGF controls endothelial-cell permeability by promoting the beta-arrestin-dependent endocytosis of VE-cadherin. Nat Cell Biol *8*, 1223-1234.

Gavard, J., and Gutkind, J.S. (2008). VE-cadherin and claudin-5: it takes two to tango. Nat Cell Biol *10*, 883-885.

Ghosh, M., Song, X., Mouneimne, G., Sidani, M., Lawrence, D.S., and Condeelis, J.S. (2004). Cofilin promotes actin polymerization and defines the direction of cell motility. Science *304*, 743-746.

Gomez, G.A., McLachlan, R.W., and Yap, A.S. (2011). Productive tension: force-sensing and homeostasis of cell–cell junctions. Trends in Cell Biology *21*, 499-505.

Gong, C., Stoletov, K.V., and Terman, B.I. (2004). VEGF treatment induces signaling pathways that regulate both actin polymerization and depolymerization. Angiogenesis *7*, 313-321.

Gonzalez-Mariscal, L., Tapia, R., and Chamorro, D. (2008). Crosstalk of tight junction components with signaling pathways. Biochimica et biophysica acta *1778*, 729-756.

Goodwin, A.M. (2007). In vitro assays of angiogenesis for assessment of angiogenic and anti-angiogenic agents. Microvascular research *74*, 172-183.

Goren, I., Muller, E., Pfeilschifter, J., and Frank, S. (2006). Severely impaired insulin signaling in chronic wounds of diabetic ob/ob mice: a potential role of tumor necrosis factor-alpha. Am J Pathol *168*, 765-777.

Gough, W., Hulkower, K.I., Lynch, R., McGlynn, P., Uhlik, M., Yan, L., and Lee, J.A. (2011). A quantitative, facile, and high-throughput image-based cell migration method is a robust alternative to the scratch assay. Journal of biomolecular screening *16*, 155-163.

Gould, G.W., and Lippincott-Schwartz, J. (2009). New roles for endosomes: from vesicular carriers to multi-purpose platforms. Nat Rev Mol Cell Biol *10*, 287-292.

Gregory, W.B. (1965). Effect of insulin on the healing of bone wounds in albino rats. Journal of dental research *44*, 487-492.

Gumbiner, B.M. (1995). Signal transduction of beta-catenin. Curr Opin Cell Biol *7*, 634-640.

Gunduz, D., Thom, J., Hussain, I., Lopez, D., Hartel, F.V., Erdogan, A., Grebe, M., Sedding, D., Piper, H.M., Tillmanns, H.*, et al.* (2010). Insulin stabilizes microvascular endothelial barrier function via phosphatidylinositol 3-kinase/Akt-mediated Rac1 activation. Arterioscler Thromb Vasc Biol *30*, 1237-1245.

Hall, A. (1998). Rho GTPases and the actin cytoskeleton. Science *279*, 509-514.

Hall, A. (2012). Rho family GTPases. Biochemical Society transactions *40*, 1378-1382.

Hanada, M., Feng, J., and Hemmings, B.A. (2004). Structure, regulation and function of PKB/AKT--a major therapeutic target. Biochimica et biophysica acta *1697*, 3-16.

Hanam, S., Singleton, C., and Rudek, W. (1983). The effect of topical insulin on infected cutaneous ulcerations in diabetic and nondiabetic mice. The Journal of foot surgery *22*, 298.

Hanke, S., and Mann, M. (2009). The Phosphotyrosine Interactome of the Insulin Receptor Family and Its Substrates IRS-1 and IRS-2. Molecular & Cellular Proteomics *8*, 519-534.

Harada, A., Furuta, B., Takeuchi, K., Itakura, M., Takahashi, M., and Umeda, M. (2000). Nadrin, a novel neuron-specific GTPase-activating protein involved in regulated exocytosis. J Biol Chem *275*, 36885-36891.

Harhaj, N.S., and Antonetti, D.A. (2004). Regulation of tight junctions and loss of barrier function in pathophysiology. Int J Biochem Cell Biol *36*, 1206-1237.

Harhaj, N.S., Felinski, E.A., Wolpert, E.B., Sundstrom, J.M., Gardner, T.W., and Antonetti, D.A. (2006). VEGF activation of protein kinase C stimulates occludin phosphorylation and contributes to endothelial permeability. Investigative ophthalmology & visual science *47*, 5106-5115.

Harris, E.S., and Nelson, W.J. (2010). VE-cadherin: at the front, center, and sides of endothelial cell organization and function. Current Opinion in Cell Biology *22*, 651-658.

Heasman, S.J., and Ridley, A.J. (2008). Mammalian Rho GTPases: new insights into their functions from in vivo studies. Nat Rev Mol Cell Biol *9*, 690-701.

Heath, J.P. (1983). Behaviour and structure of the leading lamella in moving fibroblasts. I. Occurrence and centripetal movement of arc-shaped microfilament bundles beneath the dorsal cell surface. J Cell Sci *60*, 331-354.

Heltianu, C., Bogdan, I., Constantinescu, E., and Simionescu, M. (1986). Endothelial cells express a spectrin-like cytoskeletal protein. Circ Res *58*, 605-610.

Hemmings, B.A., and Restuccia, D.F. (2012). PI3K-PKB/Akt pathway. Cold Spring Harb Perspect Biol *4*, a011189.

Hermann, C., Assmus, B., Urbich, C., Zeiher, A.M., and Dimmeler, S. (2000). Insulin-mediated stimulation of protein kinase Akt: A potent survival signaling cascade for endothelial cells. Arterioscler Thromb Vasc Biol *20*, 402-409.

Hill, C.S., Wynne, J., and Treisman, R. (1995). The Rho family GTPases RhoA, Rac1, and CDC42Hs regulate transcriptional activation by SRF. Cell *81*, 1159-1170.

Hillyer, P., Mordelet, E., Flynn, G., and Male, D. (2003). Chemokines, chemokine receptors and adhesion molecules on different human endothelia: discriminating the tissue-specific functions that affect leucocyte migration. Clinical and experimental immunology *134*, 431-441.

Hiramoto-Yamaki, N., Takeuchi, S., Ueda, S., Harada, K., Fujimoto, S., Negishi, M., and Katoh, H. (2010). Ephexin4 and EphA2 mediate cell migration through a RhoG-dependent mechanism. J Cell Biol *190*, 461-477.

Hirase, T., Kawashima, S., Wong, E.Y., Ueyama, T., Rikitake, Y., Tsukita, S., Yokoyama, M., and Staddon, J.M. (2001). Regulation of tight junction permeability and occludin phosphorylation by Rhoa-p160ROCK-dependent and -independent mechanisms. J Biol Chem *276*, 10423-10431.

Hixenbaugh, E.A., Goeckeler, Z.M., Papaiya, N.N., Wysolmerski, R.B., Silverstein, S.C., and Huang, A.J. (1997). Stimulated neutrophils induce myosin light chain phosphorylation and isometric tension in endothelial cells. Am J Physiol *273*, H981-988.

Hjerrild, M., Stensballe, A., Rasmussen, T.E., Kofoed, C.B., Blom, N., Sicheritz-Ponten, T., Larsen, M.R., Brunak, S., Jensen, O.N., and Gammeltoft, S. (2004). Identification of phosphorylation sites in protein kinase A substrates using artificial neural networks and mass spectrometry. Journal of proteome research *3*, 426-433.

Hoeben, A., Landuyt, B., Highley, M.S., Wildiers, H., Van Oosterom, A.T., and De Bruijn, E.A. (2004). Vascular endothelial growth factor and angiogenesis. Pharmacol Rev *56*, 549-580.

Hoelzle, M.K., and Svitkina, T. (2012). The cytoskeletal mechanisms of cell-cell junction formation in endothelial cells. Mol Biol Cell *23*, 310-323.

Holaska, J.M., Rais-Bahrami, S., and Wilson, K.L. (2006). Lmo7 is an emerin-binding protein that regulates the transcription of emerin and many other muscle-relevant genes. Hum Mol Genet *15*, 3459-3472.

Hornbeck, P.V., Kornhauser, J.M., Tkachev, S., Zhang, B., Skrzypek, E., Murray, B., Latham, V., and Sullivan, M. (2012). PhosphoSitePlus: a comprehensive resource for investigating the structure and function of experimentally determined post-translational modifications in man and mouse. Nucleic Acids Res *40*, D261-270.

Hotulainen, P., and Lappalainen, P. (2006). Stress fibers are generated by two distinct actin assembly mechanisms in motile cells. The Journal of Cell Biology *173*, 383-394.

Hu, Q., Guo, C., Li, Y., Aronow, B.J., and Zhang, J. (2011). LMO7 mediates cell-specific activation of the Rho-myocardin-related transcription factor-serum response factor pathway and plays an important role in breast cancer cell migration. Mol Cell Biol *31*, 3223-3240.

Hu, Z., Hung, J.H., Wang, Y., Chang, Y.C., Huang, C.L., Huyck, M., and DeLisi, C. (2009). VisANT 3.5: multi-scale network visualization, analysis and inference based on the gene ontology. Nucleic Acids Res *37*, W115-121.

Hu, Z., Mellor, J., Wu, J., and DeLisi, C. (2004). VisANT: an online visualization and analysis tool for biological interaction data. BMC bioinformatics *5*, 17.

Huang, A.J., Manning, J.E., Bandak, T.M., Ratau, M.C., Hanser, K.R., and Silverstein, S.C. (1993). Endothelial cell cytosolic free calcium regulates neutrophil migration across monolayers of endothelial cells. J Cell Biol *120*, 1371-1380.

Hurd, T.W., Fan, S., Liu, C.J., Kweon, H.K., Hakansson, K., and Margolis, B. (2003). Phosphorylation-dependent binding of 14-3-3 to the polarity protein Par3 regulates cell polarity in mammalian epithelia. Curr Biol *13*, 2082-2090.

Hussain, N.K., Jenna, S., Glogauer, M., Quinn, C.C., Wasiak, S., Guipponi, M., Antonarakis, S.E., Kay, B.K., Stossel, T.P., Lamarche-Vane, N.*, et al.* (2001). Endocytic protein intersectin-l regulates actin assembly via Cdc42 and N-WASP. Nat Cell Biol *3*, 927-932.

Huveneers, S., Oldenburg, J., Spanjaard, E., van der Krogt, G., Grigoriev, I., Akhmanova, A., Rehmann, H., and de Rooij, J. (2012). Vinculin associates with endothelial VE-cadherin junctions to control force-dependent remodeling. The Journal of Cell Biology *196*, 641-652.

Ikenouchi, J., Umeda, K., Tsukita, S., Furuse, M., and Tsukita, S. (2007). Requirement of ZO-1 for the formation of belt-like adherens junctions during epithelial cell polarization. J Cell Biol *176*, 779-786.

Ingber, D.E., and Folkman, J. (1989). How does extracellular matrix control capillary morphogenesis? Cell *58*, 803-805.

Iruela-Arispe, M.L., and Davis, G.E. (2009). Cellular and molecular mechanisms of vascular lumen formation. Dev Cell *16*, 222-231.

Ito, T., Narita, A., Hirayama, T., Taki, M., Iyoshi, S., Yamamoto, Y., Maéda, Y., and Oda, T. (2011). Human Spire Interacts with the Barbed End of the Actin Filament. Journal of molecular biology *408*, 18-25.

Itoh, M., Nagafuchi, A., Moroi, S., and Tsukita, S. (1997). Involvement of ZO-1 in cadherin-based cell adhesion through its direct binding to alpha catenin and actin filaments. J Cell Biol *138*, 181-192.

Itoh, T., Koshiba, S., Kigawa, T., Kikuchi, A., Yokoyama, S., and Takenawa, T. (2001). Role of the ENTH domain in phosphatidylinositol-4,5-bisphosphate binding and endocytosis. Science *291*, 1047-1051.

Ivanov, D.B., Philippova, M.P., and Tkachuk, V.A. (2001). Structure and functions of classical cadherins. Biochemistry Biokhimiia *66*, 1174-1186.

Ivetic, A., and Ridley, A.J. (2004). Ezrin/radixin/moesin proteins and Rho GTPase signalling in leucocytes. Immunology *112*, 165-176.

Izumi, G., Sakisaka, T., Baba, T., Tanaka, S., Morimoto, K., and Takai, Y. (2004). Endocytosis of E-cadherin regulated by Rac and Cdc42 small G proteins through IQGAP1 and actin filaments. The Journal of Cell Biology *166*, 237-248.

Izumi, Y., Hirose, T., Tamai, Y., Hirai, S., Nagashima, Y., Fujimoto, T., Tabuse, Y., Kemphues, K.J., and Ohno, S. (1998). An atypical PKC directly associates and colocalizes at the epithelial tight junction with ASIP, a mammalian homologue of Caenorhabditis elegans polarity protein PAR-3. J Cell Biol *143*, 95-106.

Jaffe, A.B., and Hall, A. (2005). Rho GTPases: biochemistry and biology. Annu Rev Cell Dev Biol *21*, 247-269.

Jenna, S., Hussain, N.K., Danek, E.I., Triki, I., Wasiak, S., McPherson, P.S., and Lamarche-Vane, N. (2002). The activity of the GTPase-activating protein CdGAP is regulated by the endocytic protein intersectin. J Biol Chem *277*, 6366-6373.

Jeyaraj, S.C., Unger, N.T., and Chotani, M.A. (2011). Rap1 GTPases: an emerging role in the cardiovasculature. Life sciences *88*, 645-652.

Joberty, G., Petersen, C., Gao, L., and Macara, I.G. (2000). The cell-polarity protein Par6 links Par3 and atypical protein kinase C to Cdc42. Nat Cell Biol *2*, 531-539.

Johnson, C., Crowther, S., Stafford, M.J., Campbell, D.G., Toth, R., and MacKintosh, C. (2010). Bioinformatic and experimental survey of 14-3-3-binding sites. Biochem J *427*, 69-78.

Johnson, C., Tinti, M., Wood, N.T., Campbell, D.G., Toth, R., Dubois, F., Geraghty, K.M., Wong, B.H., Brown, L.J., Tyler, J.*, et al.* (2011). Visualization and biochemical analyses of the emerging mammalian 14-3-3-phosphoproteome. Mol Cell Proteomics *10*, M110 005751.

Johnson, G., 3rd, Tsao, P.S., and Lefer, A.M. (1991). Cardioprotective effects of authentic nitric oxide in myocardial ischemia with reperfusion. Crit Care Med *19*, 244-252.

Jonassen, A.K., Sack, M.N., Mjos, O.D., and Yellon, D.M. (2001). Myocardial protection by insulin at reperfusion requires early administration and is mediated via Akt and p70s6 kinase cell-survival signaling. Circ Res *89*, 1191-1198.

Kadrmas, J.L., and Beckerle, M.C. (2004). The LIM domain: from the cytoskeleton to the nucleus. Nat Rev Mol Cell Biol *5*, 920-931.

Kahn, C.R., and White, M.F. (1988). The insulin receptor and the molecular mechanism of insulin action. J Clin Invest *82*, 1151-1156.

Kasuga, M., Hedo, J.A., Yamada, K.M., and Kahn, C.R. (1982a). The structure of insulin receptor and its subunits. Evidence for multiple nonreduced forms and a 210,000 possible proreceptor. J Biol Chem *257*, 10392-10399.

Kasuga, M., Karlsson, F.A., and Kahn, C.R. (1982b). Insulin stimulates the phosphorylation of the 95,000-dalton subunit of its own receptor. Science *215*, 185-187.

Katoh, K., Kano, Y., Amano, M., Onishi, H., Kaibuchi, K., and Fujiwara, K. (2001). Rho-kinase–mediated contraction of isolated stress fibers. The Journal of cell biology *153*, 569-584.

Katsoyannis, P.G. (1967). Synthetic insulins. Recent progress in hormone research *23*, 505-563.

Keiper, T., Al-Fakhri, N., Chavakis, E., Athanasopoulos, A.N., Isermann, B., Herzog, S., Saffrich, R., Hersemeyer, K., Bohle, R.M., Haendeler, J.*, et al.* (2005). The role of junctional adhesion molecule-C (JAM-C) in oxidized LDL-mediated leukocyte recruitment. FASEB journal : official publication of the Federation of American Societies for Experimental Biology *19*, 2078-2080.

Kimura, K., Ito, M., Amano, M., Chihara, K., Fukata, Y., Nakafuku, M., Yamamori, B., Feng, J., Nakano, T., Okawa, K.*, et al.* (1996). Regulation of myosin phosphatase by Rho and Rho-associated kinase (Rho-kinase). Science *273*, 245-248.

King, G.L., and Johnson, S.M. (1985). Receptor-mediated transport of insulin across endothelial cells. Science *227*, 1583-1586.

Kleppe, R., Martinez, A., Doskeland, S.O., and Haavik, J. (2011). The 14-3-3 proteins in regulation of cellular metabolism. Semin Cell Dev Biol *22*, 713-719.

Knight, Z.A., Gonzalez, B., Feldman, M.E., Zunder, E.R., Goldenberg, D.D., Williams, O., Loewith, R., Stokoe, D., Balla, A., Toth, B.*, et al.* (2006). A Pharmacological Map of the PI3-K Family Defines a Role for p110α in Insulin Signaling. Cell *125*, 733-747.

Ko, G., Paradise, S., Chen, H., Graham, M., Vecchi, M., Bianchi, F., Cremona, O., Di Fiore, P.P., and De Camilli, P. (2010). Selective high-level expression of epsin 3 in gastric parietal cells, where it is localized at endocytic sites of apical canaliculi. Proc Natl Acad Sci U S A *107*, 21511-21516.

Koh, W., Mahan, R.D., and Davis, G.E. (2008). Cdc42- and Rac1-mediated endothelial lumen formation requires Pak2, Pak4 and Par3, and PKC-dependent signaling. J Cell Sci *121*, 989-1001.

Koh, W., Sachidanandam, K., Stratman, A.N., Sacharidou, A., Mayo, A.M., Murphy, E.A., Cheresh, D.A., and Davis, G.E. (2009). Formation of endothelial lumens requires a coordinated PKCepsilon-, Src-, Pak- and Raf-kinase-dependent signaling cascade downstream of Cdc42 activation. J Cell Sci *122*, 1812-1822.

Kojima, T., Sawada, N., Chiba, H., Kokai, Y., Yamamoto, M., Urban, M., Lee, G., Hertzberg, E.L., Mochizuki, Y., and Spray, D.C. (1999). Induction of Tight Junctions in Human Connexin 32 (hCx32)-Transfected Mouse Hepatocytes: Connexin 32 Interacts with Occludin. Biochemical and Biophysical Research Communications *266*, 222-229.

Komarova, Y., and Malik, A.B. (2010). Regulation of endothelial permeability via paracellular and transcellular transport pathways. Annual review of physiology *72*, 463-493.

Kooistra, M.R., Corada, M., Dejana, E., and Bos, J.L. (2005). Epac1 regulates integrity of endothelial cell junctions through VE-cadherin. FEBS Lett *579*, 4966-4972.

Kovacs, E.M., Ali, R.G., McCormack, A.J., and Yap, A.S. (2002). E-cadherin Homophilic Ligation Directly Signals through Rac and Phosphatidylinositol 3-Kinase to Regulate Adhesive Contacts. Journal of Biological Chemistry *277*, 6708-6718.

Kowanetz, K., Husnjak, K., Höller, D., Kowanetz, M., Soubeyran, P., Hirsch, D., Schmidt, M.H.H., Pavelic, K., De Camilli, P., Randazzo, P.A.*, et al.* (2004). CIN85 Associates with Multiple Effectors Controlling Intracellular Trafficking of Epidermal Growth Factor Receptors. Molecular Biology of the Cell *15*, 3155-3166.

Krogh, A. (2008). What are artificial neural networks? Nature biotechnology *26*, 195-197.

Kubota, T., Kubota, N., and Kadowaki, T. (2013). The role of endothelial insulin signaling in the regulation of glucose metabolism. Reviews in endocrine & metabolic disorders *14*, 207-216.

Kwon, T., Kwon, D.Y., Chun, J., Kim, J.H., and Kang, S.S. (2000). Akt protein kinase inhibits Rac1-GTP binding through phosphorylation at serine 71 of Rac1. J Biol Chem *275*, 423-428.

Lamalice, L., Le Boeuf, F., and Huot, J. (2007). Endothelial cell migration during angiogenesis. Circ Res *100*, 782-794.

Lamarche, N., and Hall, A. (1994). GAPs for rho-related GTPases. Trends Genet *10*, 436-440.

Lambrechts, A., Van Troys, M., and Ampe, C. (2004). The actin cytoskeleton in normal and pathological cell motility. Int J Biochem Cell Biol *36*, 1890-1909.

Lampugnani, M.G. (2012). Endothelial cell-to-cell junctions: adhesion and signaling in physiology and pathology. Cold Spring Harbor perspectives in medicine *2*.

Lampugnani, M.G., Zanetti, A., Breviario, F., Balconi, G., Orsenigo, F., Corada, M., Spagnuolo, R., Betson, M., Braga, V., and Dejana, E. (2002). VE-Cadherin Regulates Endothelial Actin Activating Rac and Increasing Membrane Association of Tiam. Molecular Biology of the Cell *13*, 1175-1189.

Lang, P., Gesbert, F., Delespine-Carmagnat, M., Stancou, R., Pouchelet, M., and Bertoglio, J. (1996). Protein kinase A phosphorylation of RhoA mediates the morphological and functional effects of cyclic AMP in cytotoxic lymphocytes. EMBO J *15*, 510-519.

Langanger, G., Moeremans, M., Daneels, G., Sobieszek, A., De Brabander, M., and De Mey, J. (1986). The molecular organization of myosin in stress fibers of cultured cells. J Cell Biol *102*, 200-209.

Langouche, L., Vanhorebeek, I., Vlasselaers, D., Vander Perre, S., Wouters, P.J., Skogstrand, K., Hansen, T.K., and Van den Berghe, G. (2005). Intensive insulin therapy protects the endothelium of critically ill patients. J Clin Invest *115*, 2277-2286.

Larance, M., Rowland, A.F., Hoehn, K.L., Humphreys, D.T., Preiss, T., Guilhaus, M., and James, D.E. (2010). Global phosphoproteomics identifies a major role for AKT and 14-3-3 in regulating EDC3. Mol Cell Proteomics *9*, 682-694.

Laufs, U., and Liao, J.K. (1998). Post-transcriptional Regulation of Endothelial Nitric Oxide Synthase mRNA Stability by Rho GTPase. Journal of Biological Chemistry *273*, 24266-24271.

Lee, J., Pilch, P.F., Shoelson, S.E., and Scarlata, S.F. (1997). Conformational changes of the insulin receptor upon insulin binding and activation as monitored by fluorescence spectroscopy. Biochemistry *36*, 2701-2708.

Leech, C.A., Chepurny, O.G., and Holz, G.G. (2010). Epac2-dependent rap1 activation and the control of islet insulin secretion by glucagon-like peptide-1. Vitamins and hormones *84*, 279-302.

Ley, K., Laudanna, C., Cybulsky, M.I., and Nourshargh, S. (2007). Getting to the site of inflammation: the leukocyte adhesion cascade updated. Nat Rev Immunol *7*, 678-689.

Li, J., Wu, F., Zhang, H., Fu, F., Ji, L., Dong, L., Li, Q., Liu, W., Zhang, Y., Lv, A.*, et al.* (2009). Insulin inhibits leukocyte-endothelium adherence via an Akt-NO-dependent mechanism in myocardial ischemia/reperfusion. J Mol Cell Cardiol *47*, 512-519.

Li, Y.J., Guan, H., Hazarika, S., Liu, C.W., and Annex, B.H. (2007). Impaired angiogenesis following hind-limb ischemia in diabetes mellitus mice. Chinese medical sciences journal = Chung-kuo i hsueh k'o hsueh tsa chih / Chinese Academy of Medical Sciences *22*, 232-237.

Libby, P. (2012). Inflammation in atherosclerosis. Arterioscler Thromb Vasc Biol *32*, 2045-2051.

Libby, P., Lichtman, A.H., and Hansson, G.K. (2013). Immune effector mechanisms implicated in atherosclerosis: from mice to humans. Immunity *38*, 1092-1104.

Liebner, S., Cavallaro, U., and Dejana, E. (2006). The multiple languages of endothelial cell-to-cell communication. Arterioscler Thromb Vasc Biol *26*, 1431-1438.

Lin, D., Edwards, A.S., Fawcett, J.P., Mbamalu, G., Scott, J.D., and Pawson, T. (2000). A mammalian PAR-3-PAR-6 complex implicated in Cdc42/Rac1 and aPKC signalling and cell polarity. Nat Cell Biol *2*, 540-547.

Liu, W.F., Nelson, C.M., Tan, J.L., and Chen, C.S. (2007). Cadherins, RhoA, and Rac1 are differentially required for stretch-mediated proliferation in endothelial versus smooth muscle cells. Circ Res *101*, e44-52.

Liu, Y., Petreaca, M., and Martins-Green, M. (2009). Cell and molecular mechanisms of insulin-induced angiogenesis. J Cell Mol Med *13*, 4492-4504.

Mackintosh, C. (2004). Dynamic interactions between 14-3-3 proteins and phosphoproteins regulate diverse cellular processes. Biochem J *381*, 329-342.

Madigan, J.P., Bodemann, B.O., Brady, D.C., Dewar, B.J., Keller, P.J., Leitges, M., Philips, M.R., Ridley, A.J., Der, C.J., and Cox, A.D. (2009). Regulation of Rnd3 localization and function by protein kinase C alpha-mediated phosphorylation. Biochem J *424*, 153-161.

Mamdouh, Z., Chen, X., Pierini, L.M., Maxfield, F.R., and Muller, W.A. (2003). Targeted recycling of PECAM from endothelial surface-connected compartments during diapedesis. Nature *421*, 748-753.

Manning, B.D., and Cantley, L.C. (2007). AKT/PKB signaling: navigating downstream. Cell *129*, 1261-1274.

Marasciulo, F.L., Montagnani, M., and Potenza, M.A. (2006). Endothelin-1: the yin and yang on vascular function. Current medicinal chemistry *13*, 1655-1665.

Markiewicz, E., Tilgner, K., Barker, N., van de Wetering, M., Clevers, H., Dorobek, M., Hausmanowa-Petrusewicz, I., Ramaekers, F.C., Broers, J.L., Blankesteijn, W.M.*, et al.* (2006). The inner nuclear membrane protein emerin regulates beta-catenin activity by restricting its accumulation in the nucleus. EMBO J *25*, 3275-3285.

Martin-Belmonte, F., Gassama, A., Datta, A., Yu, W., Rescher, U., Gerke, V., and Mostov, K. (2007). PTEN-mediated apical segregation of phosphoinositides controls epithelial morphogenesis through Cdc42. Cell *128*, 383-397.

Mattila, P.K., and Lappalainen, P. (2008). Filopodia: molecular architecture and cellular functions. Nat Rev Mol Cell Biol *9*, 446-454.

McKenzie, J.A., and Ridley, A.J. (2007). Roles of Rho/ROCK and MLCK in TNF-alpha-induced changes in endothelial morphology and permeability. J Cell Physiol *213*, 221-228.

Medina, M.W., Theusch, E., Naidoo, D., Bauzon, F., Stevens, K., Mangravite, L.M., Kuang, Y.L., and Krauss, R.M. (2012). RHOA is a modulator of the cholesterol-lowering effects of statin. PLoS genetics *8*, e1003058.

Meek, S.E., Lane, W.S., and Piwnica-Worms, H. (2004). Comprehensive proteomic analysis of interphase and mitotic 14-3-3-binding proteins. J Biol Chem *279*, 32046-32054.

Menting, J.G., Whittaker, J., Margetts, M.B., Whittaker, L.J., Kong, G.K., Smith, B.J., Watson, C.J., Zakova, L., Kletvikova, E., Jiracek, J.*, et al.* (2013). How insulin engages its primary binding site on the insulin receptor. Nature *493*, 241-245.

Millan, J., Cain, R.J., Reglero-Real, N., Bigarella, C., Marcos-Ramiro, B., Fernandez-Martin, L., Correas, I., and Ridley, A.J. (2010). Adherens junctions connect stress fibres between adjacent endothelial cells. BMC Biol *8*, 11.

Miller, M.L., and Blom, N. (2009). Kinase-specific prediction of protein phosphorylation sites. Methods Mol Biol *527*, 299-310, x.

Mim, C., and Unger, V.M. (2012). Membrane curvature and its generation by BAR proteins. Trends Biochem Sci *37*, 526-533.

Miralles, F., Posern, G., Zaromytidou, A.I., and Treisman, R. (2003). Actin dynamics control SRF activity by regulation of its coactivator MAL. Cell *113*, 329-342.

Monaghan-Benson, E., and Wittchen, E.S. (2011). In Vitro Analyses of Endothelial Cell Permeability. In, pp. 281-290.

Montagnani, M., Chen, H., Barr, V.A., and Quon, M.J. (2001). Insulin-stimulated activation of eNOS is independent of Ca2+ but requires phosphorylation by Akt at Ser(1179). J Biol Chem *276*, 30392-30398.

Moon, S.Y., and Zheng, Y. (2003). Rho GTPase-activating proteins in cell regulation. Trends Cell Biol *13*, 13-22.

Moore, B.W., and Perez, V.J. (1967). Specific acidic proteins of the nervous system (Englewood Cliffs, N.J.: Prentice-Hall).

Moorhead, G., Douglas, P., Cotelle, V., Harthill, J., Morrice, N., Meek, S., Deiting, U., Stitt, M., Scarabel, M., Aitken, A.*, et al.* (1999). Phosphorylation-dependent interactions between enzymes of plant metabolism and 14-3-3 proteins. Plant J *18*, 1-12.

Moorhead, G., Douglas, P., Morrice, N., Scarabel, M., Aitken, A., and MacKintosh, C. (1996). Phosphorylated nitrate reductase from spinach leaves is inhibited by 14-3-3 proteins and activated by fusicoccin. Curr Biol *6*, 1104-1113.

Morrison, D.K. (2009). The 14-3-3 proteins: integrators of diverse signaling cues that impact cell fate and cancer development. Trends Cell Biol *19*, 16-23.

Moxham, C.P., Duronio, V., and Jacobs, S. (1989). Insulin-like growth factor I receptor beta-subunit heterogeneity. Evidence for hybrid tetramers composed of insulin-like growth factor I and insulin receptor heterodimers. Journal of Biological Chemistry *264*, 13238-13244.

Muller, S.L., Portwich, M., Schmidt, A., Utepbergenov, D.I., Huber, O., Blasig, I.E., and Krause, G. (2005). The tight junction protein occludin and the adherens junction protein alpha-catenin share a common interaction mechanism with ZO-1. J Biol Chem *280*, 3747-3756.

Muller, W.A. (2011). Mechanisms of leukocyte transendothelial migration. Annual review of pathology *6*, 323-344.

Muller, W.A., Weigl, S.A., Deng, X., and Phillips, D.M. (1993). PECAM-1 is required for transendothelial migration of leukocytes. The Journal of experimental medicine *178*, 449-460.

Muniyappa, R., Montagnani, M., Koh, K.K., and Quon, M.J. (2007). Cardiovascular actions of insulin. Endocr Rev *28*, 463-491.

Muniyappa, R., and Sowers, J.R. (2013). Role of insulin resistance in endothelial dysfunction. Reviews in endocrine & metabolic disorders *14*, 5-12.

Murohara, T., Horowitz, J.R., Silver, M., Tsurumi, Y., Chen, D., Sullivan, A., and Isner, J.M. (1998). Vascular endothelial growth factor/vascular permeability factor enhances vascular permeability via nitric oxide and prostacyclin. Circulation *97*, 99-107.

Murray, C.J.L., Vos, T., Lozano, R., Naghavi, M., Flaxman, A.D., Michaud, C., Ezzati, M., Shibuya, K., Salomon, J.A., Abdalla, S.*, et al.* (2012). Disability-adjusted life years (DALYs) for 291 diseases and injuries in 21 regions, 1990–2010: a systematic analysis for the Global Burden of Disease Study 2010. The Lancet *380*, 2197-2223.

Muslin, A.J., Tanner, J.W., Allen, P.M., and Shaw, A.S. (1996). Interaction of 14-3-3 with signaling proteins is mediated by the recognition of phosphoserine. Cell *84*, 889-897.

Muslin, A.J., and Xing, H. (2000). 14-3-3 proteins: regulation of subcellular localization by molecular interference. Cell Signal *12*, 703-709.

Myagmar, B.E., Umikawa, M., Asato, T., Taira, K., Oshiro, M., Hino, A., Takei, K., Uezato, H., and Kariya, K. (2005). PARG1, a protein-tyrosine phosphatase-associated RhoGAP, as a putative Rap2 effector. Biochem Biophys Res Commun *329*, 1046-1052.

Nabel, E.G., and Braunwald, E. (2012). A Tale of Coronary Artery Disease and Myocardial Infarction. New England Journal of Medicine *366*, 54-63.

Nagai-Tamai, Y., Mizuno, K., Hirose, T., Suzuki, A., and Ohno, S. (2002). Regulated protein-protein interaction between aPKC and PAR-3 plays an essential role in the polarization of epithelial cells. Genes to cells : devoted to molecular & cellular mechanisms *7*, 1161-1171.

Naumanen, P., Lappalainen, P., and Hotulainen, P. (2008). Mechanisms of actin stress fibre assembly. Journal of Microscopy *231*, 446-454.

Navarro, P., Ruco, L., and Dejana, E. (1998). Differential localization of VE- and N-cadherins in human endothelial cells: VE-cadherin competes with N-cadherin for junctional localization. J Cell Biol *140*, 1475-1484.

Navarro-Lerida, I., Sanchez-Perales, S., Calvo, M., Rentero, C., Zheng, Y., Enrich, C., and Del Pozo, M.A. (2012). A palmitoylation switch mechanism regulates Rac1 function and membrane organization. EMBO J *31*, 534-551.

Nawroth, R., Poell, G., Ranft, A., Kloep, S., Samulowitz, U., Fachinger, G., Golding, M., Shima, D.T., Deutsch, U., and Vestweber, D. (2002). VE-PTP and VE-cadherin ectodomains interact to facilitate regulation of phosphorylation and cell contacts. EMBO J *21*, 4885-4895.

Nieset, J.E., Redfield, A.R., Jin, F., Knudsen, K.A., Johnson, K.R., and Wheelock, M.J. (1997). Characterization of the interactions of alpha-catenin with alpha-actinin and beta-catenin/plakoglobin. J Cell Sci *110 (Pt 8)*, 1013-1022.

Nishimura, T., Yamaguchi, T., Kato, K., Yoshizawa, M., Nabeshima, Y., Ohno, S., Hoshino, M., and Kaibuchi, K. (2005). PAR-6-PAR-3 mediates Cdc42-induced Rac activation through the Rac GEFs STEF/Tiam1. Nat Cell Biol *7*, 270-277.

Nitert, M.D., Chisalita, S.I., Olsson, K., Bornfeldt, K.E., and Arnqvist, H.J. (2005). IGF-I/insulin hybrid receptors in human endothelial cells. Mol Cell Endocrinol *229*, 31-37.

Nobes, C.D., and Hall, A. (1995). Rho, rac, and cdc42 GTPases regulate the assembly of multimolecular focal complexes associated with actin stress fibers, lamellipodia, and filopodia. Cell *81*, 53-62.

Noma, K., Kihara, Y., and Higashi, Y. (2012). Striking crosstalk of ROCK signaling with endothelial function. Journal of cardiology *60*, 1-6.

Noren, N.K., Arthur, W.T., and Burridge, K. (2003). Cadherin Engagement Inhibits RhoA via p190RhoGAP. Journal of Biological Chemistry *278*, 13615-13618.

Nottebaum, A.F., Cagna, G., Winderlich, M., Gamp, A.C., Linnepe, R., Polaschegg, C., Filippova, K., Lyck, R., Engelhardt, B., Kamenyeva, O.*, et al.* (2008). VE-PTP maintains the endothelial barrier via plakoglobin and becomes dissociated from VE-cadherin by leukocytes and by VEGF. The Journal of experimental medicine *205*, 2929-2945.

Nystrom, F.H., and Quon, M.J. (1999). Insulin signalling: metabolic pathways and mechanisms for specificity. Cell Signal *11*, 563-574.

Obenauer, J.C., Cantley, L.C., and Yaffe, M.B. (2003). Scansite 2.0: Proteome-wide prediction of cell signaling interactions using short sequence motifs. Nucleic Acids Res *31*, 3635-3641.

Obsil, T., and Obsilova, V. (2011). Structural basis of 14-3-3 protein functions. Semin Cell Dev Biol *22*, 663-672.

Ohashi, K., Nagata, K., Maekawa, M., Ishizaki, T., Narumiya, S., and Mizuno, K. (2000). Rho-associated kinase ROCK activates LIM-kinase 1 by phosphorylation at threonine 508 within the activation loop. J Biol Chem *275*, 3577-3582.

Olsen, J.V., de Godoy, L.M., Li, G., Macek, B., Mortensen, P., Pesch, R., Makarov, A., Lange, O., Horning, S., and Mann, M. (2005). Parts per million mass accuracy on an Orbitrap mass spectrometer via lock mass injection into a C-trap. Mol Cell Proteomics *4*, 2010-2021.

Olsson, A.K., Dimberg, A., Kreuger, J., and Claesson-Welsh, L. (2006). VEGF receptor signalling - in control of vascular function. Nat Rev Mol Cell Biol *7*, 359-371.

Ooshio, T., Irie, K., Morimoto, K., Fukuhara, A., Imai, T., and Takai, Y. (2004). Involvement of LMO7 in the association of two cell-cell adhesion molecules, nectin and E-cadherin, through afadin and alpha-actinin in epithelial cells. J Biol Chem *279*, 31365-31373.

Orsenigo, F., Giampietro, C., Ferrari, A., Corada, M., Galaup, A., Sigismund, S., Ristagno, G., Maddaluno, L., Koh, G.Y., Franco, D.*, et al.* (2012). Phosphorylation of VE-cadherin is modulated by haemodynamic forces and contributes to the regulation of vascular permeability in vivo. Nature communications *3*, 1208.

Ostermann, G., Fraemohs, L., Baltus, T., Schober, A., Lietz, M., Zernecke, A., Liehn, E.A., and Weber, C. (2005). Involvement of JAM-A in mononuclear cell recruitment on inflamed or atherosclerotic endothelium: inhibition by soluble JAM-A. Arterioscler Thromb Vasc Biol *25*, 729-735.

Ott, E.B., van den Akker, N.M., Sakalis, P.A., Gittenberger-de Groot, A.C., Te Velthuis, A.J., and Bagowski, C.P. (2008). The lim domain only protein 7 is important in zebrafish heart development. Developmental dynamics : an official publication of the American Association of Anatomists *237*, 3940-3952.

Ozaki, M., Kawashima, S., Hirase, T., Yamashita, T., Namiki, M., Inoue, N., Hirata Ki, K., and Yokoyama, M. (2002). Overexpression of endothelial nitric oxide synthase in endothelial cells is protective against ischemia-reperfusion injury in mouse skeletal muscle. Am J Pathol *160*, 1335-1344.

Pannekoek, W.J., van Dijk, J.J., Chan, O.Y., Huveneers, S., Linnemann, J.R., Spanjaard, E., Brouwer, P.M., van der Meer, A.J., Zwartkruis, F.J., Rehmann, H.*, et al.* (2011). Epac1 and PDZ-GEF cooperate in Rap1 mediated endothelial junction control. Cell Signal *23*, 2056-2064.

Pasula, S., Cai, X., Dong, Y., Messa, M., McManus, J., Chang, B., Liu, X., Zhu, H., Mansat, R.S., Yoon, S.J.*, et al.* (2012). Endothelial epsin deficiency decreases tumor growth by enhancing VEGF signaling. J Clin Invest *122*, 4424-4438.

Pellegrin, S., and Mellor, H. (2007). Actin stress fibres. J Cell Sci *120*, 3491-3499.

Perrot, V., and Rechler, M.M. (2003). Characterization of insulin inhibition of transactivation by a C-terminal fragment of the forkhead transcription factor Foxo1 in rat hepatoma cells. J Biol Chem *278*, 26111-26119.

Pessin, J.E., and Saltiel, A.R. (2000). Signaling pathways in insulin action: molecular targets of insulin resistance. J Clin Invest *106*, 165-169.

Peterson, L.J., Rajfur, Z., Maddox, A.S., Freel, C.D., Chen, Y., Edlund, M., Otey, C., and Burridge, K. (2004). Simultaneous stretching and contraction of stress fibers in vivo. Mol Biol Cell *15*, 3497-3508.

Petrelli, A., Gilestro, G.F., Lanzardo, S., Comoglio, P.M., Migone, N., and Giordano, S. (2002). The endophilin-CIN85-Cbl complex mediates ligand-dependent downregulation of c-Met. Nature *416*, 187-190.

Pierre, E.J., Barrow, R.E., Hawkins, H.K., Nguyen, T.T., Sakurai, Y., Desai, M., Wolfe, R.R., and Herndon, D.N. (1998). Effects of insulin on wound healing. The Journal of Trauma and Acute Care Surgery *44*, 342-345.

Pober, J.S., and Sessa, W.C. (2007). Evolving functions of endothelial cells in inflammation. Nat Rev Immunol *7*, 803-815.

Pokutta, S., Drees, F., Takai, Y., Nelson, W.J., and Weis, W.I. (2002). Biochemical and structural definition of the l-afadin- and actin-binding sites of alpha-catenin. J Biol Chem *277*, 18868-18874.

Pokutta, S., and Weis, W.I. (2007). Structure and mechanism of cadherins and catenins in cell-cell contacts. Annu Rev Cell Dev Biol *23*, 237-261.

Pollard, T.D., and Borisy, G.G. (2003). Cellular motility driven by assembly and disassembly of actin filaments. Cell *112*, 453-465.

Pollard, T.D., and Cooper, J.A. (2009). Actin, a central player in cell shape and movement. Science *326*, 1208-1212.

Polo, S., Sigismund, S., Faretta, M., Guidi, M., Capua, M.R., Bossi, G., Chen, H., De Camilli, P., and Di Fiore, P.P. (2002). A single motif responsible for ubiquitin recognition and monoubiquitination in endocytic proteins. Nature *416*, 451-455.

Post, A., Pannekoek, W.J., Ross, S.H., Verlaan, I., Brouwer, P.M., and Bos, J.L. (2013). Rasip1 mediates Rap1 regulation of Rho in endothelial barrier function through ArhGAP29. Proc Natl Acad Sci U S A *110*, 11427-11432.

Pouyssegur, J., and Lenormand, P. (2003). Fidelity and spatio-temporal control in MAP kinase (ERKs) signalling. European journal of biochemistry / FEBS *270*, 3291-3299.

Pozuelo Rubio, M., Geraghty, K.M., Wong, B.H., Wood, N.T., Campbell, D.G., Morrice, N., and Mackintosh, C. (2004). 14-3-3-affinity purification of over 200 human phosphoproteins reveals new links to regulation of cellular metabolism, proliferation and trafficking. Biochem J *379*, 395-408.

Pradhan, D., Lombardo, C.R., Roe, S., Rimm, D.L., and Morrow, J.S. (2001). alpha - Catenin binds directly to spectrin and facilitates spectrin-membrane assembly in vivo. J Biol Chem *276*, 4175-4181.

Prasain, N., and Stevens, T. (2009). The actin cytoskeleton in endothelial cell phenotypes. Microvascular research *77*, 53-63.

Privratsky, J.R., Newman, D.K., and Newman, P.J. (2010). PECAM-1: conflicts of interest in inflammation. Life sciences *87*, 69-82.

Putilina, T., Jaworski, C., Gentleman, S., McDonald, B., Kadiri, M., and Wong, P. (1998). Analysis of a human cDNA containing a tissue-specific alternatively spliced LIM domain. Biochem Biophys Res Commun *252*, 433-439.

Qualmann, B., Koch, D., and Kessels, M.M. (2011). Let's go bananas: revisiting the endocytic BAR code. EMBO J *30*, 3501-3515.

Rask-Madsen, C., Li, Q., Freund, B., Feather, D., Abramov, R., Wu, I.H., Chen, K., Yamamoto-Hiraoka, J., Goldenbogen, J., Sotiropoulos, K.B.*, et al.* (2010). Loss of insulin signaling in vascular endothelial cells accelerates atherosclerosis in apolipoprotein E null mice. Cell Metab *11*, 379-389.

Rath, S., Kalogeris, T., Mai, N., Zibari, G., Alexander, J.S., Lefer, D., and Turnage, R.H. (2006). Insulin prevents oxidant-induced endothelial cell barrier dysfunction via nitric oxide-dependent pathway. Surgery *139*, 82-91.

Reider, A., and Wendland, B. (2011). Endocytic adaptors--social networking at the plasma membrane. J Cell Sci *124*, 1613-1622.

Reymond, N., Borg, J.-P., Lecocq, E., Adelaide, J., Campadelli-Fiume, G., Dubreuil, P., and Lopez, M. (2000). Human nectin3/PRR3: a novel member of the PVR/PRR/nectin family that interacts with afadin. Gene *255*, 347-355.

Richnau, N., and Aspenstrom, P. (2001). Rich, a rho GTPase-activating protein domain-containing protein involved in signaling by Cdc42 and Rac1. J Biol Chem *276*, 35060-35070.

Richnau, N., Fransson, Å., Farsad, K., and Aspenström, P. (2004). RICH-1 has a BIN/Amphiphysin/Rvsp domain responsible for binding to membrane lipids and tubulation of liposomes. Biochemical and Biophysical Research Communications *320*, 1034-1042.

Ridley, A.J. (2006). Rho GTPases and actin dynamics in membrane protrusions and vesicle trafficking. Trends Cell Biol *16*, 522-529.

Ridley, A.J. (2011). Life at the leading edge. Cell *145*, 1012-1022.

Ridley, A.J., and Hall, A. (1992). The small GTP-binding protein rho regulates the assembly of focal adhesions and actin stress fibers in response to growth factors. Cell *70*, 389-399.

Ridley, A.J., Paterson, H.F., Johnston, C.L., Diekmann, D., and Hall, A. (1992). The small GTP-binding protein rac regulates growth factor-induced membrane ruffling. Cell *70*, 401-410.

Ridley, A.J., Schwartz, M.A., Burridge, K., Firtel, R.A., Ginsberg, M.H., Borisy, G., Parsons, J.T., and Horwitz, A.R. (2003). Cell migration: integrating signals from front to back. Science *302*, 1704-1709.

Riento, K., Totty, N., Villalonga, P., Garg, R., Guasch, R., and Ridley, A.J. (2005a). RhoE function is regulated by ROCK I-mediated phosphorylation. EMBO J *24*, 1170-1180.

Riento, K., Villalonga, P., Garg, R., and Ridley, A. (2005b). Function and regulation of RhoE. Biochemical Society transactions *33*, 649-651.

Rikitake, Y., Mandai, K., and Takai, Y. (2012). The role of nectins in different types of cell-cell adhesion. J Cell Sci *125*, 3713-3722.

Riou, P., Kjaer, S., Garg, R., Purkiss, A., George, R., Cain, R.J., Bineva, G., Reymond, N., McColl, B., Thompson, A.J*., et al.* (2013). 14-3-3 proteins interact with a hybrid prenyl-phosphorylation motif to inhibit G proteins. Cell *153*, 640-653.

Risau, W. (1997). Mechanisms of angiogenesis. Nature *386*, 671-674.

Roberts, P.J., Mitin, N., Keller, P.J., Chenette, E.J., Madigan, J.P., Currin, R.O., Cox, A.D., Wilson, O., Kirschmeier, P., and Der, C.J. (2008). Rho Family GTPase modification and dependence on CAAX motif-signaled posttranslational modification. J Biol Chem *283*, 25150-25163.

Roh, M.H., Liu, C.J., Laurinec, S., and Margolis, B. (2002). The carboxyl terminus of zona occludens-3 binds and recruits a mammalian homologue of discs lost to tight junctions. J Biol Chem *277*, 27501-27509.

Rosenthal, J.A., Chen, H., Slepnev, V.I., Pellegrini, L., Salcini, A.E., Di Fiore, P.P., and De Camilli, P. (1999). The epsins define a family of proteins that interact with components of the clathrin coat and contain a new protein module. J Biol Chem *274*, 33959-33965.

Rosenthal, S.P. (1968). Acceleration of primary wound healing by insulin. Archives of Surgery *96*, 53.

Rossman, K.L., Der, C.J., and Sondek, J. (2005). GEF means go: turning on RHO GTPases with guanine nucleotide-exchange factors. Nat Rev Mol Cell Biol *6*, 167-180.

Rothbauer, U., Zolghadr, K., Muyldermans, S., Schepers, A., Cardoso, M.C., and Leonhardt, H. (2008). A versatile nanotrap for biochemical and functional studies with fluorescent fusion proteins. Mol Cell Proteomics *7*, 282-289.

Rotty, J.D., Wu, C., and Bear, J.E. (2013). New insights into the regulation and cellular functions of the ARP2/3 complex. Nat Rev Mol Cell Biol *14*, 7-12.

Rowland, A.F., Larance, M., Hughes, W.E., and James, D.E. (2011). Identification of RhoGAP22 as an Akt-dependent regulator of cell motility in response to insulin. Mol Cell Biol *31*, 4789-4800.

Sadot, E., Simcha, I., Shtutman, M., Ben-Ze'ev, A., and Geiger, B. (1998). Inhibition of beta-catenin-mediated transactivation by cadherin derivatives. Proc Natl Acad Sci U S A *95*, 15339-15344.

Saltiel, A.R., and Kahn, C.R. (2001). Insulin signalling and the regulation of glucose and lipid metabolism. Nature *414*, 799-806.

Sandu, O.A., Ito, M., and Begum, N. (2001). Selected contribution: insulin utilizes NO/cGMP pathway to activate myosin phosphatase via Rho inhibition in vascular smooth muscle. Journal of applied physiology (Bethesda, Md : 1985) *91*, 1475-1482.

Sanger, F., and Tuppy, H. (1951). The amino-acid sequence in the phenylalanyl chain of insulin. I. The identification of lower peptides from partial hydrolysates. Biochem J *49*, 463-481.

Saras, J., Franzen, P., Aspenstrom, P., Hellman, U., Gonez, L.J., and Heldin, C.H. (1997). A novel GTPase-activating protein for Rho interacts with a PDZ domain of the protein-tyrosine phosphatase PTPL1. J Biol Chem *272*, 24333-24338.

Sarbassov, D.D., Guertin, D.A., Ali, S.M., and Sabatini, D.M. (2005). Phosphorylation and regulation of Akt/PKB by the rictor-mTOR complex. Science *307*, 1098-1101.

Sauzeau, V., Le Jeune, H., Cario-Toumaniantz, C., Smolenski, A., Lohmann, S.M., Bertoglio, J., Chardin, P., Pacaud, P., and Loirand, G. (2000). Cyclic GMP-dependent protein kinase signaling pathway inhibits RhoA-induced Ca2+ sensitization of contraction in vascular smooth muscle. J Biol Chem *275*, 21722-21729.

Sawada, N., Li, Y., and Liao, J.K. (2010). Novel aspects of the roles of Rac1 GTPase in the cardiovascular system. Current opinion in pharmacology *10*, 116-121.

Schmelzle, K., Kane, S., Gridley, S., Lienhard, G.E., and White, F.M. (2006). Temporal dynamics of tyrosine phosphorylation in insulin signaling. Diabetes *55*, 2171-2179.

Schreml, S., Szeimies, R.M., Prantl, L., Landthaler, M., and Babilas, P. (2010). Wound healing in the 21st century. J Am Acad Dermatol *63*, 866-881.

Schulte, D., Kuppers, V., Dartsch, N., Broermann, A., Li, H., Zarbock, A., Kamenyeva, O., Kiefer, F., Khandoga, A., Massberg, S.*, et al.* (2011). Stabilizing the VE-cadherin-catenin complex blocks leukocyte extravasation and vascular permeability. EMBO J *30*, 4157-4170.

Schweitzer, K.M., Vicart, P., Delouis, C., Paulin, D., Drager, A.M., Langenhuijsen, M.M., and Weksler, B.B. (1997). Characterization of a newly established human bone marrow endothelial cell line: distinct adhesive properties for hematopoietic progenitors compared with human umbilical vein endothelial cells. Laboratory investigation; a journal of technical methods and pathology *76*, 25-36.

Sen, A., Madhivanan, K., Mukherjee, D., and Aguilar, R.C. (2012). The epsin protein family: coordinators of endocytosis and signaling. Biomol Concepts *3*, 117-126.

Senger, D.R., and Davis, G.E. (2011). Angiogenesis. Cold Spring Harb Perspect Biol *3*, a005090.

Seshasai, S.R., Kaptoge, S., Thompson, A., Di Angelantonio, E., Gao, P., Sarwar, N., Whincup, P.H., Mukamal, K.J., Gillum, R.F., Holme, I.*, et al.* (2011). Diabetes mellitus, fasting glucose, and risk of cause-specific death. N Engl J Med *364*, 829-841.

Sessa, W.C. (2005). Regulation of endothelial derived nitric oxide in health and disease. Memorias do Instituto Oswaldo Cruz *100 Suppl 1*, 15-18.

Shabanpoor, F., Separovic, F., and Wade, J.D. (2009). The human insulin superfamily of polypeptide hormones. Vitamins and hormones *80*, 1-31.

Shamir, R., Shehadeh, N., Rosenblat, M., Eshach-Adiv, O., Coleman, R., Kaplan, M., Hamoud, S., Lischinsky, S., and Hayek, T. (2003). Oral Insulin Supplementation Attenuates Atherosclerosis Progression in Apolipoprotein E-Deficient Mice. Arteriosclerosis, Thrombosis, and Vascular Biology *23*, 104-110.

Shaul, P.W. (2002). Regulation of endothelial nitric oxide synthase: location, location, location. Annual review of physiology *64*, 749-774.

Shi, J., and Wei, L. (2013). Rho Kinases in Cardiovascular Physiology and Pathophysiology: The Effect of Fasudil. Journal of cardiovascular pharmacology *62*, 341-354.

Shin, K., Straight, S., and Margolis, B. (2005). PATJ regulates tight junction formation and polarity in mammalian epithelial cells. J Cell Biol *168*, 705-711.

Shutes, A., Berzat, A.C., Cox, A.D., and Der, C.J. (2004). Atypical mechanism of regulation of the Wrch-1 Rho family small GTPase. Curr Biol *14*, 2052-2056.

Siflinger-Birnboim, A., Del Vecchio, P.J., Cooper, J.A., Blumenstock, F.A., Shepard, J.M., and Malik, A.B. (1987). Molecular sieving characteristics of the cultured endothelial monolayer. J Cell Physiol *132*, 111-117.

Simionescu, M. (2000). Structural, biochemical and functional differentiation of the vascular endothelium. Morphogenesis of Endothelium, 1-21.

Simionescu, M., Gafencu, A., and Antohe, F. (2002). Transcytosis of plasma macromolecules in endothelial cells: a cell biological survey. Microscopy research and technique *57*, 269-288.

Singer, A.J., and Clark, R.A. (1999). Cutaneous wound healing. N Engl J Med *341*, 738-746.

Skolnik, E.Y., Batzer, A., Li, N., Lee, C.H., Lowenstein, E., Mohammadi, M., Margolis, B., and Schlessinger, J. (1993). The function of GRB2 in linking the insulin receptor to Ras signaling pathways. Science *260*, 1953-1955.

Small, J.V., Rottner, K., Kaverina, I., and Anderson, K.I. (1998). Assembling an actin cytoskeleton for cell attachment and movement. Biochimica et biophysica acta *1404*, 271-281.

Soubeyran, P., Kowanetz, K., Szymkiewicz, I., Langdon, W.Y., and Dikic, I. (2002). Cbl-CIN85-endophilin complex mediates ligand-induced downregulation of EGF receptors. Nature *416*, 183-187.

Stadler, C., Rexhepaj, E., Singan, V.R., Murphy, R.F., Pepperkok, R., Uhlen, M., Simpson, J.C., and Lundberg, E. (2013). Immunofluorescence and fluorescent-protein tagging show high correlation for protein localization in mammalian cells. Nat Methods *10*, 315-323.

Steiner, D.F., and Oyer, P.E. (1967). The biosynthesis of insulin and a probable precursor of insulin by a human islet cell adenoma. Proc Natl Acad Sci U S A *57*, 473-480.

Stockton, R.A., Schaefer, E., and Schwartz, M.A. (2004). p21-activated kinase regulates endothelial permeability through modulation of contractility. J Biol Chem *279*, 46621-46630.

Stossel, T.P., Chaponnier, C., Ezzell, R.M., Hartwig, J.H., Janmey, P.A., Kwiatkowski, D.J., Lind, S.E., Smith, D.B., Southwick, F.S., Yin, H.L.*, et al.* (1985). Nonmuscle actin-binding proteins. Annual review of cell biology *1*, 353-402.

Stossel, T.P., Condeelis, J., Cooley, L., Hartwig, J.H., Noegel, A., Schleicher, M., and Shapiro, S.S. (2001). Filamins as integrators of cell mechanics and signalling. Nat Rev Mol Cell Biol *2*, 138-145.

Straight, S.W., Shin, K., Fogg, V.C., Fan, S., Liu, C.J., Roh, M., and Margolis, B. (2004). Loss of PALS1 expression leads to tight junction and polarity defects. Mol Biol Cell *15*, 1981-1990.

Sumpio, B.E., Riley, J.T., and Dardik, A. (2002). Cells in focus: endothelial cell. Int J Biochem Cell Biol *34*, 1508-1512.

Suranadi, I.W., Demaison, L., Chate, V., Peltier, S., Richardson, M., and Leverve, X. (2012). An increase in the redox state during reperfusion contributes to the cardioprotective effect of GIK solution. Journal of applied physiology (Bethesda, Md : 1985) *113*, 775-784.

Suraneni, P., Rubinstein, B., Unruh, J.R., Durnin, M., Hanein, D., and Li, R. (2012). The Arp2/3 complex is required for lamellipodia extension and directional fibroblast cell migration. J Cell Biol *197*, 239-251.

Surma, M., Wei, L., and Shi, J. (2011). Rho kinase as a therapeutic target in cardiovascular disease. Future cardiology *7*, 657-671.

Taddei, A., Giampietro, C., Conti, A., Orsenigo, F., Breviario, F., Pirazzoli, V., Potente, M., Daly, C., Dimmeler, S., and Dejana, E. (2008). Endothelial adherens junctions control tight junctions by VE-cadherin-mediated upregulation of claudin-5. Nat Cell Biol *10*, 923-934.

Takahashi, K., Nakanishi, H., Miyahara, M., Mandai, K., Satoh, K., Satoh, A., Nishioka, H., Aoki, J., Nomoto, A., Mizoguchi, A.*, et al.* (1999). Nectin/PRR: An Immunoglobulin-like Cell Adhesion Molecule Recruited to Cadherin-based Adherens Junctions through Interaction with Afadin, a PDZ Domain–containing Protein. The Journal of Cell Biology *145*, 539-549.

Takai, Y., Irie, K., Shimizu, K., Sakisaka, T., and Ikeda, W. (2003). Nectins and nectin-like molecules: roles in cell adhesion, migration, and polarization. Cancer Sci *94*, 655-667.

Takei, K., Slepnev, V.I., Haucke, V., and De Camilli, P. (1999). Functional partnership between amphiphysin and dynamin in clathrin-mediated endocytosis. Nat Cell Biol *1*, 33-39.

Takemaru, K., Fischer, V., and Li, F.Q. (2009). Fine-tuning of nuclear-catenin by Chibby and 14-3-3. Cell cycle (Georgetown, Tex) *8*, 210-213.

Takemoto, M., and Liao, J.K. (2001). Pleiotropic effects of 3-hydroxy-3-methylglutaryl coenzyme a reductase inhibitors. Arterioscler Thromb Vasc Biol *21*, 1712-1719.

Tan, W., Palmby, T.R., Gavard, J., Amornphimoltham, P., Zheng, Y., and Gutkind, J.S. (2008). An essential role for Rac1 in endothelial cell function and vascular development. FASEB journal : official publication of the Federation of American Societies for Experimental Biology *22*, 1829-1838.

Tanaka, S., Fukumoto, Y., Nochioka, K., Minami, T., Kudo, S., Shiba, N., Takai, Y., Williams, C.L., Liao, J.K., and Shimokawa, H. (2013). Statins exert the pleiotropic effects through small GTP-binding protein dissociation stimulator upregulation with a resultant Rac1 degradation. Arterioscler Thromb Vasc Biol *33*, 1591-1600.

Taniguchi, C.M., Emanuelli, B., and Kahn, C.R. (2006). Critical nodes in signalling pathways: insights into insulin action. Nat Rev Mol Cell Biol *7*, 85-96.

Taqueti, V.R., Mitchell, R.N., and Lichtman, A.H. (2006). Protecting the pump: controlling myocardial inflammatory responses. Annu Rev Physiol *68*, 67-95.

Taylor, F., Huffman, M.D., Macedo, A.F., Moore, T.H., Burke, M., Davey Smith, G., Ward, K., and Ebrahim, S. (2013). Statins for the primary prevention of cardiovascular disease. The Cochrane database of systematic reviews *1*, CD004816.

Tcherkezian, J., and Lamarche-Vane, N. (2007). Current knowledge of the large RhoGAP family of proteins. Biol Cell *99*, 67-86.

Thery, M., Pepin, A., Dressaire, E., Chen, Y., and Bornens, M. (2006). Cell distribution of stress fibres in response to the geometry of the adhesive environment. Cell motility and the cytoskeleton *63*, 341-355.

Thomas, J.L., Baker, K., Han, J., Calvo, C., Nurmi, H., Eichmann, A.C., and Alitalo, K. (2013). Interactions between VEGFR and Notch signaling pathways in endothelial and neural cells. Cellular and molecular life sciences : CMLS *70*, 1779-1792.

Thomas, P., and Smart, T.G. (2005). HEK293 cell line: a vehicle for the expression of recombinant proteins. Journal of pharmacological and toxicological methods *51*, 187-200.

Tian, Q., Feetham, M.C., Tao, W.A., He, X.C., Li, L., Aebersold, R., and Hood, L. (2004). Proteomic analysis identifies that 14-3-3zeta interacts with beta-catenin and facilitates its activation by Akt. Proc Natl Acad Sci U S A *101*, 15370-15375.

Tinti, M., Johnson, C., Toth, R., Ferrier, D.E., and Mackintosh, C. (2012). Evolution of signal multiplexing by 14-3-3-binding 2R-ohnologue protein families in the vertebrates. Open Biol *2*, 120103.

Tojkander, S., Gateva, G., and Lappalainen, P. (2012). Actin stress fibers–assembly, dynamics and biological roles. Journal of Cell Science *125*, 1855-1864.

Tojkander, S., Gateva, G., Schevzov, G., Hotulainen, P., Naumanen, P., Martin, C., Gunning, P.W., and Lappalainen, P. (2011). A Molecular Pathway for Myosin II Recruitment to Stress Fibers. Current biology : CB *21*, 539-550.

Toyofuku, T., Yabuki, M., Otsu, K., Kuzuya, T., Hori, M., and Tada, M. (1998). Direct association of the gap junction protein connexin-43 with ZO-1 in cardiac myocytes. J Biol Chem *273*, 12725-12731.

Troyanovsky, B., Levchenko, T., Mansson, G., Matvijenko, O., and Holmgren, L. (2001). Angiomotin: an angiostatin binding protein that regulates endothelial cell migration and tube formation. J Cell Biol *152*, 1247-1254.

Tsai, W.-C., Bhattacharyya, N., Han, L.-Y., Hanover, J.A., and Rechler, M.M. (2003). Insulin Inhibition of Transcription Stimulated by the Forkhead Protein Foxo1 Is Not Solely due to Nuclear Exclusion. Endocrinology *144*, 5615-5622.

Tsukita, S., Furuse, M., and Itoh, M. (2001). Multifunctional strands in tight junctions. Nat Rev Mol Cell Biol *2*, 285-293.

Tu, S., Wu, W.J., Wang, J., and Cerione, R.A. (2003). Epidermal growth factor-dependent regulation of Cdc42 is mediated by the Src tyrosine kinase. J Biol Chem *278*, 49293-49300.

Tuma, P., and Hubbard, A.L. (2003). Transcytosis: crossing cellular barriers. Physiol Rev *83*, 871-932.

Turowski, P., Martinelli, R., Crawford, R., Wateridge, D., Papageorgiou, A.P., Lampugnani, M.G., Gamp, A.C., Vestweber, D., Adamson, P., Dejana, E.*, et al.* (2008). Phosphorylation of vascular endothelial cadherin controls lymphocyte emigration. J Cell Sci *121*, 29-37.

Tzivion, G., Dobson, M., and Ramakrishnan, G. (2011). FoxO transcription factors; Regulation by AKT and 14-3-3 proteins. Biochimica et biophysica acta *1813*, 1938-1945.

Ullrich, A., Gray, A., Tam, A.W., Yang-Feng, T., Tsubokawa, M., Collins, C., Henzel, W., Le Bon, T., Kathuria, S., Chen, E.*, et al.* (1986). Insulin-like growth factor I receptor primary structure: comparison with insulin receptor suggests structural determinants that define functional specificity. EMBO J *5*, 2503-2512.

van Wetering, S., van Buul, J.D., Quik, S., Mul, F.P., Anthony, E.C., ten Klooster, J.P., Collard, J.G., and Hordijk, P.L. (2002). Reactive oxygen species mediate Rac-induced loss of cell-cell adhesion in primary human endothelial cells. J Cell Sci *115*, 1837-1846.

Vandenbroucke, E., Mehta, D., Minshall, R., and Malik, A.B. (2008). Regulation of endothelial junctional permeability. Ann N Y Acad Sci *1123*, 134-145.

Vestweber, D. (2008). VE-cadherin: the major endothelial adhesion molecule controlling cellular junctions and blood vessel formation. Arterioscler Thromb Vasc Biol *28*, 223-232.

Vestweber, D. (2012a). Novel insights into leukocyte extravasation. Current opinion in hematology *19*, 212-217.

Vestweber, D. (2012b). Relevance of endothelial junctions in leukocyte extravasation and vascular permeability. Ann N Y Acad Sci *1257*, 184-192.

Vicente-Manzanares, M., Ma, X., Adelstein, R.S., and Horwitz, A.R. (2009). Non-muscle myosin II takes centre stage in cell adhesion and migration. Nat Rev Mol Cell Biol *10*, 778-790.

Wallez, Y., and Huber, P. (2008). Endothelial adherens and tight junctions in vascular homeostasis, inflammation and angiogenesis. Biochimica et biophysica acta *1778*, 794-809.

Wang, H., Liu, Z., Li, G., and Barrett, E.J. (2006). The vascular endothelial cell mediates insulin transport into skeletal muscle. Am J Physiol Endocrinol Metab *291*, E323-332.

Wang, H., Wang, A.X., and Barrett, E.J. (2012). Insulin-induced endothelial cell cortical actin filament remodeling: a requirement for trans-endothelial insulin transport. Mol Endocrinol *26*, 1327-1338.

Wang, W., and Shakes, D.C. (1996). Molecular evolution of the 14-3-3 protein family. J Mol Evol *43*, 384-398.

Waschke, J., Baumgartner, W., Adamson, R.H., Zeng, M., Aktories, K., Barth, H., Wilde, C., Curry, F.E., and Drenckhahn, D. (2004). Requirement of Rac activity for maintenance of capillary endothelial barrier properties. American journal of physiology Heart and circulatory physiology *286*, H394-401.

Watanabe, N., Madaule, P., Reid, T., Ishizaki, T., Watanabe, G., Kakizuka, A., Saito, Y., Nakao, K., Jockusch, B.M., and Narumiya, S. (1997). p140mDia, a mammalian homolog of Drosophila diaphanous, is a target protein for Rho small GTPase and is a ligand for profilin. EMBO J *16*, 3044-3056.

Weber, C., Fraemohs, L., and Dejana, E. (2007). The role of junctional adhesion molecules in vascular inflammation. Nat Rev Immunol *7*, 467-477.

Wei, J., Mialki, R.K., Dong, S., Khoo, A., Mallampalli, R.K., Zhao, Y., and Zhao, J. (2013). A new mechanism of RhoA ubiquitination and degradation: Roles of SCFFBXL19 E3 ligase and Erk2. Biochimica et Biophysica Acta (BBA) - Molecular Cell Research *1833*, 2757-2764.

Weiss, E.E., Kroemker, M., Rudiger, A.H., Jockusch, B.M., and Rudiger, M. (1998). Vinculin is part of the cadherin-catenin junctional complex: complex formation between alpha-catenin and vinculin. J Cell Biol *141*, 755-764.

Weiss, W., Weiland, F., and Görg, A. (2009). Protein detection and quantitation technologies for gel-based proteome analysis. In Proteomics (Springer), pp. 59-82.

Wells, C.D., Fawcett, J.P., Traweger, A., Yamanaka, Y., Goudreault, M., Elder, K., Kulkarni, S., Gish, G., Virag, C., Lim, C.*, et al.* (2006). A Rich1/Amot complex regulates the Cdc42 GTPase and apical-polarity proteins in epithelial cells. Cell *125*, 535-548.

Wendland, B. (2002). Epsins: adaptors in endocytosis? Nat Rev Mol Cell Biol *3*, 971-977.

Wendland, B., Steece, K.E., and Emr, S.D. (1999). Yeast epsins contain an essential N-terminal ENTH domain, bind clathrin and are required for endocytosis. EMBO J *18*, 4383-4393.

Werner, H., Weinstein, D., and Bentov, I. (2008). Similarities and differences between insulin and IGF-I: structures, receptors, and signalling pathways. Archives of physiology and biochemistry *114*, 17-22.

Wheelock, M.J., and Johnson, K.R. (2003). Cadherin-mediated cellular signaling. Curr Opin Cell Biol *15*, 509-514.

Wildenberg, G.A., Dohn, M.R., Carnahan, R.H., Davis, M.A., Lobdell, N.A., Settleman, J., and Reynolds, A.B. (2006). p120-catenin and p190RhoGAP regulate cell-cell adhesion by coordinating antagonism between Rac and Rho. Cell *127*, 1027-1039.

Wojciak-Stothard, B., Potempa, S., Eichholtz, T., and Ridley, A.J. (2001). Rho and Rac but not Cdc42 regulate endothelial cell permeability. J Cell Sci *114*, 1343-1355.

Wojciak-Stothard, B., and Ridley, A.J. (2002). Rho GTPases and the regulation of endothelial permeability. Vascular pharmacology *39*, 187-199.

Wojciak-Stothard, B., and Ridley, A.J. (2003). Shear stress-induced endothelial cell polarization is mediated by Rho and Rac but not Cdc42 or PI 3-kinases. J Cell Biol *161*, 429-439.

Wolburg, H., and Lippoldt, A. (2002). Tight junctions of the blood–brain barrier: development, composition and regulation. Vascular pharmacology *38*, 323-337.

Woth, K., Prein, C., Steinhorst, K., Diehl, S., Boehncke, W.H., and Buerger, C. (2013). Endothelial cells are highly heterogeneous at the level of cytokine-induced insulin resistance. Experimental dermatology *22*, 714-718.

Xiao, B., Smerdon, S.J., Jones, D.H., Dodson, G.G., Soneji, Y., Aitken, A., and Gamblin, S.J. (1995). Structure of a 14-3-3 protein and implications for coordination of multiple signalling pathways. Nature *376*, 188-191.

Xiao, K., Garner, J., Buckley, K.M., Vincent, P.A., Chiasson, C.M., Dejana, E., Faundez, V., and Kowalczyk, A.P. (2005). p120-Catenin regulates clathrin-dependent endocytosis of VE-cadherin. Mol Biol Cell *16*, 5141-5151.

Xu, K., Sacharidou, A., Fu, S., Chong, D.C., Skaug, B., Chen, Z.J., Davis, G.E., and Cleaver, O. (2011). Blood vessel tubulogenesis requires Rasip1 regulation of GTPase signaling. Dev Cell *20*, 526-539.

Yaffe, M.B. (2002). How do 14-3-3 proteins work?-- Gatekeeper phosphorylation and the molecular anvil hypothesis. FEBS Lett *513*, 53-57.

Yaffe, M.B., Rittinger, K., Volinia, S., Caron, P.R., Aitken, A., Leffers, H., Gamblin, S.J., Smerdon, S.J., and Cantley, L.C. (1997). The structural basis for 14-3-3:phosphopeptide binding specificity. Cell *91*, 961-971.

Yalow, R.S., and Berson, S.A. (1961). Immunoassay of plasma insulin in man. Diabetes *10*, 339-344.

Yamada, A., Irie, K., Fukuhara, A., Ooshio, T., and Takai, Y. (2004). Requirement of the actin cytoskeleton for the association of nectins with other cell adhesion molecules at adherens and tight junctions in MDCK cells. Genes to cells : devoted to molecular & cellular mechanisms *9*, 843-855.

Yamada, S., Pokutta, S., Drees, F., Weis, W.I., and Nelson, W.J. (2005). Deconstructing the cadherin-catenin-actin complex. Cell *123*, 889-901.

Yang, L., Froio, R.M., Sciuto, T.E., Dvorak, A.M., Alon, R., and Luscinskas, F.W. (2005). ICAM-1 regulates neutrophil adhesion and transcellular migration of TNF-alpha-activated vascular endothelium under flow. Blood *106*, 584-592.

Yang, X., Lee, W.H., Sobott, F., Papagrigoriou, E., Robinson, C.V., Grossmann, J.G., Sundstrom, M., Doyle, D.A., and Elkins, J.M. (2006). Structural basis for protein-protein interactions in the 14-3-3 protein family. Proc Natl Acad Sci U S A *103*, 17237-17242.

Yip, M.F., Ramm, G., Larance, M., Hoehn, K.L., Wagner, M.C., Guilhaus, M., and James, D.E. (2008). CaMKII-mediated phosphorylation of the myosin motor Myo1c is required for insulin-stimulated GLUT4 translocation in adipocytes. Cell Metab *8*, 384-398.

Yu, Q., Gao, F., and Ma, X.L. (2011). Insulin says NO to cardiovascular disease. Cardiovascular research *89*, 516-524.

Yuan, S.Y. (2006). New insights into eNOS signaling in microvascular permeability. American journal of physiology Heart and circulatory physiology *291*, H1029-1031.

Zeng, G., Nystrom, F.H., Ravichandran, L.V., Cong, L.N., Kirby, M., Mostowski, H., and Quon, M.J. (2000). Roles for insulin receptor, PI3-kinase, and Akt in insulin-signaling pathways related to production of nitric oxide in human vascular endothelial cells. Circulation *101*, 1539-1545.

Zeng, G., and Quon, M.J. (1996). Insulin-stimulated production of nitric oxide is inhibited by wortmannin. Direct measurement in vascular endothelial cells. J Clin Invest *98*, 894-898.

Zhang, X.F., Schaefer, A.W., Burnette, D.T., Schoonderwoert, V.T., and Forscher, P. (2003). Rho-dependent contractile responses in the neuronal growth cone are independent of classical peripheral retrograde actin flow. Neuron *40*, 931-944.

Zhao, J., Bruck, S., Cemerski, S., Zhang, L., Butler, B., Dani, A., Cooper, J.A., and Shaw, A.S. (2013). CD2AP Links Cortactin and Capping Protein at the Cell Periphery To Facilitate Formation of Lamellipodia. Molecular and Cellular Biology *33*, 38-47.